

**İSTANBUL TECHNICAL UNIVERSITY ★ INSTITUTE OF SCIENCE AND TECHNOLOGY**

**INORGANIC BINDING POLYPEPTIDES AS MOLECULAR CONSTRUCTS**

**Ph.D. Thesis by  
Turgay KAÇAR**

**Department : Advanced Technologies**

**Programme : Molecular Biology-Genetics and Biotechnology**

**JANUARY 2010**

**INORGANIC BINDING POLYPEPTIDES AS MOLECULAR CONSTRUCTS**

**Ph.D. Thesis by  
Turgay KAÇAR  
(707022003)**

**Date of submission : 30 September 2009  
Date of defence examination: 12 January 2010**

**Supervisor (Chairman) : Prof. Dr. Candan TAMERLER (ITU)  
Co-Supervisor : Prof. Dr. Mehmet SARIKAYA (UW)  
Members of the Examining Committee : Prof. Dr. Pemra DORUKER (BU)  
Prof. Dr. Yusuf YAĞCI (ITU)  
Prof. Dr. Nihat BERKER (SU)  
Assoc. Prof. Ayten KARATAŞ (ITU)  
Assis. Prof. Nevin KARAGÜLER (ITU)**

**JANUARY 2010**

**İSTANBUL TEKNİK ÜNİVERSİTESİ ★ FEN BİLİMLERİ ENSTİTÜSÜ**

**ANORGANİK YAPILARA BAĞLANAN PEPTİTLERİN MOLEKÜLER  
ARAÇ OLARAK KULLANILMASI**

**DOKTORA TEZİ  
Turgay KAÇAR  
(707022003)**

**Tezin Enstitüye Verildiği Tarih : 30 Eylül 2009  
Tezin Savunulduğu Tarih : 12 Ocak 2010**

**Tez Danışmanı : Prof. Dr. Candan TAMERLER (İTÜ)  
Tez Eş Danışmanı : Prof. Dr. Mehmet SARIKAYA (WÜ)  
Diğer Jüri Üyeleri : Prof. Dr. Pemra DORUKER (BÜ)  
Prof. Dr. Yusuf YAĞCI (İTÜ)  
Prof. Dr. Nihat BERKER (SÜ)  
Doç. Dr. Ayten KARATAŞ (İTÜ)  
Yrd. Doç. Dr. Nevin KARAGÜLER (İTÜ)**

**OCAK 2010**

## FOREWORD

This study would not have been accomplished without the support of many people. Firstly, I would like to thank my advisors, Professor Mehmet Sarikaya (UW) and Professor Candan Tamerler (ITU) for their patience, understanding and guidance. I am also grateful to Professor Sarikaya for allowing me to visit his labs during my PhD study, which was a great opportunity to improve my scientific vision and abilities, leading to significant increase in quality of my research.

I would like to thank all members in Professor Sarikaya, especially to Dr. H. Fong, Dr. M. Hnilova, Dr. E. Oren, Dr. Y. Hayamizu, C. Gresswell, B. Wilson, C. So, and J. Park, for their invaluable help and friendship during my visits.

Also, I would like to thank Asst. Prof. N. Gul Karaguler (ITU) and Assoc. Prof. A. Yazgan Karatas (ITU) for their guidance and help in proteomics experiments.

I would like to acknowledge my friends; M. Gungormus, S. Cetinel, H. Yazici, U. O. Seker, E. Yuca, B. Taktak, V. Demir, and D. Sahin all whom I shared unforgettable experiences with.

I would like to acknowledge my collaborators; Prof. D. Ginger (UW), Prof. A. Jen (UW) and their students; Dr. M. Zin, Dr. Y. Chen, K. Munechika, and J. Wei.

I would like to thank the funding agencies for their financial support throughout my PhD research: UW-DURINT (Defense University Research Initiative on Nano technology) through the Army Research Office (US-ARO), the GEMSEC (Genetically Engineered Materials and Engineering Center) through NSF-MRSEC at the UW, and ITU Institute of Science and Technology through Turkish State Planning Organization.

My final and best regards are for my family. I am so pleased that I have a loving and supportive mother who always believes in me.

January 2010

Turgay Kaçar

Molecular Biology and Genetics  
Faculty of Science and Letters



## TABLE OF CONTENTS

	<u>Page</u>
<b>FOREWORD .....</b>	<b>v</b>
<b>TABLE OF CONTENTS.....</b>	<b>vii</b>
<b>ABBREVIATION .....</b>	<b>xi</b>
<b>LIST OF TABLES .....</b>	<b>xiii</b>
<b>LIST OF FIGURES .....</b>	<b>xv</b>
<b>SUMMARY .....</b>	<b>xxi</b>
<b>ÖZET.....</b>	<b>xxiii</b>
<b>1. INTRODUCTION.....</b>	<b>1</b>
1.1 Nanobiotechnology .....	1
1.2 Protein Immobilization.....	3
1.2.1 Physical immobilization .....	3
1.2.2 Chemical immobilization.....	8
1.2.2.1 Non-specific immobilization .....	10
1.2.2.2 Site-Specific immobilization .....	13
1.2.3 Bioaffinity immobilization.....	16
1.2.3.1 Biotin-Avidin system .....	17
1.2.3.2 His-Tag system .....	18
1.2.3.3 DNA-directed immobilization .....	20
1.3 Protein/Peptide Patterning for Micro/Nanoarrays.....	23
1.3.1 Microcontact printing .....	24
1.3.2 Dip-pen lithography.....	26
1.3.3 Photolithography .....	29
1.4 Nano/micro fabrication of inorganic structures .....	31
1.4.1 Nanoparticle synthesis .....	32
1.4.2 Photolithography .....	34
1.4.3 Electron-beam lithography.....	35
1.4.4 Nanosphere lithography.....	37
1.5 Optical Detection Methods in Biosensors .....	38
1.5.1 Fluorescence based detection .....	39
1.5.2 Localized surface plasmon resonance spectroscopy .....	42
1.5.3 Surface plasmon resonance spectroscopy .....	45
1.6 GEPI in Nanobiotechnology.....	47
1.6.1 Isolation of GEPIs using combinatorial biology protocols.....	48
1.6.2 Bioinformatics and molecular binding characterization for GEPIs .....	51
1.6.3 Current and potential applications of GEPIs.....	54
<b>2. MATERIALS AND METHODS .....</b>	<b>59</b>
2.1 Peptide and Nanoparticle Synthesis .....	59
2.1.1 Solid state synthesis of peptides .....	59
2.1.2 Synthesis of silica nanoparticles.....	61
2.1.3 Noble metal nanoparticles.....	61
2.1.4 Decoration of silica nanoparticles with gold nanoparticles .....	62
2.1.5 Preparation of silica core gold nanoshells .....	63

2.2 Expression and Purification of Enzymes .....	64
2.2.1 Strain and plasmids .....	64
2.2.2 Growth and purification of enzymes .....	64
2.3 Preparation of PDMS Stamps for $\mu$ CP. ....	65
2.3.1 Master preparation. ....	65
2.3.2 PDMS stamp preparation.....	65
2.4 Preparation of Patterned Substrates. ....	66
2.4.1 Micropatterned gold substrates by $\mu$ CP .....	66
2.4.2 Noble metal nanostructures by NSL .....	66
2.5 Enzymatic Activity Assays .....	67
2.5.1 Quantification of enzyme activity in solution .....	67
2.5.2 Quantification of immobilized enzyme activity.....	67
2.6. Immobilization of Nanoparticles and Proteins through GEPI.....	68
2.6.1 Self assembly of nanoparticles on inorganic substrates .....	68
2.6.2 $\mu$ CP of enzymes on gold substrates .....	68
2.6.3 $\mu$ CP of QBP-F on quartz substrates .....	69
2.6.4 Co-immobilization of Fluorescein and SA-QDs .....	69
2.6.5 Co-immobilization of noble metal nanoparticles and SA-QDs on glass .	69
2.6.6 Dip-pen lithography of GEPI.....	70
2.7 LSPR based Biomolecule Detection.....	71
2.7.1 Anti-AP detection using immobilized gold NP on glass.....	71
2.7.2 SA-AP Detection using silver nanostructures deposited on glass .....	71
2.8 Characterization Techniques .....	72
2.8.1 Quartz crystalline microbalance spectroscopy .....	72
2.8.2 Atomic force microscopy .....	73
2.8.3 Surface plasmon resonance spectroscopy .....	74
2.8.4 Fluorescence and darkf-field microscopy .....	75
2.8.5 Transmission electron microscopy.....	76
2.8.6 Scanning electron microscopy .....	77
<b>3. RESULTS AND DISCUSSION.....</b>	<b>79</b>
3.1 Oriented Enzyme Immobilization on Gold .....	79
3.1.1 Purification and characterization of bifunctional enzymes .....	79
3.1.2 Binding and assembly of 5GBP1-AP on gold substrates .....	82
3.1.3 Peptide mediated self-immobilization of enzyme on micro-patterned surfaces .....	87
3.2 Nanoparticle Immobilization through Self-assembly of GEPI .....	93
3.2.1 Gold nanoparticle immobilization on glass .....	93
3.2.2 Silica nanoparticle immobilization on gold.....	98
3.2.3 Silver nanoparticle immobilization on glass.....	101
3.3 Micropatterning of Nanoparticles, Fluorophores and Enzyme .....	103
3.3.1 Microcontact printing of FITC through quartz binding peptide .....	103
3.3.2 Co-immobilization of QD and FITC using quartz binding peptide .....	107
3.3.3 Co-immobilization of QD and metal noble nanoparticles using bifunctional inorganic binding peptide.....	113
3.3.4 Microcontact printing of Alkaline phosphatase on gold .....	120
3.3.5 Dip-pen lithography of inorganic binding peptides .....	122
3.4 LSPR based detection of Biomolecules using GEPI and GEPI-Protein Constructs.....	125
3.4.1 Preparation of LSPR active silver nanostructures using NSL .....	125
3.4.2 Probe and target assembly on silver nanostructures .....	127

3.4.3 Probe and target assembly on gold nanoparticles immobilized on glass	128
3.5 Preparation of Gold Nanoparticle-Silica Nanoparticle conjugates and Gold Nanoshells (Silica core).....	134
3.5.1 Decoration of silica nanoparticles with gold nanoparticles .....	134
3.5.2 Gold Formation on Silica nanoparticles. ....	138
3.6 Conclusions.....	146
<b>REFERENCES .....</b>	<b>153</b>
<b>APPENDICES.....</b>	<b>181</b>
<b>CURRICULUM VITA.....</b>	<b>191</b>





## ABBREVIATIONS

<b>aa</b>	: Amino acid
<b>A (Ala)</b>	: Alanine
<b>R (Arg)</b>	: Arginine
<b>N (Asn)</b>	: Asparagine
<b>D (Asp)</b>	: Aspartic acid
<b>C (Cys)</b>	: Cysteine
<b>E (Glu)</b>	: Glutamic acid
<b>Q (Gln)</b>	: Glutamine
<b>G (Gly)</b>	: Glycine
<b>H (His)</b>	: Histidine
<b>I (Ile)</b>	: Isoleucine
<b>L (Leu)</b>	: Leucine
<b>K (Lys)</b>	: Lysine
<b>M (Met)</b>	: Methionine
<b>F (Phe)</b>	: Phenylalanine
<b>P (Pro)</b>	: Proline
<b>S (Ser)</b>	: Serine
<b>T (Thr)</b>	: Threonine
<b>W (Trp)</b>	: Tryptophan
<b>Y (Tyr)</b>	: Tyrosine
<b>V (Val)</b>	: Valine
<b>AFM</b>	: Atomic force microscopy
<b>AgBP</b>	: Silver binding peptide
<b>AP</b>	: Alkaline phosphatase
<b>Anti-AP</b>	: Antibody against AP
<b>AuBP</b>	: Gold binding peptide
<b>Bi-GEPI</b>	: Bifunctional GEPI
<b>DEAE</b>	: Diethylaminoethyl
<b>DF</b>	: Darf-field
<b>DMF</b>	: Dimethylformamide
<b>DMSO</b>	: Dimethyl sulfoxide
<b>DPN</b>	: Dip-pen nanolithography
<b>EBL</b>	: Electron beam lithography
<b>EDX</b>	: Energy-dispersive X-ray
<b>ELISA</b>	: Enzyme-linked immunosorbent assay
<b>E. coli</b>	: Escherichia coli
<b>FITC</b>	: Fluorescein isothiocyanate
<b>FM</b>	: Fluorescence microscopy
<b>FRET</b>	: Fluorescence resonance energy transfer
<b>GBP1</b>	: Gold binding peptide with “MHGKTQATSGTIQS” sequence
<b>5GBP1-AP</b>	: Genetic fusion of 5 repeats of GBP1 to AP
<b>6GBP1-AP</b>	: Genetic fusion of 6 repeats of GBP1 to AP
<b>7GBP1-AP</b>	: Genetic fusion of 7 repeats of GBP1 to AP

<b>9GBP1-AP</b>	: Genetic fusion of 5 repeats of GBP1 to AP
<b>GEPI</b>	: Genetically engineered polypeptides for inorganic surfaces
<b>GEPI-bio</b>	: Biotinylated GEPI
<b>IPTG</b>	: Isopropyl $\beta$ -D-1-thiogalactopyranoside
<b>LFM</b>	: Lateral force microscopy
<b>LSP</b>	: Localized surface plasmon
<b>LSPR</b>	: Localized surface plasmon resonance
<b>LSPR <math>\lambda_{\max}</math></b>	: Wavelength of LSPR extinction band maximum
<b>NIR</b>	: Near infrared
<b>NP</b>	: Nanoparticle
<b>PBS</b>	: Phosphate buffered saline
<b>PDMS</b>	: Polydimethylsiloxane
<b>PMSF</b>	: Phenylmethanesulphonyl fluoride
<b>QBP</b>	: Quartz binding peptide
<b>QCM</b>	: Quartz crystalline microbalance
<b>SA-AP</b>	: Streptavidin-linked Alkaline phosphatase
<b>SA-QD</b>	: Streptavidin-coated quantum dot
<b>SA-QD(565)</b>	: Streptavidin-coated quantum dot (light-emitting at 565 nm)
<b>SA-QD(605)</b>	: Streptavidin-coated quantum dot (light-emitting at 605 nm)
<b>SAM</b>	: Self-assembled monolayer
<b>SEM</b>	: Scanning electron microscopy
<b>SPP</b>	: Surface plasmon polariton
<b>SPR</b>	: Surface plasmon resonance
<b>TEM</b>	: Transmission electron microscopy
<b>TEOS</b>	: Tetraethyl orthosilicate
<b><math>\mu</math>CP</b>	: Microcontact printing
<b><math>\lambda</math></b>	: Wavelength

## LIST OF TABLES

	<b><u>Page</u></b>
<b>Table 1.1:</b> Mostly used functional groups in proteins and functionalities of the required surfaces.....	8
<b>Table 2.1:</b> Sequence, MW, pI, and Net Charge of Synthesized Peptides. ....	61
<b>Table 3.1:</b> The parameters of binding kinetics for 5GBP1-AP and AP on bare Au surfaces obtained by SPR.....	86



## LIST OF FIGURES

	<u>Page</u>
<b>Figure 1.1</b> : Models for SAMs of (a) alkanethiolates on gold and (b) alkylsiloxanes on SiO <sub>2</sub> surface. ....	9
<b>Figure 1.2</b> : Schematic representation of amine chemistry on (a) NHS-Derivatized and (b) Aldehyde-Derivatized Surfaces.....	11
<b>Figure 1.3</b> : Schematic representation of thiol chemistry on (a) Maleimide-Derivatized, (b) Disulfide-Derivatized, and (c) Vinyl Sulfone-Derivatized Surfaces Models for SAMs of (a) alkanethiolates on gold and (b) alkylsiloxanes on SiO <sub>2</sub> surface. ....	11
<b>Figure 1.4</b> : Schematics of carboxyl chemistry through carbodiimide. ....	13
<b>Figure 1.5</b> : (a) Random immobilization of proteins, (b) oriented immobilization of proteins.....	14
<b>Figure 1.6</b> : Schematically representation of the site-specific biomolecule immobilization via “click” chemistry.....	14
<b>Figure 1.7</b> : Schematically representation of Thiazolidine ring formation through peptide ligation between N-terminal cysteine and ester glycoaldehyde. ....	15
<b>Figure 1.8</b> : Reaction mechanism of Staudinger Ligation.....	16
<b>Figure 1.9</b> : Binding mechanism of the His-tagged protein to a Ni-NTA surface.. ..	19
<b>Figure 1.10</b> : Schematic representation of the construction of a SPR sensor via DDI and streptavidin bridging. ....	22
<b>Figure 1.11</b> : Scheme of (a) fabrication of PDMS stamp and (b) its use for $\mu$ CP of proteins. ....	25
<b>Figure 1.12</b> : Schematic representation of DPN. The AFM tip, thiol molecule, and gold film are utilized as “nib”, “ink”, and “paper”, respectively.....	27
<b>Figure 1.13</b> : Conventional photoresist technology applied to the silane SAMs for fabrication of a template for protein immobilization... ..	30
<b>Figure 1.14</b> : Top-down and bottom-up approaches meet on the scale.. ..	32
<b>Figure 1.15</b> : Steps in photolithography using positive and negative photoresists....	35
<b>Figure 1.16</b> : Steps in EBL to produce Au nanostructures.....	36
<b>Figure 1.17</b> : Steps in the fabrication of Ag nanostructures by NSL.....	38
<b>Figure 1.18</b> : The principles for the biosensor.....	39
<b>Figure 1.19</b> : Fluorescence parameters used for obtaining the sensor response.....	40
<b>Figure 1.20</b> : Different possibilities for the generation of a signal from fluorescent dye on sensor-target interaction.. ..	41
<b>Figure 1.21</b> : Schematic representation of a localized surface plasmon. ....	43
<b>Figure 1.22</b> : The extinction spectra of NSL-fabricated silver nanostructures in different size and shape. ....	45
<b>Figure 1.23</b> : Schematic representation of a surface plasmon polariton. ....	46
<b>Figure 1.24</b> : Schematic diagram for the Kretschmann configuration. ....	47
<b>Figure 1.25</b> : Schematic diagram for phage- and cell-surface display techniques. ....	50
<b>Figure 1.26</b> : Bioinformatic approach for desing of second generation GEPIs. ....	53

<b>Figure 1.27</b> : Potential application areas of GEPIs. ....	55
<b>Figure 2.1</b> : Image of CS-Bio peptide synthesizer... ..	60
<b>Figure 2.2</b> : Image of Waters HPLC.....	60
<b>Figure 2.3</b> : Schematic representation of experimental setup for LSPR detection on NSL-fabricated nanoarray. ....	72
<b>Figure 2.4</b> : The setup for the QCM. ....	73
<b>Figure 2.5</b> : The image of the Atomic Force Microscope in the chamber for acoustic and mechanical isolation. ....	74
<b>Figure 2.6</b> : The setup for SPR spectroscopy.....	75
<b>Figure 2.7</b> : The optical microscope dedicated for fluorescence and dark-field imaging. ....	76
<b>Figure 2.8</b> : Philips EM420 Transmission electron microscope. ....	77
<b>Figure 2.9</b> : JEOL JSM 7000F Scanning electron microscope with EDX detector...78	
<b>Figure 3.1</b> : SDS–PAGE of 5GBP1-AP purification steps.....	80
<b>Figure 3.2</b> : The image of 10% SDS gel of the purified constructs with the molecular weight marker. ....	81
<b>Figure 3.3</b> : Phosphatase activity of the molecular constructs, nGBP1-AP. ....	81
<b>Figure 3.4</b> : Gold binding activity of nGBP1-AP constructs by quartz crystal microbalance analysis (protein concentration: 2.5 µg/ml). ....	82
<b>Figure 3.5</b> : AFM image of gold substrate following self-assembly of 5GBP1-AP (protein concentration: 3 µg/ml). The area corresponds to 500 nm x 500 nm scans. ....	83
<b>Figure 3.6</b> : Digitally magnified Figure 3.5 is represented in pseudo-3-dimensional presentation at 150 nm x 150 nm area to show surface topography following the immobilization of 5GBP1-AP. ....	84
<b>Figure 3.7</b> : AFM image of gold substrate following self-assembly of AP (protein concentration: 3 µg/ml). The area corresponds to 500 nm x 500 nm scans. ....	84
<b>Figure 3.8</b> : Digitally magnified Figure 3.7 is represented in pseudo-3-dimensional presentation at 150 nm x 150 nm area to show surface topography following the immobilization of AP.....	85
<b>Figure 3.9</b> : SPR spectroscopy results of AP and 5GBP1-AP binding to bare gold surfaces at 4 µg/ml concentration. ....	86
<b>Figure 3.10</b> : Surface coverage of AP and 5GBP1-AP has been calculated using the Langmuir isotherm model based on the SPR experiments ..... 86	
<b>Figure 3.11</b> : Schematic representation of the experimental procedure for the generation of two-dimensional arrays of immobilized proteins on a patterned substrate fabricated through µCP ..... 88	
<b>Figure 3.12</b> : Topographic image of the microarray of immobilized AP. .... 88	
<b>Figure 3.13</b> : AFM image of the microarray of immobilized AP at higher magnification. .... 89	
<b>Figure 3.14</b> : Topographic image of the microarray of immobilized 5GBP1-AP. ... 89	
<b>Figure 3.15</b> : AFM image of the micro-array of immobilized 5GBP1-AP at higher magnification. .... 90	
<b>Figure 3.16</b> : The calculated AP activities per unit area for AP and 5GBP1-AP corresponding to self-assembly (SA) of each enzyme on the non- patterned (NP) and micropatterned (µP) gold substrates..... 92	
<b>Figure 3.17</b> : Procedure for GEPI directed nanoparticle immobilization..... 94	
<b>Figure 3.18</b> : DF image of gold nanoparticle immobilization on glass using AuBP1 ..... 95	

<b>Figure 3.19 :</b>	DF image of gold nanoparticle immobilization on glass using QBP1	95
<b>Figure 3.20 :</b>	DF image of gold nanoparticle immobilization on glass treated only with PBS	95
<b>Figure 3.21 :</b>	(a) DF and (b) AFM images of gold nanoparticle immobilization on glass using Bi-GEPI-1.	97
<b>Figure 3.22 :</b>	(a) DF and (b) AFM images of gold nanoparticle immobilization on glass using Bi-GEPI-2.	97
<b>Figure 3.23 :</b>	(a) DF and (b) AFM images of gold nanoparticle immobilization on glass using Bi-GEPI-3.	97
<b>Figure 3.24 :</b>	(a) DF and (b) AFM images of gold nanoparticle immobilization on glass using Bi-GEPI-4.	98
<b>Figure 3.25 :</b>	DF image of silica nanoparticle immobilization on gold using AuBP1	98
<b>Figure 3.26 :</b>	DF image of silica nanoparticle immobilization on gold using QBP1.	99
<b>Figure 3.27 :</b>	DF image of silica nanoparticle immobilization on gold treated only with PBS.	99
<b>Figure 3.28 :</b>	(a) DF and (b) AFM images of immobilized silica nanoparticles on gold through Bi-GEPI-1 assembly.	100
<b>Figure 3.29 :</b>	(a) DF and (b) AFM images of immobilized silica nanoparticles on gold through Bi-GEPI-2 assembly.	100
<b>Figure 3.30 :</b>	(a) DF and (b) AFM images of immobilized silica nanoparticles on gold through Bi-GEPI-3 assembly	100
<b>Figure 3.31 :</b>	(a) DF and (b) AFM images of immobilized silica nanoparticles on gold through Bi-GEPI-4 assembly	101
<b>Figure 3.32 :</b>	DF image of Ag nanoparticle immobilization on gold using AgBP1.	102
<b>Figure 3.33 :</b>	DF image of silver nanoparticle immobilization on gold using QBP1.	102
<b>Figure 3.34 :</b>	DF image of silver nanoparticle immobilization on glass treated only with PBS.	102
<b>Figure 3.35 :</b>	DF image of silver nanoparticle immobilization on glass using Bi-GEPI-5.	103
<b>Figure 3.36 :</b>	Schematic representation for PDMS patterning of QBP1-F on quartz..	105
<b>Figure 3.37 :</b>	FM image of the quartz substrate after micropatterning with fluorescein alone, as the control	105
<b>Figure 3.38 :</b>	FM image of the quartz substrate after micropatterning with QBP1-F	106
<b>Figure 3.39 :</b>	FM image of the quartz substrate after micropatterning with BSA-F, as another control	106
<b>Figure 3.40 :</b>	Comparisons of fluorescence intensity of fluorescein molecules immobilized through itself, BSA and QBP1	107
<b>Figure 3.41 :</b>	FM images of the micropattern of QBP1-F on glass surface at (a) lower and (b) higher magnifications	107
<b>Figure 3.42 :</b>	Schematic representation of PDMS patterning of QBP1-bio on a solid substrate.	109
<b>Figure 3.43 :</b>	FM image of the micropattern formed through directed assembly of SA-QD following the PDMS stamping of QBP1-bio on quartz.	109



<b>Figure 3.44 :</b>	FM image of the quartz substrate after the PDMS stamping of QBP2-bio followed by SA-QD assembly .....	110
<b>Figure 3.45 :</b>	FM image of the gold substrate after the PDMS stamping of QBP1-bio followed by SA-QD assembly .....	110
<b>Figure 3.46 :</b>	FM image of the gold substrate after the PDMS stamping of QBP2-bio followed by SA-QD assembly .....	111
<b>Figure 3.47 :</b>	Schematics of QBP1-F assembly on a quartz substrate pre-patterned using QBP1-bio/SA-QD.....	112
<b>Figure 3.48 :</b>	FM image of a micropattern of directed immobilized SA-QD via the QBP1-bio patterned surface .....	112
<b>Figure 3.49 :</b>	FM image of the micropattern formed by the immobilization of QBP1-F conjugate on the unfilled microlines, using the substrate as in Figure 3.48 .....	113
<b>Figure 3.50 :</b>	Digital overlay of the images in Figure 3.48 and Figure 3.49, demonstrating the utility of QBP1 both as a molecular ink for stamping, for directing the immobilization of QDs, and a mediated molecular assembler for a fluorescent molecule.....	113
<b>Figure 3.51 :</b>	Schematics for co-immobilization of metal nanoparticle and green/red QD on glass through $\mu$ CP and self-assembly of GEPIs.....	114
<b>Figure 3.52 :</b>	DF image of the micropattern formed through $\mu$ CP of Bi-GEPI-1 followed by gold nanoparticle assembly and then, PBS incubation followed by green SA-QD(565) assembly .....	115
<b>Figure 3.53 :</b>	FM image of the micropattern formed through $\mu$ CP of Bi-GEPI-1 followed by gold nanoparticle assembly and then, PBS incubation followed by green SA-QD(565) assembly. ....	115
<b>Figure 3.54 :</b>	DF image of the substrate prepared through $\mu$ CP of PBS followed by gold nanoparticle assembly and then, sequential QBP1-bio and SA-QD(565) assembly. ....	116
<b>Figure 3.55 :</b>	FM image of the substrate prepared through $\mu$ CP of PBS followed by gold nanoparticle assembly and then, sequential QBP1-bio and SA-QD(565) assembly .....	116
<b>Figure 3.56 :</b>	DF image of the micropattern formed through $\mu$ CP of Bi-GEPI-1 followed by gold nanoparticle assembly then, sequential QBP1-bio and SA-QD(565) assembly. ....	117
<b>Figure 3.57 :</b>	FM image of the micropattern formed through $\mu$ CP of Bi-GEPI-1 followed by gold nanoparticle assembly then, sequential QBP1-bio and SA-QD(565) assembly .....	117
<b>Figure 3.58 :</b>	DF image of the micropattern formed through $\mu$ CP of Bi-GEPI-5 followed by silver nanoparticle assembly and then, PBS incubation followed by red SA-QD(605) assembly.....	118
<b>Figure 3.59 :</b>	FM image of the glass substrate prepared through $\mu$ CP of Bi-GEPI-5 followed by silver nanoparticle assembly and then, PBS incubation followed by SA-QD(605) assembly .....	118
<b>Figure 3.60 :</b>	DF image of the substrate prepared through $\mu$ CP of PBS followed by silver nanoparticle assembly and then, sequential QBP1-bio and SA-QD(605) assembly .....	119
<b>Figure 3.61 :</b>	FM image of the substrate prepared through $\mu$ CP of PBS followed by silver nanoparticle assembly and then, sequential QBP1-bio and SA-QD(605) assembly .....	119

<b>Figure 3.62 :</b>	DF image of the micropattern formed through $\mu$ CP of Bi-GEPI-5 followed by silver nanoparticle assembly then, sequential QBP1-bio and SA-QD(605) assembly.....	120
<b>Figure 3.63 :</b>	FM image of the micropattern formed through $\mu$ CP of Bi-GEPI-5 followed by silver nanoparticle assembly then, sequential QBP1-bio and SA-QD(605) assembly.....	120
<b>Figure 3.64 :</b>	Schematics for $\mu$ CP of (a) AP and (b) 5GBP1-AP on gold followed by labeled Anti-AP coupling..	121
<b>Figure 3.65 :</b>	FM image of the micropattern formed through $\mu$ CP of AP followed by labeled Anti-AP incubation..	122
<b>Figure 3.66 :</b>	FM image of the micropattern formed through $\mu$ CP of 5GBP1-AP followed by labeled Anti-AP incubation. ....	122
<b>Figure 3.67 :</b>	Schematics for DPN of GEPI-bio on inorganic substrate followed by SA-QD assembly.....	123
<b>Figure 3.68 :</b>	FM image of the microarray formed through DPN of QBP1-bio followed by SA-QD assembly..	124
<b>Figure 3.69 :</b>	LFM image of DPN-patterned QBP1 on silica substrate.....	124
<b>Figure 3.70 :</b>	DF image of polystyrene monolayer prior to silver deposition.....	125
<b>Figure 3.71 :</b>	DF image of NSL-fabricated silver nanostructures following metal deposition and removal of polystyrene beads.....	126
<b>Figure 3.72 :</b>	AFM image of NSL-fabricated silver nanostructures with line profile analysis..	126
<b>Figure 3.73 :</b>	Pseudo-3-dimensional presentation of the AFM image of NSL-fabricated silver nanostructures shown in Figure 3.72.....	127
<b>Figure 3.74 :</b>	LSPR spectra of NSL-fabricated Ag nanoarray (nanosphere D= 450 nm, the height of Ag nanotriangle; $d_m$ = 50nm) for each step in SA-AP detection.....	128
<b>Figure 3.75 :</b>	Comparison of probe assembly by LSPR spectroscopy.....	129
<b>Figure 3.76 :</b>	Immuno-detection of Anti-AP (25 $\mu$ g/ml) using LSPR based biosensor composed of gold nanoparticles immobilized through Bi-GEPI-1 and a genetically engineered fusion probe, 5GBP1-AP... ..	130
<b>Figure 3.77 :</b>	Immuno-detection of Anti-AP (25 $\mu$ g/ml) using LSPR based biosensor composed of gold nanoparticles immobilized through Bi-GEPI-1 and the control protein, AP... ..	131
<b>Figure 3.78 :</b>	The red shift upon functionalization of probe-assembled gold nanoparticles on glass slide by Anti-AP with different concentrations .....	132
<b>Figure 3.79 :</b>	Red shifts at LSPR $\lambda_{max}$ obtained from (a) the non-specific binding of Anti-AP on glass functionalized with gold nanoparticle film, (b) the specific binding of the same target to 5GBP1-AP immobilized on gold nanoparticles attached to the glass cover slip, and (c) the non-specific binding of Anti-MBP on the same substrate represented in b.....	133
<b>Figure 3.80 :</b>	TEM image of synthesized silica nanoparticles..	134
<b>Figure 3.81 :</b>	Gold nanoparticle attachments to silica nanoparticle pre-functionalized by Bi-GEPI-1..	135
<b>Figure 3.82 :</b>	SEM image of gold nanoparticle attachments to silica nanoparticle pre-functionalized by Bi-GEPI-1 (at lower magnification)..	136
<b>Figure 3.83 :</b>	SEM image of gold nanoparticle attachments to silica nanoparticle pre-functionalized by Bi-GEPI-1 (at higher magnification).....	136

<b>Figure 3.84 :</b> SEM image of gold nanoparticle attachments to silica nanoparticles in absence of Bi-GEPI-1..	137
<b>Figure 3.85 :</b> Extinction spectra of free gold nanoparticles and 20/148 nm Au/SiO <sub>2</sub> ensembles. Arrows indicate the position of the extinction maxima of each spectrum..	138
<b>Figure 3.86 :</b> Scheme for GEPI-based gold nanoshell (Au-shell@Silica-core) preparation.....	139
<b>Figure 3.87 :</b> Comparison for number of bound Bi-GEPIs per silica nanoparticle .....	139
<b>Figure 3.88 :</b> Extinction spectra of control 1, control 2, and the nanostructures (sample) prepared using the protocol depicted in Figure 3.86 with formaldehyde.....	141
<b>Figure 3.89 :</b> SEM image of control 1 where only silica nanoparticles were exposed to gold ion solution under reducing condition.....	142
<b>Figure 3.90 :</b> SEM image of control 2 where only formaldehyde was exposed to gold ion solution .....	142
<b>Figure 3.90 :</b> SEM image of control 2 where only formaldehyde was exposed to gold ion solution .....	142
<b>Figure 3.91 :</b> SEM image of nanostructures synthesized using the protocol shown in Figure 3.86 in combination with formaldehyde (at lower magnification).....	143
<b>Figure 3.92 :</b> SEM image of nanostructures synthesized using the protocol shown in Figure 3.86 in combination with formaldehyde (at higher magnification).....	143
<b>Figure 3.93 :</b> Characterization of silica nanoparticle by (a) SEM, (b) with EDX spectroscopy. ....	144
<b>Figure 3.94 :</b> Characterization of gold nanoparticles obtained from control experiment-1 by (a) SEM, (b) with EDX spectroscopy.....	145
<b>Figure 3.95 :</b> Characterization of gold nanoshells by (a) SEM, (b) with EDX spectroscopy .....	145
<b>Figure A.1 :</b> Adsorption isotherms for QBP1 and QBP2 based on SPR spectroscopy.....	182
<b>Figure A.2 :</b> FM images of the glass substrate after micropatterning of QBP1-F...	183
<b>Figure A.3 :</b> FM image of PBS buffer-stamped quartz substrate following SA-QD(605) incubation. ....	184
<b>Figure A.4 :</b> (a) AFM image of NSL-fabricated Au NP array, (b) Section analysis .....	185
<b>Figure A.5 :</b> 3D AFM image of NSL-fabricated Au NP array represented in Figure A.4. ....	186
<b>Figure A.6 :</b> SPR sensogram upon binding of AgBP1 on silver coated-SPR chip..	187
<b>Figure A.7 :</b> TEM image of synthesized silica NPs. ....	188
<b>Figure A.8 :</b> EDX spectrum was taken from blank spot on Aluminum mount (as background), showing negligible Si and Au signals.....	189

## INORGANIC BINDING POLYPEPTIDES AS MOLECULAR CONSTRUCTS

### SUMMARY

Molecular biomimetics has emerged from the inspiration from nature regarding to the interactions between biomolecules and inorganic materials at molecular level. This area has potential to provide novel molecular tools involving polypeptides with affinity towards inorganic surfaces. These peptides are used to produce new hybrid materials with advanced properties that can be utilized for various applications in different areas such as biotechnology, nanotechnology, and micro/nanoelectronics. Inorganic binding peptides, known as genetically engineered polypeptides for inorganic surfaces (GEPIs), are isolated using combinatorial biology protocols such as phage- and cell-surface display technologies. Following successful qualitative and quantitative molecular characterization using FM, SPR, QCM, and AFM, these peptides were used in this thesis as assembler, linker, and synthesizer to fabricate new functional platforms for different purposes avoiding potential problems or limitations associated with the conventional chemical methods. Firstly, due to the specific surface recognition and ease of genetic manipulation, utilization of gold binding peptide (GBP1) as a molecular linker genetically fused to AP enzyme was demonstrated for site-specific protein immobilization on non-patterned and micro-patterned gold substrates. Moreover, in protein and nanoparticle patterning, GEPIs were shown to be successful “ink” (molecular linker) for lithography techniques, *i.e.*  $\mu$ CP and DPN. Through self-assembly process, bifunctional GEPIs containing two different inorganic binding sequences, *e.g.*, gold, silver and silica were used to immobilize gold and silver nanoparticles on silica and also, silica nanoparticle attachment was accomplished on gold substrates. At nano-scale level, Bi-GEPI was also used to decorate silica nanoparticles with gold nanoparticles. As an application of these platforms that GEPIs provide the assembly of nanoparticles and probe molecules, optical hybrid sensors composed of noble metal nanostructures and GEPI-linked probes were fabricated and utilized to detect appropriate targets. For example, glass slides where gold nanoparticles were assembled *via* Bi-GEPI, were utilized as platform to achieve the detection of target molecules (Anti-AP) with concentration of down to ~30 nM through a GEPI-based probe, 5GBP1-AP. Apart from assembly and micro/nano-organization of proteins and nanoparticles on solid substrates, GEPI was also employed in synthesis of optically active hybrid nanostructures where the peptide acted as nucleation site for gold formation around silica nanoparticles, resulting a red shift at corresponding LSPR  $\lambda_{\text{max}}$  from vis to IR region where biological components in tissue barely absorb the light. Overall, the results reported in this thesis clearly show that polypeptides with binding affinity and specificity towards inorganic surfaces have great potential to prepare new functional platforms at different scale and under ambient conditions, which then, can be used for various purposes such as in preparation of protein micro/nano-arrays, biosensors, and reagents for molecular imaging and targeting.



## ANORGANİK YAPILARA BAĞLANAN PEPTİTLERİN MOLEKÜLER ARAÇ OLARAK KULLANILMASI

### ÖZET

Moleküler biyobenzetim, doğada varolan, biyomoleküllerin anorganik yapılar ile olan moleküler seviyedeki ilişkilerinden esinlenerek ortaya çıkmıştır. İleri derecede gelişmiş özelliklere sahip hibrid malzemelerin üretilmesi için anorganik yapılara bağlanabilen peptitlerin de içinde bulunduğu yeni moleküler araçlar sunmaktadır. Bu peptitlerden yararlanılarak yapılacak malzemeler biyoteknoloji, nanoteknoloji, ve mikro/nanoelektronik gibi birçok alanda kullanılabilir. Terminolojide genetik olarak modifiye edilmiş anorganik yapılara bağlanabilen peptitler (GEPI) olarak bilinen bu moleküler araçlar, faj- ve hücre- gösterimi gibi kombinatoriyel biyolojide kullanılan methodlarla elde edilirler. FM, SPR, QCM, ve AFM gibi teknikler ile karakterize edildikten sonra GEPI'ler; bu tezin içerdiği çalışmalarda moleküler ölçekte organize edici, bağlayıcı, sentezleyici olarak kullanılmış, bu sayede aynı amaçlar için klasik olarak kullanılan sentetik moleküllerin taşıdığı dezavantajlar ortadan kaldırılarak farklı uygulamalara hizmet edebilecek, fonksiyonel yeni platformlar hazırlanmıştır. İlk olarak, spesifik olarak yüzeyi tanıması ve protein mühendisliğindeki uygulanabilirliği baz alınarak, altına bağlanabilen peptitlerden biri olan GBP1'in, AP enzimine eklenmesi sonucu ortaya çıkan recombinant proteinin mikro desenli veya düz altın yüzeylere belli bir noktadan (site-specific) tutunması gösterilmiştir. Ayrıca, GEPI'lerin  $\mu$ CP ve DPN gibi desenleme teknikleri kullanılarak yüzeye mikro/nano boyutlarda desenleri oluşturulmak suretiyle protein ve nanoparçacık arrayleri hazırlanmasında bağlayıcı molekül olarak kullanılabilecekleri gösterilmiştir. İki farklı anorganik yapıya bağlanan aminoasit dizileri içeren iki fonksiyonlu peptitlerin (Bi-GEPIs) kullanılması ile nanoparçacıkların yüzeye immobilize ("Self-assembly" yoluyla) olmaları sağlanmıştır. Altın ve gümüş nanoparçacıklarının cam yüzeyine; silika nanoparçacıklarının da altın yüzeyine bu peptitler aracılığı ile tutunabildikleri gösterilmiştir. Ayrıca, makro büyüklükte düz bir yüzey yerine nano boyutlardaki silika parçacıkları da uygun Bi-GEPI kullanılarak altın nanoparçacıkları ile dekore edilmiştir. GEPI'lerin nanoparçacık ve de prob molekülünü organize etmesinden yararlanarak elde edilen platformların bir uygulaması olarak, hibrid optik sensörler hazırlanmış ve uygun hedef moleküllerin algılamasında kullanılmıştır. Bu uygulamaların bir tanesinde, cam üzerine Bi-GEPI kullanılarak immobilize edilen altın nanoparçacıklar ve onların üzerine bağlanan 5GBP1-AP prob molekülünden oluşan sensör, hedef molekülü olan Anti-AP deteksiyonunda  $\sim 30$  nM'ye kadar inebilmiştir. Protein ve nanoparçacıkların immobilizasyonu ve mikro/nano boyutlardaki organizasyonlarının sağlanması dışında, GEPI'ler, optik olarak aktif, hibrid nanoyapıların oluşturulmasında da kullanılmış; silika nanoparçacıklarının etrafının altın ile kaplanmasını sağlamıştır. Sonuç olarak elde edilen bu parçacıkların LSPR  $\lambda_{maks}$ 'sında görünür bölgeden IR bölgesine kayma gözlenmiştir ki bu bölgede biyolojik materyaller ışığı çok az absorbe etmektedirler. Genel olarak bakıldığında bu doktora çalışmasında elde edilen sonuçlar, açıkça GEPI'lerin yeni, fonksiyonel ve farklı ölçeklerde platformların ortam koşullarında hazırlanmasında kullanılabilecek

kapasitede olduğunu ve daha sonra bu platformların da protein mikro/nanoarray sistemler, biyosensörler, moleküler görüntüleme ve hedefleme gibi amaçlar için kullanılabileceklerini göstermektedir.

## 1. INTRODUCTION

### 1.1 Nanobiotechnology

The first concept of the possibility to manipulate matter at the nano-level was proposed by Richard Feynman during his lecture entitled “There’s Plenty of Room at the Bottom” back in December 1959. In his talk, he discussed the use of atomic blocks to assemble at a molecular level, saying that “The principles of physics, as far as I can see, do not speak against the possibility of maneuvering things atom by atom. It is not an attempt to violate any laws; it is something, in principle, that can be done; but in practice, it has not been done because we are too big” [1, 2]. In recent definitions, “nanotechnology is the understanding and control of matter at dimensions of roughly 1 to 100 nanometers, where unique phenomena enable novel applications”[2].

Today, since the knowledge on synthesizing and manipulating the materials at nanoscale has been growing, the key challenge in nanotechnology is to be able to produce nanodevices with stronger properties and wider range of functions comparing to those readily provided by modern microchips [3-6]. As a tool box consisting of the huge number of nanostructures that can be formed through self-assembly are developed, these nanodevices with new mechanical, optical, or electronic properties can be fabricated using appropriate set of self-organized elements [3, 7].

Nanobiotechnology is a subset of nanotechnology where biology gives the inspiration and/or the end goal. It is defined as engineering and manufacturing at nanoscale using biological precedence for guidance (Nano-Biomimetics) or traditional nanotechnology applied to the needs in biotechnology [2, 7, 8]. Specifically, molecular biomimetics, proposed by Sarikaya *et al.* and relied on the specific interactions of protein/peptides with inorganics to control structures and functions of biological hard and soft tissues, has been emerged to address the issues in biotechnology, cooperatively utilizing nanotechnology and molecular biology [7,



9, 10]. In molecular biomimetics [11-13], new hybrid materials and devices that could be useful for various applications in biotechnology can be prepared under mild conditions at molecular level through the interactions between the biological components such as proteins and peptides, and the inorganic structures such as gold and silica [7, 10]. Moreover, this area could allow us to understand the dynamic of self-assembly in detail from the nature so that these biomimetic nanostructures can be fabricated *via* controlled self-assembly process [2, 7, 14, 15].

An example of advances in nanotechnology is on disease treatment that is in conjunction with the emerging fields of molecular medicine and personalized medicine [2]. It is certain that cellular level control is not possible without the help from nanotechnology. The ability of nanotechnology enables us to make progress in early detection, diagnostics, prognostics and the selection of therapeutic strategies, yielding ‘multiplexing’ that is, to detect a broad multiplicity of molecular signals and biomarkers in real time [16].

The possibilities of developing nanostructures such as nanocantilevers, nanotubes, and nanoparticles, are attracting more attention [2]. By systematically combining them with preferred therapeutic and biological targeting moieties it can be doable to prepare a very large number of multifunctional, novel, personalized therapeutic agents [16]. For example, multifunctionality including the avoidance of biobarriers and biomarker-based targeting, and the reporting of therapeutic efficacy is the fundamental advantage of the nanostructures used for the cancer-specific delivery of therapeutic and imaging agents [16].

With new advances in bionanotechnology where collaborative efforts from different fields have been accumulated, molecular understanding of cellular function in health and disease is improved by nanotools [2]. As a consequence, clinicians have started to diagnose diseases much faster with higher sensitivity and specificity. In other words, the distinctions of basic and applied science have merged, synergizing each other to improve human health [2].

## 1.2 Protein Immobilization

Immobilization can be defined as the attachment of the molecules to the surface. As a result, mobility of the attached molecules is either decreased or canceled [17-19]. DNA and proteins are the most common biomolecules involved in various applications for biotechnology, necessitating efficient immobilization on inorganic substrates. For example, high-throughput screening of candidate drugs generally needs biosensors based on solid supports, *e.g.*, for mimicking the receptor-drug interactions [20]. Other examples of industrial applications for proteins bound to solids include affinity chromatography, protein chips, cell separation, drug delivery, etc. [18, 20-22]. Due to the fundamental structural difference between DNA and proteins, their immobilization requires different strategies. DNA is i) uniformly structured, ii) stable, iii) highly resistant to the activity loss, and has only one interaction site with target molecule, *i.e.* complementary DNA. In comparison, proteins i) have many different structures, ii) include heterogeneous hydrophobic and charged domains, iii) are highly sensitive to any changes in the three-dimensional structure causing to activity loss, iv) can have many interaction spots [23].

The reusability and increased stability of biomolecules are major advantages of the immobilization. However, activity of proteins can be reduced due to the random orientation and structural deformation during the attachment. In fact, the immobilization shouldn't affect conformation and function of the molecule to fully retain the biological activity [17]. There are many immobilization techniques that are mainly based on three mechanisms as follows: physical, chemical and bioaffinity immobilization [17, 22].

### 1.2.1 Physical Immobilization

Considering numerous practical applications of immobilized proteins, as well as the economical potential in the area mentioned above, it is the fact that the research area of interfacial behavior of the biomolecules has been quite progressive during the past few decades. Although initial attempts for the protein immobilization was based on physically adsorption of the molecules, this has become less important due to the limitations of physically adsorbed layers, such as activity loss, desorption or exchange in multi-component protein systems, etc [20]. Basically, proteins can adsorb at surfaces via intermolecular forces, mainly ionic bonds and hydrophobic and

polar interactions. Mostly, the resulting layer is to be heterogeneous and randomly oriented, since each molecule may have different optimum conformation to minimize the repulsive forces from the surface and previously attached protein, during the adsorption [17, 22]. Furthermore, high-density packing may sterically block active sites of proteins, decreasing the functional properties [17]. However, it should be also noted that the physical adsorption of proteins constitutes the first step of chemical immobilization involving covalent bonding of proteins at the surface as a second step.

During protein adsorption at a surface, five major subprocesses in the adsorption process can be distinguished: (1) movement of proteins toward the surface, (2) actual attachment to the surface, (3) adsorption at higher surface coverage which is hindered to lateral repulsion between proteins in solution and at the surface; (4) structural and/or orientational rearrangements in the adsorbed proteins; (5) desorption of proteins from the surface [24]. This affinity may be enhanced by the possibility of structural changes within protein and is therefore related to the structural stability of the protein [24]. Furthermore, many proteins undergo conformational changes and generally, their ordered structural content is decreased at the adsorption process [20]. The adsorption of proteins to surfaces is mainly determined by van der Waals, hydrophobic, electrostatic interactions and hydrogen bonding [20, 24, 25]. For example, under conditions of electrostatic repulsion to hydrophobic surfaces, protein adsorption is limited by Gibbs energy barrier whereas such a barrier is barely felt at the hydrophobic methylated surfaces [24].

Surface properties of the inorganic materials directly affect the physical attachment of protein; also surface modification may be needed to increase the protein adsorption for technical applications. The surface hydrophobicity is one of the surface properties that one can control over a wide range. Furthermore, hydrophobic interactions between the solid surface and the protein would be expected to be more favorable comparing to hydrophilic interactions in terms of protein adsorption. This is also frequently, but not always, observed experimentally [20, 24-26]. As an example, the preferential adsorption of fibrinogen at a hydrophobicity gradient surface was demonstrated by Elwing *et al.* As the hydrophobicity of the surface was decreased, reduction at the adsorption of the protein was observed [26]. Besides, to increase the hydrophobic interactions between the inorganic surface and the protein,

peptide blocks composed of hydrophobic aminoacids, such as Ala, Ile, Trp, were inserted into a synthetic protein domain derived from *Staphylococcal* Protein A (Z domain). It was found that the protein adsorption was not detected at hydrophilic silica whereas increasing length of the hydrophobic insertion resulted in an increase at Z adsorption on methylated (hydrophobic) silica [27].

Electrostatic interactions between the inorganic surface and the protein may also enhance the protein adsorption. Generally, for the proteins undergoing limited or no interfacial conformational changes, *e.g.* lysozyme, cytochrome c, subtilisin, and RNase, there is interplay between electrostatic and hydrophobic interactions [20]. For example, the adsorption of bovine pancreas ribonuclease at a (hydrophobic) negatively charged polystyrene surface was found to be high at both above and below the protein isoelectric point, highlighting the primary adsorption driving force, here, is other type of interactions, presumably, hydrophobic interactions instead of electrostatic interactions [20, 25]. On the other hand, at a hydrophilic and charged surface (haematite), the adsorption mechanism mainly proceeds through electrostatic considerations between the surface and the protein with opposite charge [20].

Another attempt by Mamlsten *et al.* was carried out to explore the interplay between hydrophobic and electrostatic interactions by means of protein adsorption at a inorganic surface. The effects of insertion of three different type of amino acid blocks, *i.e.* (AlaTrpTrpPro)<sub>n</sub> (T)<sub>n</sub>, (AlaTrpTrpAspPro)<sub>n</sub> (N)<sub>n</sub> and (AlaTrpTrpLysPro)<sub>n</sub> (P)<sub>n</sub> on adsorption of ZZ protein at a number of surfaces were investigated [28]. Electrostatic interactions were the major factors in case of hydrophilic surfaces investigated. Regardless to type of peptide insertion, the net negatively charged resultant proteins were found not to adsorb at a hydrophilic and negatively charged silica surface. However, there was extensive adsorption at a positively charged hydrophilic diaminocyclohexane plasma polymer surface for all proteins investigated. In the case of hydrophobic and negatively charged methylated silica, both hydrophobic and electrostatic interactions were found to be of importance. Also, peptide insertions were found to have major effect on the protein interfacial behavior [28].

For the proteins undergoing large conformational changes on adsorption, *e.g.* BSA, nonelectrostatic driving forces considerably take roles. Hence, the adsorption usually

does not follow the electrostatic interactions. Moreover, the adsorption is governed also by other effects, such as van der Waals and hydrophobic interactions [20, 29].

Especially in biomedical applications, PEG derivatives are mostly used reagents in the literature to prevent the protein adsorption at a solid surface [30-33]. If the PEG chains are sufficiently long and molecule density is high enough at the surface, PEG modified surfaces display very low protein adsorption. The main reason of the efficient repulsive characteristics of the PEG layer is two-fold [30, 34]. Firstly, dense and thick layer of the PEG derivatives maintain a strong steric hinderance for the proteins [34]. Secondly, the adsorption driving forces are absent. For example, since the typical PEG-layers are uncharged, electrostatic interactions are insufficient for the protein attachment [34]. Also, PEG molecules can interact with the water molecules, preventing van der Waals interactions between the surface and the protein [30]. Under these conditions, it is really hard for a protein to attach to the PEG-modified surface unless it can penetrate through the PEG layer and reach the bare surface.

It should be noted that the protein-surface interactions are not only the parameters for the adsorption. It depends on a combination of interactions between the protein, the surface and the solvent. Once the solvent becomes a poorer for a protein in terms of solvation, the possibilities for formation of a separate macroscopic phases (phase separation), protein self-association, and adsorption at a interface all become more favorable [20].

For some of the proteins, the adsorption at a surface can be increased with worsening the solvency conditions. As an example of this, it was demonstrated that the BSA had an increased tendency for aggregative adsorption at quartz with worsening the solvency by additions of an increasing concentrations of ammonium sulfate [35]. The protein solvency can be also decreased by thermal denaturation. Since proteins undergo denaturation at elevated temperatures, changing their structural conformation, this causes the exposure of the hydrophobic domains hidden in the protein core, which tends to reduce the aqueous solubility [20]. For example, fibrinogen,  $\beta$ -lactoglobulin displayed higher surface activity with increasing temperature [36-38].

It is well known that some proteins such as BSA, human serum albumin (HSA), tend to form oligomeric structures at certain conditions. Especially, for more flexible

protein structures, association of the monomers leads a decrease in the conformational entropy per segment, yielding an increased adsorption [20]. For instance, the studies on adsorption of BSA, HSA and  $\beta$ -lactoglobulin indicate that homodimer version of these biomolecules adsorbs preferentially over the unassociated protein molecules [39-41]. Nevertheless, adsorption is generally favored by self-association, or when the adsorbing species is the aggregate [20].

On the other hand, there are some proteins, *e.g.* RNase, cytochrome c and lysozyme that undergo limited conformational changes during adsorption, approximating the behavior of rigid particles [20]. Here, the major adsorption driving force generally occurs from the electrostatic considerations [42]. In addition, as an example for investigating the effect of protein conformational stability on degree of interfacial conformational change on adsorption, T4 lysozyme and its mutants displaying different structural stability were chosen. The results indicated that the loss of  $\alpha$ -helix content in the protein structure with a decreasing stability yields larger adsorption-induced conformational changes at silica particles [43]. It was also found that a stronger protein-surface attraction causes a larger degree of conformational changes on adsorption [44].

From the point of view of biotechnology, it should be noted that adsorption can drastically affect the biological activity of the protein. For most of the protein systems, the biological activity necessitates the retained protein structure. However, adsorption-induced conformational changes can cause at least partially loss in the activity of the protein such as enzymatic activity (in the case of enzyme), molecular recognition (in the case of antibody) [20, 45, 46]. Therefore these conformational changes should be reduced or eliminated for efficient protein-surface based systems. For example, if a protein undergoes adsorption through interaction between its active site and the surface, the molecule will be no longer active, even at a retained native conformation. Moreover, the thickness, structure and density of adsorbed layer may affect the biological activity due to the insufficient accessibility of the target molecules, *e.g.*, substrate molecules for enzymes, to the adsorbed protein [17, 20].

### 1.2.2 Chemical Immobilization

Immobilization of densely packed and 2D ordered protein monolayers, that was firstly studied by Langmuir *et al.* [47, 48], can be prepared on a surface consisting of active groups that are able to form covalent bonds with the protein molecules [17, 49, 50]. Potential functional groups in proteins for covalent bonding and the functionalities for the surface are listed in Table 1.1.

**Table 1.1:** Mostly used functional groups in proteins and functionalities of the required surfaces [17].

Side Groups	Amino acids	Surfaces
-NH <sub>2</sub>	Lys, hydroxyl-Lys	carboxylic acid active ester (NHS) epoxy
-SH	Cys	aldehyde maleimide pyridyl disulfide vinyl sulfone
-COOH	Asp, Glu	amine
-OH	Ser, Thr	epoxy

Although irreversible attachment of the protein to the surface with a high coverage is feasible, the orientation of the immobilized molecule is often random, yielding a loss in biological activity. In other words, the coupling reactions between the functional groups on the surface and the residues present on the exterior of the protein are very difficult to control the final molecule orientation so that the molecule's direction on the surface varies from one protein to another [17, 45]. For example, in the case of diagnostic devices, the IgG molecules should be immobilized in a position that Fab fragments be directed towards the solution phase to display the molecular recognition activity [51]. Also, during the immobilization process, amino acids located at active site of the protein should remain intact. Unlike random immobilization, well-defined attachments can provide reproducible and site-specific (oriented) immobilization, causing minimum activity loss. Site-specific immobilization requires the functionalization of the molecules or the surface modification or both [17, 51-53]. In ideal case, protein with only one active amino acid for the chemical attachment gives the site-specific immobilization [50, 51, 53].

In general, the solid surface is treated with appropriate linkers forming self-assembled monolayers (SAM), *e.g.*  $\omega$ -substituted alkanethiols for gold and aminoalkylsilanes for glass, prior to immobilization step (Figure 1.1) [54]. Functionalized silanes are one of the first class of SAM that can be for the chemical immobilization of the proteins to both silicone and silicone dioxide surfaces [50, 54]. The surface of silica is formed from silanol ( $-\text{Si}-\text{OH}$ ) and siloxane ( $-\text{Si}-\text{O}-\text{Si}-$ ) groups. The chemical attachment of silane molecules to the silanol groups enables modification of the surface with various functional groups (Table 1.1). The resultant cross-linked siloxane on the surface can now provide the high concentration of functional groups that, in turn, will be activated for covalent binding of the proteins [50].

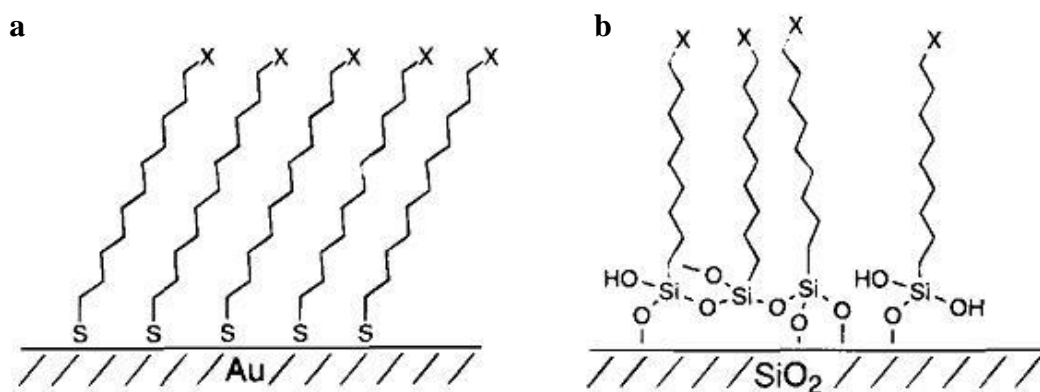


**Figure 1.1:** Models for SAMs of (a) alkanethiolates on gold and (b) alkylsiloxanes on  $\text{SiO}_2$  surface [54].

The silane monomers such as alkoxysilanes, alkyltrichlorosilanes can form a film on the  $\text{Si}/\text{SiO}_2$  surface by diffusion either from an organic solvent or gas phase, depending on the molecular weight and functional group of the silane monomers. In both cases, the resultant substrate should be heated for the polymerization of deposited silane layer [54-56]. The silanization of alkoxysilanes generally tends to form randomly ordered multilayer films of molecules chemisorbed on the surface. For example, in the case of (3-aminopropyl)triethoxysilane, the alkoxy groups of the silane molecules react with trace amount of water in the solution to form silanol groups ( $-\text{Si}-\text{OH}-$ ), leading to formation of siloxane oligomers in the solution. Here, the slowest step of the film formation is the chemisorption to the surface where  $-\text{Si}-\text{O}-\text{Si}-$  bonds are formed through the reaction between silanol groups of oligomers and the  $\text{Si}/\text{SiO}_2$  surface. The chain of chemisorbed oligomers grows by lateral interaction



with monomers from the solution. The monomers with three available alkoxy groups for the reaction might not be hydrolyzed at the same time. Therefore, the 3D condensation of oligomers chemisorbed on the surface and partially hydrolyzed silane molecules from the solution is the main reason for the formation of multilayer films [50].

Another common way for producing highly ordered and densely packed SAMs with variety of functional groups enabling the further surface functionalization is the chemisorption of  $\omega$ -substituted alkanethiols from solution (or vapor) onto the gold substrate (Figure 1.1) [54, 57-59]. The sulfur atoms coordinate to the gold atoms of the surface, yielding the trans-extended alkyl chains tilted about 30 degrees from the normal to the surface [54]. This approach can be used to prepare surfaces that host affinity ligands for the specific binding proteins or enable the covalent coupling of the protein and the alkanethiols chemisorbed on the surface, depending on the functional group (X) at the end of the thiol molecule (Figure 1.1) [17, 54, 57-59]. Comparing to the SAMs of silane molecules, the organized thiol monolayers can be formed in a short time, however, it should be noted that the SAMs of alkanethiols are less stable than siloxane polymers due to rapid oxidation [50, 60, 61]. Also, both thiol and silane based molecules are toxic reagents, addressing to environmental considerations.

The strategies for the chemical immobilization of the protein on a solid surface coated with SAMs of the appropriate molecules depend on the functionalities on both the protein and the linker molecule chemisorbed on the surface.

#### **1.2.2.1 Non-specific Immobilization**

Generally, all of the functional groups summarized in Table 1.1 can react with suitable types of modified surfaces, yielding covalent bonding towards protein immobilization.

a) Amine Chemistry: Globular proteins usually contain lysine residues on the external surface of the globule that can be used for the binding. However, their abundance may cause multipoint attachment as well as restriction on conformational flexibility. *N*-Hydroxysuccinimide (NHS) is the most commonly used agent to activate the surface derivatized with SAMs consisting of carboxylic end. Subsequently, proteins bind efficiently to the support activated as NHS ester through

formation of an amide bond between the linker and lysine residue (Figure 1.2a) [50, 62-64]. Several parameters such as pH, ionic strength, protein concentration affect the efficiency of the chemical bonding [17]. However, the coupling is completed in minutes and results in densely packed protein monolayers covalently linked to the solid support [50].

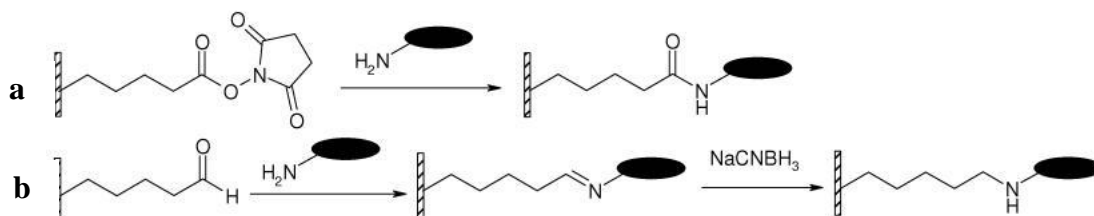


**Figure 1.2:** Schematic representation of amine chemistry on (a) NHS-Derivatized and (b) Aldehyde-Derivatized Surfaces [17].

Apart from the carboxyl group, an aldehyde group on the linker molecule reacts with amino group of the lysine residue, leading to the formation of a labile Schiff's base that can be stabilized by reduction creating a stable secondary amine linkage (Figure 1.2b) [65, 66]. Aldehyde-amino chemistry has been widely utilized for years for protein immobilization on different surfaces [67-69]. Aldehyde derivatization has been also used to prepare patterned collagen-type protein col3a1 surfaces to study cell adhesion [70].

b) Thiol Chemistry: Proteins that have exposed cysteine residues can be covalently immobilized onto the surfaces with appropriate functionalities, *e.g.* sulfhydryl- or maleimide-derivatized SAMs [71-73]. Figure 1.3 shows possible approaches on thiol chemistry for protein attachment.

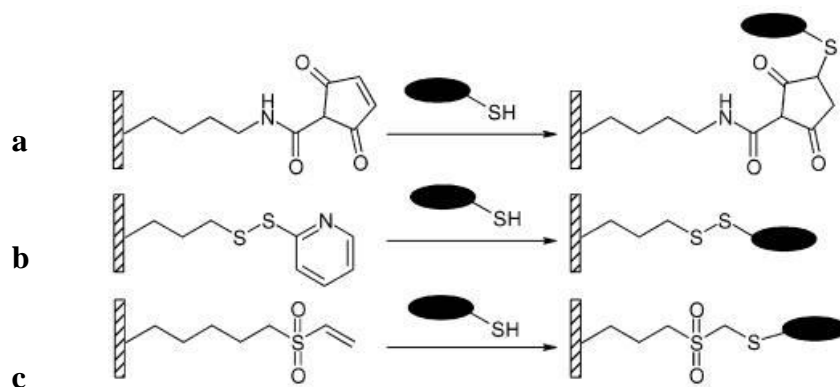


**Figure 1.3:** Schematic representation of thiol chemistry on (a) Maleimide-Derivatized, (b) Disulfide-Derivatized, and (c) Vinyl Sulfone-Derivatized Surfaces [17].

The double bond of maleimide readily reacts with all hydroxy, amine or thiol groups found on the matrix to form a stable carbon-carbon, carbon-nitrogen or carbon-sulfur bond. Therefore, the maleimide based molecules such as homobifunctional (bis (maleimido)hexane) (BMH) and heterobifunctional (N-( $\epsilon$ -maleimidocaproyl) succinimide (EMCS) and 3-maleimidopropionic acid *N*-hydroxysuccinimide ester (MPANHS), are used to form the covalent bond between the surface containing amine or hydroxyl groups and the cysteine residue of the protein (Figure 1.3a) [71, 74-76]. As an example, maleimide based linker molecule reacts with the amino group from the surface, yielding an amide bond between linker molecule and amino-functionalized surface. Then, following the removal of the hydrolyzed NHS from the surface, the protein with available cysteine residue can be chemically linked to the surface through the reaction of the terminal maleimide group of the linker with sulfhydryl group of the residue (Figure 1.3a) [75]. Here, the advantages of maleimide chemistry over the attachment *via* disulphide bond, represented in Figure 3.1b, are that the reaction is faster and the  $-NH_2$  surface is chemically more stable than the one with  $-SH$  group [50]. Furthermore, since the maleimide groups react selectively with Cys residues of the protein, this approach allows one to immobilize the proteins directly from the solution [50].

Disulphide exchange reactions can be used for formation of disulphide bridging between Cys residues of the protein and the surface coated with disulphide reagents such as Pyridyl disulfides (Figure 3.1b) [17, 77, 78]. The major disadvantage of this approach is that reversibility of the linkage by exposure to reducing agents may cause a problem in terms of stable protein immobilization [17]. Also, the immobilization generally takes place in aqueous/organic mixture since the disulphide reagents are quite insoluble in water based environment [17]. In Figure 3.1c, Cys residue reacts with Vinyl sulfone, yielding addition of the protein to the sulfone reagent bound to the surface [17]. This reaction is known to be Cys-selective and favorable under mild and physiological conditions [79]. The pH is the key parameter since reaction of the sulfone with thiol groups is effective within a range of 7-9.5, whereas a slower reaction with amine groups takes place generally above pH 9. Beside thiol selectivity, water stability is also another advantage of this approach [17].

c) Carboxyl Chemistry: Glutamic acid (Glu) and Aspartic acid (Asp) on surface of the protein can be used to attach the molecule on the aminated surfaces. If the carboxyl group of these residues is activated with a reagent such as carbodiimide (CDI), covalently coupling of the protein to the amino groups attached on the surface occurs (Figure 1.4) [17, 80, 81]. The major advantage of the carboxyl chemistry is that the activation of the protein takes place in mild conditions. Also, the required concentration of the CDI is low ( $\sim 1\text{mM}$ ), preventing the activity loss in terms of enzyme immobilization [82].

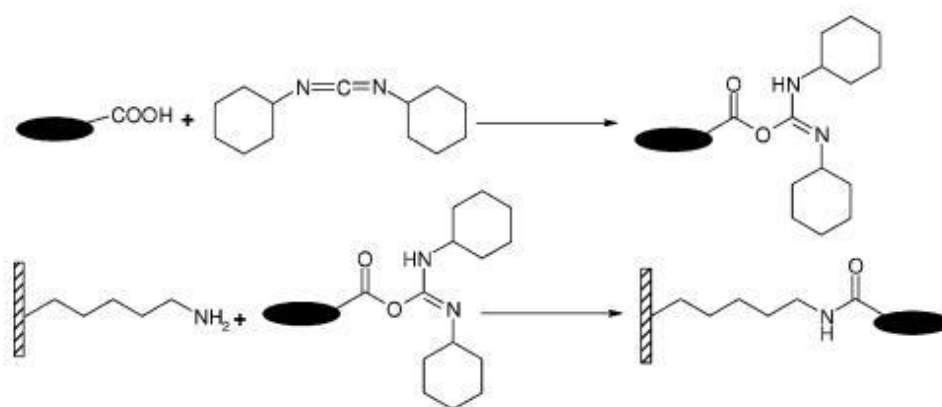


**Figure 1.4:** Schematics of carboxyl chemistry through carbodiimide [17].

#### 1.2.2.2 Site-Specific Immobilization

Efficient immobilization requires that proteins should be oriented on the surface in such a way that their active sites are exposed to the aqueous environment. However, in most cases, immobilization causes partial or total of biological activity due to the random orientation of the protein on the surface [45, 46, 83-85]. The main reason for random orientation is the uncontrolled attachment through multi amino acids in the protein sequence. Random and oriented immobilization is schematized in Figure 1.5 [85]. There have been several efforts on developing techniques to orient proteins on surfaces through single point attachment, leading the active site accessible for the further applications. Mostly used ones are as follows;

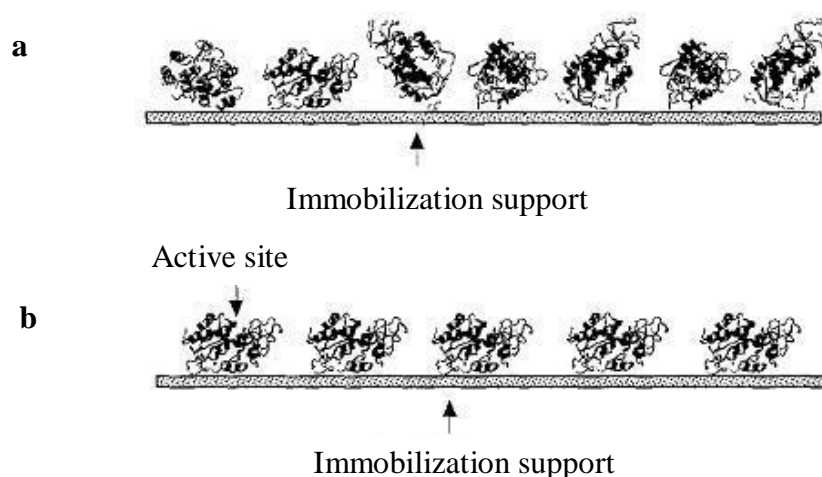


**Figure 1.5:** (a) Random immobilization of proteins, (b) oriented immobilization of proteins [85].

a) “Click” Chemistry: 1,3 Dipolar cycloaddition of an azide and alkyne to form 1,2,3- triazole has been called “click” chemistry due to simple procedure and purification steps, yielding new products (Figure 1.6) [86-89]. So, it is very feasible to introduce alkyne and azide into macromolecules such as carbohydrates and proteins, without any effect to their stability [17]. The reactants are also stable and do not react with common organic reagents or functional groups in biomolecules [87]. The formation of triazole is irreversible and usually quantitative [17, 87]. In addition, the reaction requires an extremely mild and regioselective copper(I) catalyst system [87].

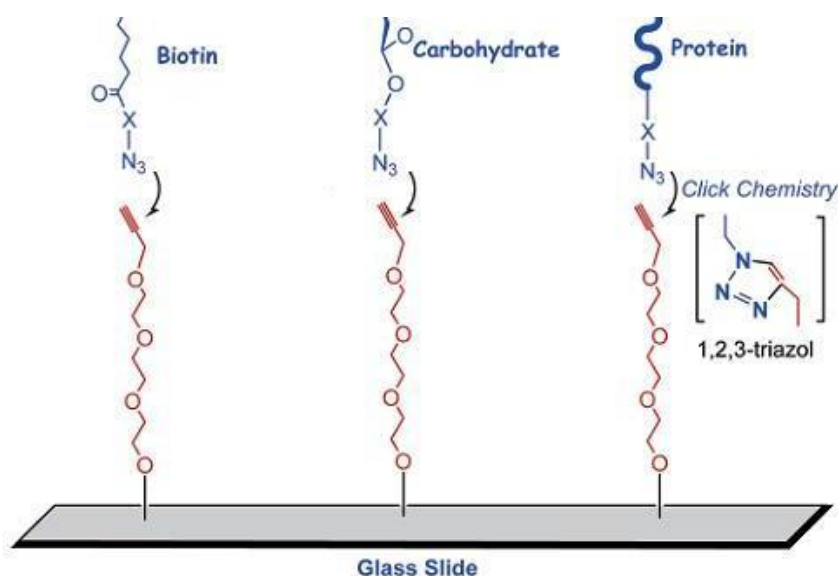


**Figure 1.6:** Schematically representation of the site-specific biomolecule immobilization via “click” chemistry [87].

“Click” chemistry can be a useful approach to prepare uniform, high-density surface immobilization of biomolecules in an oriented fashion since the unique properties of this reaction can be transferable to surface-bound reactants and will likely provide access to a growing variety of novel functionalized surfaces [17, 89]. As an example, in situ preparation of SAM of azide-terminated molecules bound to the surface was carried out through a Diels-Alder reaction between cycloaddition terminus of a bifunctional PEG linker carrying an alkyne group at the opposite end and *N*-( $\epsilon$ -Maleimidocaproyl) EMC-derivatized glass slide [87]. Subsequently, various types of biomolecules such as lactose, biotin, recombinant thrombomodulin, were stably immobilized using “click” chemistry without any occurrence of side products (Figure 1.6).

b) Peptide Ligation: Unprotected peptides and proteins can be chemically coupled to each other using peptide ligation via a variable chemoselective capture step followed by an intramolecular acyl transfer reaction [17, 90, 91]. This chemoselective capture necessitates a nucleophile or electrophile proximally located at the N-terminus of the molecule and another compatible electrophile or nucleophile that is also proximally placed at the C-terminus. The chemoselective interaction between the nucleophile and electrophile pair forces the C- and N-termini into such a close proximity to allow an intramolecular acyl transfer reaction forming an amide bond [17, 91]. An ester or a thioester is required for C-terminus whereas N-Terminal cysteine, histidine, serine and threonine, having weak-base nucleophiles such as thiol, amine, or hydroxyl groups spatially separated by two atoms from  $\alpha$ -amine, have been shown to be the most appropriate. Here, the chemoselective capture of the N-terminal cysteine and ester glycoaldehyde leads to the formation of a thiazolidine ring, followed by formation of a proline mimic via acy migration (Figure 1.7) [17].

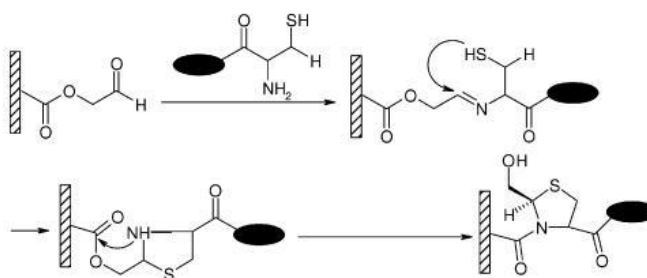


**Figure 1.7:** Schematically representation of Thiazolidine ring formation through peptide ligation between N-terminal cysteine and ester glycoaldehyde [17].

c) Staudinger Ligation: Staudinger ligation is a general method for the covalent uniform immobilization of peptides and protein, requiring an azide group and a functionalized phosphine-containing (thio)ester [53, 83, 92]. The reaction of the azide group to the phosphino(thio)ester is both rapid and high-yielding, forming an amide via iminophosphorane intermediate (Figure 1.8) [17, 83]. Also, the reaction is favorable at room temperature in aqueous or wet organic solvents and compatible with the unprotected functional groups of proteinogenic amino acids [83].

The first application of Staudinger ligation for protein immobilization was demonstrated by Soellner *et al.* In this work, glass slides were treated with chemical reagents to form phosphinothioester bound to the surface. Azido-modified ribonuclease S' was then spotted onto the surface, leading to site-specific immobilization of the protein [83].

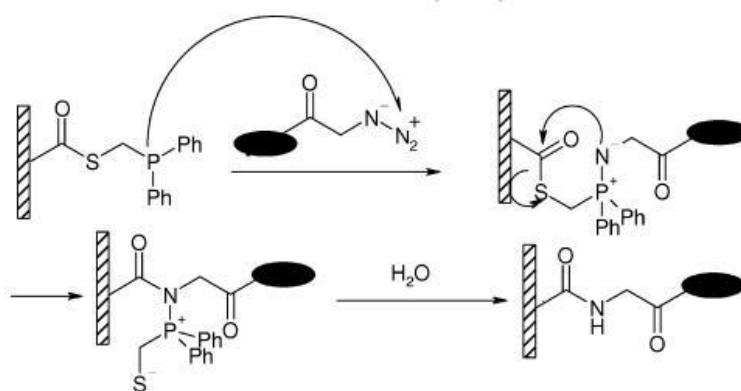


**Figure 1.8:** Reaction mechanism of Staudinger Ligation [17].

In chemical immobilization strategies requiring the activation of SAM bound to the surface, it should be noted that the reaction between the activated group and the protein must be carried out very rapidly under mild conditions that result in a stable covalent bond, to prevent denaturation of the protein and contamination of the surface [50].

### 1.2.3 Bioaffinity Immobilization

Bioaffinity reactions provide gentle immobilization technique that maintains the homogeneous attachment as well as the ability to detach the protein, regenerating the surface for the next use [17, 50, 85, 93-95]. Especially, using of these types of attractions was firstly started for the purification of recombinant proteins. Affinity tags that can be specific antibody epitopes, posttranslational modification sites, a

single amino acid residue, or a peptide sequence provide a handle on the expressed recombinant protein that permits for immobilization from a specific site on the biomolecule to the solid support coated with appropriate entity that the tag is specific to [85, 93, 96]. Mostly, this can be achieved by ligating DNA sequences of the affinity tag peptide/protein to either 5' or 3' end of the gene. Moreover, in some cases, the fusion protein can be designed to have a cleavage site in between the protein and the tag, giving an opportunity to remove the affinity segment by enzymatic or chemical reaction following the purification step [85, 93, 96].

### **1.2.3.1 Biotin-avidin system**

One of the most powerful approach to design a surface for protein immobilization involves the modification of the surface such as gold, silica, with biotinylated linkers [6, 50, 97, 98]. Biotin is low molecular weight ligand (MW: 244 g/mol) that can strongly and specifically bind to the protein avidin (from the egg white) or the bacterial protein streptavidin with an extremely high binding constant ( $K_d: 10^{15} \text{ M}^{-1}$ ) [17, 98, 99].

Avidin, tetrameric glycoprotein soluble in aqueous, is also stable over wide pH and temperature ranges. It has capacity for binding up to four biotin molecules through very fast bond formation that is also unaffected by pH, temperature, organic solvents, enzymatic proteolysis and other denaturing agents [17]. Although streptavidin has different amino acid composition, molecular weight and pI, it is a closely related tetrameric protein with similar affinity to biotin. Furthermore, using chemical and genetic engineering, the properties of these proteins could be improved, resulting enhanced stability and/or controlled biotin binding [17].

Due to its small size, biotin can be attached to the macromolecules such as proteins, peptides and the resultant conjugate retains the both activities. The biotinylation of the molecules also requires specific reagents for the activation of the functional groups involved in the conjugation reaction [6, 17, 50, 85]. For example, the NHS ester of biotin and biotin hydrazide are the mostly used chemical reagents, specifically targeting the amine groups and carboxyl or carbohydrates, respectively [100, 101].

The attachment of the biotin to a solid substrate also requires the surface activation. As an example, in the case of NHS derivative of biotin, the surface should be



aminated with an appropriate reagent such as, 4-aminophenylmercuric acetate for silanized glass [100]. Following the activation, the free amino groups can react with NHS biotin, leading the biotinylation of the surface. Binding of avidin to biotinylated-SAMs provides a protein layer that is shielding the metal surface. Immobilized avidin, consisting of four identical subunits, has at least two binding sites available for the biotinylated molecules in surrounding media [50]. However, the binding of avidin to the closed-packed biotinylated-SAMs turned out to be with low affinity whereas; loosely packed biotinylated layers show significantly higher binding affinity to the avidin [102]. For this reason, the density of the biotin on the surface should be controlled using mixed SAMs composed of two types of thiol/silane molecules, *i.e.* one biotinylated and one not [17].

### 1.2.3.2 His-tag system

Polypeptide tags can be used for the site specific immobilization of the proteins. Tags are located at defined positions, preferably, sufficiently far away from the active site of the protein to maintain a higher bioactivity [17]. Due to its small size, compatibility with the organic solvents, low immunogenicity, and effective purification under native and denaturing conditions, Poly(His) is one of the most common tags. Since The sequence of histidines can form complexes with metal ions such as  $\text{Zn}^{+2}$ ,  $\text{Cu}^{+2}$ ,  $\text{Ni}^{+2}$  and  $\text{Co}^{+2}$ , the fusion of His tag to the proteins facilitates the metal affinity chromatography (IMAC) and leads to site-specific immobilization [85, 103-106]. For example, the interaction between His-tagged protein and nickel-chelated complex, such as Ni-nitriloacetic acid (NTA), involves the octahedral coordination of the nickel ion with two valences occupied by two imidazole groups from the His-tag and four ligands given by the NTA molecule (Figure 1.9) [93]. Here, NTA is covalently attached to the surface of purification column and then loaded with the divalent metal cation,  $\text{Ni}^{+2}$ . This interaction is still stable even in the presence of 8 M urea, 10 mM  $\beta$ -mercaptoethanol or detergents, enabling purification of the proteins that form inclusion bodies [85, 107].

To explore the effect of the length of the histidine tag on the immobilization efficiency, a poly(His) containing two to six histidine residues fused to the enzyme dihydrofolate reductase (DHFR) was expressed and their binding to the IMAC support was studied [105]. It was found that the fusion protein with a  $(\text{His})_2$  tag did

not bind to the support in the presence of 6 M guanidine HCl whereas, (His)<sub>6</sub> tag provided 90% of the attachment of the enzyme to the same support. Also, same study showed that histidine tags consisting of more than six residues was problematic in terms of expression of the fusion protein, leading to low fusion protein recovery.

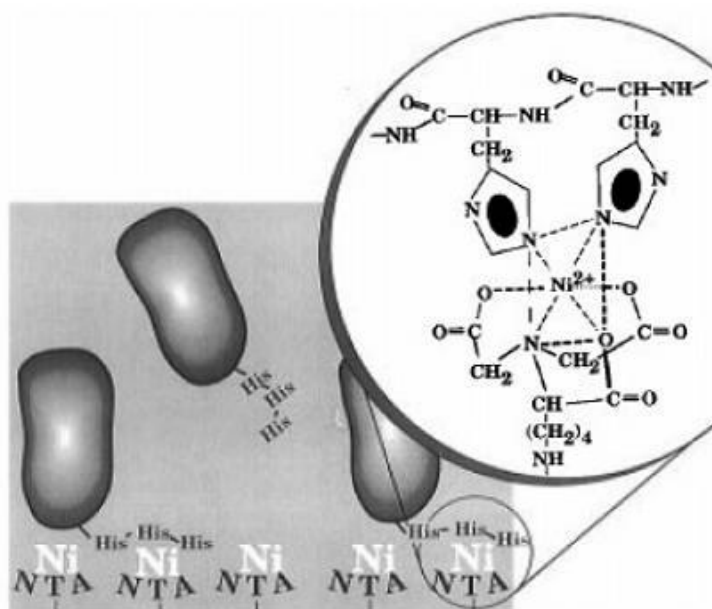


**Figure 1.9:** Binding mechanism of the His-tagged protein to a Ni-NTA surface [93].

Oriented immobilization of recombinant proteins fused to insert peptide sequence consisting of Ala-His-Gly-His-Arg-Pro has also been shown [108]. The results showed that the fusion proteins had affinity to IMAC support loaded individually with  $\text{Zn}^{+2}$ ,  $\text{Cu}^{+2}$ ,  $\text{Ni}^{+2}$  and  $\text{Co}^{+2}$ . Here, Arginine improved the water solubility whereas; Proline was used to increase the resistance to proteolysis. Also, site-specific immobilization of His-tagged lactate dehydrogenase {(His)<sub>4</sub>LDH},  $\beta$ -glucuronidase {(His)<sub>4</sub> $\beta$ -glu}, galactose dehydrogenase {(His)<sub>5</sub>galDH}, and the complex between (His)<sub>5</sub>protein A and horseradish peroxidase-labeled immunoglobulins were reported by Carlsson *et al.* [109]. In this study, the behavior of the enzymes (dimeric or tetrameric) was investigated. It was shown that the relative activities of the tetrameric enzymes LDH and  $\beta$ -glu were higher comparing to the dimeric enzyme galDH. The immobilized tetrameric enzymes preserved the activities similar to the corresponding soluble enzymes. Furthermore, it was highlighted that the enzymes had higher activity when zinc ion was used as a metal ligand. However, in the case of copper,

longer stability was achieved. The difference in stability was addressed to copper ion having non-specific interactions with the protein [109].

The SAMs modified with NTA molecule have been used to immobilize proteins on glass slides and gold surfaces [93, 110-112]. For example, in one of these studies, A T-cell receptor (scTCR) construct was used as a model protein to test the immobilization capacity and the activity retention using SAM of alkanethiols terminated with NTA on gold coated SPR slide [111]. The binding of histidine to the Ni-NTA complex is rapid, and reversible upon addition of a competitive ligand, such as histidine or imidazole, however His-tag system has few drawbacks, such as non-specific binding of His-tag to the metals such as gold, [113-115], metal dependent non-specific protein adsorption to the NTA support, and low affinity of the His-tag to the  $\text{Ni}^{+2}$ -NTA complex ( $K_d = 10 \mu\text{M}$ ) [17].

#### **1.2.3.3 DNA-directed immobilization**

In recent years, several attempts have been made to immobilize proteins using DNA hybridization since DNA pairing is stable and robust. The problems in protein microarrays resulted from random attachment can be solved using oligonucleotide-directed immobilization due to the high stability of DNA oligomers and site-selectivity of nucleotide base pairing [97, 116, 117]. Moreover, nature supplies a comprehensive toolbox containing specific ligases, nucleases and other DNA-modifying enzymes, which can be used for manipulating the DNA with atomic precision to build molecular constructions [117-119].

Conjugation of protein and DNA molecules can enable the preparation of the arrays in which biomolecules are located in an oriented way on the substrates although the incorporation of oligonucleotides into large proteins is still poorly developed [17]. To be able to achieve DNA-directed immobilization (DDI), protein of the interest is required to be coupled with ssDNA oligomers, providing a specific recognition site for the complementary pair that is covalently attached to the surface [17, 116, 117]. DNA-protein conjugates can be obtained from different strategies, *i.e.*, direct covalent attachment, bifunctional linkers, interaction via a streptavidin bridge, and expressed protein ligation [120, 121].

Enzymes are excellent candidates for DNA-directed immobilization. As an example, oligonucleotide–enzyme conjugates obtained from 5'-thiolated oligonucleotides and

calf intestine alkaline phosphatase (AP), horseradish peroxidase or  $\beta$ -galactosidase were immobilized through target DNA attached to the nitrocellulose, probing the nucleic acids [122]. The DNA-AP conjugate enabled the detection of attomol amounts of target DNA. Similarly, conjugates of AP and streptavidin, labeled with short 10mer biotinylated oligonucleotides, were used as probes in nucleic-acid hybridization detection [122]. A fungal lipase conjugated with an oligonucleotide conjugate was prepared to generate a thermostable probe for hybridization assays and biosensors [123]. Besides, DNA-directed immobilization has been also used for antibody attachment. With antibody-DNA conjugates, magnetic beads were functionalized and utilized for the cell sorting [124] and also, micro-biochips were prepared [125, 126].

Preparation of biosensors and mixed arrays containing both nucleic acids and proteins for various applications is doable with DNA-directed immobilization due to the reversibility and site-selectivity of Watson-Crick base pairing [117, 127]. Recent developments in this immobilization technique allowed the researchers to use synthetic DNA analogs (pyranosyl-RNA oligomers) as recognition elements for the addressable immobilization of antibodies and peptides [117]. Signal enhancement in both QCM and SPR based sensors was achieved using DDI of DNA-functionalized gold nanoparticles to detect DNA hybridization [128, 129]. DNA-coated gold nanoparticles were also functionalized with DNA-antibody conjugates to use as reagents in sandwich immunoassays [130]. The DDI approach has been also combined with dip-pen nanolithography to write thiolated compounds with less than 30-nm line-width resolution on gold substrates [131].

Sensor platforms can be prepared using more than one bioaffinity interactions. Figure 1.10 schematically represents preparation of the SPR surface using both DDI and streptavidin-biotin coupling [97]. After streptavidin is immobilized on a mixed biotinylated/OEG SAM, biotinylated ssDNA is attached to streptavidin. Antibodies conjugated to the complementary ssDNA (red) are then immobilized on the sensor surface via hybridization whereas those conjugated to non-complementary ssDNA (blue) do not bind [97].

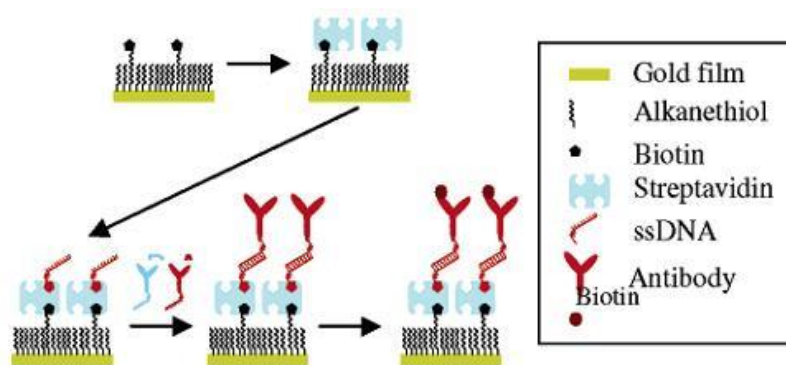


**Figure 1.10:** Schematic representation of the construction of a SPR sensor via DDI and streptavidin bridging [97].

Apart from the bioaffinity interactions mentioned here so far, protein immobilization can be carried out by designing a protein expression system that protein of the interest is genetically fused to some other peptides or proteins, *e.g.* glutathione S-transferase (GST), maltose binding protein (MBP) and FLAG-peptide, providing the binding affinity to certain chemical substances [132-138]. For example, GST-tagged proteins have affinity to glutathione whereas MBP-tagged proteins can bind to maltose molecule. Not only does this strategy work for the immobilization of proteins but also it can be used for the protein purification [85, 137, 138]. Furthermore, due to their specific interaction with the  $F_c$  constant region of IgG molecules, protein A and protein G can be also utilized for immobilization of the antibodies, making the Fab variable region accessible for the antigen binding [94, 139]. However, the major disadvantages of this method are that the control on the orientation of Protein A is difficult and only certain classes of antibodies are able to bind to it [17].

Although recent advances in biotechnology have improved the protein immobilization, the lack of optimal ways to do it has been still remaining as the major challenge. Many methods have been attempted to achieve a full coverage of surface with the highest retained protein activity for the best detection. SAM thiol- and silane-based molecules have been extensively studied due to their higher coverage on the corresponding surface as well as their capacity for the chemical modification upon various applications. Bioaffinity interactions such as biotin-streptavidin and DNA base pairing also made an impact on site-specific immobilization of proteins.

However, to be able build new devices with higher performance such as biochips and sensors, new strategies allowing site-specific and stable immobilization of proteins are urgently needed [17].

### **1.3 Protein/Peptide Patterning for Micro/Nanoarrays**

Arrays have become an increasingly diverse set of tools for biological studies as their use expands rapidly [116, 140, 141]. Likewise, development of the array technologies, formats and protocols has been in progress [116]. Basically, arrays contain collections of different capture molecules attached to a substrate (usually a glass slide) at predefined locations within a certain pattern [116, 142, 143]. The types of capture biomolecules used in arrays include DNA [144], proteins [145], carbohydrates [146], drug-like molecules [147], cells [148], tissues [149] and so on. For example, a protein microarray provides a multiplex approach to investigate protein-protein interactions, to investigate the substrates for protein kinases, to identify transcription factor protein-activation, or to identify the targets of biologically active small molecules [116, 140]. Among the protein arrays, the most common array type is antibody microarray, where antibodies are immobilized onto the solid substrate and used as capture molecules (probe) to detect proteins in the solution exposed to the array [150].

Array technology is the most promising approach that allows the large-scale analyses of genome/protein functions (comprehensive proteome) and/or analyses focusing on the limited functions (focused proteome) simultaneously and rapidly [140]. DNA micro-array technology is one of the powerful analytical methods to address those issues, analyzing mRNA transcript levels expressed under various conditions [140]. But, it is also known that mRNA expression level and the corresponding protein abundances (or activities) do not always correlate due to the changes in translation rates and protein lifetimes [140, 151, 152]. Moreover, post-translational modifications, such as proteolysis, phosphorylation, glycosylation, or acetylation, are not considered in the analysis of mRNA transcripts, although many signaling pathways mediate such structural alterations [140]. Hence, in order to overcome these difficulties, protein array technology has emerged to make large-scale analysis of proteins in miniaturized fashion [116, 140, 150].

The attachment of the proteins to the solids has already mentioned in section 1.2. In this section, the most common patterning techniques for the fabrication of protein arrays will be discussed.

### **1.3.1 Microcontact printing**

Microcontact printing ( $\mu$ CP) is one of the soft lithography techniques, developed by George Whitesides and consisting of a non-photolithographic strategy based on self-assembly and replica molding for carrying out micro- and nanofabrication [153]. Soft lithography is called “soft” because an elastomeric stamp or mold is the part that transfers the molecules (ink) to the substrate through conformal contact of the patterned surface and this approach uses flexible organic molecules and materials instead of the rigid inorganic materials commonly utilized during the fabrication of microelectronic systems [153]. Using soft lithography, patterns and structures with feature sizes ranging from 30 nm to 100  $\mu$ m can be fabricated by an elastomeric stamp with patterned relief structures on its surface [153]. For example, this approach has been successfully used to prepare scaffolds for cell growth [154], nanotube formation [155], nanowire organization [156], microfluidic systems [157], and biosensing [158]. Specifically,  $\mu$ CP also provides a robust, effective and low-cost method for fabrication of protein patterns [159-164].

Microcontact printing was introduced in 1993 as a novel method for patterning SAMs of alkanethiols onto gold substrates [165, 166]. In this work, an elastomer, polydimethylsiloxane (PDMS), was used to form a patterned stamp, which transfers the thiols (ink) to gold surface. The printed SAMs of thiols can serve as template for attachment of biomolecules such as proteins, using the immobilization approaches mentioned in Section 1.2. As proteins adsorb preferentially to some surfaces but are repelled from others, tailoring the surface properties of gold by patterning SAMs provides the efficient capability of depositing proteins from solution into patterned region [160, 167, 168]. Generally, micropatterned area consisting of alkanethiols acts as hydrophobic sites where proteins will deposit from the solution following the untouched area is passivated with thiolated PEGs [31].

Direct printing of proteins onto solid substrate is also possible. PDMS provides a hydrophobic surface similar to polystyrene used for adsorption of proteins for immunoassays. Also, flexible PDMS stamps ensure conformal contact with various

solid substrates. Since, almost any pattern can be fabricated on PDMS stamp, conformal contact of the stamp inked with the protein can be achieved in many different geometrically controlled ways, transferring the protein from stamp to the surface of the substrate [160]. Figure 1.11 represents the steps for the fabrication of PDMS stamp and subsequently, its use to print proteins on surfaces *via* non-specific interactions between protein and the solid surface [160]. Firstly, viscous liquid PDMS prepolymer is mixed with curing agent and the mixture is poured onto a microfabricated silicon mold to form the surface relief of the stamp (Figure 1.10a). Generally curing step is occurred by overnight incubation at 70 °C. The stamp is peeled off the mold and can be now used for protein printing. Basically, PDMS stamp is incubated with the ink, *i.e.* protein solution to cover its micro features with monolayer of protein, which after rinsing and drying, can be transferred to the surface of the solid substrate by conformal contact.

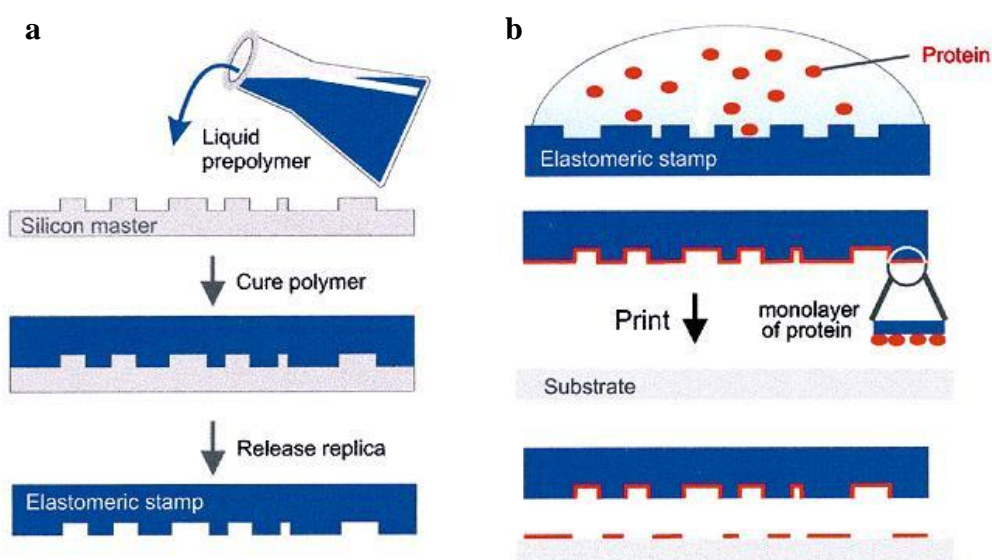


**Figure 1.11:** Scheme of (a) fabrication of PDMS stamp and (b) its use for  $\mu$ CP of proteins [160].

For an efficient protein transfer from the stamp to the solid substrate, an important requirement is that time between drying of the stamp (after its inking) and printing of the protein should be very short. For example, the efficiency of the protein transfer decreases substantially, leading to incomplete patterning if the stamp is kept in a dry state (at 55% ambient humidity) for  $\sim 1$  min [160]. Moreover, the transfer of the proteins is a fast process and can be achieved with contact duration of few seconds [159-161]. It was also demonstrated that the patterns obtained by  $\mu$ CP of proteins



have high contrast due to the mechanical stability of the pattern of the stamp and because printed proteins are not diffused [160].

In microarray technology, biological activity of the proteins should be retained even after a patterning process. An important characteristic of  $\mu$ CP is that many proteins preserve their biological function after printing [169]. Also, combination of  $\mu$ CP with standard biomedical procedures such as fluorescence labeling and enzyme-linked immunosorbent assaying (ELISA) is possible [169, 170]. The activity of stamped Rhodamine-labeled antibodies or stamped alkaline phosphatase could be still detected by fluorescence microscopy [160]. Furthermore,  $\mu$ CP of biological material was applied to fabricate patterns of proteins, lipids, [171] and polyaminoacids [172], for cell attachment [173, 174], for biosensing [175], for AFM studies [176], and for binding assays [169, 174].

Microcontact printing seems to be a robust method for protein patterning. Interestingly,  $\mu$ CP can transfer proteins onto a variety of substrate materials with hydrophilic or hydrophobic surfaces. Bare and silanized glass, gold, silicon and silicon oxide, polystyrene, PMMA (polymethylmethacrylate) are already tested [160, 169]. Here, it should be noted that the attachment is based on non-specific interactions between the surface and the bound molecules. Hence, certain proteins may not survive on the solid surface through adsorption force [169]. So, an appropriate linker can be patterned on the surface, yielding a handle for the protein to attach the solid.

### **1.3.2 Dip-pen lithography**

Dip-Pen technology, wherein ink adsorbed on a sharp object is delivered to a paper substrate via capillary forces, is approximately 4000 years old and has been used extensively throughout history to transport molecules on macroscale dimensions [4]. Similarly, Dip-Pen Lithography (DPN), a type of scanning probe lithography, employs the tip of an AFM to fabricate micro- and nanoscaled structures by material deposition onto a substrate [4]. The AFM tip transports the molecules (ink) to the substrate surface using a solvent meniscus that forms in ambient atmospheres. Structures with features ranging from several hundreds of nanometers to sub-50 nm can be fabricated using this technique [4]. For the first demonstration, the AFM tip was used to write 1-octadecanethiol molecules with 30 nm line-width resolution on

gold surface. Here, a water meniscus forms between the AFM tip coated with thiol molecule and the gold film. The transport rate for the thiol molecule and DPN resolution are dependent on the size of the meniscus, which is controlled by humidity (Figure 1.12) [4].

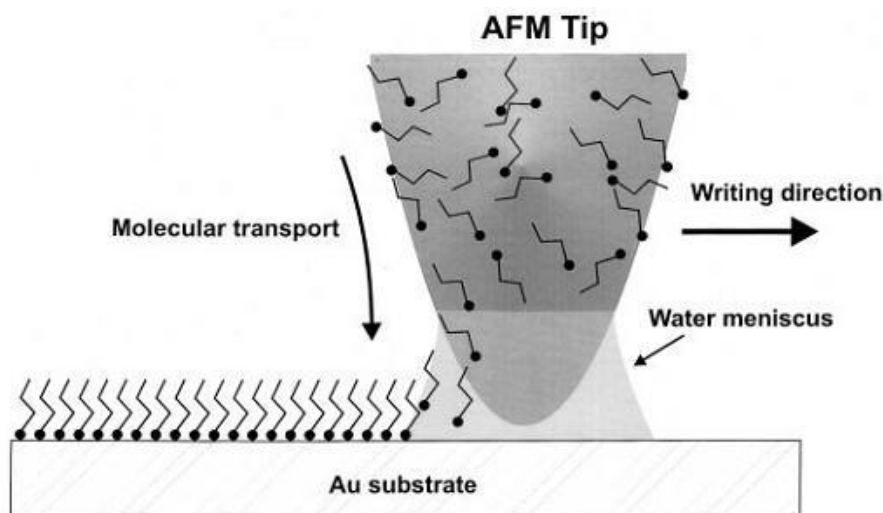


**Figure 1.12:** Schematic representation of DPN. The AFM tip, thiol molecule, and gold film are utilized as “nib”, “ink”, and “paper”, respectively [4].

Several different parameters also affect the formation, structure, and stability of the deposited material (ink). The formation and stability of the structure are dependent on the strength of the interaction between the substrate and the ink as well as the amount of adhesion between the ink being deposited and the AFM tip [177, 178]. Surface charge is one reason of this interaction; the static interaction between charged surface of the substrate and oppositely charged molecule (ink) will lead to the material deposition onto the substrate [177, 179]. Moreover, if the interaction between the ink and the AFM tip is too strong, it may cause poor material deposition; or if it is too weak, the ink will not stay on the tip long enough to be transferred onto surface of the substrate, also, there may not be enough amount of molecules on the tip to produce the structure [180]. The cohesion between the ink already deposited and the ink on tip affects the ink transfer from the ink to the surface [177, 180]. Another parameter that influences the DPN is temperature. Especially, if the ink is biomolecule such as DNA, protein, temperature affects the solubility and diffusion rate of the molecules, which influences the size of the nanopatterns [177]. Another factor in stability is to choose an appropriate solvent. The shape of the deposit can be influenced by the amount of solvent in the material. Evaporation of the solvent from

the material makes the deposits harden [180]. Additionally, the dimensions of pattern can be adjusted by the speed of tip. As the tip movement gets faster, the size of the pattern will be smaller [179].

In comparison with DPN,  $\mu$ CP allow one to fabricate the entire patterns onto substrate by stamping the ink molecules directly in one step [153, 165], which is an advantage over a serial patterning technique such as DPN [4]. However, DPN provides an opportunity that one can selectively deposit different types of materials at specific sites within certain type of nanostructures so that DPN can serve as a complementary patterning technique with  $\mu$ CP for micro- and nanofabrication [153, 165]. Also, DPN needs relatively small amount of molecular substance to deliver to a substrate in nanolithographic fashion that doesn't necessitate any resist, stamp, complicated processing methods whereas, there are different types of printing techniques that rely on scanning probe instruments, electron beams to make the patterns, utilizing additional organic molecules as resist layers [181-183].

The strong properties of DPN have provoked the researchers to utilize the technique for biomolecule patterning. DNA and protein were used as ink and were successfully patterned within nanoscopic dimensions ( $<200$  nm) by DPN [178, 184, 185]. Protein/peptide nanopatterns have been prepared by either indirect method necessitating resists [186] or prefabricated chemical affinity templates that serve as linker for protein attachment [185] or direct method relied on direct deposition of protein in which chemical modification of the AFM was carried out [178]. In the latter case, the AFM tip was coated with gold and incubated in thiol solution prior to inking. The hydrophilic tip with the carboxylic acid-terminated SAMs of the thiol molecule facilitated protein adsorption throughout its incubation in protein solution. During the patterning of the protein, the interaction between the cysteine residues of the proteins and the gold surface provides a strong driving force for protein deposition [178]. Based on this approach, they could produce nanopatterns ( $\sim 45$  nm) of two different proteins, *i.e.* IgG and lysozyme, that are still biologically active after the patterning process. Moreover, DPN-fabricated nanoarrays of anti-p24 antibody were demonstrated to screen for the human immunodeficiency HIV-1 virus (HIV-1) p24 antigen in serum samples [187]. In contrast to previous study, here, the antibody nanoarrays were fabricated using DPN-patterned 16-mercaptohexadecanoic acid (MHA) nanodots as templates for antibody immobilization. The detection of p24 was

evaluated using AFM; the anti-p24 features increased in height by  $2.3 \pm 0.6$  nm. This height increase could be further enhanced by sandwiching the captured p24 protein with anti-p24-functionalized gold nanoparticles. As an important result, this work demonstrates that DPN fabricated nanoarray-based assays can go beyond the detection limit of conventional enzyme-linked immunosorbent assays by orders of magnitude [187]. Apart from proteins [178, 185, 187-189], peptides [190-192], and DNA [184, 193] viruses [187, 194-196] and bacteria [197] have been patterned using DPN through either indirect or direct adsorption methods.

DPN is very straightforward and powerful method for patterning of molecules onto substrate at resolutions comparable to those achieved with much more expensive lithographic methods, such as electron-beam lithography [4, 198]. The reports cited here clearly show that the DPN-fabricated nanoarrays of biological molecules are valuable tools for different areas such as proteomics, genomics, and medicine. Also, DPN provides an ability to fabricate smaller, densely packed and multi-component arrays of proteins that preserve the biological activity [178]. In addition, fabricating the arrays with these properties can enable new screening technologies and start to study important fundamental issues regarding biomolecular recognition that are not addressable with microarrays [178, 198].

### 1.3.3 Photolithography

Photolithography, began in the late 1950s, is a patterning technique used to transfer shapes and designs onto a surface coated with photoresist materials [177]. Over the years, this technique has been reached to a point where it is now one of the most successful technologies used in the field of microfabrication to produce semiconductors for computers and arrays for biosensing [153, 177, 199]. In protein array technology, patterning is basically done using chemical linkers with different active groups (see section 1.2.2 and section 1.2.3) to create a heterogeneous monolayer [19]. For example, silane coupling agents have been used as linker for attaching proteins to silica since they can survive the organic solvent systems needed for removal of the photoresist [19, 200-202].

Basic procedure for patterning of silane molecules using photoresist is described in Figure 1.13 [19]. The substrate, *i.e.* silica, is spin-coated with polymeric photoresist and then covered with a photomask (step 1-2) followed by UV exposure (step 3). The

regions of photoresist layer that are not blocked by the mask become decomposed by UV irradiation resulting in being washed away with the solvent rinse. These regions are now bare and available for the attachment of amino-terminated silane molecules (step 4). The substrate treated with silane is now exposed to a hydrophobic chemical reagent such as methyl or alkyl terminated silane, resulting in a mixed monolayer interface (step 5) [19].

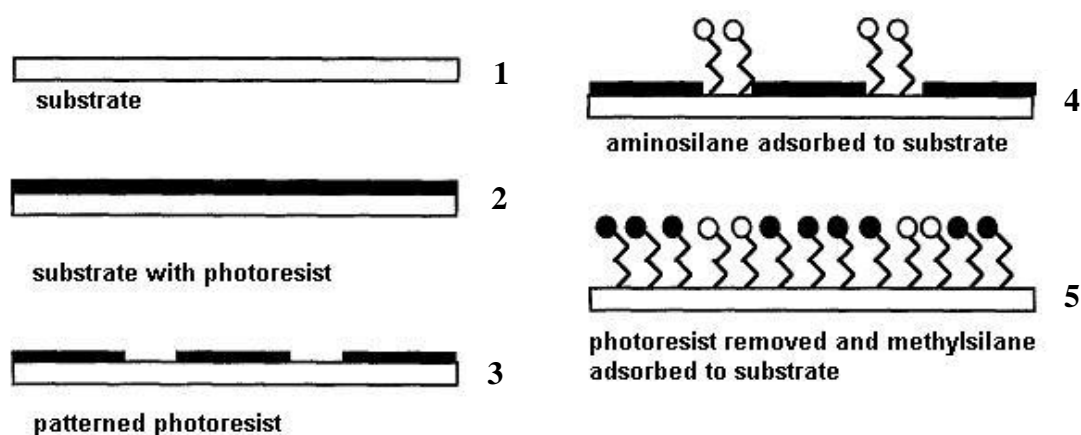


**Figure 1.13:** Conventional photoresist technology applied to the silane SAMs for fabrication of a template for protein immobilization [19].

Another approach for protein patterning through photolithography is to use chemically labile species, which can be activated upon UV irradiation to bind target molecules [203-205]. Oppositely, UV exposure can be used to deactivate the chemical species, *e.g.* the conversion of thiol groups to sulfonates [74]. Arylazide [204, 206], nitrobenzyl [207], diazirine [203, 208] derivatives are the mostly used reagents for this approach.

Photoresist-based protein patterning is based on a well-established technology. Varying the end group on the linker molecule (Figure 1.13) allows one to produce arrays of different proteins. However, the biggest disadvantage is the effect of the patterning process on the final protein activity [19]. The chemicals used in the protocol such as solvents and photoresist can denature the proteins. Additionally, in the case of incomplete surface coverage of the linker, *e.g.* silane or thiol based molecules, the “sites” that are favorable for the nonspecific binding of protein can form on the substrate [19]. Using photochemical methods involving photochemically labile molecules minimizes the negative effect of solvents and reactants on protein activity [19]. But, its limited ability to control the surface energy of the background

region can cause increased non-specific binding that may be minimized by introduction of blocking proteins such as BSA [19, 116]. It should be also noted that photomasking must be conducted either *via* backmasking through a transparent substrate or through some air gap to prevent any damage to the photoresist on the substrate [19, 177].

Traditionally, photolithography is used to fabricate nano/microsurface topologies for biomedical applications [209]. To date, arrays for enzymatic assays [63, 210], immunoassays [211, 212], controlled cell growth [213, 214], DNA and peptide libraries [207, 215] have been successfully produced by photolithography methods. Besides, photolithography has been evolving to produce more efficient products. For example, to be able to minimize the activity loss in proteins that can be caused from harsh chemicals used as photoresist, novel biocompatible photoresists have been developed [216, 217].

#### **1.4 Micro/nano Fabrication of Inorganic Structures**

Interest in production of micro- and nano- inorganic structures has been increasing due to their valuable applications in human life such as semiconductors in computers, nanoscaled devices and structures for biosensing and drug delivery [6, 21, 116, 177]. Comparing the materials used in last centuries in electrical devices such as millimeter-sized copper wires to new advanced materials such as (sub)micrometer-sized optical and electronical parts can allow one to understand the importance of these developments [218]. In addition, the synergic combination of nanotechnology with biology and medicine has yielded a new field of science “Nanomedicine” aiming the development of robust nanotools for the prevention, diagnosis, and treatment of many diseases [2].

In nature, size dimensions of biomolecular components are typically in the range of around 5 to 200 nm. On the other hand, man-made devices can be miniaturized down to about 40 nm using conventional top-down processes (miniaturization processes) such as photolithography [199]. Although there is an interest for further miniaturization due to the commercial requirements, conventional top-down technologies don't seem to be eligible for large-scale production of the components smaller than 40 nm. This fact has triggered the development of bottom-up strategies involving self-assembly of (macro)molecular and colloidal building blocks to create larger, functional devices (Figure 1.14) [218, 219]. In addition, Sarikaya and co-

workers proposed to use peptides and proteins as molecular blocks to fabricate hybrid and hetero-functional nanodevices [7, 9]. In this section, conventional micro-/nanofabrication techniques including nanoparticle synthesis will be mentioned. Biomimetic approach, involving preparation or synthesis of inorganic nanostructures by using biological components, will be discussed in Section 6.

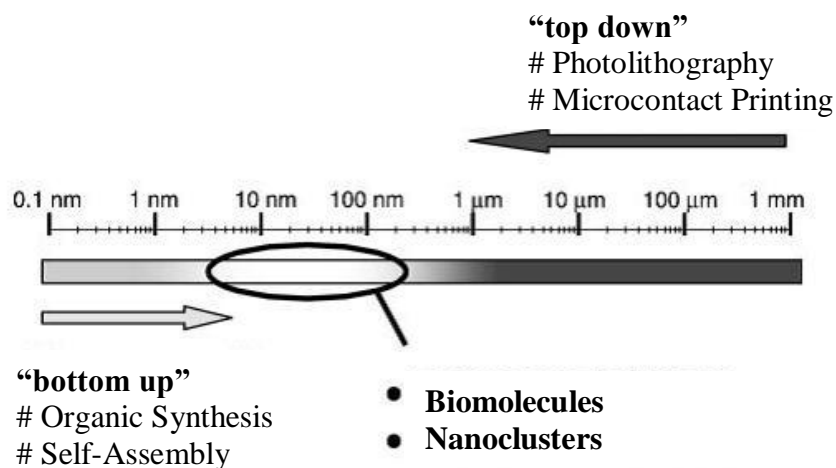


**Figure 1.14:** Top-down and bottom-up approaches meet on the scale [218].

### 1.4.1 Nanoparticle synthesis

Inorganic nanoparticles are very attractive blocks to fabricate larger structures [218, 220, 221]. Basically, nanoparticles should fulfill following requirements [218]; firstly, they need to display certain function that can be applied to corresponding device, such as biosensors. Secondly, their assembly should be controllable through specific recognition. Thirdly, the size of these building blocks should be suitable to bridge the gap between the submicrometer dimensions that are doable by conventional top-down approach and the dimensions that are addressable by bottom-up approaches, such as chemical synthesis and supramolecular self-assembly [218]. Nanoparticles comprised of noble metals, metal oxides, semiconductors can be synthesized readily in large quantities from various materials by simple chemical methods with a range of one to several hundred nanometers in size [220, 222, 223]. Generally, the nanoparticles show strong optical, electronic, magnetic, and catalytic properties which are not displayed by their corresponding bulk forms and which are often size-dependent [218, 224]. The synthesis of commonly used nanoparticles will be briefly mentioned as follows.

Due to their plasmonic properties, noble metal nanoparticles such as gold and silver are one of the most popular nanomaterials [221, 224-227]. Generally their synthesis is based on reduction of gold or silver derivatives. In the case of gold nanoparticle synthesis, the most popular one is citrate reduction of  $\text{HAuCl}_4$  in water, which was developed by Turkevitch in 1951 [228]. Citrate to gold ratio is determined the size of the particles [221]. Since the interaction between citrate and gold nanoparticle is weak, this method is very effective when a loose shell of ligands is required around the gold core to prepare gold nanoparticle-based materials [5, 221]. Reducing agents other than citrate such as sodium borohydride, formaldehyde and hydroxylamine have been also used for gold formation [56, 221, 229]. Also, synthesis of silver nanoparticles has been extensively studied [222, 226, 227]. Silver nitrate is common silver source for the synthesis. Using different capping agents such as polymers, thiols, one can precisely control the shape of gold and silver nanoparticles which also tune their optical properties [224].

Metal nanoshells are new class of nanostructures with highly tunable optical properties. They are composed of dielectric core nanoparticle, e.g. silica, surrounded by nanometer- thick metal layer, e.g. gold [230]. The first experimental procedure for the synthesis of nanoshells consisted of an  $\text{Au}_2\text{S}$  dielectric core surrounded by Au shell [231]. This method allows one to prepare gold nanoshells displaying plasmon resonance peaks at longer wavelengths, ranging from  $\sim 520$  nm to  $\sim 900$  nm. However, lacking the control of the nanoparticle core and shell dimensions as well as large amount of gold colloid formation as byproduct are the major restrictions [230]. Many of these restrictions could be overcome by a new method where gold layer is grown on a dielectric silica nanoparticle [56]. Silica nanoparticles are synthesized via reduction of tetraethylorthosilicate under basic conditions [232] and then functionalized with aminopropyltriethoxysilane (APTES). Subsequently, the small gold nanoparticles (1-2 nm) are attached to silica nanoparticle via the bifunctional APTES molecule. Attached gold nanoparticles serve as nucleation sites for further Au layer formation on silica surface when the gold nanoparticle decorated silica nanoparticles are incubated in  $\text{HAuCl}_4$  solution followed by formaldehyde addition [56].

Semiconductor nanocrystals, called as quantum dots (QDs), also highly light absorbing and luminescent, have taken attention for the potential nanophotonic applications [220, 233]. QDs with narrow size distribution can be chemically



synthesized in organic solvent at elevated temperature [234, 235]. Triocyl phosphine oxide (TOPO) is generally used as capping agent for the QDs during the synthesis to prevent the agglomeration in the organic solvents such as toluene or chloroform [234, 236, 237]. By varying the size of QD, any color emission is possible [220]. QDs composed of ZnSe, CdSe, CdS, and CdTe emit the light in the visible region [220, 238] whereas InAs, InP, and PbS shift the emission to the near-infrared (NIR) [239-241].

#### **1.4.2 Photolithography**

Photolithography is one of the dominant methods for manufacturing in microelectronics industry. It can pattern ~40-nm wide features with 193-nm wavelength light [199]. The most advanced photolithographic systems are based the projection of collimated light through a quartz plate that supports a patterned chromium mask composing of openings with linear dimensions approximately four times larger than the final image projected onto a photoresist located at the focal plane. Typically, photoresist is an organic material that can crosslink and become insoluble or that can decompose and get soluble in organic solvents following UV exposure [199, 242, 243].

There are two types of photoresist materials; positive and negative. Positive photoresist becomes soluble when exposed to UV light (Figure 1.15). So, when the mask is placed onto the positive photoresist, the exposed areas, that are not covered by the mask will be washed away by the appropriate organic solution called “developer”. As a result, the shape of the mask will be transferred onto underlying wafer [177, 199]. In contrast, negative photoresist materials become insoluble (crosslinked) under UV light. Following the exposure, once the mask has been removed and the substrate has been rinsed with developer, the photoresist covered by the mask is washed away, leaving the photographic negative of the mask on the wafer (Figure 1.15) [177, 199]. Photolithography offers an ability to carry out large-scale production of devices with sub-50-nm resolution. To be able to produce smaller features, the technique requires further advances, such as shifting the imaging wavelength to shorter region [199, 244]. This blue shift requires new photoresists to alter the wavelength sensitivity and resolution of the resist [245, 246] as well as new light sources and, especially, new types of optics based on reflection rather than transmission to focus the light [199, 247, 248].

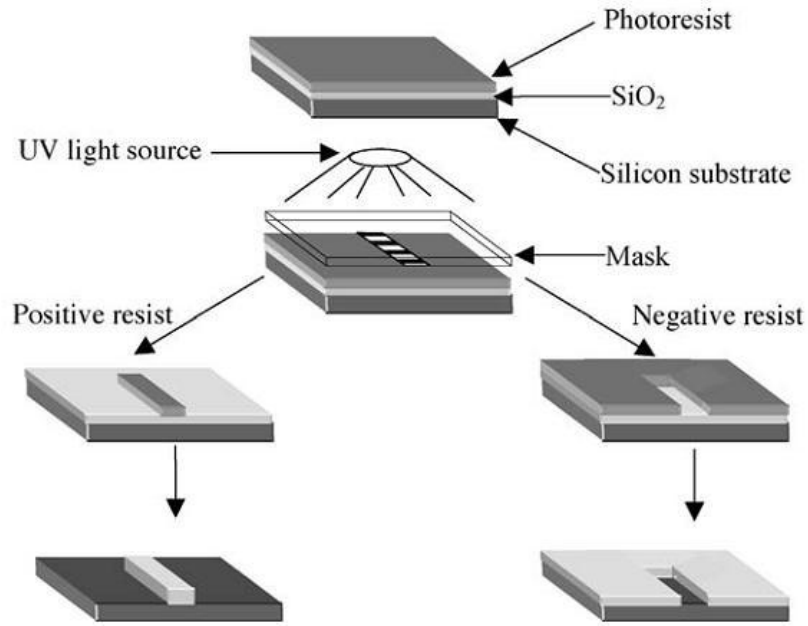


**Figure 1.15:** Steps in photolithography using positive and negative photoresists [177].

### 1.4.3 Electron beam lithography

Electron beam lithography (EBL) has been also used in the production of semiconductors and patterning of masks for other types of lithography such as optical lithography [177]. In this case, focused electron beams in scanning electron microscopy (SEM) or transmission electron microscopy can be utilized to generate patterned nanostructures on an electron-sensitive resist film [249]. Typically, the wafer coated with a layer of resist, *e.g.* poly(methyl methacrylate) (PMMA), is mounted on electron microscope. Tightly focused beam of electrons is then scanned across the surface. Interaction of the electron beam with the resist breaks the chains in the polymer, leading to formation of micropores. This fact causes the resist to be more soluble in a developing solution (Figure 1.16). Following the development, the substrate is coated with inorganic material, *e.g.* Au, Ag. Finally, resultant wafer is rinsed with organic solvent, *i.e.* acetone to remove the rest of photoresist coated with Au, yielding Au nanostructures on the surface [249].

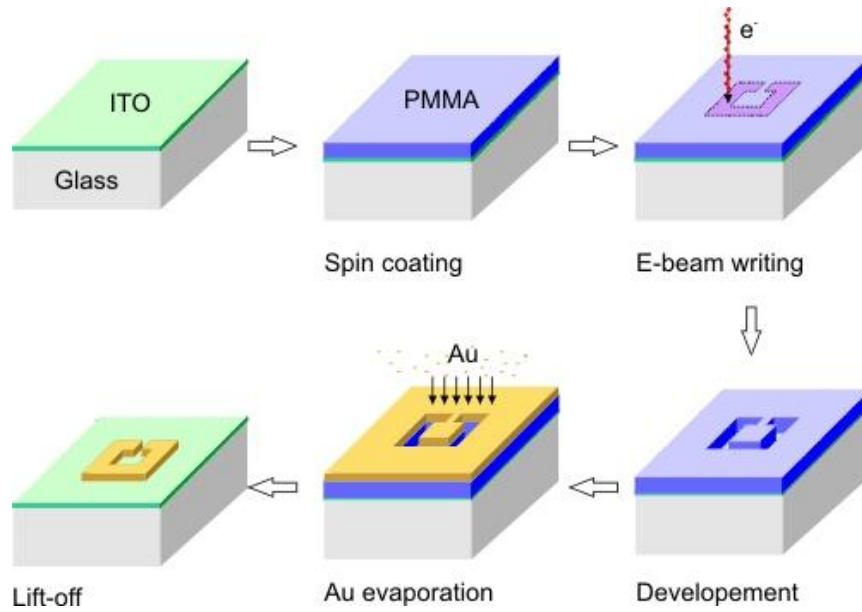


**Figure 1.16:** Steps in EBL to produce Au nanostructures [250].

This technique allows one to prepare nanosized patterns with high resolution on the resist surface by using correct parameters such as energy of the beam. The high-energy electron beams with short wavelength (for example,  $\sim 0.005$  nm for 50 keV electrons) provides e-beam writing with an extremely high resolution [249]. For example, 0.25-nm focused spots are possible [251, 252]. In this technique, the resolution is mainly dependent on the scattering of primary and secondary electrons in the resist film and the substrate. Well-defined arrays with sub50-nm features can be routinely fabricated by EBL [199]. Moreover, the structures as fine as  $\sim 2$  nm have been also fabricated by using thin (10-100 nm) membranes as substrate to minimize the limitation caused by scattering [253].

EBL is a serial process that e-beam scans across the film of resist so that it is inefficient approach for the mass production due to the prolonged process time (approximately 1h) per 4 inch-wafer [254]. This rate of patterning limits scanning beam lithography techniques to small areas or low densities of features. Hence, EBL is mostly used to produce the photomasks for photolithography or to fabricate nanostructures in small quantities for research purposes [249]. Also, for some specific purposes such as certain niche applications where optical lithography is unsuccessful, EBL is used, *e.g.* fabrication of high-frequency GaAs field-effect transistor (FET) devices that requires resolution down to  $\sim 100$  nm and manufacturing of low-volume products [249].

#### 1.4.4 Nanosphere lithography

Nanosphere lithography (NSL) is a powerful and simple method to make nanoparticle arrays which precisely controls shape, size and interparticle spacing [255, 256]. The first step of this method is the self-assembly of monodisperse polystyrene or SiO<sub>2</sub> nanospheres with diameter  $D$  to form a colloidal crystal mask for metal deposition. Negatively charged nanospheres are drop coated onto a substrate such as mica or chemically treated glass cover slip which also has negative charge. These particles freely move until they reach the lowest energy configuration. Capillary forces bring them together resulting in crystallization as hcp pattern on substrate during evaporation of water (solvent). Naturally, nanosphere masks have a variety of defects due to nanosphere polydispersity, site randomness, point defects (vacancies), line defects and polycrystalline domains cause different defects in nanosphere masks. Typical defect-free domain sizes are in the range of 10 to 100  $\mu\text{m}$ . Following nanosphere mask formation, deposition of metal or other material is carried out through the nanomask to form a film with controlled thickness. Finally, sonication of the substrate will yield a nanoparticle array with desired thickness, shape and size (Figure 1.17) [255].

NSL is very cheap and straightforward technique to fabricate nanosensors comprised of arrays of optically active metal nanostructures. Varying either the size of the nanospheres or the thickness of metal coated through the mask clearly changes the optical properties of the resultant nanometallic material [257]. For example, the deposition of 40 nm of Ag over a single-layer mask self-assembled from 390 nm nanospheres produces nanotriangles with Localized surface plasmon resonance (LSPR)  $\lambda_{\text{max}}$  at  $\sim 620$  nm whereas 50 nm deposition of Ag through same mask yields those with a LSPR  $\lambda_{\text{max}}$  at  $\sim 580$  nm [257]. Using these arrays as platform, optical detection of biomolecules such as streptavidin, biomarker for Alzheimer's disease was demonstrated [6, 258]. Although the sensing requires inexpensive setup containing only light source, flowcell, and spectrometer coupled to computer, the detection limit can reach down to few hundreds of target molecules [255].

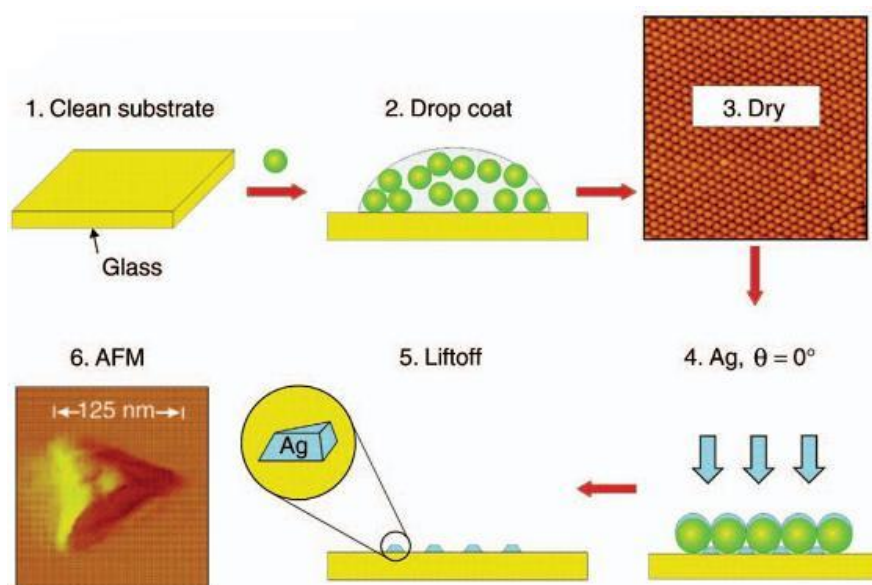


**Figure 1.17:** Steps in the fabrication of Ag nanostructures by NSL [255].

Alternatively, if the deposited metal film on the nanosphere mask is not removed (step 4 in Figure 1.17), the resulting surface, referred to as a metal (e.g., Ag) “film over nanosphere” (FON) surface, is robust plasmonic material for Surface enhanced raman scattering (SERS) [255, 256, 259, 260]. Changing the size of the nanosphere forming the mask and thickness of the metal deposition will also affect the optical properties of resultant metal FON. For example, the deposition of 200 nm of Ag over 390 nm and 600 nm nanospheres gives a metal film with dip position at ~530 nm and ~750 nm, respectively [257]. Metal FON have been also used to detect biocomponents such as glucose and spores [261, 262].

### 1.5 Optical Detection Methods for Biosensing

A biosensor is a device that can quantitatively detect biomolecules, such as proteins, environmental pollutants, pathogenic microbes viruses in a single step [257, 263, 264]. Fundamentally, these devices convert ligand-receptor coupling reaction to an output signal by means of various signal transduction methods including optical, piezoelectric, magnetic, mass spectrometric, etc (Figure 1.18) [6, 263]. Due to their potential applications in areas such as environmental protection, clinic assays, and food industry, there has been enormous effort in the development of new biosensing techniques [263]. Biosensors allow the detection of interaction between the probe unit and the target to be direct and fast comparing to classical bioassays, such as ELISA, which require complex procedure with addition of auxiliary reagents.

Since the transducing principle enables to discriminate between free and bound molecules, biosensors don't require separation or use of additional reagents [265]. Furthermore, detection methods should offer high signal-to-noise ratio, low instrumentation costs, good resolution, and reproducible results with high throughput [140]. In this section, most commonly used optical biosensing techniques will be mentioned.

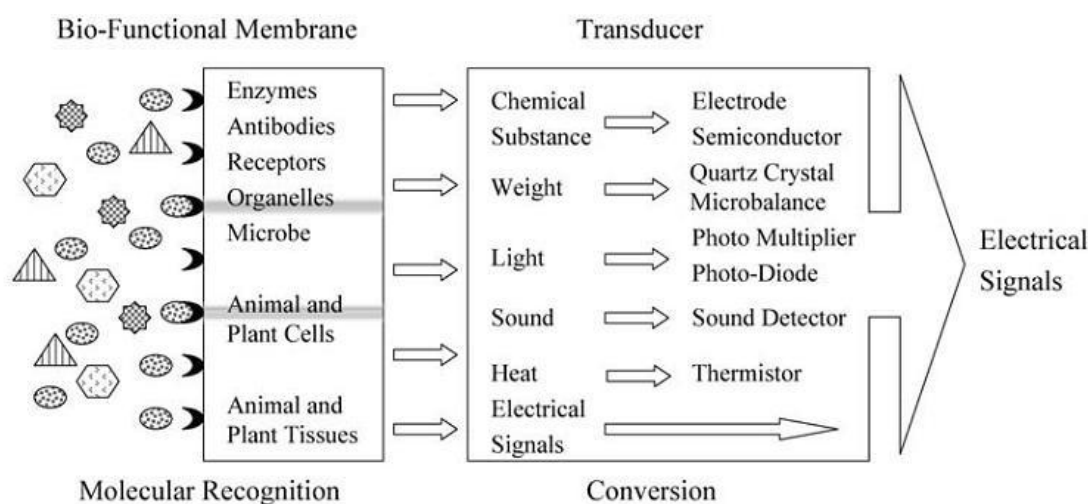


**Figure 1.18:** The principles for the biosensor [263].

### 1.5.1 Fluorescence based detection

Among all existing techniques, fluorescence is most sensitive one to detect intermolecular interactions and is inexpensive and easy to use for practical applications [265]. In sensing applications, detection is based on a change in fluorescence properties of molecular probe that happens when it interacts with the target molecule [266]. Therefore, this probe displays both biological recognition as well as fluorescence activity. As a simple example, fluorescent recognition element is a dye that also exhibits binding affinity towards a certain target (chemical sensor). For most of the applications, integration of one or two dyes at appropriate positions in the molecular recognition element that is specific binder to the target is needed [265]. Although it is a flexible and common approach, there are rigorous requirements for the building of the fluorescent recognition unit, the dye structure and photophysical mechanism of its response, and the fluorescence parameter(s) to be used in detection [265].

Figure 1.19 summarizes the fluorescence parameters to monitor the sensor response [265]. Fluorescence intensity ( $I$ ) is the simplest parameter that can be measured in the steady-state spectrum at particular excitation ( $\lambda_{ex}$ ) and emission ( $\lambda_{em}$ ) wavelengths.  $I$  measured in relative units is sensitive to all quenching effects. Its dependence on excitation wavelength  $I(\lambda_{ex})$  and on emission wavelength  $I(\lambda_{em})$  give the excitation and the emission spectra, respectively. Positions of their maxima may be sensitive to intermolecular interactions of reporting dye. The rate of emission decay gives the fluorescence lifetime. The emission anisotropy is obtained by recording fluorescence emission at two perpendicular polarizations, vertical and horizontal. All of these parameters can be measured as a function of excitation and emission wavelengths [265].

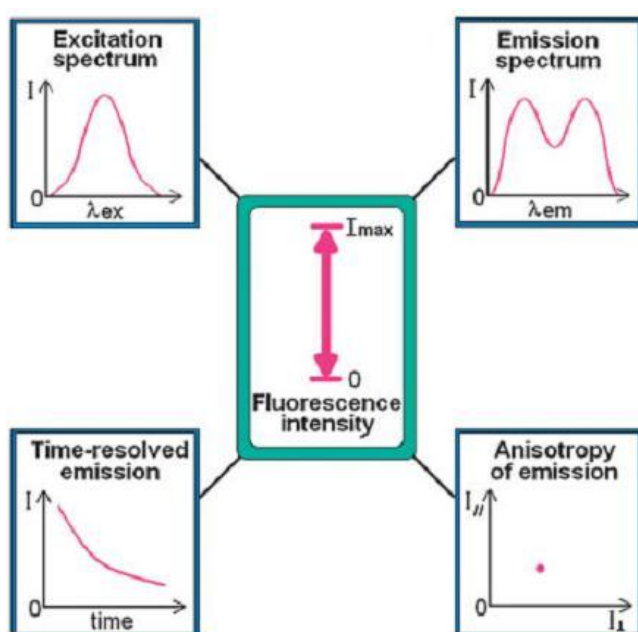


**Figure 1.19:** Fluorescence parameters used for obtaining the sensor response [265].

Organic dyes that contain extended  $\pi$ -electronic systems with excitation and emission in visible range of the spectrum are mostly used in fluorescence based sensors. Additionally, coordinated transition metal ions can be utilized as fluorophore since they exhibit luminescence emission with extended lifetimes [267]. Among biological molecules, the green fluorescent protein (GFP) and its analogs are very interesting for intracellular studies [268]. Furthermore, semiconductor conductor crystals (also known as quantum dots), such as CdSe, CdS, can generate very strong fluorescence emission that is very useful for biosensing [220].

In fluorescence based sensing, probe-target complex formation causes a change in fluorescence parameters of the probe-dye construct mediated by photophysical processes in the dye. These changes occurred at the molecular level are produced either by a change in the distance between two dyes or between a dye and a quencher (Figure 1.20-a), or by a change in environment of a single dye. For the sensing systems containing single dye, the change can be realized in two ways; 1) the dye located in a site far from the recognition site of the target undergoes a conformational changes following probe-target complex formation (Figure 1.20-b), 2) the dye can directly contact with the target by involving the recognition process and this interaction appears as change in the parameters of fluorescence emission (Figure 1.20-c) [265].

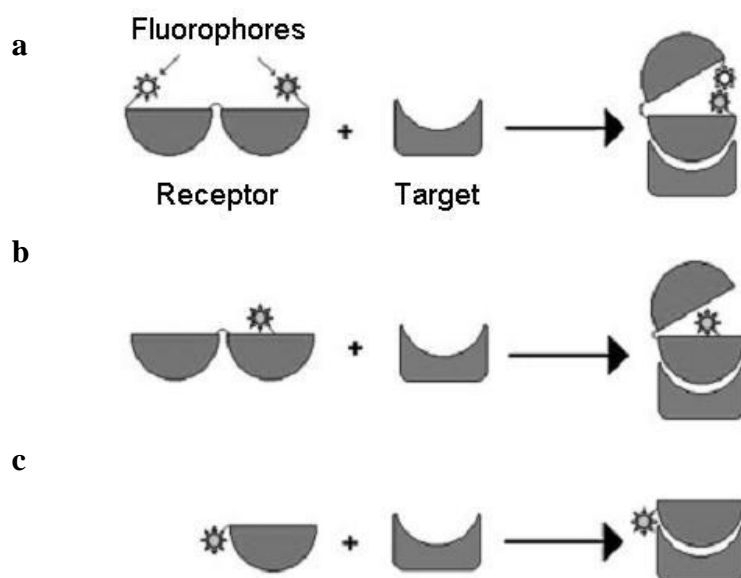


**Figure 1.20:** Different possibilities for the generation of a signal from fluorescent dye on sensor-target interaction [265]. Upon binding to target molecule, a conformational change in the receptor unit changes: (a) the distance and therefore the interaction between two fluorophores or between a fluorophore and a quencher, (b) the interaction of the fluorophore with the receptor and/or its exposure to the solvent. (c) the environment of the fluorophore, leading to a direct interaction between the dye and the bound target.

In fluorescence sensors involving dye and quencher, the distance and efficiency of interaction between two moieties (the dye and the quencher) can be manipulated in such a way that they change upon target binding. Here, intermolecular electron transfer (ET) can be involved in quenching where at short distances an electron can be captured by an excited-state electron acceptor from closely located electron donor



causing a loss of ability for the light emitting [265]. This principle can easily find applications in DNA hybridization technologies. For example, one can design a DNA hairpin where probe ssDNA is flanked by complementary sequences with either donor or acceptor molecule [269]. In absence of target, DNA forms hairpin structure by hybridization of the complementary regions that brings the acceptor and donor molecule into close proximity causing quenching. Upon specific hybridization to the target DNA, the hairpin shows a conformational change leading to separation of complementary flanking ends with a strong increase in fluorescence since the donor and acceptor molecules are now, away from each other.

In fluorescence resonance energy transfer (FRET) sensor, the efficiency depends highly on the distance between the donor and acceptor dyes. The energy transfer from the one molecule (the donor) being initially excited to other (the acceptor) being able to receive the energy and to convert it to its own emission is possible at distances of 10–60 Å and sometimes up to 100 Å [265]. The formation of the target-the fluorescent sensor complex results in a change in the proximity range between the two dyes, leading to an increase in the intensity of the acceptor fluorescence, and a decrease in the donor fluorescence. FRET can provide an easy and convenient way for determining the target concentration. During the sensing event, the switching between donor and acceptor emissions can be recorded as the ratio of the corresponding emission intensities, providing compensation for various instrumental factors as well as the concentration of sensor molecules [265, 270].

### **1.5.2 Localized surface plasmon resonance spectroscopy**

Localized surface plasmon resonance (LSPR) spectroscopy of metallic nanostructures is a robust technique for chemical and biological sensing applications [256]. Basically, a surface plasmon resonance (SPR) is occurred by the materials that possess a negative real and small positive imaginary dielectric constant. This resonance is caused by a coherent oscillation of the surface conduction electrons excited by electromagnetic radiation [271]. There are two types of surface plasmons; the propagating and the localized [255]. Localized surface plasmons (LSPs) that oscillate around the nanoparticle with a frequency, called as the LSPR, is generated when the light interacts with the particles much smaller than the incident wavelength (Figure 1.21), [271]. The LSPR occurs in metallic nanoparticles, mostly silver and gold, in the 10-200 nm size range and results in enhancement at the electric field (**E**) near the

particle surfaces such that  $|\mathbf{E}|^2$  can be 100–10,000 times stronger in intensity than the incident field [255]. The enhanced electric field nearby the particles has a spatial range on the order of 10–50 nm and is highly dependent on the nanoparticle size, shape and local environment [255, 256]. On the other hand, propagating plasmons, generally known as surface plasmon polaritons (SPPs), (will be discussed in the following subsection) require a planar platform containing a thin film of silver and gold with thicknesses within the range of 10–200 nm. Comparing to LSP, propagating surface plasmons lead to smaller field enhancements (10–100 times) and larger spatial range (~1000 nm) [255].

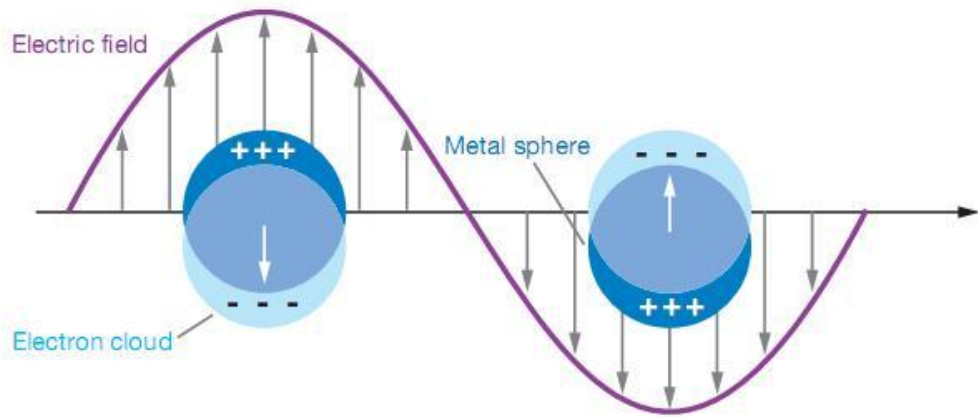


**Figure 1.21:** Schematic representation of a localized surface plasmon [271].

Both the SPR and the LSPR are very sensitive to changes in the local dielectric environment [224, 257, 272]. Based on this fact, the plasmonic materials have been already used in instruments which provide monitoring of the thermodynamics and kinetics of biological interactions using SPR spectroscopy [273, 274]. In SPR spectroscopy, researchers use thin (~50 nm) metal films, mostly gold, as the sensing platform. These platforms can generate SPPs. Besides, with recent development of synthetic techniques, such as colloid chemistry based nanoparticle synthesis, and NSL, researchers have started to achieve controlled fabrication and manipulation of metallic nanostructures and to use them in new applications that take advantage of the LSPR [6, 257, 258].

For LSPR based sensing, the changes in the local environment are detectable through an LSPR wavelength-shift measurement, although a variant of angle-resolved sensing for the LSPR is also possible [275]. The sensor converts the changes in local refractive index caused by the changes in local environment, to wavelength shifts of

the LSPR extinction band maximum ( $\text{LSPR}_{\lambda_{\text{max}}}$ ). As mentioned above, upon the interaction between metal nanoparticles and the light, a collective oscillation of the conduction electrons around the particles occurs and this leads to LSPR extinction which results in wavelength-selective absorption with extremely large molar extinction coefficients ( $\sim 3 \times 10^{11} \text{ M}^{-1} \text{ cm}^{-1}$ ), resonant Rayleigh scattering with efficiency equivalent to that of  $10^6$  fluorophores [257].  $\text{LSPR}_{\lambda_{\text{max}}}$  is also dependent on the size, shape, composition, and dielectric environment of the nanoparticles [224, 226, 255]. The simplest theoretical model for the extinction  $E(\lambda)$  of sphere nanoparticles can be demonstrated by Eq 1.1 [255, 257];

$$E(\lambda) = \frac{24\pi^2 N a^3 \varepsilon_m^{3/2}}{\lambda \ln(10)} \left[ \frac{\varepsilon_i}{(\varepsilon_r + \chi \varepsilon_m)^2 + \varepsilon_i^2} \right] \quad (1.1)$$

where  $N$  is Avagadro's number,  $a$  the radius of the sphere,  $\varepsilon_m$  the external dielectric constant, and  $\varepsilon_i$  and  $\varepsilon_r$  are the imaginary and real portion of dielectric constant of the metal. The effects of particle shape are normalized with the factor  $\chi$ , which has value of 2 for a perfect sphere, and increases directly with the nanoparticle's aspect ratio. The effect of the aspect ratio on the extinction of the nanoparticle can be demonstrated by Figure 1.22. Here, one can easily tune the  $E(\lambda)$  by NSL-fabrication of nanostructures with different aspect ratio [255]. The tuning of optical properties of nanoparticles can also effect the sensing capability of LSPR sensors [257]. LSPR sensors can sense the binding of target molecules at very low concentration [6]. Furthermore the LSPR sensors are potentially applicable for *in vivo* detection in biological cells since the sensing components are at nano-scale [257].

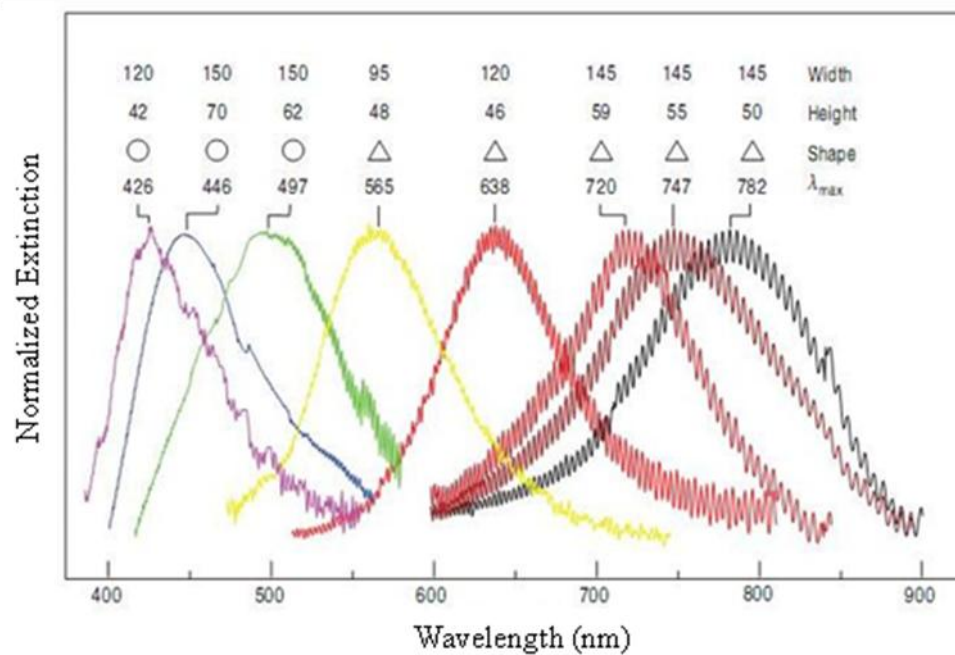


**Figure 1.22:** The extinction spectra of NSL-fabricated silver nanostructures in different size and shape (modified from [255]).

### 1.5.3 Surface plasmon resonance spectroscopy

Surface plasmon resonance (SPR) spectroscopy is, perhaps, the most extensively utilized optical technique for various biological and chemical sensing applications such as detection of glucose and urea, DNA binding assays, immunosensing for immunoassays (for proteins, hormones, drugs, viruses whole bacteria, etc.) [276]. SPR spectroscopy is associated with the SPPs that propagate in the x- and y- directions along the metal-dielectric interface, for a distance range from tens to hundreds of microns, and diminish evanescently in the z- direction with 1/e decay lengths on the order of 200 nm (Figure 2.23) [271, 277]. When the light hits the metal film, the interaction between the metal surface and the electromagnetic wave produce SPPs along the metal-dielectric interface, that are so sensitive to any change in dielectric environment. For the SPR sensors, the binding of target molecule to the probe molecule at the gold surface alters the surrounding environment of thin metal film, leading shifts in the plasmon resonance condition which can be monitored in three modes: 1) wavelength shift, 2) angle resolved, and 3) imaging. In modes 1 and 2, sensor records the reflectivity of light from the metal surface as function of either wavelength (at constant angle of incidence), or angle of incidence (at constant wavelength).

However, the mode utilizes light of both incident angle and constant wavelength to scan a certain two-dimensional region of the metal film, mapping the reflectivity of the surface as a function of position [271].

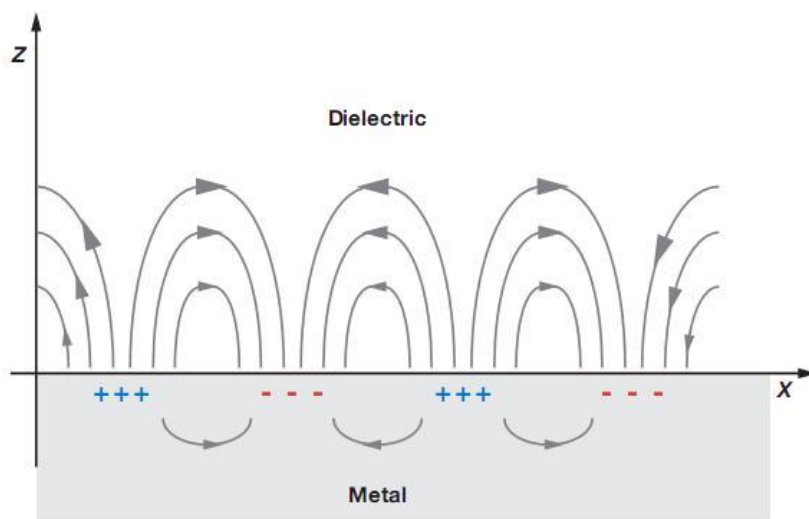


**Figure 1.23:** Schematic representation of a surface plasmon polariton [271].

In SPR sensors, the Kretschmann configuration is mostly used setup to excite plasmons [278]. The configuration is depicted in Figure 2.24. A glass slide is coated with a 40-to 50 nm-thick gold or silver film by vacuum deposition. Then, the biosensing layer containing probe molecule is attached to the metal surface by immobilization techniques including, mostly, SAMs of thiol molecules (see Section 1.2.2). The slide is then coupled to a prism through an index-matching fluid followed by getting the light incident at the prism. The reflection of the light is monitored. At a certain  $\theta_{sp}$ , a surface plasmon is generated by coupling of the electromagnetic wave to the interface while an evanescent field propagates away from the interface, that moves away up to 100 nm above and below the metal surface. At this angle, the reflectivity signal decreases, resulting in a dip. In the case of bare metal film, this dip in reflectivity occurs at one angle. However, for the metal film coated with sensing layer, this angle shifts (mode 2). Upon the binding of target molecules to the sensing layer, a further red shift in the SPR coupling angle occurs. Simply, the sensor converts the target binding to the angular shift (change in  $\theta_{sp}$ ) [276]. Alternatively, this can be also applied to the mode 1 where the reflectivity of the light is recorded as a function of wavelength at constant  $\theta_{sp}$  [279].

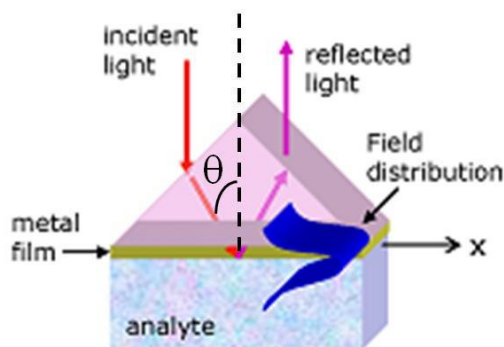


**Figure 1.24:** Schematic diagram for the Kretschmann configuration (modified from [280]).

Both propagating SPR and LSPR sensors have an intrinsic advantage over other optical biosensors such as fluorescence based systems that necessitate a fluorophore or other label to sense the binding event [256, 281]. The response of LSPR and SPR sensors is related with the amount of bound molecule, thin layers and refractive index [257]. These sensors also allow researchers to monitor real-time information for various binding events being used in biotechnology and medicine [256, 257]. In terms of the changes in bulk refractive index, SPR spectroscopy gives higher sensitivity comparing to LSPR spectroscopy [282, 283]. However, the responses of two techniques are comparable when sensing the short-range changes in the refractive index due to a molecular adsorption layer [282]. In other words, SPR sensors provide larger sensing volume since the electromagnetic field decay length is 40-50 times longer than that of LSPR sensors [271].

## 1.6 GEPI in Biotechnology

Over the last decade, genetically engineered peptides for inorganic solids (GEPIs) have emerged, taking advantage of molecular biomimetics where different disciplines such as materials science and molecular biology are utilized to understand the interactions between materials and biomolecules by taking lessons from the nature [7, 11]. Existence of hybrid materials, in nature, that contain highly ordered nanostructures with strong functionality including such as advanced optical and mechanical properties has influenced researchers to pay attention for understanding of the relation between constituents of those materials, biological components *e.g.* proteins, and inorganic structures, at molecular level [7]. Here, with applying the

knowledge obtained from the nature, the challenge is to be able to produce new materials or devices with advanced properties for different purposes while synthetic processes are not capable of [7]. At this point, GEPIs will be important molecular tools to achieve this task. Recent studies pioneered by Sarikaya and co-workers [7, 10, 284] have demonstrated that inorganic-binding peptides have great potential for various applications in different areas in conjunction with nanotechnology such as nanobiotechnology, medicine, nanoelectronics [7, 10, 13]. Following successful isolation and characterization of these peptides, they have been used as assembler, linkers, and synthesizers in proof-of-principle implementations [285-288]. To be able to demonstrate the development towards novel functional materials, this section includes isolation and characterization of GEPIs as well as their potential applications.

#### **1.6.1 Isolation of GEPIs using combinatorial biology protocols**

There are several approaches to isolate inorganic-binding proteins. Traditionally, extraction of these biomolecules from the hard tissues was mostly used in 1990s, however it wasn't efficient due to complicated and time-consuming procedures for isolation and purification of proteins [10, 289, 290]. Also, there are other existing proteins known to bind inorganic surfaces, *e.g.* amelogenin [290-292], a major protein in enamel, sillicatein (extracted from skeletons of diatoms) [293-295]. Utilization of these proteins as molecular tools for hybrid systems provides limited applicability owing to proteins' size and the requirements for the working conditions [10]. Furthermore, these proteins bind to inorganic surfaces non-specifically *via* chemisorption or physisorption [10, 18, 296].

As an alternative and rational approach to obtain surface-specific proteins, recombinant proteins would be designed using molecular biology protocols. In the absence of precise surface topography of a given solid material and binding mechanism of biomolecules to the surface, the appropriate molecule with high affinity to the desired inorganic surface could be either designed using site-directed mutagenesis of the existing proteins or selected as polypeptide motif among peptide libraries [10]. Since peptides have shorter sequences, responsible aminoacid motifs for the inorganic-binding function can be easily explored, providing valuable database for the molecular binding mechanism studies. Also, they can be genetically

or chemically fused to other molecules without loss of their binding function, to obtain multifunctional molecular constructs [10].

With advances in molecular biology, combinatorial selection techniques, emerged more than two decades ago, have been used for the studies on protein-protein interactions that are very important for applications in biology, biotechnology, and medicine, such as drug and vaccine development. The first application of combinatorial methods to identify peptides that bind to inorganic surfaces was conducted by Brown [297]. He selected the peptides for  $\text{Fe}_2\text{O}_3$ . Following that, these combinatorial methods have been also used for isolating peptide sequences binding to various inorganic materials including noble metals (*e.g.*, Au [298, 299], platinum [279], and silver [300]), semiconductors (*e.g.*, GaAs [301], ZnS and CdS [302]), minerals (*e.g.*, hydroxyapatite [288], sapphire [303]) and metal oxides (*e.g.*,  $\text{SiO}_2$  [304], ZnO [305],  $\text{Cu}_2\text{O}$  [305],  $\text{TiO}_2$  [306]) and even polymers [307, 308].

Phage- and cell-surface display methods that utilize the certain part of the outer components of the organism have been mostly used [299, 309]. Basically, DNA sequences of random peptides are inserted into genome of the host organisms where they will be expressed as a part of the proteins located at the surface of organism, *e.g.*, major or minor coat proteins on phage and lipoprotein or flagellar protein of *E. coli* [279, 288, 298, 299, 305]. *In vitro* selection of GEPIs are carried out by biopanning step where the library of phage or cell clones containing huge amount of random peptides displayed on the corresponding part of the organisms is exposed to desired inorganic material as target (Figure 1.25). Following unbound clones are washed away; the bound ones are eluted by chemical or physical methods such as treatment with buffer containing certain amount of detergent [288] and probe sonication [310], respectively. This is followed by amplification step where population of bound clones is increased for the subsequent biopanning round. Generally, 3-5 cycles of biopanning step give clones with the peptides displaying high-affinity to target material, that are then individually isolated and prepared for DNA sequencing to indentify the peptide sequences [279, 298].



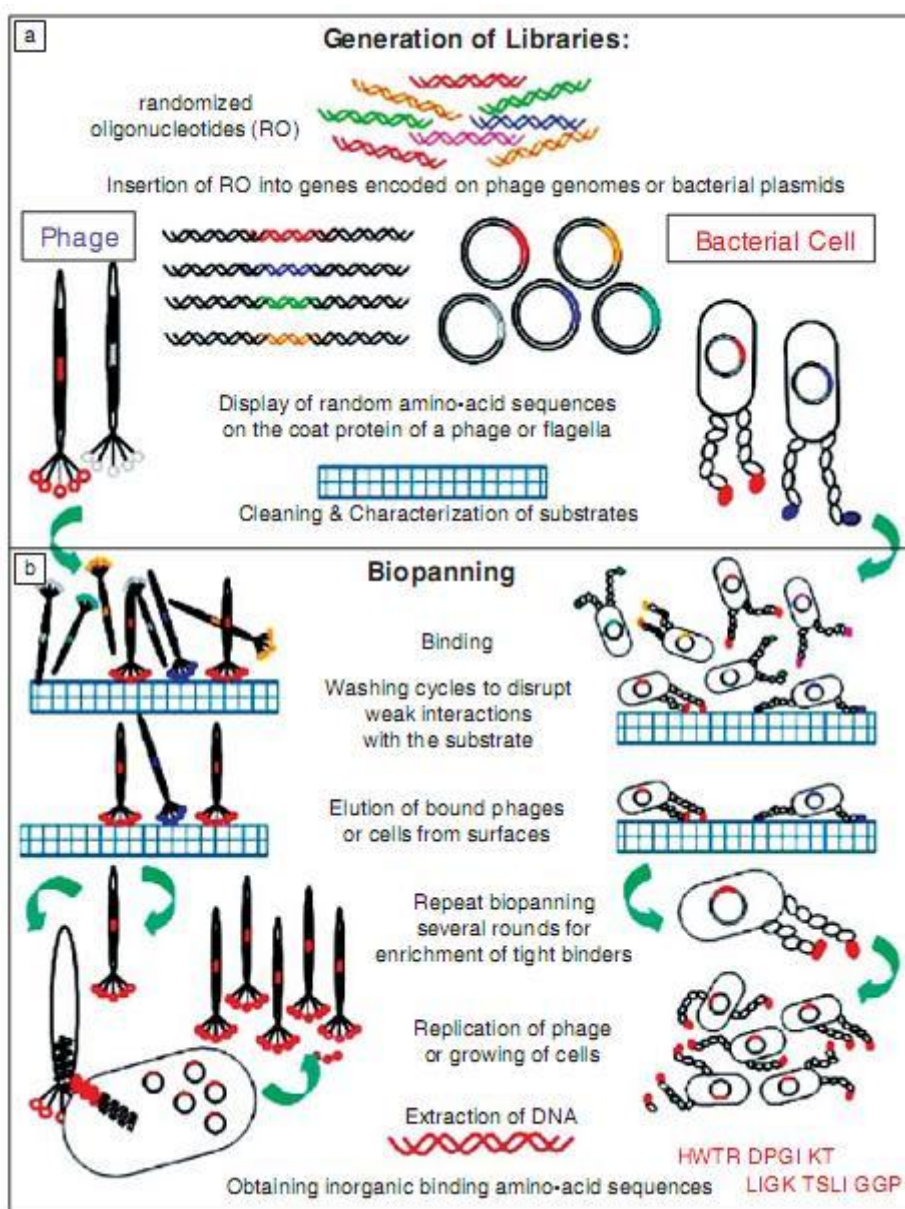


**Figure 1.25:** Schematic diagram for (a) cell-surface and (b) phage- display techniques [7].

Generally, around 50 different clones identified by DNA sequencing are then semi-quantitatively characterized by a protocol, developed by Sarikaya group, involving fluorescence microscopy and ELISA, as first step of general characterization of GEPIs [10, 288, 298]. Simply, each clone (already selected as binders) is amplified again and then exposed to target material. Following washing steps, bound clones are fluorescently labeled with either M13-antibody-FITC conjugate or DNA dye in case of phage or cell, respectively. Under fluorescence mode, the bound cells are basically counted if cell surface display is the case or for phage display, surface coverage of bound phages on the inorganic powder is to be calculated. Based on the number of

bound cells or the surface coverage on material coming from the bound phages, the affinities of the clones are sorted from “strong” to “weak”. For phage display, same protocol can be applied to the ELISA where the reagents are directly added into powder solution containing bound phage labeled with M13-antibody-HRP conjugate, followed by absorbance measurements [288]. Surely, higher number of bound phage will result in quicker enzyme reaction.

Technically, both display protocols have advantages and disadvantages. Since cell-surface doesn't necessitate any other organism but itself, to amplify and replicate the DNA, the efficiency for generating peptide sequences is higher comparing to phage-display, unlikely requiring cell and phage. Additionally, if the powder form of the target materials is chosen, the flagellar proteins may not be suitable for the peptides to be displayed on due to that their fragile structure can fail during centrifuging, resulting in loss of bound clones. Phage- and cell-surface display techniques provide peptide sequences with certain affinity to the target inorganic materials. Although one can find common binding motive among the sequences selected against a protein [309, 311], peptide-solid material interactions generally result in broad binding amino acid patterns among the selected inorganic-binding sequences, leading researchers to do further quantitative binding characterization. Heterogeneity of the surface and complex binding mechanisms involved in the interaction between the peptide and surface may be the explanation [7, 312].

### **1.6.2 Bioinformatics and molecular binding characterization for GEPIs**

Inorganic-binding peptides with certain affinity have been demonstrated to be experimentally selected by combinatorial biology protocols. However, size of the library may not be enough to cover all possibilities to reach the best sequence through directed evolution [10]. Therefore, experimentally selected peptides (first generation) can be improved to increase the binding ability and material-specificity using various tools such as bioinformatics [304], site-directed mutations, and conformational constraints [298].

The interaction between proteins and solids that already exists in nature has been studied to understand the surface recognition as well as binding mechanism of the proteins not only for bioprocesses such as biomineralization [291, 313, 314], also for making novel hybrid materials where GEPIs can be used as molecular tools in

synthesis, structural organization towards multifunctionality [7, 10]. These studies showed that the proteins, in nature, that exhibit similar functions also have aa sequence similarity to each other [315]. Based on this finding, Sarikaya and his co-workers proposed a theory that recognizing one surface may necessitate certain sequence similarity among the peptides selected for the same material [304]. Furthermore, to examine this theory and to be able to design new peptides (second generation) with improved affinity as well as material-specificity, a methodology that combines different sequence alignment techniques resulting in material-specific scoring matrices has been developed by same group [304]. Following FM characterization, based on the surface affinity, the experimentally- selected peptides are categorized in to three groups; strong, moderate, and weak. The sequence alignment methods [316] and the standard scoring matrices [317] are applied to the experimentally-selected sequences to generate a new material-specific sequence scoring matrix that can determine the aa pattern among the strong binders with a certain score [304]. To design new peptides with higher affinity, the resultant sequence scoring matrix that is specific to certain material is applied to millions of aa sequences that are generated by computer and similarity score for each generated peptide is calculated. Among them, the peptides with highest or lowest similarity score are defined as “strongest” or “weakest”, respectively, comparing to experimentally-selected strong binders [304].

First demonstration of this methodology was successfully carried out for quartz binding peptides [304]. Also, one can separately generate scoring matrix for different materials and then using these different material-specific matrices, one can design multifunctional peptides that have recognition abilities for multiple surfaces [312]. This procedure requiring initial aa sequence database provided by experimental phage- or cell- surface display in conjunction with FM characterization can be applied to any inorganic surface (Figure 1.26).

Although there are significant achievements on isolating or designing of inorganic-binding peptides, their surface recognition and assembly mechanisms haven't understood clearly. However, there is already extensive work to quantify their affinity to solids, which is very important for the applications. Using SPR and QCM, adsorption and desorption of the peptides for a certain solid can be easily monitored, providing molecular binding kinetic parameters under various buffering conditions

[279, 298, 318]. Finger print of peptide adsorption may be also obtained by X-ray photoelectron spectroscopy (XPS), time-of-flight secondary ion mass spectroscopy (TOF-SIMS) [319], Fourier transform infrared spectroscopy [320]. Since the molecular conformation of the peptides is a key for understanding the binding mechanism on the inorganic surface, solid- and liquid-state nuclear magnetic resonance (NMR) spectroscopy can provide quantitative information on molecular conformations of peptides [321] but the contribution of solid-NMR method is limited due to the interference coming from the solid surface [10].

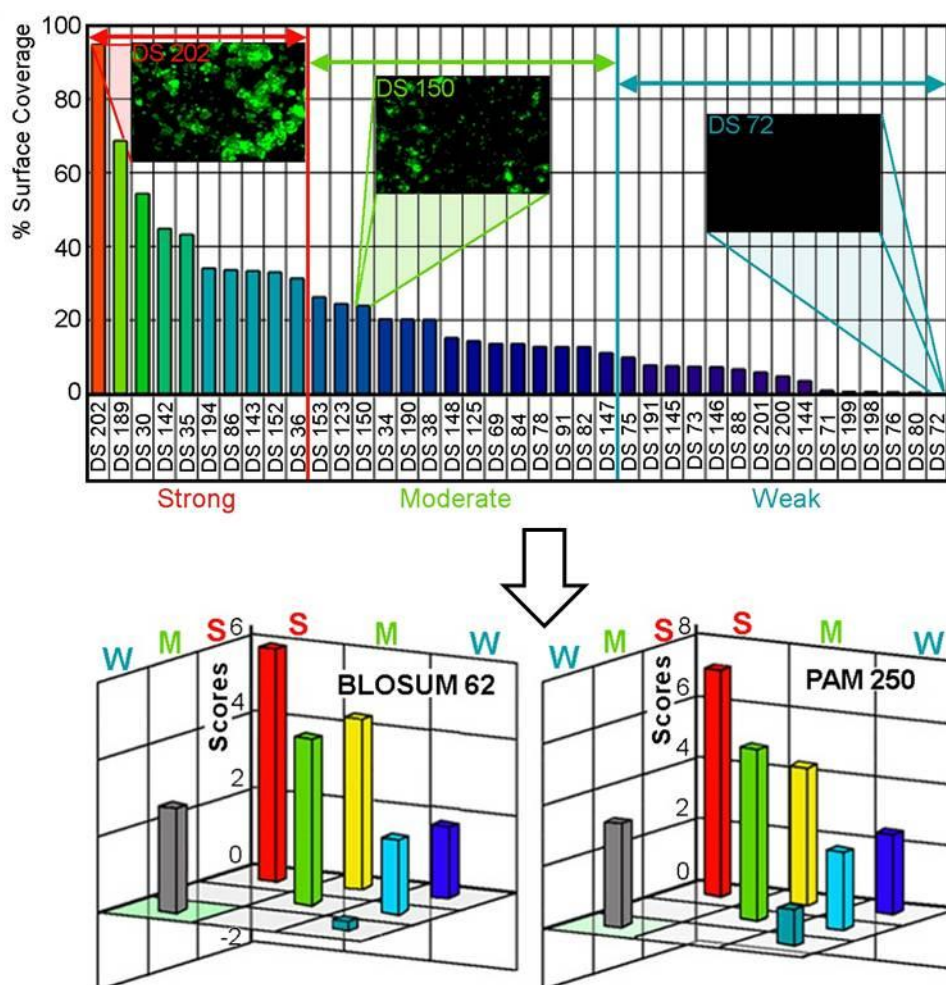


**Figure 1.26:** Bioinformatic approach for desing of second generation GEPIs [304]. Experimentally selected and categorized peptide sequences (upper) are used to calculate similarity scoring matrices (lower) that are utilized to select 2<sup>nd</sup> generation GEPI sequences among computationally created peptide sequences.

Generally, GEPIs have short sequences (7-12 aa), leading to different possible secondary structures in the solution. Using circular dichroism (CD), the structures of peptides in solution and on the surface can be determined [298]. With combination of

SPR, QCM and CD measurements, one can associate the binding affinity with conformational data. For example, using SPR and CD, Hnilova *et al.* showed that linear and constrained (through Cys-Cys bonding) forms of same gold binding sequence displayed different structures, resulting in different affinities to gold surface [298]. Additionally, atomic force microscopy (AFM) is powerful technique to gain insight into assembly and diffusion of the peptide on the solid surface [322]. Also, molecular recognition and specific assembly of the GEPI on a given single crystalline surface can be analyzed using AFM and computational methods such as molecular simulation [323].

None of these techniques can answer all fundamental questions by itself, however advances in the molecular spectroscopic techniques and analytical approach including combination of appropriate methods will provide more quantitative information on peptide assembly. As the knowledge on the peptide recognition and assembly processes increases, novel peptides with tailored binding and higher material-specificity will be designed for the control of solid/peptide interface, leading to assembly/formation of new hybrid materials [10].

### **1.6.3 Current and potential applications of GEPIs**

Controlled attachment and assembly of biomolecules and nano-components onto inorganic substrates are very important issues to build new materials and devices for various applications, especially in nano- and biotechnology [324, 325]. To overcome the limitations imposed by conventional linkers such as silane- and thiol-based molecules, GEPI can be an alternative to achieve these tasks due to peptides' ability for inorganic surface recognition [7, 10]. Bioinformatics and molecular biology protocols such as site-directed mutation, can allow tailoring of GEPIs to tune their binding and material-selective properties [10]. Potential application areas of GEPIs in bio- and nanotechnology are summarized in Figure 1.27.

Protein immobilization is one of the applications where GEPI has great potential. GEPI sequences are genetically inserted into proteins, providing a linkage between molecule and the desired inorganic surfaces to prepare functional hybrid platforms for a variety of practical applications [10]. Such hybrid platforms, containing genetically engineered molecular constructs with site-specific solid-binding peptides, could be potential novel ways of efficient immobilization of proteins under ambient conditions [46, 61, 299, 303, 326].

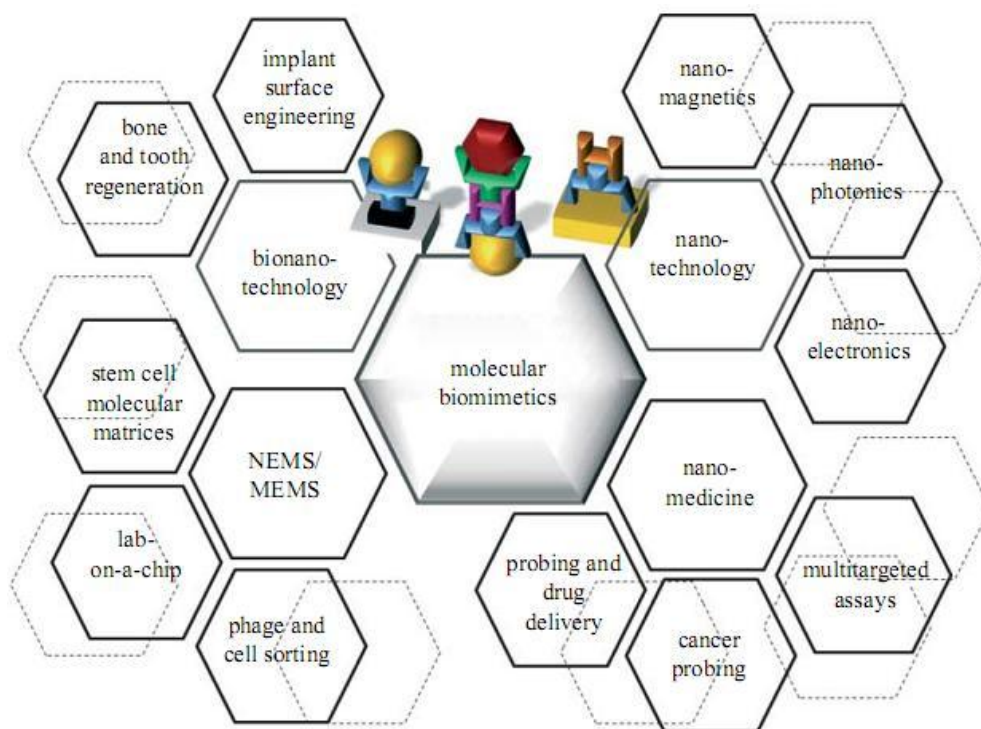


**Figure 1.27:** Potential application areas of GEPIs [284].

Gold-binding peptides, selected by cell surface display [299], are one of the first examples of GEPIs. They were selected using random peptide libraries expressed on the outer surface of *E. coli* as part of the maltodextrin porin, LamB protein. Among the selected peptides, GBP1 (MHGKTQATSGTIQS) has been well characterized by Sarikaya group [286, 311, 318]. Moreover, the GBP1 sequence does not contain cysteine which forms a covalent thiol linkage to gold, as in alkanethiols that form SAMs.

The GBP1 sequence has been used as fusion partner with different proteins [61, 327]. In one of these studies, by insertion of GBP1 sequence into alkaline phosphatase molecule (AP), a surface plasmon resonance (SPR) biosensor was constructed [327]. Here, the seven-repeat gold-binding peptide (7GBP1-AP) was immobilized on SPR chip. However, attached AP molecule was then cleaved off by trypsin from an unspecified region of GBP1, possibly still leaving a residual bound GBP1 layer on to gold which was then used to link probe molecules prior to antibody detection. In another study, immobilization of enhanced green fluorescent protein, severe acute respiratory syndrome (SARS) coronavirus envelope protein and core streptavidin of *Streptomyces avidinii* on gold surface was achieved in conjunction with GBP1-6Histidine as fusion partner [61]. Due to gold affinity of histidine-tag [113-115], the



existence of histidine-tag in the molecular constructs precludes the effect of GBP1 as a molecular linker for immobilization of those proteins on to gold surface. Although these studies aimed to utilize GBP1 as molecular linker, the full potential of GBP1 sequence has not been demonstrated.

GBP1 sequence was also used for gold nanoparticle and quantum dot (QD) immobilization on gold surface. In nanoparticle attachment work, three-repeat GBP1 was PDMS-stamped on gold surface, providing a micro-sized template for gold nanoparticle assembly [285]. Preferential assembly of QD on multipatterned substrates containing platinum and gold micro-pads was also achieved by same three-repeat GBP1 sequence [286]. Due to its material-specific recognition, streptavidin coated quantum dots could be immobilized on only gold pads through biotinylated version of the peptide.

Apart from biomolecule and nanoparticle assembly, gold-binding peptides, selected by Brown [299], were also used for biomimetic synthesis of gold nanoparticles where peptides were found to accelerate nanoparticle growth and to alter the morphology of the particles [311]. Here, the growth of gold nanoparticles was proposed to be influenced by peptide-binding to gold embryos in solution and acidifying the local media around the particles. Furthermore, instead of using single sequence, tandem repeats of the individual gold-binding sequence were found to be more effective to control the particle growth [311]. Biomimetic gold nanoparticle synthesis opened a novel route for inorganic material synthesis where inorganic-binding peptides could act as synthesizer and nano-organizer in the structure of resultant material. In literature, inorganic-binding peptide based material synthesis has been applied to fabrication of various inorganic structures such as silver [300], Cu<sub>2</sub>O [287], silica [328], hydroxyapatite [288], Ti<sub>2</sub>O [306].

The examples reported in literature have clearly shown the potential utilization of GEPIs. New advances in designing and engineering of molecular constructs where GEPIs act as linker, synthesizer, and erector would provide better platforms for controlling cell differentiation, and tissue engineering [10]. Nanoparticle systems functionalized with inorganic-binding peptide based multi probes would be the key for drug delivery [9]. Furthermore, the peptides fused with synthetic molecules could serve as heterofunctional building blocks in different areas such as molecular electronics, magnetics, and photonics [10, 301, 329]. This thesis can open a route

towards some of the advanced applications mentioned above. Here, new protocols in fabrication of functional platforms have been developed in conjunction with different assembly techniques as well as nano/micro patterning methods. Using novel bifunctional molecular constructs, the area of GEPI-based nanoparticle and protein immobilization has been expanded. The resultant platforms were also used for building of optical sensors to detect the biomolecules. Also, a new route for preparation of hybrid nanostructures with tunable optical properties has been reported.





## **2. MATERIALS and METHODS**

### **2.1 Peptide and Nanoparticle Synthesis**

#### **2.1.1 Solid state synthesis of peptides**

An automated solid-phase peptide synthesizer (CS336X, CS-Bio Inc., Menlo Park, USA, Figure 2.1) was utilized to synthesize GEPIs through Fmoc-chemistry. In this approach, modified amino acids (Chempep, USA), where N-terminus and side chain of amino acids were protected by a Fmoc group and an appropriate protecting group, respectively, were used. In the reaction vessel, the Wang resin (Novabiochem, USA) pre-loaded with F-moc protected first amino acid was treated with 20% piperidine in DMF to remove the Fmoc group, which was monitored by UV-absorbance at 301 nm. The incoming amino acid separately activated with HBTU (Sigma Aldrich, USA) in DMF was transferred into the vessel and incubated with the resin for 45 min. After washing the resin with DMF, the same protocol was applied for addition of the next amino acids. In the case of biotinylation, biotin (Biotin-OPN, EMD Biosciences, USA) was dissolved in 1:1 DMF:DMSO and then activated with 0.45 M HBTU. The peptide bound resin was incubated with pre-activated biotin solution for overnight. The addition of biotin was confirmed by Ninhydrin test. Besides, QBP1-F was commercially synthesized (United Biochemical Research, USA).

Following the synthesis, the peptide-resin conjugate was applied to the cocktail containing 90:5:3:2 TFA:thioanisole:EDT:anisole under nitrogen for 3 h to remove peptide from the resin as well as blocking agents from the side chains of the peptide. The peptide solution was then filtered to separate the resin and the peptide. The cleaved peptide was precipitated in cold ether followed by lyophilization (Virtis Benchtop K, SP Industries, Inc, USA) to get crude product. The purification was carried out by HPLC (Waters, USA) using C-18 column (Gemini, USA) under reverse-phase conditions (see Figure 2.2). Firstly, lyophilized peptide powder was dissolved in ~25/75 % (v/v) Acetonitrile:DI water mixture and injected into HPLC. At the column, isocratic gradient of Acetonitrile was maintained for 2 min and then linear gradient of DI water with 1%/min for analytical (at a rate of 1 ml/min) and

0.5%/min for semi-prep scales (at a rate of 10 ml/min) was employed. Each peak monitored by the UV detector at 280 nm and 215 nm was collected and characterized by MALDI-TOF mass spectrometry with reflectron (RETOF-MS) on an Autoflex II (Bruker Daltonics, USA) mass spectrometer located in Department of Medicinal Chemistry at University of Washington. Synthesized peptides were listed in Table 2.1. The MW and pI parameters for each peptide were calculated through ExPASy Proteomics Server [330].

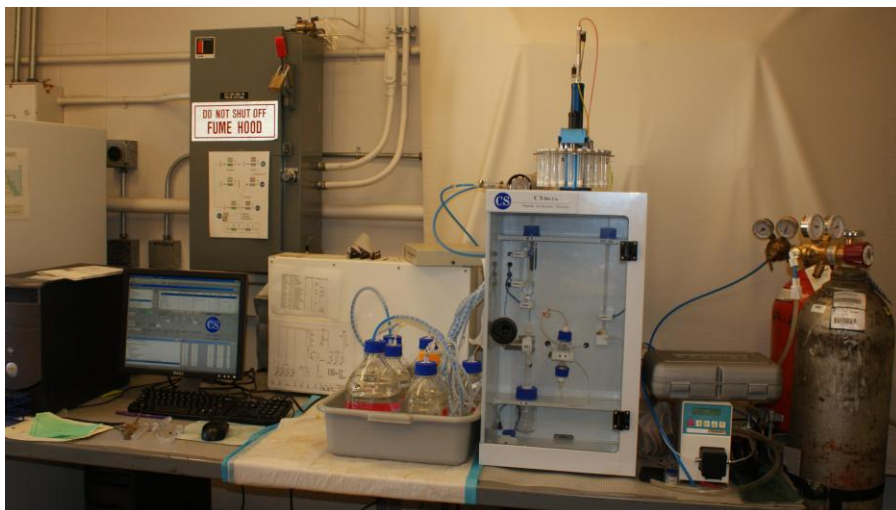


**Figure 2.1:** Image of CS-Bio peptide synthesizer.

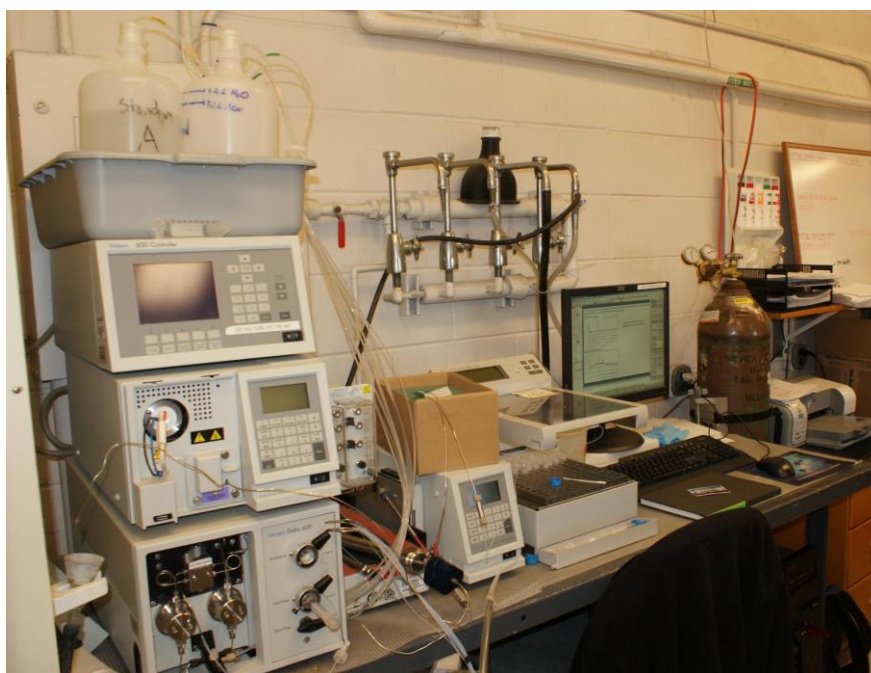


**Figure 2.2:** Image of Waters HPLC.

**Table 2.1:** Sequence, MW, pI, and Net Charge of Synthesized Peptides

Name	Sequence	MW (g/mol)	pI	Net Charge at pH 7.4
Bi-GEPI-1	PPPWLPLYMPPWSGGGWAGAKRLV LRRE	3075.6	10.9	+
Bi-GEPI-2	PPPWLPLYMPPWSPPPWAGAKRLVL RRE	3195.8	10.9	+
Bi-GEPI-3	WAGAKRLVLRREGGGPPPWLPLYM PPWS	3075.6	10.9	+
Bi-GEPI-4	WAGAKRLVLRREPPPPPPWLPLYMP PWS	3195.8	10.9	+
Bi-GEPI-5	CGPEQLGVRKELRGVGPCGGGPPP WPLYMPPWS	3519.1	8.1	+
Bi-GEPI-6	PWLPPSLPPWPPGGGRWKARWFV RRRV	3252.9	12.6	+
AuBP1	WAGAKRLVLRRE	1454.7	11.7	+
AgBP1	CGPEQLGVRKELRGVGPC	1898.2	8.1	+
QBP1	PPPWLPLYMPPWS	1467.7	6.0	-
QBP2	CINQEGAGSKDK	1249.4	6.1	-

### 2.1.2 Synthesis of silica nanoparticles

3 ml of 30% ammonia (Fisher Scientific, USA) was poured into the flask containing 50 ml ethanol. Then, 1.5 ml of tetraethyl orthosilicate (TEOS), (Alfa Aesar, USA) was added to the mixture and the solution was stirred overnight. Size of nanoparticles was found to be  $148 \pm 10$  nm and assuming that all of the TEOS was consumed and the nanoparticle's density is  $2 \text{ g/cm}^3$ , the concentration was calculated to be  $\sim 4 \times 10^{12}$  nanoparticles/ml showing consistency with the literature [56, 232]. Finally, ethanol was replaced with PBS buffer by three times 5 min. centrifugation at 2400 rpm.

### 2.1.3 Noble metal nanoparticles

$\sim 80$  nm silver nanoparticles prepared by photochemical reactions following borohydride reduction of  $\text{AgClO}_4$  were provided by K. Munechika from Ginger Group (University of Washington) [331]. 50 and 15 nm gold nanoparticles were

purchased from Ted Pella Inc, USA. All nanoparticles were used as received. Besides, gold nanoparticles were also synthesized using following procedure called citrate reduction method. 1mM of HAuCl<sub>4</sub> (20 ml) was heated up till boiling. 2 ml of 1% sodium citrate was then added to the reaction flask being stirred at medium speed. The color of the solution was quickly changed from pale yellow to firstly dark grey and finally to dark red. After 15 min. stirring and cooling, the gold nanoparticle solution was centrifuged at 2000 rpm to remove the agglomerates. Supernatant was used for the decoration experiments. Gold formation activity of Bi-GEPIs was also tested as follows; 1 mM of HAuCl<sub>4</sub> solution was reduced in presence of 83 µM peptide instead of citrate. Gold nanoparticle formation was then monitored by TECAN UV-vis spectrometer (plate reader) at 520 nm.

#### **2.1.4 Decoration of silica nanoparticles with gold nanoparticles**

Silica nanoparticles were incubated with  $83 \times 10^{-6}$  M of bifunctional peptide solution in PBS for 2h, where the final volume was 500 µl. Following centrifuging at 2400 rpm for 5min, the supernatant (SN) was removed. The pellet was dissolved in DI water and centrifuged again with the same setup. Water washing step was repeated twice and the last volume of the pellet was set to 500 µl.

Silica NPs pretreated with bifunctional peptide were incubated with 15 nm gold NP for overnight without any agitation. Gold NP/Silica NP mol ratio ( $\Phi$ ) was 2000 ( $r_{\text{gold}}$ : radius of gold nanoparticle;  $r_{\text{silica}}$ : radius of silica naoparticle in Eq 2.1). Unbound gold NPs were removed by combination of centrifuging and washing steps that was mentioned above. Another experiment in which silica NPs were incubated in blank PBS buffer prior to gold NP incubation was also carried out as the negative control (no peptide condition). Gold NP attachment was monitored by UV-vis spectrophotometer (TECAN, USA) in 96-well plate. Gold NP- functionalized silica NPs and negative control were scanned over the UV-Vis regions. Also, spectra of silica NPs and gold NPs were recorded. Finally, silica NPs decorated with gold NPs were characterized by SEM (See Section 2.8.6).

$$\Phi = \frac{r_{\text{gold}}^2}{4\pi r_{\text{silica}}^2} \quad (2.1)$$

In order to calculate the number of peptide bound to the surface of silica nanoparticle, firstly,  $\epsilon$  ( $M^{-1} cm^{-1}$ ), the extinction coefficient of the peptide was determined, using Eq 2.2 in which  $A_i$  is the absorbance of the peptide solution at 280 nm,  $C_i$  is the initial concentration of peptide,  $83 \times 10^{-6} M$ ,  $l$  is the light path length, 0.3 cm. Secondly,  $C_{SN}$ , the concentration of SN was calculated using Eq 2.3 where  $A_{SN}$  is the absorbance of SN,  $\epsilon$  is the extinction coefficient calculated by Eq 2.2,  $l$  is the optical path length, 0.3 cm. Finally, Eq 2.4 provided the number of peptide bound to the silica nanoparticles, #P on Silica NP. Here,  $C_i$  is the initial concentration of peptide,  $C_{SN}$ , is the concentration of SN, calculated using Eq 2.3,  $V$  is the volume of solution in the well,  $10^{-4} l$ ,  $N$  is the Avogadro number and # of Silica NP is the number of silica nanoparticles in the well,  $\sim 10^{11}$  particles /  $10^{-4} l$ . Coverage experiments were repeated three times. All absorbance values were subtracted from those obtained from blank solutions.

$$A_i = \epsilon \times l \times C_i \quad (2.2)$$

$$A_{SN} = \epsilon \times l \times C_{SN} \quad (2.3)$$

$$\#P \text{ on Silica NP} = [(C_i - C_{SN}) \times V \times N] / \# \text{ of Silica NP} \quad (2.4)$$

### 2.1.5 Preparation of silica core gold nanoshells

To grow the gold overlayer on the silica nanoparticles pretreated with bifunctional peptides (See Section 2.1.4), a suitable solution containing a reducible gold salt was prepared. In a glass bottle, 25 mg of  $K_2CO_3$  was dissolved in 100 ml of DI water. After 10 min of stirring,  $HAuCl_4$  solution in water was added at a final concentration of 0.375 mM. After 30 min. stirring, the color of the solution was changed from transparent yellow to colorless. 2  $\mu l$  of the solution of silica nanoparticles covered with bifunctional peptides were injected in to a vigorously stirred 4 ml aliquot of the colorless gold solution. Subsequently, 20  $\mu l$  of %36 formaldehyde solution was added to the mixture. Over the course of 2-4 min, the solution changed from colorless to blue [332]. The nanoshells were then centrifuged at 2400 rpm for 5 min. and redispersed in DI water. UV-vis spectra of nanoshells were recorded using a plate reader (TECAN, USA) over the range from 300 to 1000 nm.

## **2.2 Expression and Purification of Enzymes**

### **2.2.1 Strain and plasmids**

The *E. coli* S2157 cells harboring either the plasmid pSB2991 that encodes AP or one of the plasmids, *i.e.* pSB3057, pSB3055, pSB3053, and pSB3127 encoding 5-, 6-, 7-, and 9-repeat tandem gold binding polypeptide fused to AP, respectively, were provided by S. Brown (University of Copenhagen, Denmark) [299].

### **2.2.2 Growth and purification of enzymes**

S2157 cells with one of the plasmids mentioned in Section 2.2.1 were grown in yeast extract tripton (YT) medium containing 100 µg/ml ampicillin at 34<sup>0</sup>C with shaking until the absorbance at 600 nm of 0.5. Subsequently, the cells were harvested from the broth by centrifugation after inducing with 1mM of IPTG for 6h. Next, the periplasmic fraction containing the enzyme was isolated by cold osmotic shock protocol. Prior to purification, all buffers were prepared freshly and 1 mM PMSF was added as protease inhibitor. The shock fluid was concentrated by 10 kDa Amicon Ultra centrifugal filter device (Millipore, USA) and passed through DEAE-Sephacel column (Sigma, USA) equilibrated in 20 mM Tris-HCl (pH 8.0) buffer. After washing the column with the same buffer, enzyme fractions were eluted with 20mM Tris-HCl, making a gradient from 0.0 to 0.1M NaCl. The fractions containing the desired protein were pooled and concentrated to 5.0 mL by 10 kDa Amicon centrifugal filter device and passed over Sephacryl HS200 column (GE Healthcare, USA) in 10mM Tris-HCl (pH 7.5), 50 mM NaCl, 1.0 mM MgCl<sub>2</sub>. The eluted fractions containing the purified enzyme were then pooled. Protein concentration was determined by using Bradford protein assay with bovine serum albumin as the standard. Protein fractions at each step of purification were analyzed by SDS/PAGE (10% (w/v) gel) under denaturing conditions and the proteins were stained with Coomassie Blue [311, 333, 334]. Molecular weight marker was purchased from Bio-Rad Labs, Hercules, CA. The gel images were analyzed by Total Lab Software (ver 2.01) to determine the experimental molecular weight of enzymes.

## **2.3 Preparation of PDMS Stamps for $\mu$ CP**

### **2.3.1 Master preparation**

The silicon wafer was prepared through cleaning procedure in which the wafer was sonicated in acetone for 5 min, then incubated in methanol for a min, and, lastly, dried under stream of nitrogen. The cleaned substrate was spin-coated with negative photoresist, SU-8 2035 (Microchem, USA) through two subsequent steps; 500 rpm for 5 sec and 3000 rpm for 45 sec. Photoresist-coated wafer was incubated for 3 min on hotplate that was set to 65<sup>0</sup>C, and then kept for 6 min following ramping up to 95<sup>0</sup>C. Soft-baked wafer was then exposed to UV light ( $\lambda$ = 365 nm) for 20 sec through a photomask where the micropatterns were printed on. For the post exposure baking, UV-exposed wafer was kept at 65<sup>0</sup>C for 1 min and then at 95<sup>0</sup>C for 6 min on hotplate. Micropatterns produced on the photoresist were developed through incubating the photoresist coated silicon wafer in SU-8 200 developer (Microchem, USA) for 5 min. Finally, the wafer (master) was incubated at 200<sup>0</sup>C for hard baking.

### **2.3.2 PDMS stamp preparation**

A small petri dish with one droplet of tridecafluoro-1,1,2,2-tetrahydrooctyl)-1-trichlorosilane was placed into the bottom of the desiccator whereas the master was located at upper part of it. Desiccator was closed and left for 30 min under vacuum. This treatment step makes the master surface hydrophobic so that the PDMS sticking on the master is avoided. The modification can be controlled by putting a drop of water on the master to see if the droplet is formed. If it is formed, master is ready to use. CAUTION: the silane molecule is toxic and the fume hood is necessary.

Viscous pre-polymer and the curing agent (Sylgard 184 Elastomer kit, Dow Corning, USA) were mixed with ratio of 10:1 (w/w) and poured onto the treated master. Following degassing for removing the formed air bubbles, the viscous mixture spread on the master was cured at 70<sup>0</sup>C for overnight. The PDMS and master were separated and the elastomer stamp was cut into the smaller pieces. The stamps were then washed several times with ethanol and dried with nitrogen before use (see Figure 1.11).



## **2.4 Preparation of Patterned Substrates**

### **2.4.1 Micropatterned gold substrates by $\mu$ CP**

Gold (~25 nm thick) coating onto single-crystal silicon (100) oriented wafers (Silicon Sense, USA; 100 mm in diameter, ~500  $\mu$ m thick) were carried out by electron-beam evaporation following pre-coating with a layer of titanium (~2nm thick).

The substrates were fractured into slides (~2 cm x 2 cm) for  $\mu$ CP of oligo (ethylene glycol)-terminated alkanethiols (OH-(OCH<sub>2</sub>)<sub>3</sub>-SH). The PDMS stamps were washed several times with ethanol, and then dried in a flow of nitrogen prior to use. The inking was performed by immersing the stamp in 5mM of OH-(OCH<sub>2</sub>)<sub>3</sub>-SH solution in ethanol for 2 min. The inked stamp was dried in nitrogen and brought into a conformal contact with the gold surface for ~20 s. The patterned substrates were rinsed copiously in ethanol, dried under nitrogen, and were used immediately for the self-assembly of the proteins. After each cycle of inking and printing, the stamps were cleaned by ultrasonication in a 2:1 solution of water and ethanol for 5 min.

### **2.4.2 Noble metal nanostructures by NSL**

Glass cover slips (VWR, USA) were cleaned in a piranha solution (1:3 30% H<sub>2</sub>O<sub>2</sub>/H<sub>2</sub>SO<sub>4</sub>) at 80°C for 30 min. CAUTION: Piranha solution is a corrosive and strongly oxidizing agent. The glass substrates were left for cooling to room temperature and then rinsed with copious amounts of water followed by sonication for 60 min in 5:1:1 H<sub>2</sub>O/NH<sub>4</sub>OH/30% H<sub>2</sub>O<sub>2</sub>. Next, the glass cover slips were thoroughly rinsed with water and stored in water until used. 10  $\mu$ l of colloidal nanosphere (polystyrene beads, d= 0.45  $\mu$ m or 1.5  $\mu$ m from Invitrogen, USA) solutions was drop-coated onto cleaned glass cover slip in order to obtain mono layer of nano-masks due to drying step at room temperature. The substrate was placed in precision etching coating system (Gatan Inc.) for Ag/Au coating, operating at 6 keV, 10 mA/cm<sup>2</sup> ion current density, and 6x10<sup>-5</sup> Torr vacuum. Silver and gold targets (with 99.99% purity) were purchased from Gatan Inc. Thickness of metal deposition was ~50 nm. Subsequently, metal-coated substrate was immersed in ethanol and sonicated briefly. Then, the glass substrate was rinsed with ethanol thoroughly [255].

## 2.5 Enzymatic Activity Assays

### 2.5.1 Quantification of enzyme activity in solution

Various concentrations (0.5–3.0  $\mu\text{g/ml}$ ) of Alkaline phosphatase (AP) in 10 mM Tris–HCl (pH 7.5), 10 mM  $\text{MgCl}_2$  (Reaction buffer) were assayed with 5.5 mM pNPP for 30 min. The release of p-nitrophenol (pNP) was recorded by 96-well TECAN plate reader (San Jose, CA) at 405 nm. The AP activity was calculated from Beer-Lambert law as follows (Eq. 2.5):

$$\text{Enzymatic activity (mmol/min)} = \frac{V \times \text{OD}_{405\text{nm}}}{\varepsilon \times \text{incubation time}} \quad (2.5)$$

where  $\varepsilon$  is the molar extinction coefficient ( $\text{M}^{-1} \text{cm}^{-1}$ ) which for pNP is  $\varepsilon = 1.78 \times 10^4 \text{ M}^{-1} \text{cm}^{-1}$ ; V is the final assay volume (ml);  $\text{OD}_{405\text{nm}}$  is the absorbance divided by the light-path length ( $\text{cm}^{-1}$ ). After calculating the average of the triplicate assays, the blank values were subtracted from those of  $\text{OD}_{405\text{nm}}$  [334].

### 2.5.2 Quantification of immobilized enzyme activity

In order to quantify the AP activity, the reaction buffer (800 ml), containing 3.0  $\mu\text{g/ml}$  of enzyme, was incubated with either non-patterned or micro-patterned gold substrate in microfuge tubes and shaken at room temperature for 16 h. At the end of the incubation period, the substrate was taken out of the tubes and, washed with DI water and buffer solution. These were then dried by a flow of nitrogen before AFM characterization or activity assays. Also, as a control, the retained activity of the immobilized enzymes was determined by assaying the activity of the free enzyme in solution. The percentage of the retained enzymatic activity on the non-patterned gold surfaces was calculated as follows (Eq 2.6) [334]:

$$\text{Retained Enzymatic activity, \%} = \frac{\text{Enzyme Activity}_{5\text{GBP1-AP on substrate}}}{\text{Enzyme Activity}_{5\text{GBP1-AP in solution}}} \times 100 \quad (2.6)$$

## **2.6. Immobilization of Nanoparticles and Proteins through GEPI**

### **2.6.1 Self assembly of nanoparticles on inorganic substrates (Gold and Silica)**

Glass cover slips (VWR, USA) were sonicated firstly in acetone for 20 min and then in isopropyl alcohol (IPA) for 30min. For noble metal nanoparticle (Au or Ag) immobilization, 33  $\mu\text{M}$  of bifunctional peptide solutions in PBS buffer were dropped on the cleaned glass substrate and incubated at room temperature for 2h. The cover slips were then thoroughly rinsed with DI water and then dried in a flow of nitrogen. Similar to the peptide assembly, either gold or silver nanoparticle solution was dropped on the glass substrate pretreated with peptide and left to incubate at again room temperature for 40 min. After rinsing with DI water and drying under nitrogen flow, the glass cover slips were immediately examined using optical microscope under dark-field (DF) conditions and AFM (see Section 2.8.2 and 2.8.4).

The same procedure was applied to immobilize silica nanoparticles but in this case, gold coated glass cover slips (see Section 2.4.1) and silica nanoparticles were used as the platform and nanoentities, respectively. After immobilization, the substrates were scanned using DF imaging and AFM (see Section 2.8.2 and 2.8.4).

### **2.6.2 $\mu\text{CP}$ of enzymes on gold substrates**

100  $\mu\text{l}$  of 50  $\mu\text{g/ml}$  of enzyme in reaction buffer was dropped onto the patterned side of the PDMS stamp and incubated for 15 min. The enzyme solution was gently removed by pipette from the surface of the stamp and then dried with nitrogen following brief washing with DI water. Gold coated glass substrates (see Section 2.4.1) were thoroughly rinsed by isopropanol and ethanol and then, dried with inert gas. The clean substrate was then brought to contact with the surface of the stamp and pressed using force for 10 sec and left on the stamp surface for up to 10min. The substrate was separated from the stamp and the side contacted with the stamp was washed with DI water for 2min and dried under a flow of nitrogen.

Besides, 2  $\mu\text{l}$  of monoclonal Anti-AP (0.5  $\text{mg/ml}$ , Invitrogen, USA) was diluted to 10  $\mu\text{l}$  with the reaction buffer. Into this solution, 5  $\mu\text{l}$  of FITC-labeled IgG<sub>2a</sub> secondary antibody (Invitrogen, USA) was added. Following 30 min of incubation on ice at the shaker with lower speed, the mixture was again diluted up to 500  $\mu\text{l}$  with the reaction buffer and applied to the gold surface pre-stamped with enzyme for 1h at

room temperature. The substrates were then rinsed with DI water and dried with nitrogen prior to FM characterization (see Section 2.8.4).

### **2.6.3 $\mu$ CP of QBP-F on quartz substrates**

The patterned side of the PDMS stamp was incubated with the peptide conjugate, BSA-F or fluorescein (54  $\mu$ M) in PBS buffer for 5 min. The peptide solution was removed by pipette from the surface of the stamp, which was then dried with inert gas following brief washing with DI water. Quartz substrates were thoroughly washed by isopropanol and ethanol and then, dried with nitrogen. The clean substrate was then applied to the surface of the stamp and pressed using force for 10 sec and left on the stamp surface for 10 min. The substrate was removed from the stamp and the side contacted with the stamp was rinsed with DI water for 2 min and dried with nitrogen. The substrates were characterized with FM (see Section 2.8.2). The fluorescence measurements of the substrates were performed by Ocean Optics Spectrometer coupled to the fluorescence microscope. Since the labeling degree is  $\geq 7$  (mol ratio of fluorescein to BSA), 7.7  $\mu$ M of BSA-F that is equivalent to the number of fluorescein molecules in 54  $\mu$ M moles of QBP1-F was used [335].

### **2.6.4 Co-immobilization of Fluorescein and SA-QDs**

Following the stamping of biotinylated peptides using the procedure explained in Section 2.6.3, streptavidin-coated Quantum Dots (20 nM in PBS buffer), emitting the light at 605 nm, SA-QD(605) (Invitrogen, USA), was drop-coated onto the substrate and allowed to incubate for 15 min. The substrates were then rinsed with DI water for 2 min and dried under a stream of nitrogen. In order to produce micropatterns of two different target molecules, i.e., QDs and fluorescein, following SA-QD(605) assembly, the quartz substrate was drop-coated with QBP1-F (54  $\mu$ M) in PBS buffer and incubated for 15 min. Before FM characterization, the substrate was again rinsed with DI water for 2 min and then dried with nitrogen [335].

### **2.6.5 Co-immobilization of noble metal nanoparticles and SA-QDs on glass**

Following cleaning procedure for the glass slides (see Section 2.6.1), the PDMS stamping of bifunctional peptides was carried out on the cleaned substrates using the procedure described in Section 2.6.3, except the concentration was 33  $\mu$ M. Gold or silver nanoparticles were then dropped onto dried glass and incubated for 30-40 min.

The substrates were treated with QBP-bio (54  $\mu$ M) molecules for 2 h and subsequently, incubated with a 20 nM solution of either SA-QD(605) or SA-QD(565) (Invitrogen, USA) for 10 min. After each assembly step (peptide or nanoparticle) the substrates were rinsed in DI water and dried under nitrogen flow. For the control, the procedure was applied to two more substrates where the assembly of either bi-functional peptide or QBP-bio was replaced with blank PBS incubation. All substrates were checked with the optical microscope under fluorescence and DF mode (see Section 2.8.4).

In addition, detergent treatment and sonication were effective methods for removal of peptide molecules bound to the PDMS stamp, making the stamp reusable. After the PDMS experiments, the stamp was washed with DI water and placed in a small Petri dish containing detergent prepared with 0.2% Triton X-100 in PBS buffer. Stamps were then sonicated for 10 min in order to remove unwanted particles from the surface. After sonication, stamps were again washed with ethanol and put in desiccator for the next use following drying with inert gas.

#### **2.6.6 Dip-pen lithography of GEPI**

Silicon nitride probes (Type A, NanoInk, USA) incubated in plasma cleaner for 5 min were used for writing of GEPIs. Then, DPN tips were immersed in ink, GEPI, solution prepared in either DI water or phosphate carbonate (PC) buffer (1 to 5mM in PC buffer; 55mM  $\text{KH}_2\text{PO}_4$ /45mM  $\text{Na}_2\text{CO}_3$ / 200mM NaCl) for 3-5 sec. The inked tips were then dried under a stream of compressed gas (Falcon, USA). The silicon substrates (Silicon Quesnt Int., USA) were cut and sonicated in acetone and IPA for 25 min each. All substrates were incubated in plasma cleaner for 5 min just before the experiments. DPN writing and AFM imaging were carried out using NanoInk Nscriptor scanning probe microscope in ambient conditions (temperature 21–24°C, relative humidity 30%–50%). The substrates were then rinsed with DI water. In the case of biotinylated peptide patterning, the substrates were incubated with 20 nM SA-QD for 10 min. Subsequently, following washing step with DI water and the substrates were dried under nitrogen flow and characterized under fluorescence microscope [336].

## **2.7 LSPR based Biomolecule Detection**

### **2.7.1 Anti-AP detection using immobilized gold NP on glass**

5GBP1-AP solution (90 nM) prepared in reaction buffer was drop-coated and incubated on the gold nanoparticles immobilized on the glass surface (See Section 2.6.1). AP molecule was also used as the control for probing. Following thorough rinsing with DI water and drying under nitrogen, binding of the target molecule was achieved by repeating the probe assembly procedure with various concentrations of Anti-AP (Invitrogen, USA), in the reaction buffer. As a control experiment, Anti-Maltose Binding Protein (Invitrogen, USA) was also used. The incubation period for each assembly was 2 h at room temperature.

Transmission spectra of each substrate were recorded using Agilent (USA) 8453 UV-Vis spectrometer in air just after gold nanoparticle immobilization (as bare), enzyme (as probe) and antibody (as target) assembly. Spectral data were plotted and LSPR  $\lambda_{\text{max}}$  for each step was determined using software Origin 7.0.

### **2.7.2 SA-AP Detection using silver nanostructures deposited on glass**

Ag nanostructures fabricated on glass (See Section 2.4.2) was placed in custom-made flow cell mounted onto optical microscope, and then rinsed with copious amount of methanol, ethanol and lastly DI water (Experimental setup is depicted in Figure 2.3). 8  $\mu\text{M}$  biotinylated peptide (in DI water) solution was incubated in flow cell for overnight. Following that, DI water was passed through flow cell as the washing step. Subsequently, 100 nM SA-AP (in DI Water) solution was introduced into the cell and incubated for 3 h. Following washing step with DI water, biotin (500  $\mu\text{M}$ ) in DI water was injected and incubated for 15 min. Then washing step was done to remove free biotin and SA-AP/biotin conjugates.

Transmission spectra of the same spot on Ag nanoarrays were recorded using Ocean Optics (USA) USB2000 spectrometer coupled to the microscope via 600  $\mu\text{m}$ -fiber optic cable (Thorn Lab., USA). Prior to the measurements, the substrate was washed by pumping DI water through the flowcell. The spectral measurements were taken; firstly before the functionalization of nanoarray with biotinylated peptide, secondly after biotinylated peptide incubation, thirdly after SA-AP incubation and finally after

biotin incubation. Each spectrum collected from the Ag nanoarray was normalized by the spectrum recorded separately from white reference.

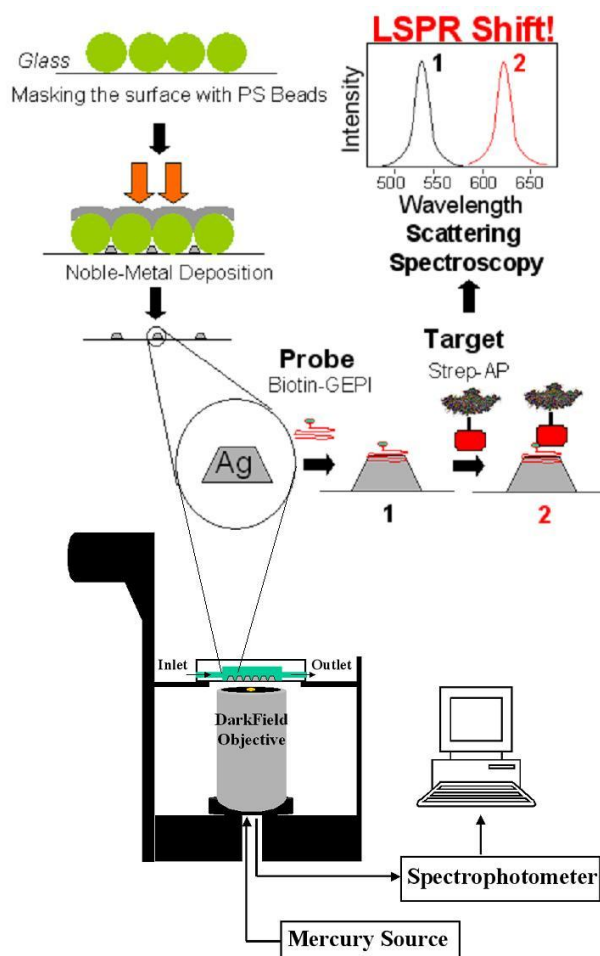


**Figure 2.3:** Schematic representation of experimental setup for LSPR detection on NSL-fabricated nanoarray.

## 2.8 Characterization Techniques

### 2.8.1 Quartz crystalline microbalance spectroscopy

A typical Collpitts oscillator, which has a buffer amplifier was utilized as the oscillation electronic circuit. The voltage of 12 V DC was applied to the oscillator circuit to drive the crystal and the frequency was measured with a Hewlett-Packard frequency counter (Model No: 53131A 225 Hz Universal Counter, Agilent Technologies, USA). The QCM electrodes with a fundamental resonant frequency of 10 MHz, were obtained from International Crystal Manufacturing Co., USA. The crystals were coated on both sides with a 100 Å -thick chromium followed by a 1,000 Å -thick gold films. The crystal surfaces were optically polished before metal

coating. The diameter of the crystals and electrodes used were 5 and 8.8 mm, respectively. Before starting the experiments, the crystals with the gold electrode were firstly cleaned with 1:3 (v/v) 30% $\text{H}_2\text{O}_2/\text{H}_2\text{SO}_4$ , “piranha solution,” for 5 min at room temperature and then rinsed with DI water. The crystals were then used immediately following getting dried under a flow of nitrogen gas. To establish a stable baseline, a sufficient volume of the reaction buffer was introduced into the cell before adding the enzyme solution. The frequency change of the crystal in pure buffer was recorded for 30–60 min. Following the equilibration with buffer, desired amount of enzyme in buffer was introduced into the cell and the frequency change was recorded continuously (Figure 2.4).



**Figure 2.4:** The setup for the QCM.

### 2.8.2 Atomic force microscopy

The samples were scanned using an AFM using a Digital Instruments Multimode scanning probe microscope with a Nanoscope IIIa controller, USA under acoustic and mechanical isolation (Figure 2.5). High frequency (~300 kHz) silicon nitride cantilevers were purchased from Molecular Imaging, USA and used at a scanning velocity of ~3  $\mu\text{m}/\text{s}$  in order to reduce feedback artifacts. Topographic feature sizes and cross-sectional analysis were performed using the Nanoscope software (ver 5.3r1) provided with the AFM by Digital Instruments Co., USA.





**Figure 2.5:** The image of the Atomic Force Microscope in the chamber for acoustic and mechanical isolation.

### 2.8.3 Surface plasmon resonance spectroscopy

The SPR measurements were carried out by a four-channel instrument (Kretschmann configuration) developed by the Radio Engineering Institute, Czech Republic [279]. Moreover, the setup consists of a polychromatic light source (Ocean Optics, USA) coupled with an optical fiber and an Ocean Optics SD 2000 detector (Figure 2.6). The data were collected using WinSpectral 1.03; this software was supplied along with the instrument. This program normalizes the acquired SPR spectrum using the dip in the wavelength shift at regular intervals which then is fit with a 4th-order polynomial for generating the metric sensogram as a function of time. During the experiments, a baseline was established by pumping the reaction buffer first, and then the 6-port valve (Upchurch Scientific, USA) was switched to protein/peptide solution until a full saturation was achieved. The concentration range was 5-100  $\mu\text{g/ml}$ . The buffer was then pumped once again (at a rate of 80  $\mu\text{L/min}$ ) to monitor the desorption behavior.

The Langmuir isotherm model was used to deduce the kinetics of the adsorption process using the experimental SPR data. Here, firstly,  $k_{\text{observable}}$  was calculated using Eq 2.7; where  $C$  is the protein concentration, and  $k_a$  and  $k_d$  are the association and

dissociation constants, respectively. Next, the equilibrium constant ( $K_{eq}$ ) and the equilibrium surface coverage ( $\theta$ ) data were obtained using Eq 2.8 and Eq 2.9, respectively [279, 318, 334].

$$k_{obs} = (k_a \times C) + k_d \quad (2.7)$$

$$K_{eq} = k_a / k_d \quad (2.8)$$

$$\theta = C / [C + (1/K_{eq})] \quad (2.9)$$

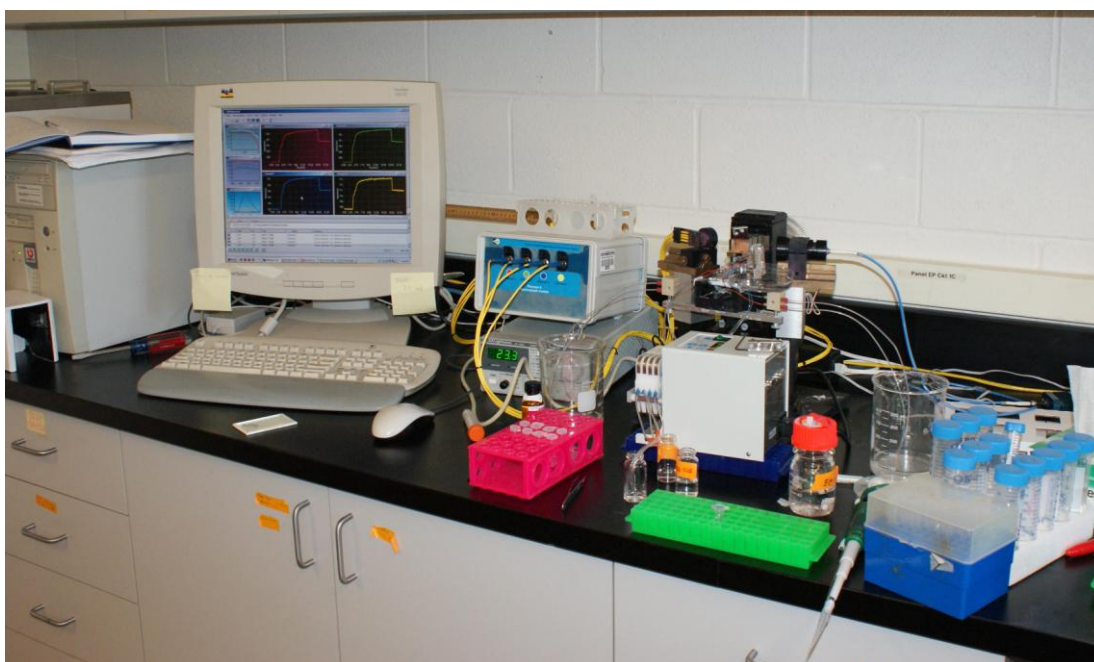


**Figure 2.6:** The setup for SPR spectroscopy.

#### 2.8.4 Fluorescence and dark-field microscopy

The dried substrates taped on glass slides were mounted on a Nikon Eclipse TE-2000U Optical Microscope (Nikon, Japan) coupled with a Hamamatsu ORCA-ER cooled charge-coupled device (CCD) camera (Figure 2.7). FITC (exciter 460–500, dichroic 505, emitter 510–560, Nikon) and QD605 (exciter 320–460, dichroic 475, emitter 605/40nm Chroma Technology Co, USA), QD565 (exciter 320–460, dichroic 475, emitter 565/40nm Chroma Technology Co, USA) filter sets were used for QBP1-F, SA-QD(605) and SA-QD(565) detection, respectively. Dark-field mode was maintained by 50X and 100X DF lenses and DF filter set from Nikon, Japan.

The mercury illumination (X-cite 120, EXFO, USA) was utilized as the light source. The images are recorded through Metamorph Software (Universal Imaging, USA).

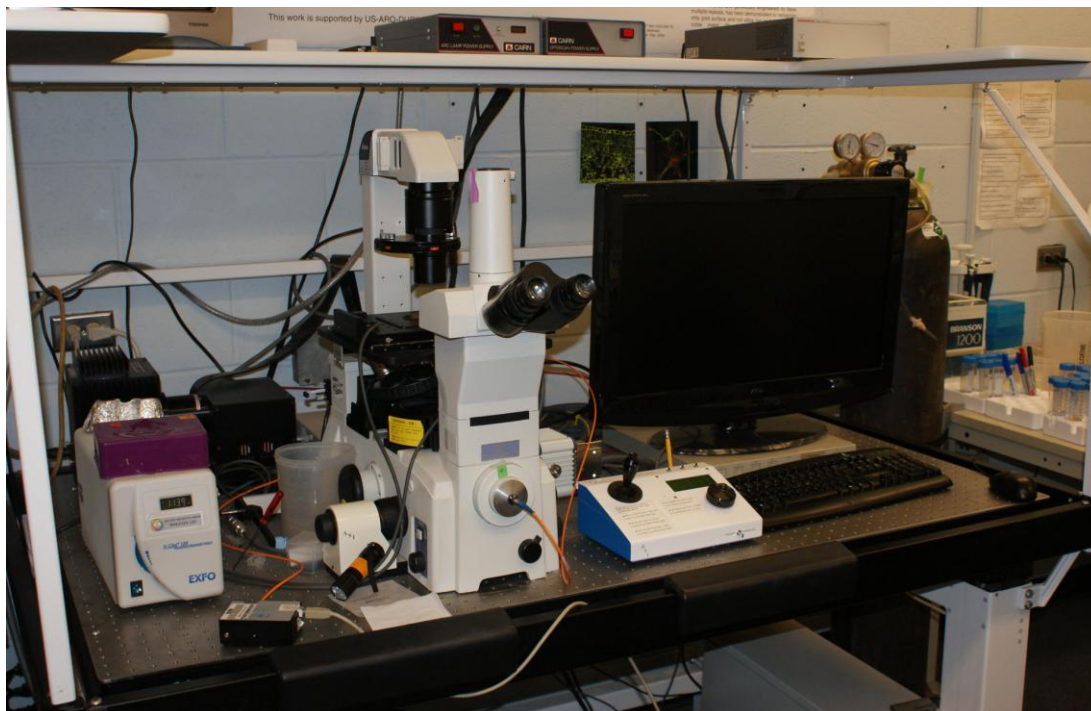


**Figure 2.7:** The optical microscope dedicated for fluorescence and dark-field imaging.

### **2.8.5 Transmission electron microscopy**

Philips EM420 TEM was used to image the nanoparticles (Figure 2.8). Prior to characterization, nanoparticles were rinsed with DI water to remove the salt and then drop-coated on copper TEM grid coated with carbon film (Ted Pella, USA). Excess of the nanoparticle solution was removed using tissue paper and then the grid was allowed to dry under vacuum. 100 kV were used as accelerating voltage. The projection of the nanoparticles was printed on photographic negatives (Kodak, USA) that were then developed in the dark room.



**Figure 2.8:** Philips EM420 Transmission Electron Microscope.

#### **2.8.6 Scanning electron microscopy**

Either immobilized nanoparticles or free nanoparticles were scanned under JSM-7000F (JEOL, Japan) coupled with the attachments for Energy-dispersive X-ray (EDX) spectroscopy (Figure 2.9). The solid substrates and the free nanoparticles were rinsed with DI water to remove the salt residues and the contaminants. Following drying process under a flow of nitrogen, solid substrates were directly mounted onto aluminum cylinder using carbon tape. In the case of nanoparticle solution, a couple of drops from the solution were directly put on a clean aluminum mount and dried under vacuum. The aluminum mount loaded with sample was placed into the microscope. The working acceleration voltage was 10kV. Both the digital images and EDX spectra of the samples were recorded using the software provided by the company.





**Figure 2.9:** JEOL JSM-7000F Scanning Electron Microscope with EDX detector.

### 3. RESULTS AND DISCUSSION

Molecular biomimetics relying on the inspiration from nature regarding to the interactions between biomolecules and inorganic materials at molecular level, has ability to provide novel molecular tools containing GEPIs (see Section 1.6) to produce new hybrid materials with advanced properties. GEPIs are isolated using phage- and cell-surface display technologies. Following molecular characterization steps, in this section, these peptides were used as assembler, linker, and synthesizer to fabricate new functional platforms for different purposes without the potential problems or limitations associated with the conventional chemical methods. Firstly, oriented immobilization of GEPI-enzyme conjugate was achieved on patterned and non-patterned gold substrates. Moreover, in protein and nanoparticle patterning, GEPIs were shown to be successful ink for microcontact printing and dip-pen nanolithography. Through self-assembly process, bifunctional GEPIs containing two different binding sequences were used as molecular linkers for nanoparticle immobilization such as gold and silica, on solid substrates. As application of these platforms, optical hybrid sensors composed of noble metal nanostructures and GEPI-linked probes were fabricated. GEPI was also employed in synthesis of optically active hybrid nanostructures where the peptide acted as nucleation site for gold formation around silica nanoparticles, resulting a red shift at corresponding LSPR  $\lambda_{\max}$  from vis to NIR region.

#### 3.1 Oriented Enzyme Immobilization on Gold

##### 3.1.1 Purification and characterization of bifunctional enzymes

In earlier studies by Tamerler *et al.*, based on the hypothesis that the increase in the number of the tandem GBP1 repeat would increase the binding activity to gold, 3-repeat GBP1 was shown to have better binding than that of single-repeat GBP1 [286, 318]. Here, the increasing repeat number of the GBP1 sequence in Alkaline phosphatase (AP), starting from 5-repeat ( $n= 5, 6, 7, 9$ ) was chosen to evaluate the effect on the bi-functional activities [334]. Multiple tandem repeats of cell surface

display-selected gold binding peptide were genetically fused to the enzyme, AP, at the N-terminus. The plasmids encoding the wild-type AP and the bi-functional constructs (nGBP1-AP) were expressed in *E. coli* S2157 cells. The expressed enzymes were secreted from the cytoplasm to the periplasmic space. Wild-type or bi-functional AP in the periplasmic fluid was purified by employing two successive steps: ion-exchange and gel filtration chromatography. The purified samples were run onto SDS-PAGE to verify their purity and molecular weights (Figure 3.1 and 3.2). The protein bands of AP, 5GBP1-AP, 6GBP1-AP, 7GBP1-AP, and 9GBP1-AP were, approximately, at the following kDa values (compared to the theoretical molecular weights in parentheses), respectively: 46.5 (50.1), 54.5 (57.4), 55.3 (58.8), 56.0 (60.3), and 58.0 (63.1). The molecular weights of the proteins purified are comparable to *E. coli* AP, a homodimer with a molecular weight of 89 kDa [337].

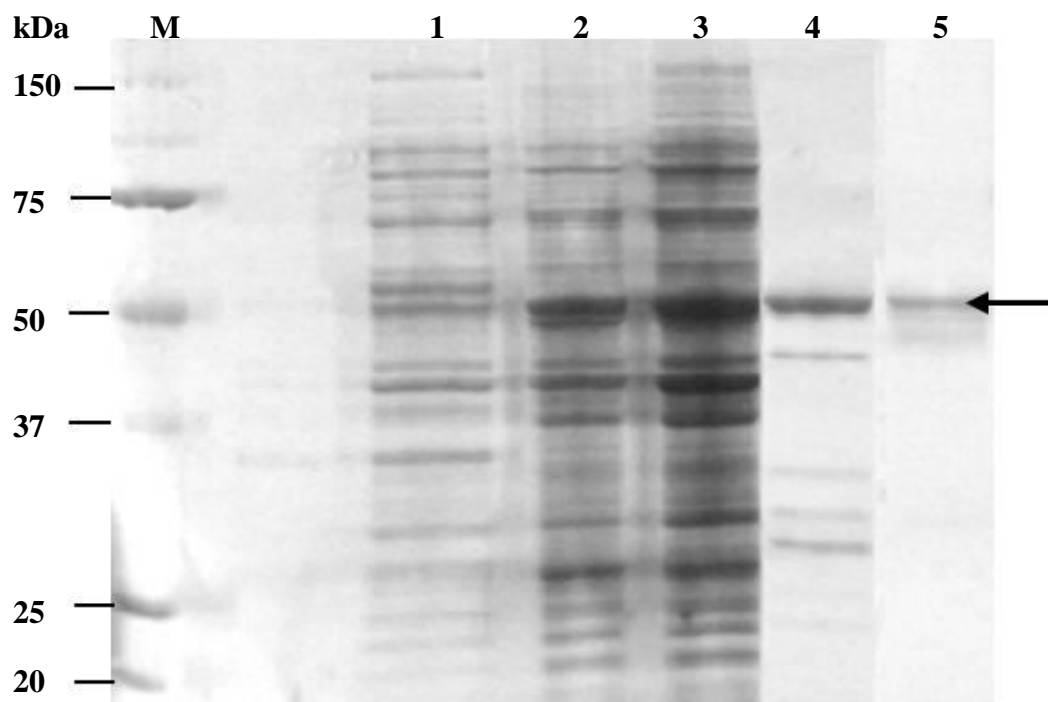


**Figure 3.1:** SDS-PAGE of 5GBP1-AP purification steps. The arrow indicates 54.5 kDa band of 5GBP1-AP. **Lane M:** Molecular weight marker with corresponding molecular masses at the left, **lane 1:** Induced culture, **lane 2:** periplasmic fluid, **lane 3:** periplasmic fraction concentrated by centrifugal filter tube, **lane 4:** DEAE chromatography, **lane 5:** gel filtration chromatography [334].

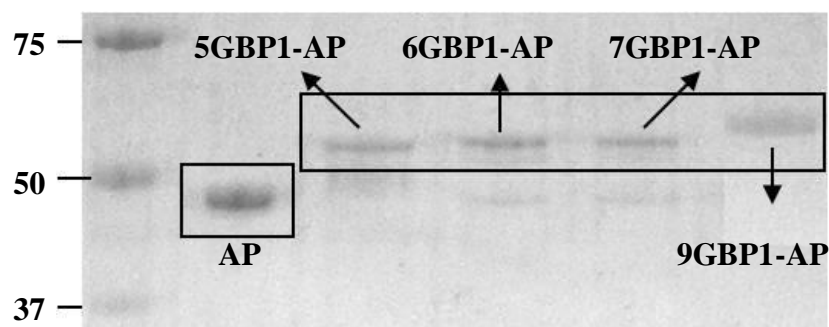


**Figure 3.2:** The image of 10% SDS gel of the purified constructs with the molecular weight marker [334].

The bi-functionality of enzymes was evaluated for both phosphatase and gold binding activities using biochemical, spectroscopic, and molecular imaging protocols. The AP activities of the wild-type protein and fusion constructs were measured spectrophotometrically using pNPP as a substrate (Figure 3.3). We then monitored the gold binding activities of bi-functional enzymes on gold electrode using QCM (Figure 3.4). The 5GBP1-AP and 6GBP1-AP presented higher gold binding activity compared to either 7GBP1-AP or 9GBP1-AP. The 5GBP1-AP had also the highest phosphatase activity; this fusion construct, therefore, was chosen to carry out the subsequent directed immobilization studies [334].

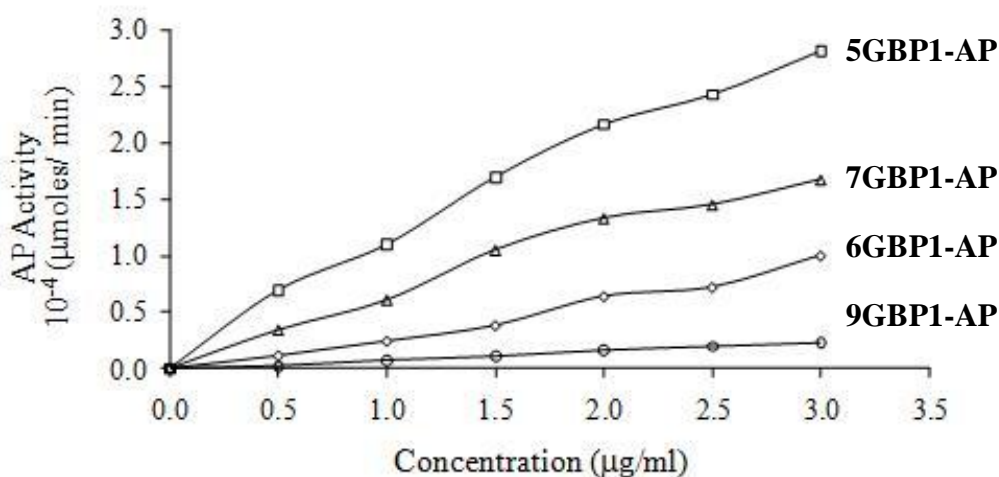


**Figure 3.3:** Phosphatase activity of the molecular constructs, nGBP1-AP [334].



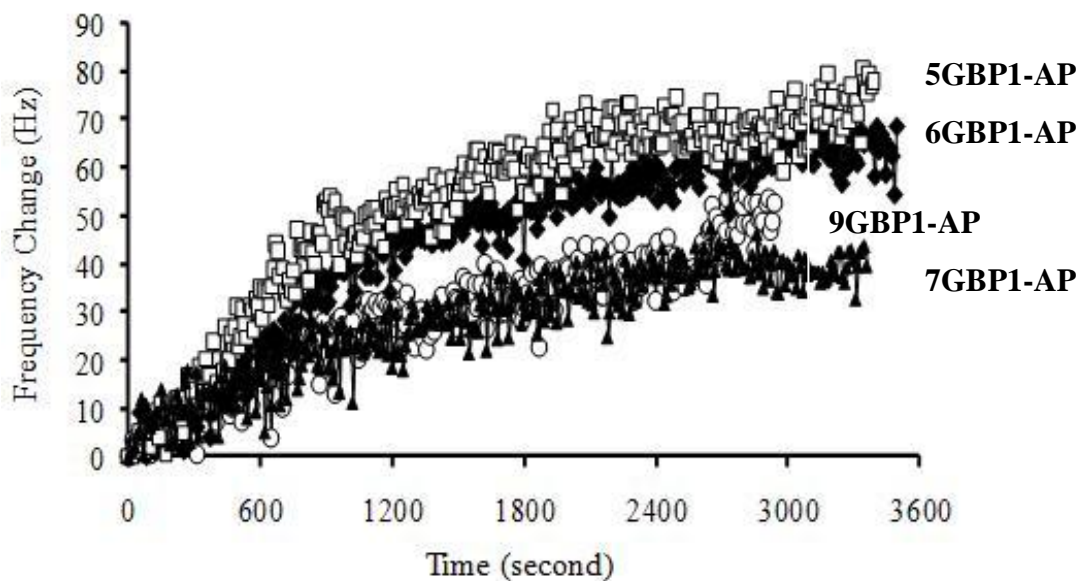


**Figure 3.4:** Gold binding activity of nGBP1-AP constructs by quartz crystal microbalance analysis (protein concentration: 2.5  $\mu\text{g/ml}$ ) [334].

### 3.1.2 Binding and assembly of 5GBP1-AP on gold substrates

The directed immobilization and the resulting morphology of the AP and the 5GBP1-AP on gold substrate were examined using non-contact mode AFM (Figure 3.5-3.8). The dimensions of the immobilized enzymes obtained from AFM characterization are comparable with the molecular dimensions of the bacterial AP obtained from the Protein Data Bank, as: 9.77 nm x 5.40 nm x 4.75 nm [338]. Upon closer inspection, it can be recognized that the 5GBP1-AP units are significantly more discrete and well packed on the surface (Figure. 3.5 and 3.6) than the wild-type AP (Figure 3.7 and 3.8). The peak-to-peak analyses of the topography of the images from the two substrates also yielded insights into the packing density of the particles. In the case of 5GBP1-AP, a higher packing density, with a peak-to-peak separation of  $11.0 \pm 2.9$  nm, was observed compared to AP alone, with  $\sim 16.0 \pm 1.5$  nm, as shown in the representative cross-sectional measurements in Figure 3.6 and 3.8. Since the same tip was used to produce the AFM images from both of the samples, the discrepancy in feature sizes was not seen to arise from experimental artifacts, such as tip convolution. The evidence of agglomeration in the AP sample, without the fusion peptide, can also be recognized by comparing the z (height) data between the two sets of images. From Figure 3.6 and 3.8, the cross sections reveal an average height variation of almost double that of the actual size of the 5GBP1-AP ( $8 \pm 4$  nm). This observation suggests that there may be multiple layers of AP in the absence of GBP1,

possibly due to agglomeration normal to the surface or misorientation of the protein with its longest axis normal to the surface. In the case of the 5GBP1-AP construct, a discrete and closely packed monolayer was formed with a thickness closest to the c-dimension of AP, that is,  $6\pm1$  nm. This result suggests, therefore, that the enzyme has likely been oriented right side up (i.e., enzymatic sites facing the solution) by the gold binding peptide. Additionally, Figure 3.5 and 3.7 also show undulating plateau-like features throughout the surface of about  $\sim 30$  nm, indicative of the polycrystalline gold grain structure of the underlying surface. With these observations and peak-to-peak measurements, it can be reasoned that the surface in Figure 3.5 and 3.6 is more indicative of a uniformly thin and oriented molecular layer than those observed in Figure 3.7 and 3.8 where AP was used [334].

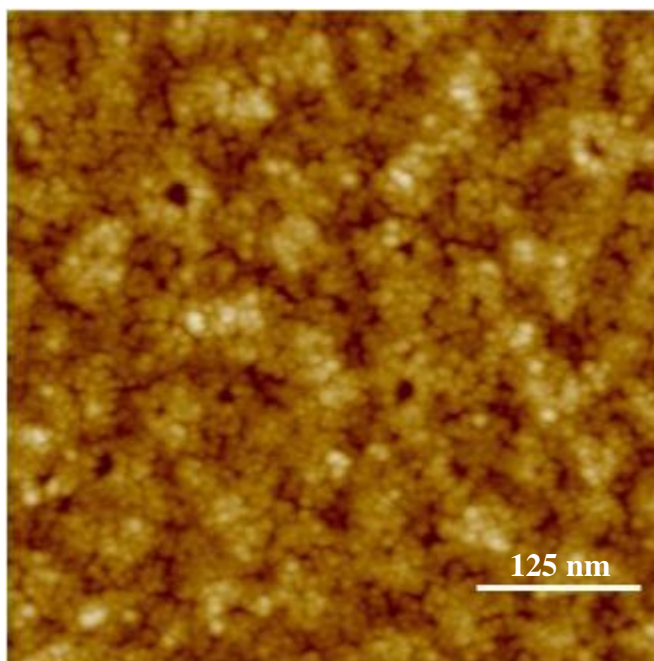


**Figure 3.5:** AFM image of gold substrate following self-assembly of 5GBP1-AP (protein concentration: 3  $\mu\text{g/ml}$ ). The area corresponds to 500 nm x 500 nm scans [334].

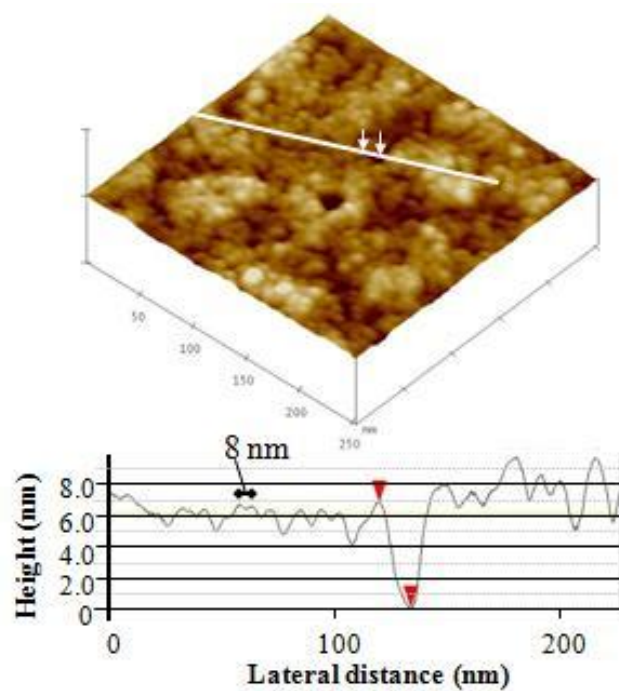


**Figure 3.6:** Digitally magnified Figure 3.5 is represented in pseudo-3-dimensional presentation at 150 nm x 150 nm area to show surface topography following the immobilization of 5GBP1-AP [334].

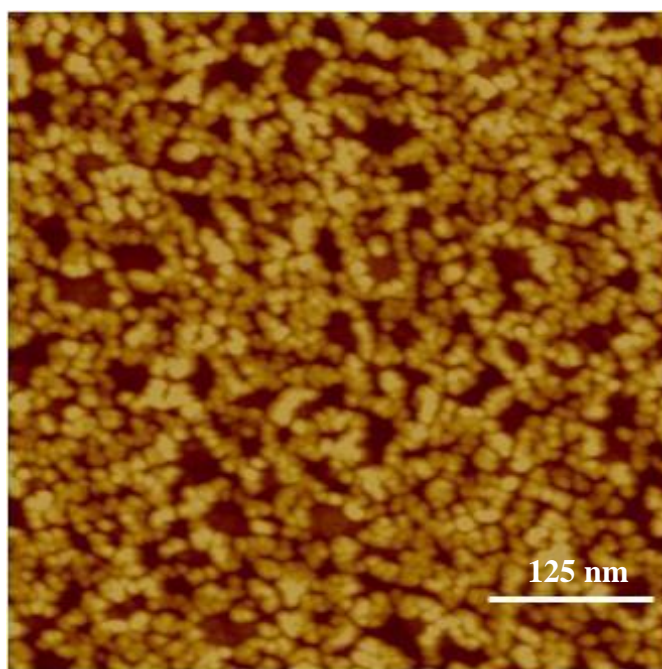


**Figure 3.7:** AFM image of gold substrate following self-assembly of AP (protein concentration: 3  $\mu\text{g/ml}$ ). The area corresponds to 500 nm x 500 nm scans [334].

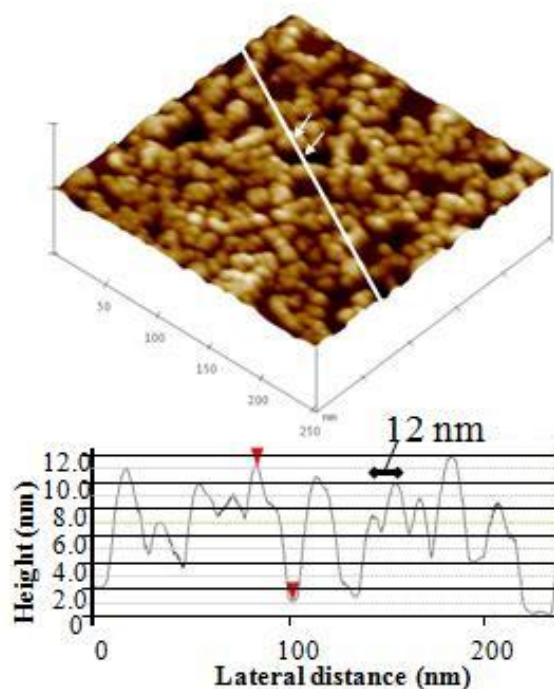


**Figure 3.8:** Digitally magnified Figure 3.7 is represented in pseudo-3-dimensional presentation at 150 nm x 150 nm area to show surface topography following the immobilization of AP [334].

The SPR experiments were also conducted on gold substrate to study binding kinetics of the fusion product. Through these studies, the overall coverage of the enzyme on the gold surface was also calculated. Firstly, the control experiments for binding studies were carried out using the control AP where we know that the enzyme alone can non-specifically bind to gold. The molecular adsorption profiles of the 5GBP1-AP, however, reveal a significant increase in adsorption, due to material specific binding activity provided to the enzyme by the gold binding peptide (Figure 3.9). As a result, based on the Langmuir adsorption model fit to both sets of the SPR data, it is found that 5GBP1-AP displays a higher surface coverage than that of the control AP (Figure 3.10). Based on the model, the calculated kinetic parameters for both enzymes are tabulated in Table 3.1. Depending on the concentration used, 5GBP1-AP reached to nearly 90% surface coverage with an equilibrium adsorption constant ( $K_{eq}$ ) of  $1.65 \times 10^8$  [334]. This value is comparable to the adsorption of alkanethiol on gold, the first step for the gold surface functionalization prior to protein immobilization in conventional chemical approaches [339, 340].

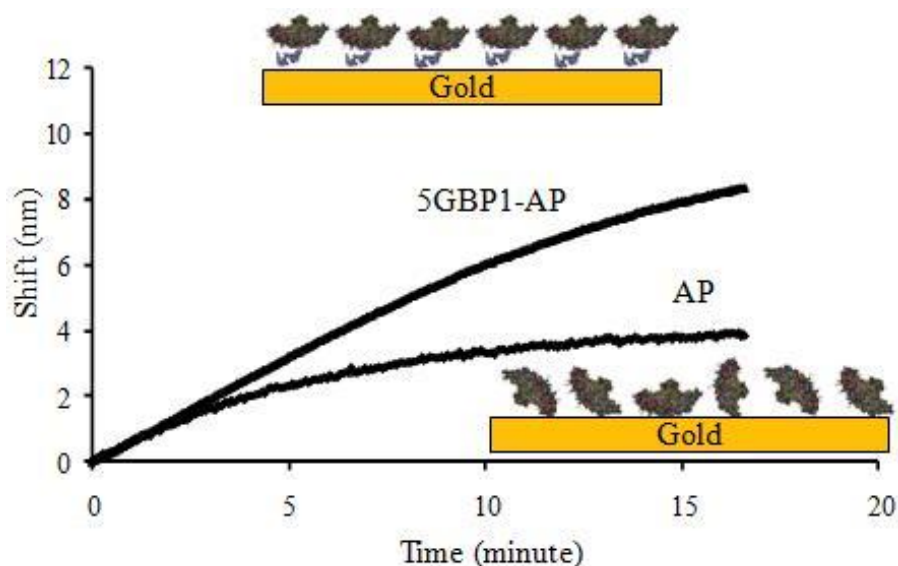


**Figure 3.9:** SPR spectroscopy results of AP and 5GBP1-AP binding to bare gold surfaces at 4  $\mu\text{g/mL}$  concentration (“Shift” corresponds to the change in the dip position of the SPR). The schematics in the figure show possible scenarios for directed and non-specific immobilization of the enzyme, respectively [334].

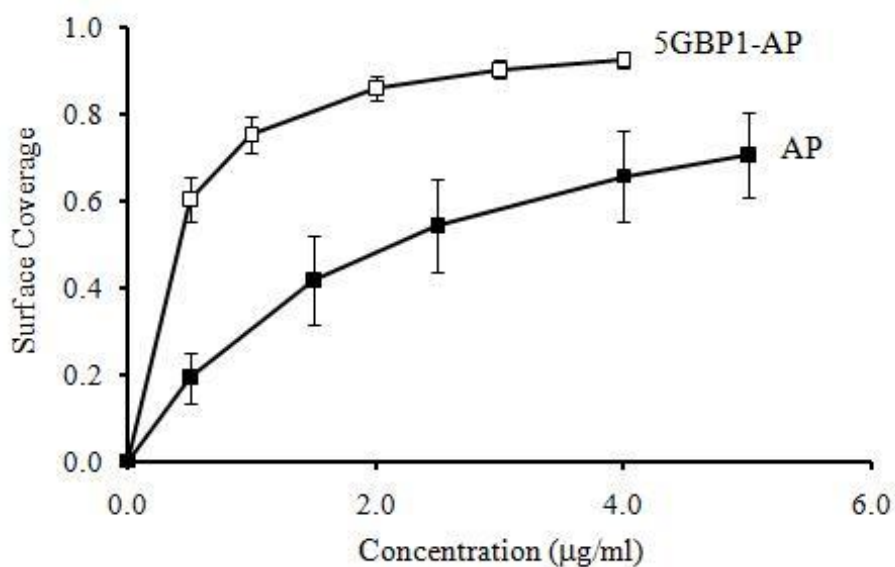


**Figure 3.10:** Surface coverage of AP and 5GBP1-AP has been calculated using the Langmuir isotherm model based on the SPR experiments [334].

**Table 3.1:** The parameters of binding kinetics for 5GBP1-AP and AP on bare Au surfaces obtained by SPR [334].

	$k_a [\text{M}^{-1}\text{s}^{-1}]$	$k_d [\text{s}^{-1}]$	$K_{eq} [\text{M}^{-1}]$
AP	$1.35 \pm 0.26 \times 10^4$	$6.00 \pm 0.16 \times 10^{-4}$	$2.24 \pm 0.22 \times 10^7$
5GBP1-AP	$3.19 \pm 0.12 \times 10^4$	$1.94 \pm 0.05 \times 10^{-4}$	$1.65 \pm 0.12 \times 10^8$

### 3.1.3 Peptide Mediated Self-Immobilization of Enzyme on Micro-Patterned Surfaces

As mentioned in Section 1.3, protein array technologies necessitate efficient patterning of biomolecules on selected micro-patterned substrates providing spatial immobilization on an inorganic surface. This is possible using various lithography techniques, for example, soft lithography [153], dip-pen lithography [185], and photolithography [341]. Taking advantage of the gold binding activity of the 5GBP1-AP fusion construct, in this section, we studied whether the enzyme could be directed-assembled on a patterned substrate. Among a variety of pattern fabrication methods, micro-contact printing ( $\mu$ CP) has proven to be a versatile technique which does not necessitate the use of expensive traditional lithographic equipments [153]. Using  $\mu$ CP, therefore, a variety of biological molecules can be patterned on solid surfaces with sub-micron features over a large area ( $>1\text{cm}^2$ ). For pattern formation, oligo(ethylene glycol)-terminated alkanethiols ( $\text{OH}-(\text{OCH}_2)_3\text{-SH}$ ) are generally used which are known to resist protein adsorption on to gold [342]. The remaining, bare, gold regions are then functionalized using thiolatemolecules designed for the desired protein coupling. Rather than the two-stage thiol linkage for protein immobilization, here, the peptide-based linkage of the fusion enzyme was examined. It should be pointed out that the position of the GBP insertion, at the N-terminus of AP, is opposite to the active site of the enzyme (as depicted in the inset of Figure 3.9) [334].

As demonstrated in Figure 3.11, and described in Materials and Methods Section, micro-patterned substrates that effectively cover large areas of the surface (millimeters) with a SAM, specifically, oligo(ethylene glycol)-terminated alkanethiols, providing a few mm-diameter circular, bare gold regions were prepared. The effect of the immobilization protocol on the efficiency of adsorption and in the enzyme activity was explored by using either the AP alone or the 5GBP1-AP fusion. The AFM images (Figure 3.12-3.15, recorded in tapping mode with silicon cantilever at scan rate= 1.5 Hz) show that both the wild-type and the hybrid construct bind to the gold regions of the patterned surface. However, the molecular packing is denser (high number density of enzyme immobilized) and more homogenous in the case of 5GBP1-AP compared to the wild-type AP (Figure 3.12 vs. 3.14). In fact, the coverage area of 5GBP1-AP, determined by AFM, was ~40% higher than that of AP alone (Figure 3.13 vs. 3.15) [334].



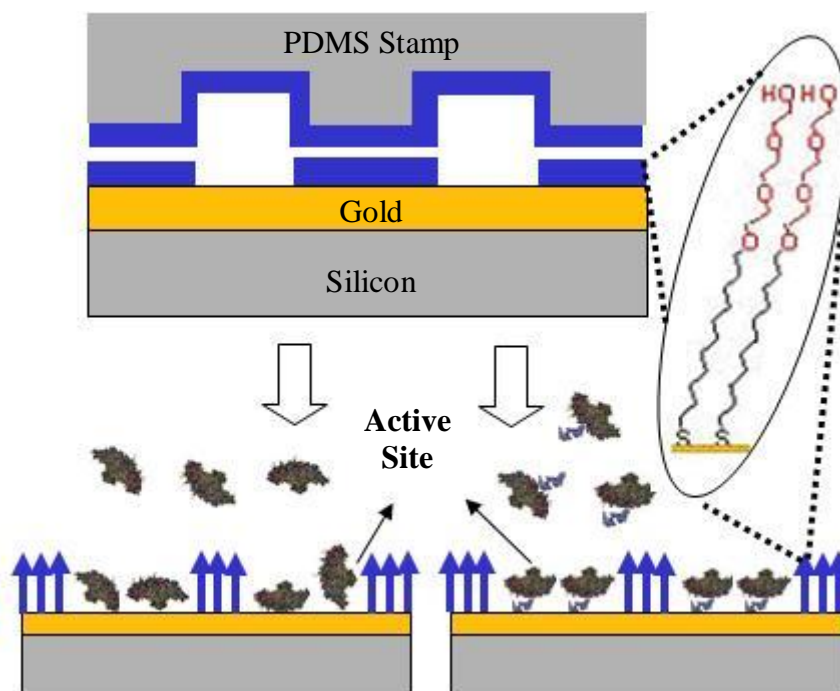


**Figure 3.11:** Schematic representation of the experimental procedure for the generation of two-dimensional arrays of immobilized proteins on a patterned substrate fabricated through  $\mu$ CP (black arrows show active site of the enzyme) [334].

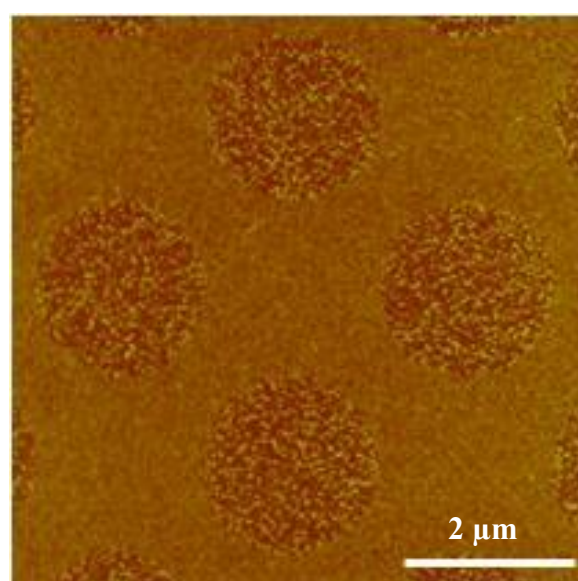


**Figure 3.12:** Topographic image of the microarray of immobilized AP [334].

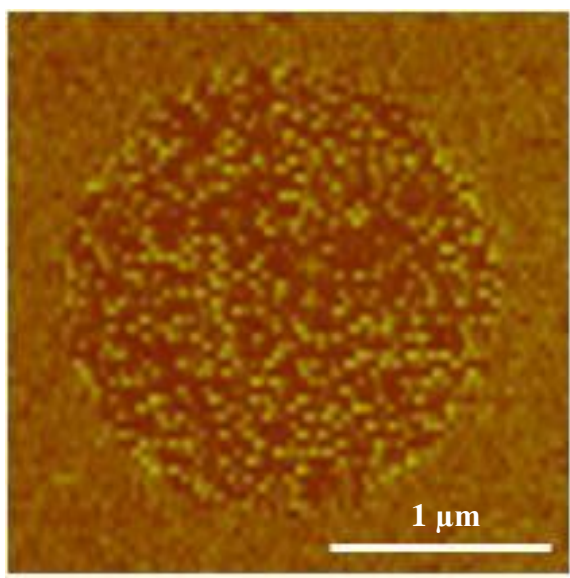


**Figure 3.13:** AFM image of the microarray of immobilized AP at higher magnification [334].

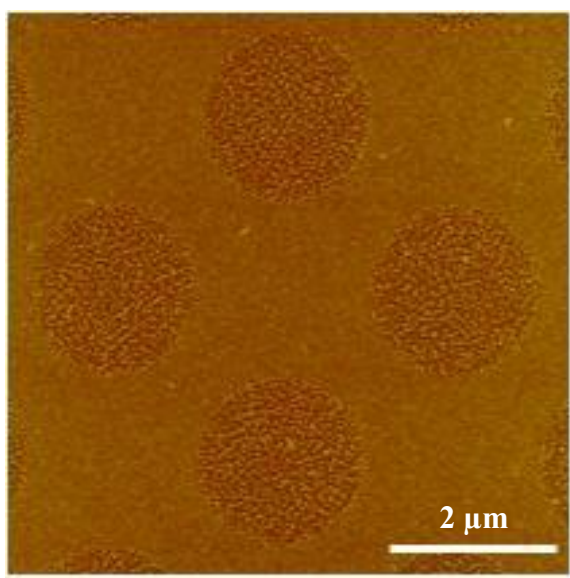


**Figure 3.14:** Topographic image of the microarray of immobilized 5GBP1-AP [334].



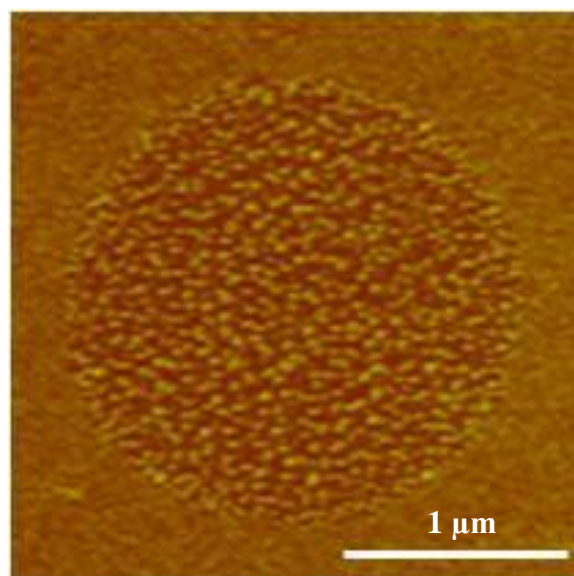


**Figure 3.15:** AFM image of the micro-array of immobilized 5GBP1-AP at higher magnification [334].

In the present experiments, the enzyme was immobilized on the gold substrate while keeping the same amount of free enzyme in solution as the reference. The prepared solution, incubated at room temperature, was assayed to quantify the enzymatic activity (see Materials and Methods Section) which was assessed under several different conditions. First, the amount of enzyme activity transferred from solution to the non-patterned gold surface was estimated. To assess this, the percentage of retained enzymatic activity by taking the ratio of the activity on the surface to that in the solution was calculated. It was found that, when immobilized; only 2% ( $\pm 0.4$ ) of wild-type AP activity was transferable onto non-patterned gold surface, whereas in case of 5GBP1-AP, transferable activity to the surface was 66% ( $\pm 0.6$ ). The enzymatic activities obtained from both the non-patterned and the micro-patterned substrates were normalized by the corresponding surface area of the substrate available for binding (Figure 3.16). This yielded a value (in  $\mu\text{mol}/\text{min}/\mu\text{m}^2$ ) of  $\sim 1.8$  times higher for 5GBP1-AP as compared to the wild-type AP even on the non-patterned surfaces [334]. This result also supports our earlier findings discussed above in reference to the AFM (Figure 3.5-3.8) and SPR (Figure 3.9 and 3.10) analyses in which higher and more homogenous coverage of 5GBP1-AP were observed compared to a lower coverage and non-homogenous immobilization of the wild-type AP. Similar to above, the enzyme activity on the micro-patterned-substrates was also investigated (Figure 3.12-3.15) [334]. In general, one observes an increase in the enzymatic activity of both the wild-type and fusion enzymes when

targeted immobilized on the micro-patterned surfaces (Figure 3.16). The increase, however, was more prominent in the fusion protein with the GBP linker than when this linker was absent. In fact, the immobilization of the AP enzyme with GBP linker on the patterned surface resulted in three times higher enzymatic activity compared to the wild-type AP on the non-patterned substrate. Here, the double-advantage of using genetically engineered peptide for inorganics (GEPI) as the fusion linker as well as the effect of assembly in a confined area as a result of patterning was effective simultaneously to result in enhanced performance of the enzyme. While a GEPI allows the control of immobilization of the enzyme relative to the substrate, the high number density of packing possibly increases the folding stability of the protein [343]. The key parameter in the process of immobilization of enzymes onto a solid surface is the ability to keep the active site available for the catalytic reactions for high efficiency while maintaining the stability of the enzyme on the solid surface [344, 345]. Various residues or domains of a given protein may interact with a given solid. These interactions are often non-specific and result in protein adsorption with loss of function as well as a loss of long term stability [346]. As schematically shown in the inset of Figure 3.9, non-specific binding of AP may lead to the blocking of the active site of the enzyme which, in turn, may cause a loss of AP activity. In this context, the GBP1 linkage provides an oriented self-immobilization of the enzyme with retained activity, as demonstrated here. Our results also show that enzymatic activity per unit area can be enhanced by directing the fusion construct on to spatial locations on a micro-patterned surface via directed assembly using the inorganic binding peptide. Here, it may be suggested that directed assembly provides the self-localization of the molecular construct on a confined surface leading to a higher number of protein adsorption per unit surface area. Therefore, the inorganic binding peptide, that is, GBP1, not only provides specific adsorption onto gold substrate but it also, through its genetic fusion, allows oriented immobilization of enzyme leaving its catalytic site available to carry out the reactions relatively freely. The molecular platform used here can be utilized successfully for self-immobilization of enzymes in their biologically active state on any solid materials (silica, graphite, etc.) using the appropriate GEPI linker specific to that substrate, for example, silica binding peptide for silica surface, graphite-binding peptide for graphite, and gold binding peptide for gold surface [334].

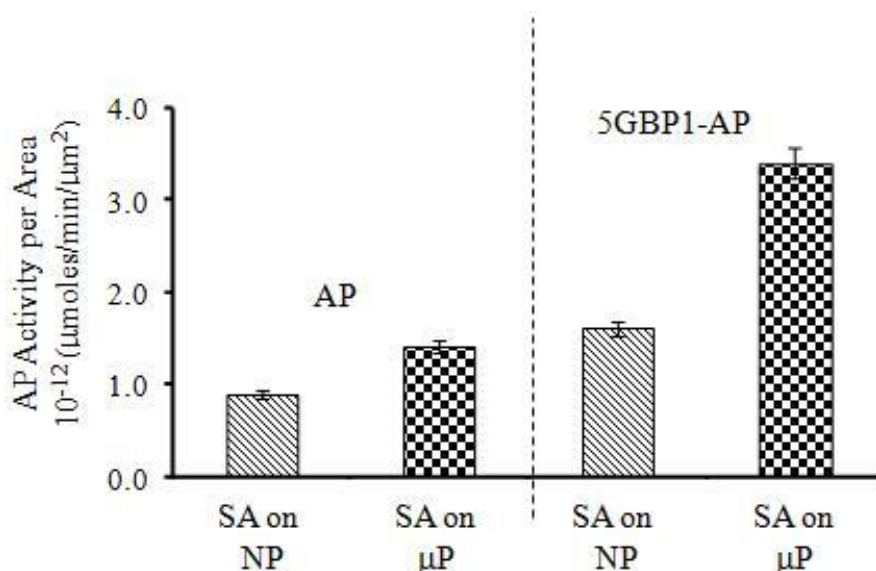


**Figure 3.16:** The calculated AP activities per unit area for AP and 5GBP1-AP corresponding to self-assembly (SA) of each enzyme on the non-patterned (NP) and micropatterned ( $\mu$ P) gold substrates. The AP activity per unit area for both enzymes was obtained by normalizing the activity of enzyme by the corresponding surface area available ( $22.4 \times 10^6$  and  $64.0 \times 10^6 \mu\text{m}^2$  for micro-patterned and non-patterned, respectively) [334].

As observed, the enzyme activity of the bare AP ( $28.8 \times 10^{-4} \mu\text{mol/min}$ ) is approximately fifteen times higher than that of the 5GBP1-AP fusion protein when measured in solution. Therefore, it appears that the enzyme does lose its activity in the hybrid form. However, this should not necessarily be a general trend for all enzymes. Here, the hybrid constructs comprising of different repeat number of the gold binding peptide at the N-terminus of the AP may not be the ideal site for fusion. Therefore, to obtain the optimum enzymatic performance, one may need to perform a genetic search for a permissive site [347]. The knowledge of the permissive site, therefore, would provide the position for genetic fusion of the inorganic-binding peptide on to the molecule with the highest retained enzymatic activity while also allowing solid binding functionality of the fusion. Furthermore, many proteins do bind to gold surface non-specifically; therefore other solids, most notably, silica, may be a better substrate for enzyme immobilization through inorganic silica-binding peptide [335]. Finally, the possible “confinement effect” observed here on the patterned surface caused higher enzyme activity because of the higher number of “correctly” immobilized and homogeneously distributed enzymes in a confined space. This may be due to the limited surface area available for enzyme

immobilization for a given concentration from the solution. While the inorganic binding activity of the fused GEPI allows solid binding and proper display (orientation) of the enzyme on the solid surface, the area confinement may also increase the high density assembly and, therefore, the activity of the enzyme [334].

### **3.2 Nanoparticle Immobilization through Self-assembly of GEPI**

#### **3.2.1 Gold nanoparticle immobilization on glass**

Beside proteins, as a linker, GEPI has also potential use to immobilize nanoparticles. Previously, another gold binding peptide (3R-GBP) was used for the assembly of gold nanoparticles on gold surface [285]. Here, to immobilize gold nanoparticles, the gold binding peptide (AuBP1) and the quartz binding peptide (QBP1), isolated and characterized by Sarikaya group [298, 304], were chemically fused together *via* either a flexible triplet of Glycine (GGG) or a rigid bridge of Proline triplet (PPP), yielding bifunctional peptides (Bi-GEPIs). Also, each inorganic binding sequence was placed at either N- terminus or C-terminus. All of the chemically synthesized peptides used for this work are listed in Table 2.1, including each one's sequence, molecular weight (MW), isoelectric point (pI) as well as net charge at pH 7.4 (working pH). It should be noted that Lysine (K) and Arginine (R) are always positively charged at neutral pH so that the peptide sequences that have these amino acid residues are also positively charged at pH 7.4.

The bifunctionality of the peptides was simply tested in gold and silica nanoparticle immobilization in which peptides were used as linkers between the substrate and the nanoparticle. Figure 3.17 shows a schematic illustration of experimental procedure including peptide assembly and nanoparticle immobilization steps. Subsequently, the samples were examined using AFM and optical microscope dedicated for DF imaging. Since nanoparticles scatter the white light efficiently, DF imaging is very fast characterization technique to monitor the attachment. However, to be able to get detailed information on surface coverage at atomic scale, we reasoned to utilize AFM.

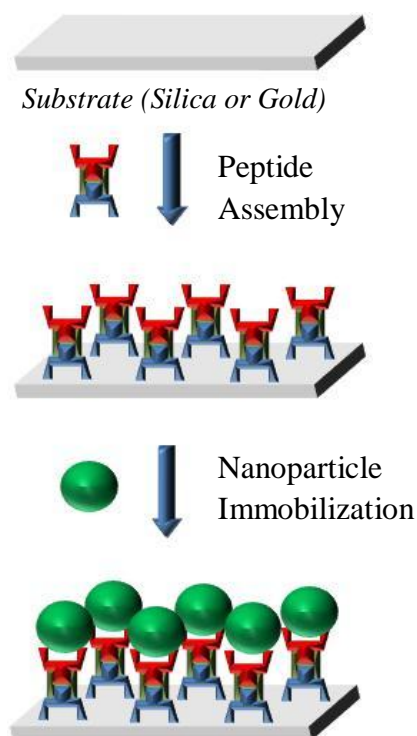


**Figure 3.17:** Procedure for GEPI directed nanoparticle immobilization.

The first experiment demonstrates the control experiments for gold nanoparticle attachment on glass substrates. For the control, gold binding region (AuBP1) alone as well as silica binding region (QBP1) alone was used as linker. After the protocol in Figure 3.17 was performed with the control peptides, the substrates were scanned under optical microscope with dark-field conditions. There was no successful gold nanoparticle attachment but only few particles due to the non-specific interactions (Figure 3.18 and Figure 3.19). There was another control experiment where the glass substrate was treated with blank PBS buffer instead of any peptide treatment. Similar to the former controls in Figure 3.18 and Figure 3.19, no gold immobilization was observed (Figure 3.20).

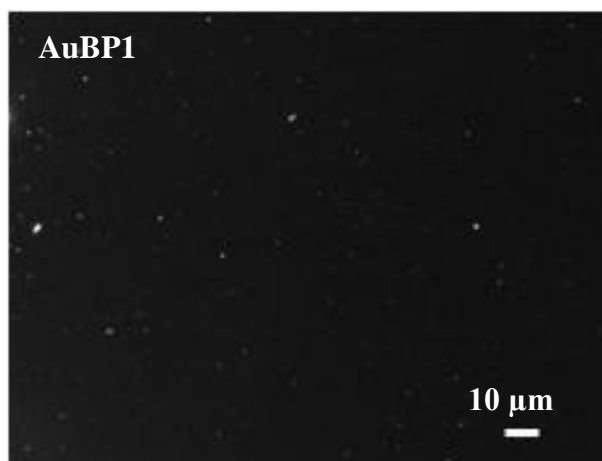


**Figure 3.18:** DF image of gold nanoparticle immobilization on glass using AuBP1.

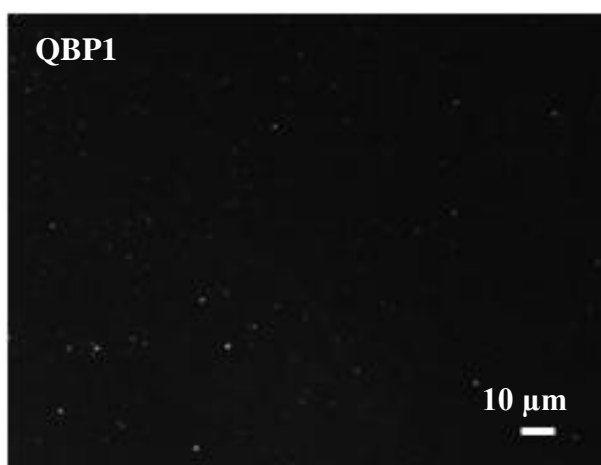


**Figure 3.19:** DF image of gold nanoparticle immobilization on glass using QBP1.

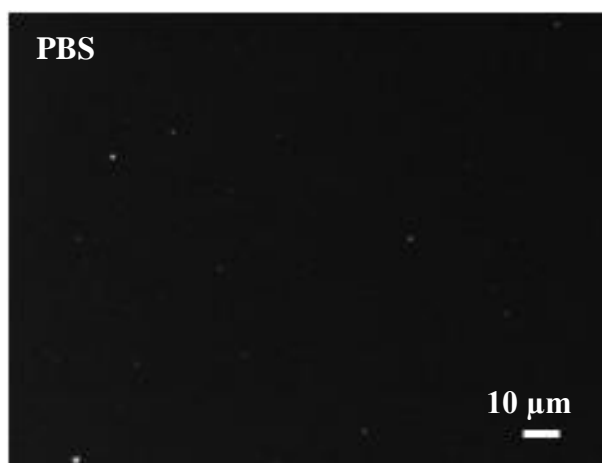


**Figure 3.20:** DF image of gold nanoparticle immobilization on glass treated only with PBS.

Secondly, the same procedure (Figure 3.17) was repeated with Bi-GEPI1-4. Among the resultant substrates, those treated with Bi-GEPI-1 and Bi-GEPI-2 have higher surface coverage obtained from immobilized gold nanoparticles (Figure 3.21 and 3.22). The net charge of peptides at the working pH would be a crucial point, due to the electrostatic interactions between the peptides and the glass surface as well as between the nanoparticles and the peptides. Since gold nanoparticle and all peptide solutions are at pH 7.4, the net charge of each peptide at the same pH is considered (Table 2.1). In the experimental procedure depicted in Figure 3.17, firstly, the peptide assembly brings the peptides into contact with the negatively charged glass surface. As the second step, gold nanoparticles electrostatically stabilized by the negative citrate anions are incubated with the same substrate. If the electrostatic interaction was the only case, all Bi-GEPIs and AuBP-1 that have positive charge, would work for the negatively charged gold nanoparticle attachment on negatively charged glass surface. In addition, regardless to the triplet linker placed in between the gold and silica binding sequences, Bi-GEPI-1 and -2 (Figure 3.21 and 3.22) in which QBP-1 sequence is at the N-terminus showed better gold nanoparticle attachment comparing to Bi-GEPI-3 and Bi-GEPI-4 (Figure 3.23 and 3.24). The reason might be that the assembly of Bi-GEPI-1 and -2 on glass results in structural changes on the surface yielding a favorable conformation of gold binding region for the further binding to nanoparticle. However, in the case of Bi-GEPI-3 and -4, either peptide assembly on the surface may hinder the gold binding region resulting low yield in nanoparticle attachment or placing the gold binding region at the N-terminus may decrease the peptide's affinity towards silica.

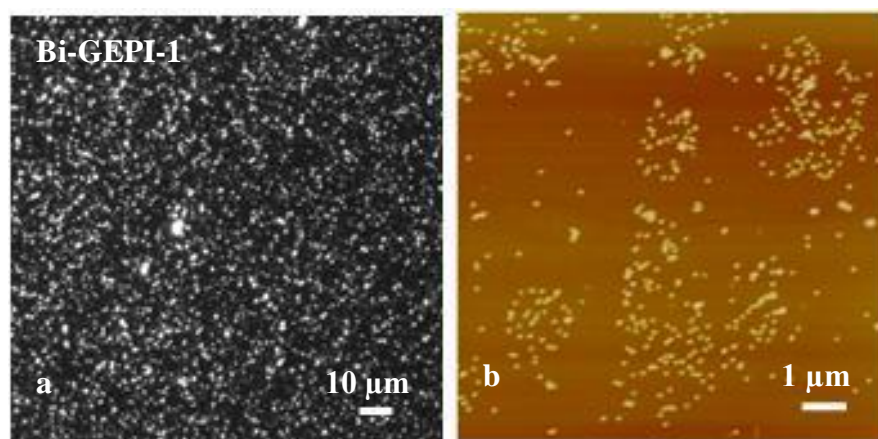


**Figure 3.21:** (a) DF and (b) AFM images of gold nanoparticle immobilization on glass using Bi-GEPI-1.

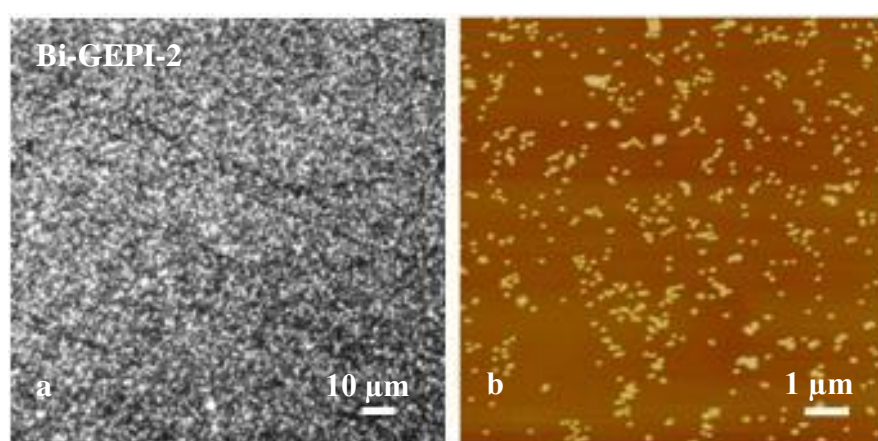


**Figure 3.22:** (a) DF and (b) AFM images of gold nanoparticle immobilization on glass using Bi-GEPI-2.

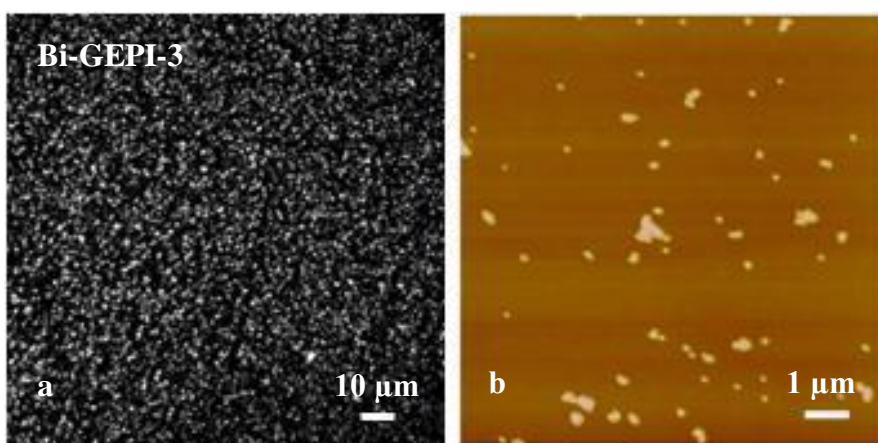


**Figure 3.23:** (a) DF and (b) AFM images of gold nanoparticle immobilization on glass using Bi-GEPI-3.



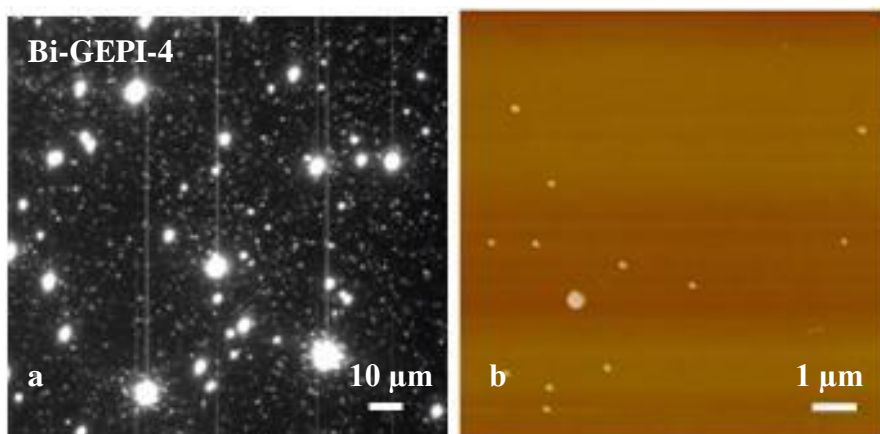


**Figure 3.24:** (a) DF and (b) AFM images of gold nanoparticle immobilization on glass using Bi-GEPI-4.

### 3.2.2 Silica nanoparticle immobilization on glass

Parallel to the gold nanoparticle attachment on glass surface, the Bi-GEPIs were also used as linker to immobilize silica nanoparticles on gold coated glass substrate. As the control, similar to gold nanoparticle immobilization, the procedure was repeated on the gold surface using either AuBP1 or QBP1 peptide or blank buffer as the peptide assembly step. DF imaging shows that these controls cannot lead to successful silica nanoparticle immobilization (Figure 3.25-3.27).

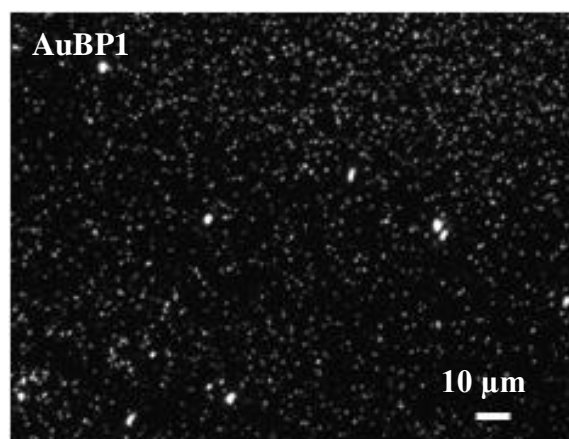


**Figure 3.25:** DF image of silica nanoparticle immobilization on gold using AuBP1.

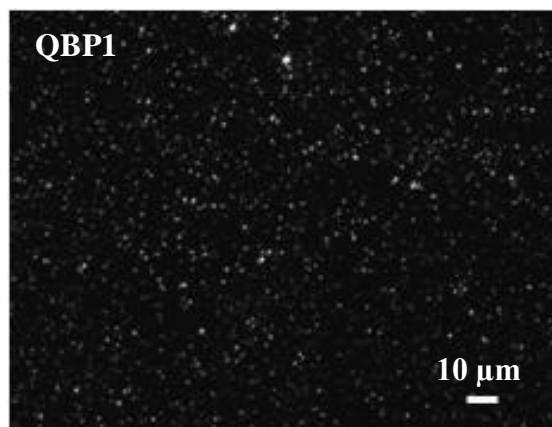


**Figure 3.26:** DF image of silica nanoparticle immobilization on gold using QBP1.

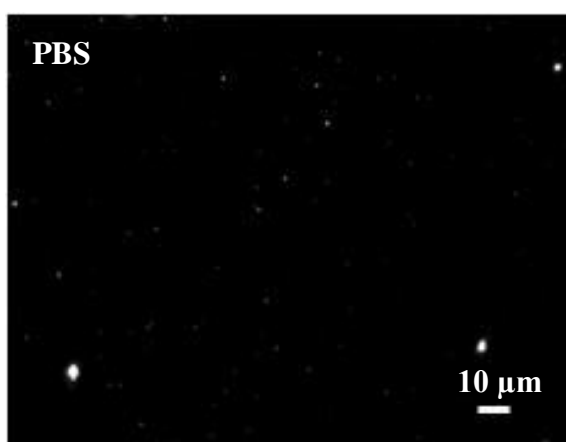


**Figure 3.27:** DF image of silica nanoparticle immobilization on gold treated only with PBS.

Next, following the experimental procedure shown in Figure 3.17 was employed for each bifunctional peptide; the gold substrates were scanned under AFM and dark-field. However, in the case of bifunctional peptides, the results indicate that all Bi-GEPIs can work for the silica attachment on gold surface (Figure 3.28-3.31). Based on the AFM results, almost complete surface coverage was achieved. Here, it is clear that Bi-GEPIs retain silica binding activity upon their self-assembly on gold film, regardless to our choices for spacer and flanking of the inorganic binding regions. Assembly of Bi-GEPIs on gold film can change the conformation of the peptides in which gold binding region is brought to the contact with the gold surface whereas silica binding region is become accessible for the nanoparticle. Again, it is really hard to state that this is just the issue of electrostatic interactions since positively charged AuBP1 shows very poor performance in negatively charged silica nanoparticle attachment (Figure 3.25).

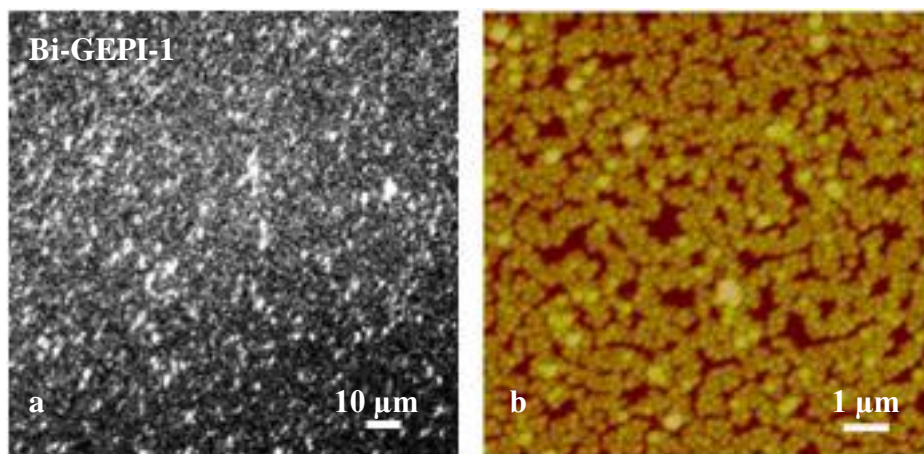


**Figure 3.28:** (a) DF and (b) AFM images of immobilized silica nanoparticles on gold through Bi-GEPI-1 assembly.

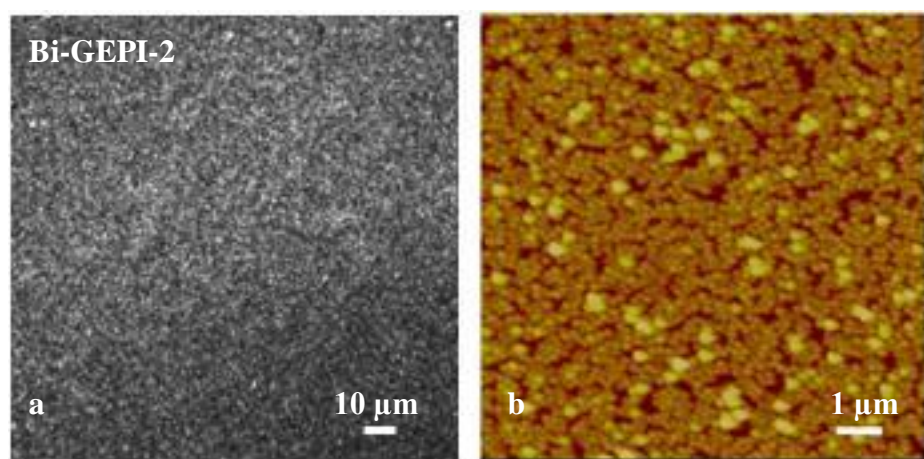


**Figure 3.29:** (a) DF and (b) AFM images of immobilized silica nanoparticles on gold through Bi-GEPI-2 assembly.

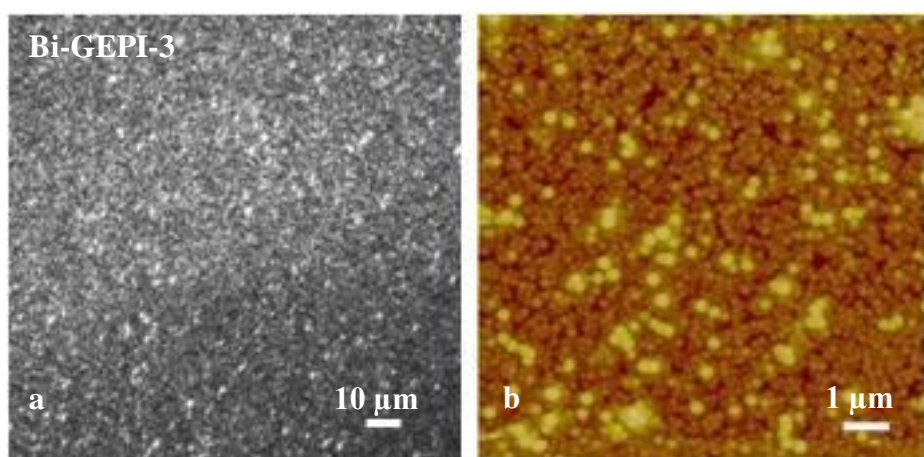


**Figure 3.30:** (a) DF and (b) AFM images of immobilized silica nanoparticles on gold through Bi-GEPI-3 assembly.

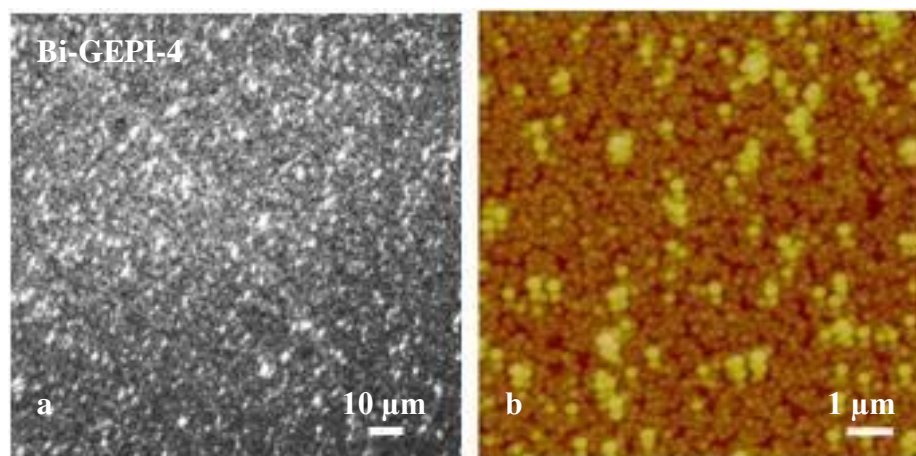


**Figure 3.31:** (a) DF and (b) AFM images of immobilized silica nanoparticles on gold through Bi-GEPI-4 assembly.

It is possible that the structure of the Bi-GEPIs on the inorganic surface may change due to self-assembly of the peptides. Bi-GEPI-1 and -2 still protect the binding site for the next nanoparticle, *i.e.*, gold or silica attachment even after their immobilization on the solid platform, *i.e.*, silica or gold. It is certain that GEPI-directed nanoparticle immobilization on inorganic substrates was achieved, through simple assembly procedure and under ambient conditions. Here, the results show that location of the binding regions is important and QBP1 site should be at the N terminus of the bifunctional GEPI in the case of gold and silica nanoparticle attachment. Moreover, the linker choice may also affect the bifunctionality. The rigid linker, triplet of prolin, showed better performance for both gold and silica nanoparticle attachment.

### 3.2.3 Silver nanoparticle immobilization on glass

Similar to gold nanoparticle assembly, silver nanoparticle attachment on glass substrate was also studied using Bi-GEPI-5 comprising of silver binding sequence fused to quartz binding sequence through Gly triplet, as linker. Here, the procedure in Figure 3.17 was applied with Bi-GEPI-5 and the controls, *i.e.* AgBP1, QBP1 and PBS alone. None of the control experiments shows successful silver attachment under Dark-field (Figure 3.32-3.34).

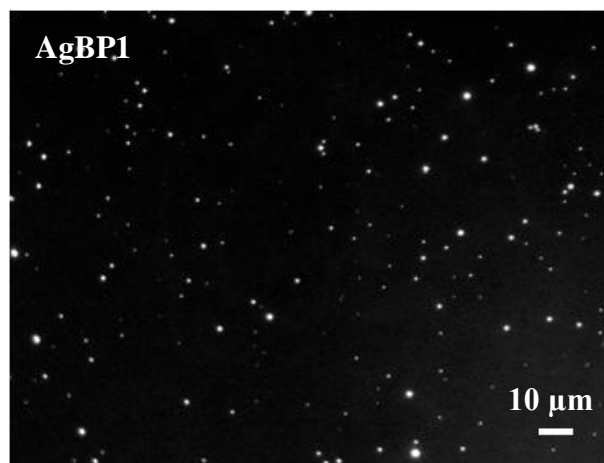


**Figure 3.32:** DF image of silver nanoparticle immobilization on gold using AgBP1.

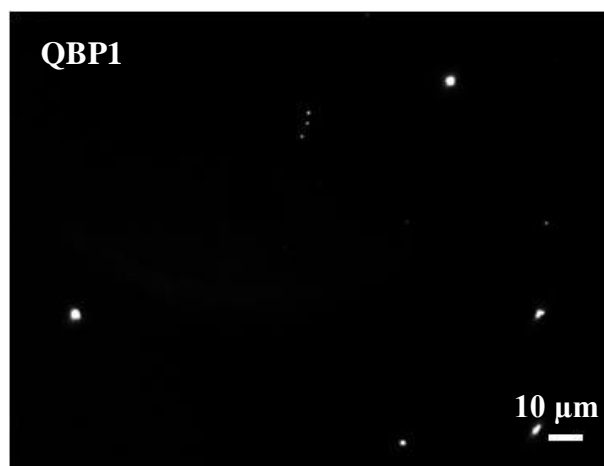


**Figure 3.33:** DF image of silver nanoparticle immobilization on gold using QBP1.

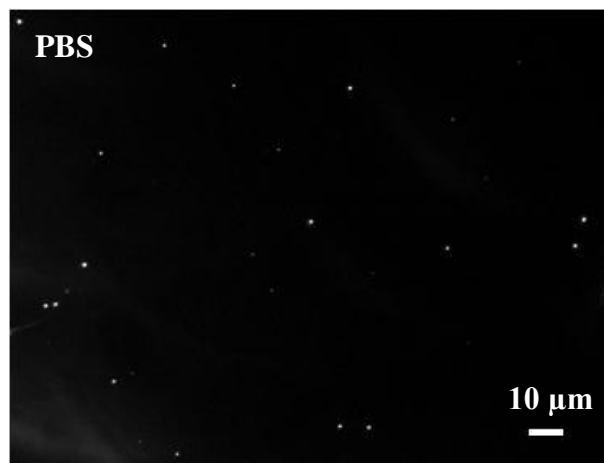


**Figure 3.34:** DF image of silver nanoparticle immobilization on glass treated only with PBS.

However, DF characterization indicated the assembly of silver nanoparticles on the glass surface pre-functionalized with Bi-GEPI-5 (Figure 3.35) since the linker provided the bridging between silver nanoparticle and the glass. The large bright spots are attributed to the silver nanoparticle agglomerates in the figure.

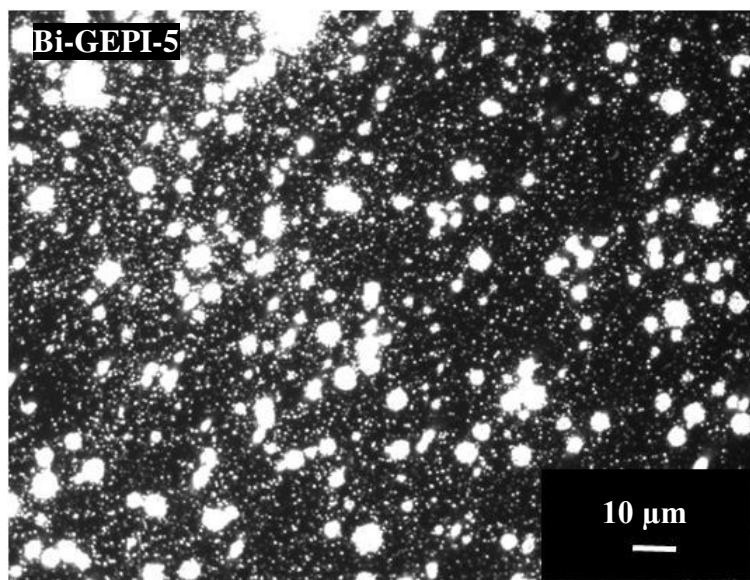


**Figure 3.35:** DF image of silver nanoparticle immobilization on glass using Bi-GEPI-5.

Overall results for the nanoparticle immobilization are convincing; the procedure for the attachment is very simple and efficient under ambient conditions. Using bifunctional GEPI, assembly of different types of nanoparticles *i.e.* gold, silver and silica is favorable on inorganic surfaces *i.e.* gold and silica.

### 3.3 Micropatterning of Nanoparticles and Fluorophores on Silica

#### 3.3.1 Micro-contact printing of FITC through Quartz Binding Peptide

In this section, micropatterning of two different photoactive target molecules, fluorescent quantum-dot nanocrystals and fluorescein, on quartz surface, immobilized via quartz-binding peptides was demonstrated (see Materials and Methods Section). The fabrication process incorporates a combination of microcontact printing and directed self-assembly processes successively. The patterned substrates were examined using fluorescence microscopy to demonstrate the bifunctionality and the quality of the pattern fabrication. The results show that the attachment of quantum dots or photoactive molecules on a substrate is material-specific. For example, when



silica is the substrate, a quartz-binding peptide (QBP) is successfully used as the linker whereas none of the QBP sequences worked on a gold substrate for the attachment of those fluorophores.

Here, QBP1 and QBP2 sequences were specifically chosen as strong and weak binders to quartz surfaces, respectively. The molecular binding characteristics of these two peptides have been quantitatively determined using various techniques, including surface plasmon resonance spectroscopy (SPR) [304]. Based on the SPR data, the apparent adsorption rate constants ( $k_{\text{observable}}$ ) of QBP1 and QBP2 were calculated to be  $0.43 \text{ s}^{-1}$  and  $0.068 \text{ s}^{-1}$ , respectively. The  $k_{\text{observable}}$  values represent the initial adsorption rates for each of the peptides on the silica surface (Appendix A1). For use as molecular inks in the PDMS stamping experiments, both peptides were chemically synthesized and were then either biotinylated, namely QBP-bio, or conjugated with fluorescein via the reactive isothiocyanate group, QBP-F. The QBP-bio conjugates were then labeled with fluorescent quantum-dot nanocrystals (QD) linked to streptavidin protein (SA-QD) [335]; here SA is known to have strong molecular recognition to biotin.

The first experiment demonstrates micropatterning of a functional target molecule (fluorescein) conjugated to QBP1 onto a quartz surface using microcontact printing. Figure 3.36 shows a schematic illustration describing the PDMS stamping of the QBP1-F conjugate molecules used as ink. In this experiment, fluorescein was chosen as the target molecule, due to its chromogenic property resulting in the emission of green light at  $\lambda = 530 \text{ nm}$ . As a control, fluorescein was attempted to stamp on the quartz substrate alone. As shown in Figure 3.37, there is no contrast when the patterned substrate was imaged through a fluorescein isocyanate (FITC) filter using a fluorescence microscope. The result of this control experiment indicates that the target molecule by itself has no affinity to quartz substrate. Then fluorescein-conjugated molecule, QBP1-F, as the molecular ink was used to produce a pattern on the quartz substrate, following the stamping procedure shown in Figure 3.36. The fluorescence microscopy image in Figure 3.38 clearly reveals high contrast, in which the green lines are indicative of the micropatterned QBP1-F molecules. Besides fluorescein, the procedure was repeated using an Albumin–fluorescein isothiocyanate conjugate, BSA-F, as another control molecule (Figure 3.39) [335].

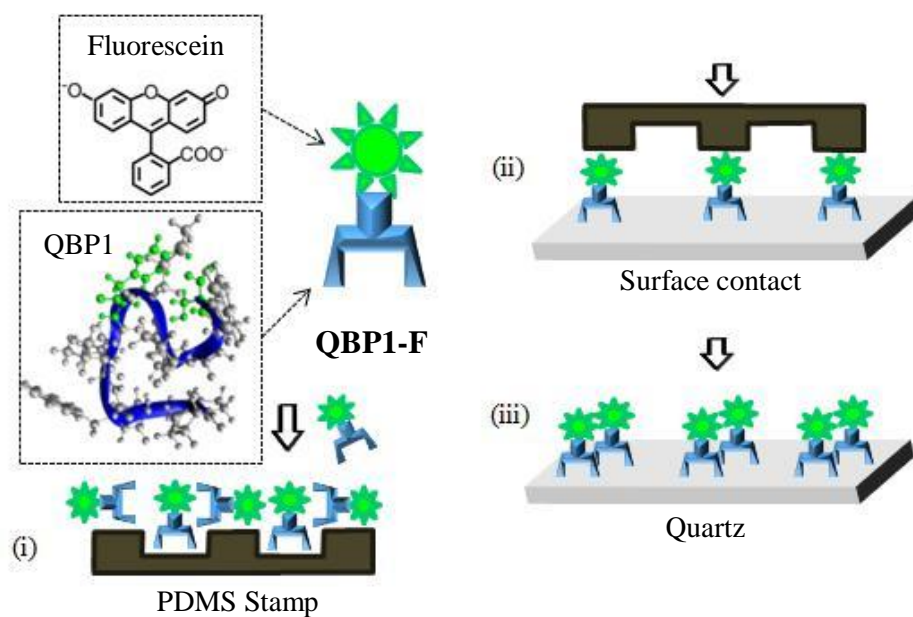


**Figure 3.36:** Schematic representation for PDMS patterning of QBP1-F on quartz [335].

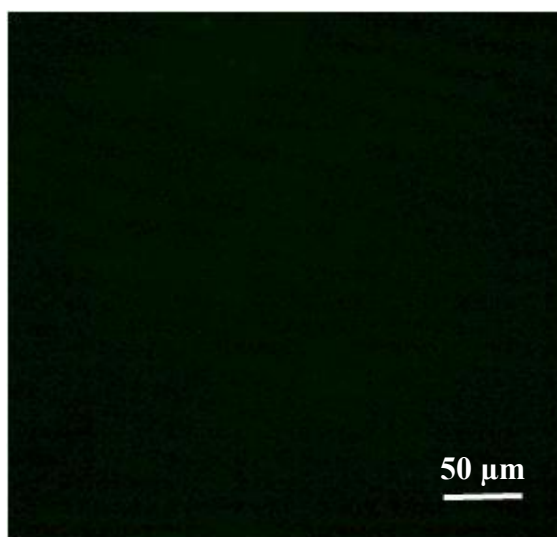


**Figure 3.37:** FM image of the quartz substrate after micropatterning with fluorescein alone, as the control [335].



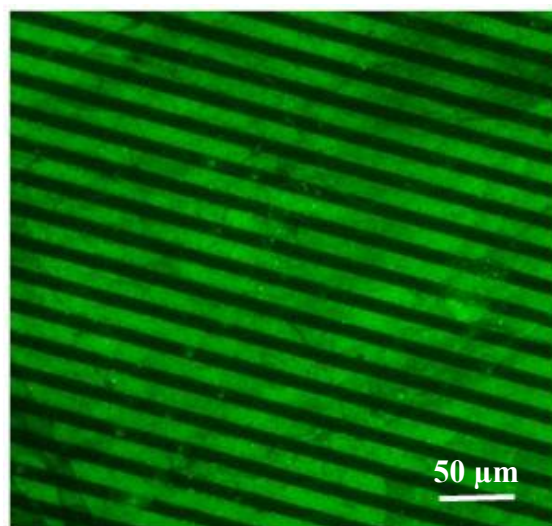


**Figure 3.38:** FM image of the quartz substrate after micropatterning with QBP1-F [335].

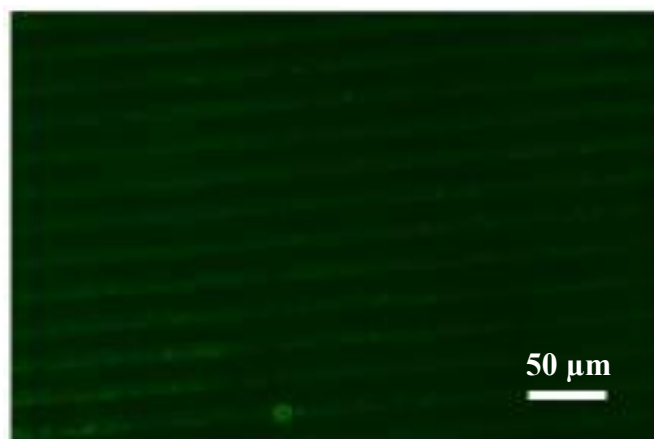


**Figure 3.39:** FM image of the quartz substrate after micropatterning with BSA-F, as another control [335].

Comparison between the fluorescence intensity measurements recorded from these three samples (Figure 3.37-3.39) clearly shows that the QBP1-mediated fluorescein-molecule immobilization was an order of magnitude more efficient than that mediated by BSA (Figure 3.40). This result demonstrates the utility of the inorganic-binding peptide, i.e., QBP1, as a linker mediating the immobilization of a fluorescent molecule, fluorescein, on silica using the microcontact printing technique.

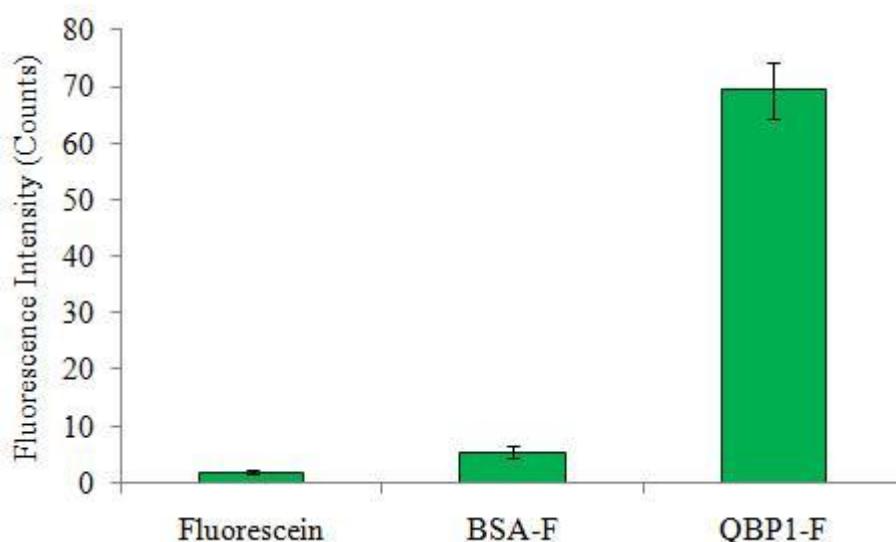


**Figure 3.40:** Comparisons of fluorescence intensity of fluorescein molecules immobilized through itself, BSA and QBP1 [335].

Also, PDMS stamps with different types of micro reliefs were fabricated to produce different micropatterns of fluorescein molecule linked to QBP1 on glass surface (Figure 3.41 and Appendix A2). Results show that QBP1 can also produce successful micropatterns on glass surface as it does on quartz.

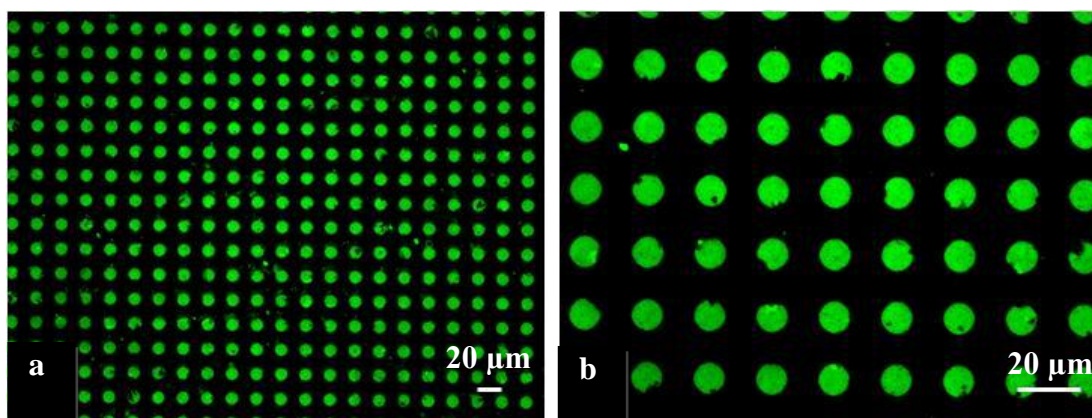


**Figure 3.41:** FM images of the micropattern of QBP1-F on glass surface at (a) lower and (b) higher magnifications.

### 3.3.2 Co-immobilization of QD and FITC using Quartz Binding Peptide

Parallel to the experiment in previous section, the biotinylated QBP was utilized as an ink for microcontact printing to generate a micropattern of a probe, *i.e.*, biotin, conjugated peptide. This way, the fabricated pattern would be biofunctional against streptavidin, and could be used as a template for the assembly of streptavidin-coated QDs through biotin-streptavidin molecular recognition. In this case, we first used a

PBS buffer (phosphate buffered saline) alone as the control experiment, stamping it on the quartz surface using PDMS, to produce a PBS pattern that was then incubated by SA-QD. The result show that the PBS buffer alone used as an ink does not allow immobilization of QDs (Appendix A3). The utility of QBP-bio as a PDMS ink to generate a functional micropattern is shown schematically in Figure 3.42. The micropatterned surface would then be incubated with SA-functionalized QDs, allowing its directed immobilization only on the stamped regions. Here, both strong and weak quartz binding peptides, i.e., QBP1-bio and QBP2-bio, respectively were used. The latter one was for the negative control experiment. Figure 3.43 and 3.44 demonstrate the affinities of the quartz-binding peptides on quartz surface. The experimental procedure schematically described in Figure 3.42 was carried out using QBP1-bio as the molecular linker for the successful directed immobilization of SA-QD, as shown in Figure 3.43. When QBP2-bio was used, instead, as the ink in PDMS patterning, because of its weak binding characteristics, no SA-QD immobilization was possible, as demonstrated in the negative control experiment displayed in Figure 3.44. Finally, to demonstrate the material-specificity of QBP1-bio for quartz, gold was chosen as the substrate and the procedure was repeated. Again, as shown in Figure 3.45 and 3.46, no SA-QD was immobilized on the patterned gold substrate, using either the strong- or the weak-binding peptide. These experiments indicate that QBP1 has a unique material-specific property, at least between quartz and gold substrates, in which it can immobilize probe molecules (e.g., biotin) on quartz, rendering the surface highly biofunctional [335].

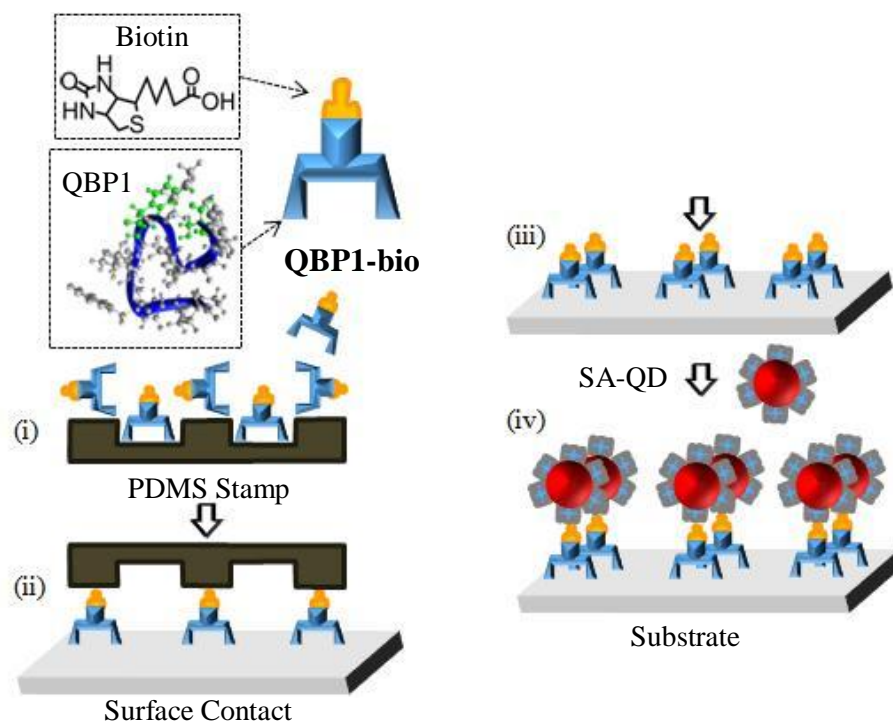


**Figure 3.42:** Schematic representation of PDMS patterning of QBP1-bio on a solid substrate [335].

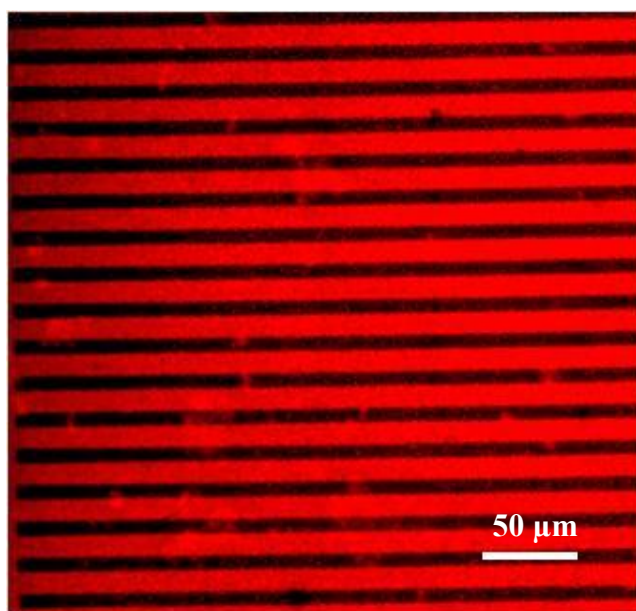


**Figure 3.43:** FM image of the micropattern formed through directed assembly of SA-QD following the PDMS stamping of QBP1-bio on quartz [335].

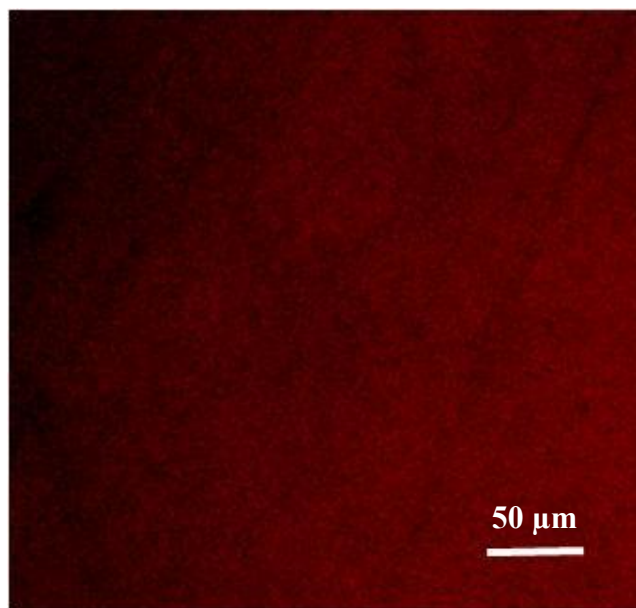


**Figure 3.44:** FM image of the quartz substrate after the PDMS stamping of QBP2-bio followed by SA-QD assembly [335].

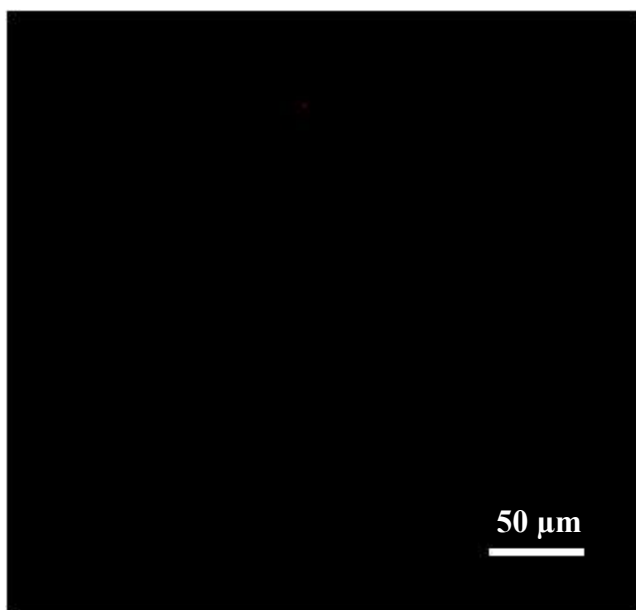


**Figure 3.45:** FM image of the gold substrate after the PDMS stamping of QBP1-bio followed by SA-QD assembly [335].

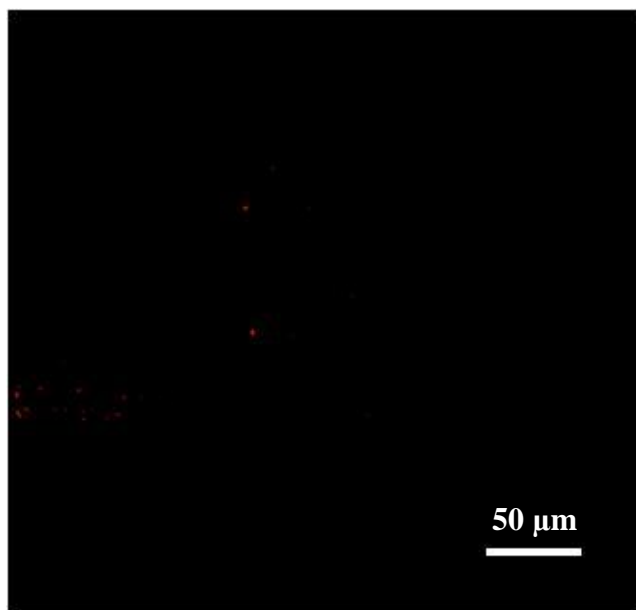


**Figure 3.46:** FM image of the gold substrate after the PDMS stamping of QBP2-bio followed by SA-QD assembly [335].

Next, we use two different nano-entities, QDs and fluorescent molecules, and sequentially assemble them on a micropatterned surface utilizing the material-specificity of the inorganic-binding peptide. In this case, directed immobilization of the QDs is followed by the GEPI-mediated assembly of the fluorescent molecule, using the procedure schematically illustrated in Figure 3.47. The directed immobilization of SA-QD on a QBP1-bio-patterned surface is shown in Figure 3.48 as red stripes, imaged with a fluorescent microscope using a QD605 filter, revealing contrast similar to that in Figure 3.43. Here, the dark stripes represent the regions originally unoccupied, exposing the bare quartz surface (Figure 3.43 or Figure 3.47(i)). Next, following the procedure in Figure 3.47, the assembly of the fluorescent molecule, i.e., fluorescein, is mediated using the QBP1-F molecular conjugate. The assembled conjugate molecules are imaged, as shown in Figure 3.49, using a FITC filter. At this step, the QBP1-F molecular conjugate diffuses towards the regions of the substrate previously unoccupied, after the initial directed immobilization of QDs. Both images in Figure 3.48 and 3.49 were recorded from the same area of the sample, showing regular alternating lines of red and green stripes, corresponding to the directed- assembled QDs and mediated-assembled fluorescein molecules, respectively.



This result demonstrates that the QBP1 sequence acts as an efficient molecular linker as well as a versatile PDMS ink [335]. Furthermore, the result demonstrates here the coassembly of two diverse nano-entities without the involvement of complex surface modification, often involved in silane-based procedures [348, 349].

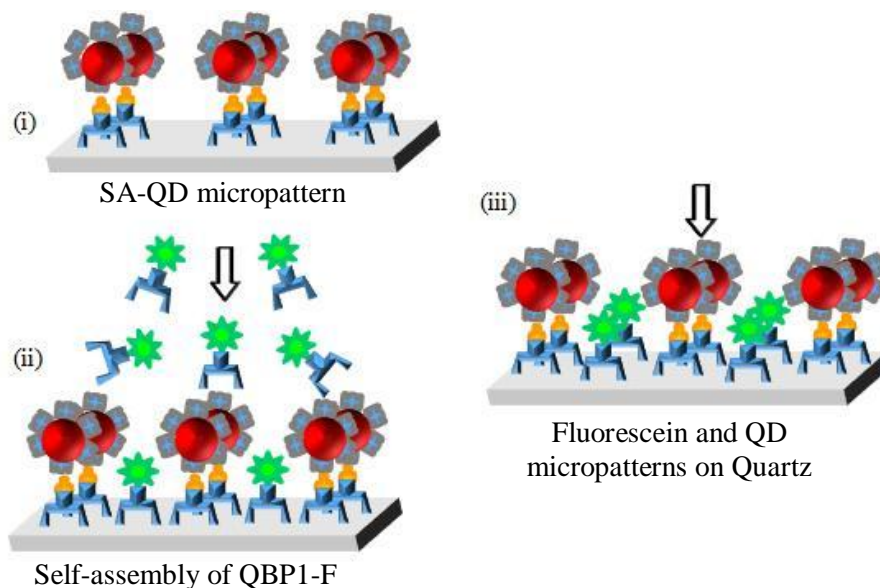


**Figure 3.47:** Schematics of QBP1-F assembly on a quartz substrate pre-patterned using QBP1-bio/SA-QD [335].

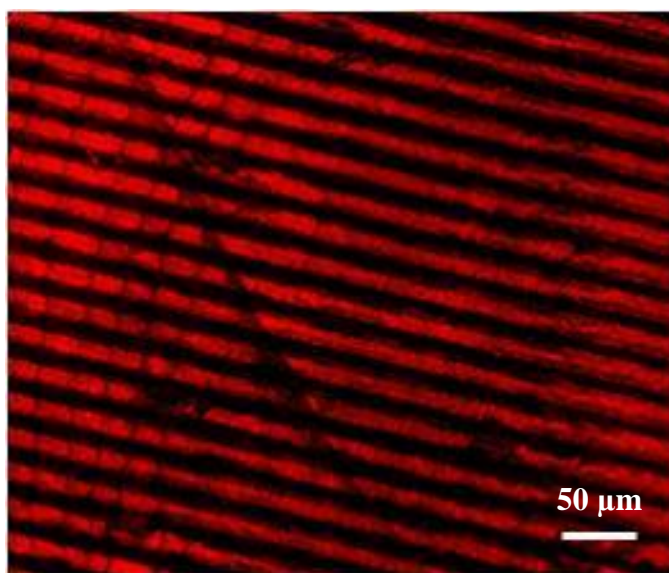


**Figure 3.48:** FM image of a micropattern of directed immobilized SA-QD via the QBP1-bio patterned surface [335].

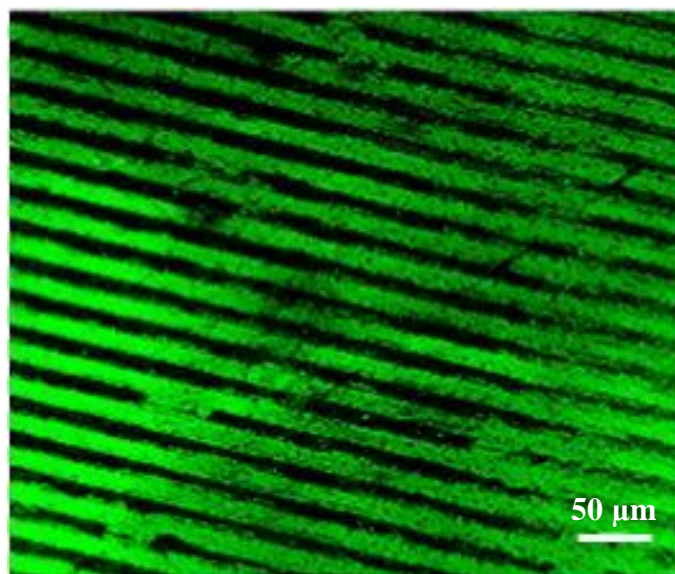


**Figure 3.49:** FM image of the micropattern formed by the immobilization of QBP1-F conjugate on the unfilled microlines, using the substrate as in Figure 3.48 [335].

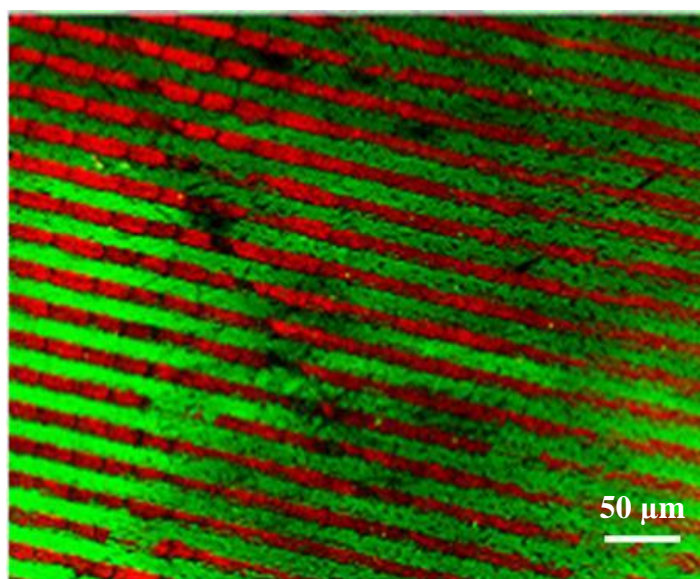


**Figure 3.50:** Digital overlay of the images in Figure 3.48 and Figure 3.49, demonstrating the utility of QBP1 both as a molecular ink for stamping, for directing the immobilization of QDs, and a mediated molecular assembler for a fluorescent molecule [335].

### 3.3.3 Co-immobilization of QD and Metal Noble Nanoparticles using Bifunctional Inorganic-Binding Peptide

The results obtained in Section 3.2.1 and 3.3.2 are encouraging to study co-immobilization of QDs and metal nanoparticles on glass substrate. In those sections, nanoparticle immobilization through self-assembly of Bi-GEPIs on glass and



successful QD assembly on quartz surface micropatterned with QBP1-bio were demonstrated. Here, a novel procedure for the co-immobilization of QDs and metal nanoparticles on same glass substrate using corresponding GEPIs is represented. The procedure, simply shown in Figure 3.51, involves both  $\mu$ CP of Bi-GEPI followed by metal nanoparticle assembly and then, self assembly of QBP1-bio and SA-QD. The substrates were then characterized by optical microscope with dark-field and fluorescence modes.

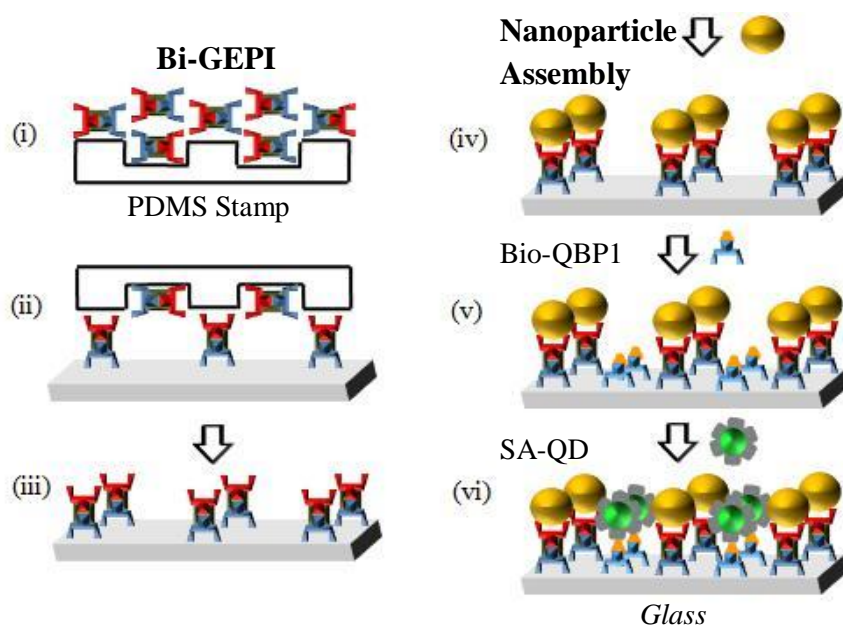


**Figure 3.51:** Schematics for co-immobilization of metal nanoparticle and green/red QD on glass through  $\mu$ CP and self-assembly of GEPIs.

Initially, two different control experiments where either QBP1-bio assembly (Figure 3.51 (v)) or Bi-GEPI printing (Figure 3.51 (i-iii)) was replaced with PBS incubation were carried out. In case of switching QBP1-bio assembly with PBS treatment, arrays of 50 nm gold nanoparticles could be imaged under dark-field (Figure 3.52). However, there was almost no indication for the QD attachment to the surface when the filter was switched to QD565 filter of fluorescence mode (Figure 3.53). Bi-GEPI-1 used for this experiment provided the assembly of gold nanoparticles, leading to bright arrays of gold nanoparticles detected with dark-field mode. On the other hand, since there was no appropriate linker for the SA-QD(565), green emission indicating the QD presence on the surface was so dimmed.

Parallel to this experiment, the procedure in Figure 3.51 was applied to another glass substrate, however this time; PBS alone was used in  $\mu$ CP step as the ink. Subsequent

characterization under dark field and fluorescence mode revealed that gold nanoparticle attachment was not successful since Bi-GEPI-1 was replaced with PBS (Figure 3.54) whereas green emission indicated the successful QD attachment to the substrate (Figure 3.55). Here, the QBP1-bio covered all over the surface, leading to dense SA-QD(565) assembly.

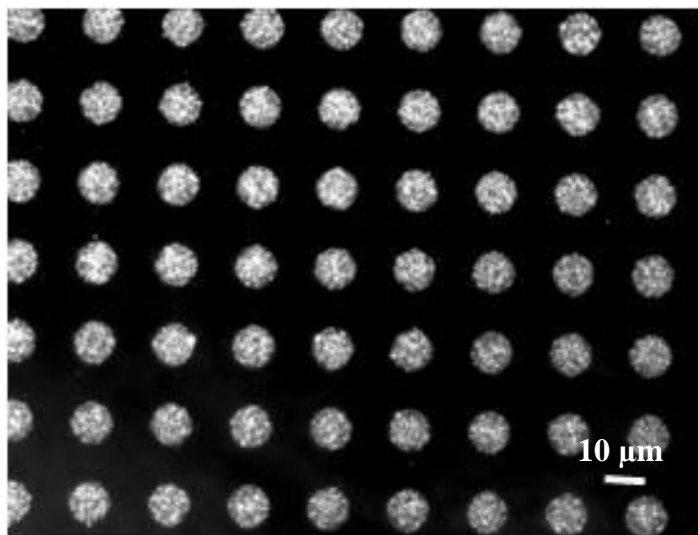


**Figure 3.52:** DF image of the micropattern formed through  $\mu$ CP of Bi-GEPI-1 followed by gold nanoparticle assembly and then, PBS incubation followed by green SA-QD(565) assembly.

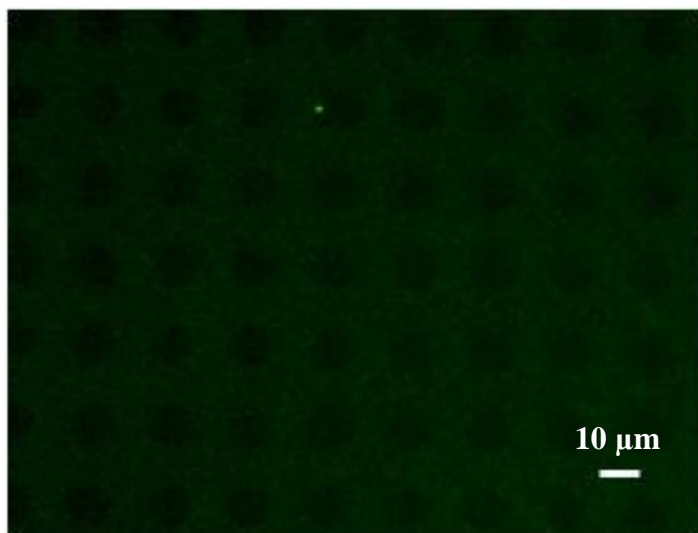


**Figure 3.53:** FM image of the micropattern formed through  $\mu$ CP of Bi-GEPI-1 followed by gold nanoparticle assembly and then, PBS incubation followed by green SA-QD(565) assembly.

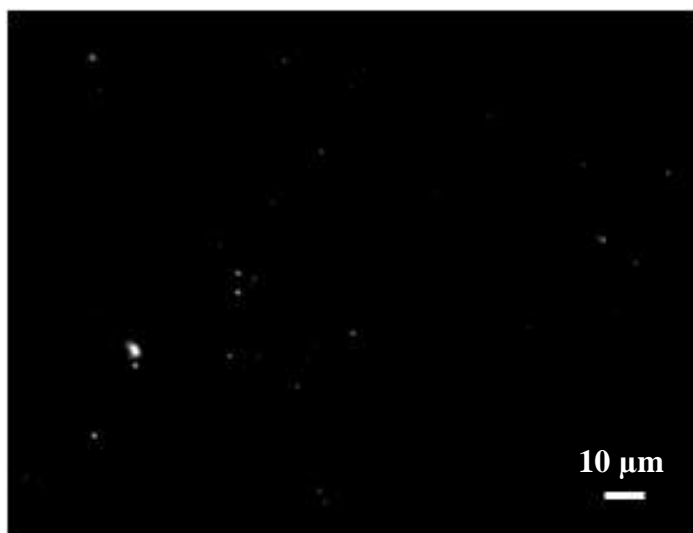


**Figure 3.54:** DF image of the substrate prepared through  $\mu$ CP of PBS followed by gold nanoparticle assembly and then, sequential QBP1-bio and SA-QD(565) assembly.

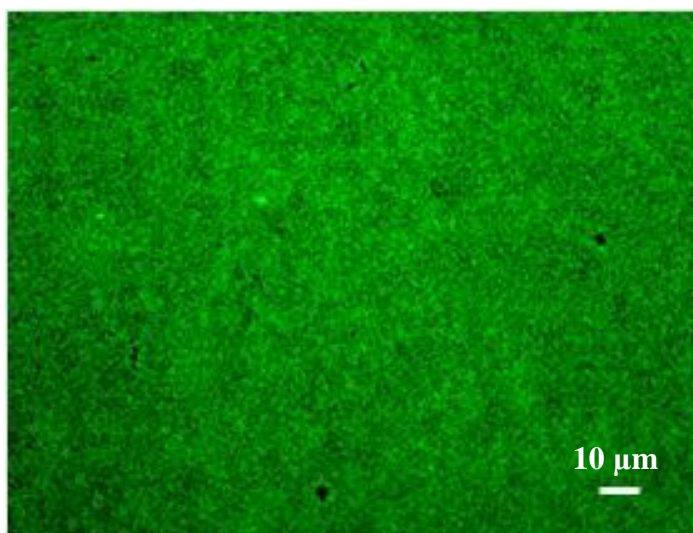


**Figure 3.55:** FM image of the substrate prepared through  $\mu$ CP of PBS followed by gold nanoparticle assembly and then, sequential QBP1-bio and SA-QD(565) assembly.

Finally, when two linkers, *i.e.* Bi-GEPI-1 and QBP1-bio are utilized at the corresponding steps in Figure 3.51, co-immobilization of gold nanoparticle and SA-QD is achieved. Both gold nanoparticles assembled through stamped Bi-GEPI-1 and QDs attached through QBP1-bio readily assembled on the surface can be detected by dark-field and fluorescence modes, respectively (Figure 3.56 and 3.57).

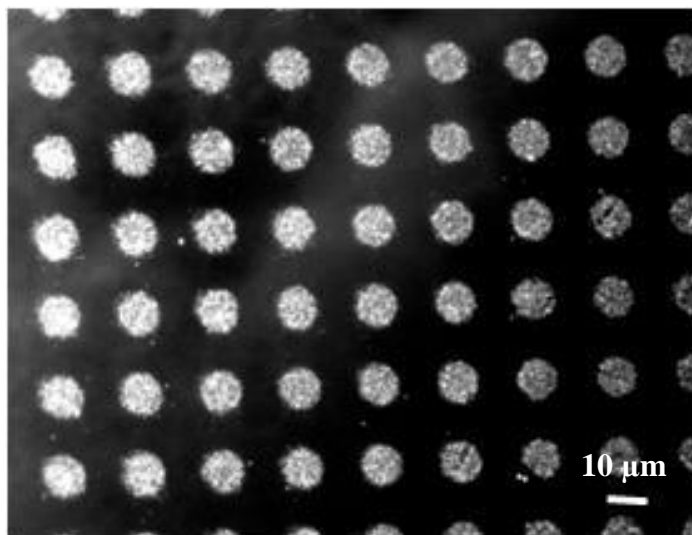


**Figure 3.56:** DF image of the micropattern formed through  $\mu$ CP of Bi-GEPI-1 followed by gold nanoparticle assembly then, sequential QBP1-bio and SA-QD(565) assembly.

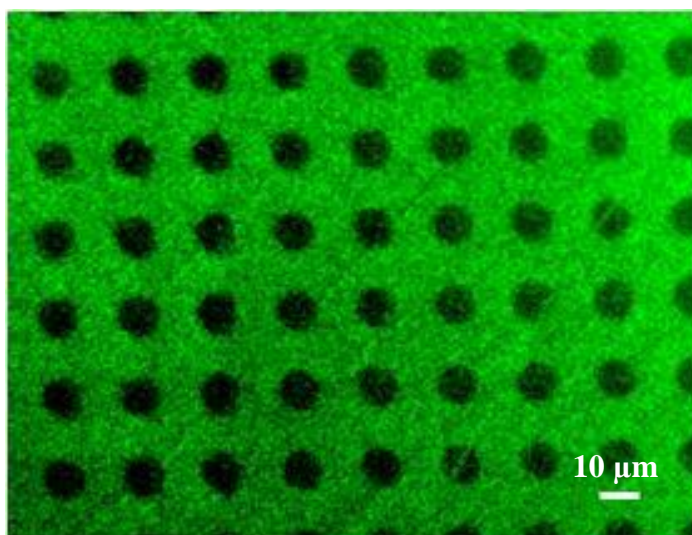


**Figure 3.57:** FM image of the micropattern formed through  $\mu$ CP of Bi-GEPI-1 followed by gold nanoparticle assembly then, sequential QBP1-bio and SA-QD(565) assembly.

Furthermore, using Bi-GEPI-5 composed of AgBP1 chemically linked to QBP1 through flexible GlyGlyGly bridge and QBP1-bio in the procedure shown in Figure 3.51, co-immobilization of silver nanoparticles and QDs could be achieved. Similar to co-immobilization of gold nanoparticle and QD case, Bi-GEPI-5 and QBP1-bio were exchanged with PBS at the corresponding steps, forming the control experiments. Naturally, when QBP1-bio was replaced with PBS, only arrays of silver nanoparticles were detected under dark-field since microprinted Bi-GEPI had the silver binding ability (Figure 3.58) whereas, there was no linker for red SA-QD(605)

to attach to the glass, leading to dark fluorescence image through QD605 filter (Figure 3.59). On the other hand, switching Bi-GEPI-5 with PBS didn't lead to formation of arrays of silver nanoparticles (Figure 3.60) but assembled QBP1-bio provided SA-QD attachment to the surface, yielding red emission coming from the all surface that could be detected in fluorescence mode with QD605 filter (Figure 3.61).

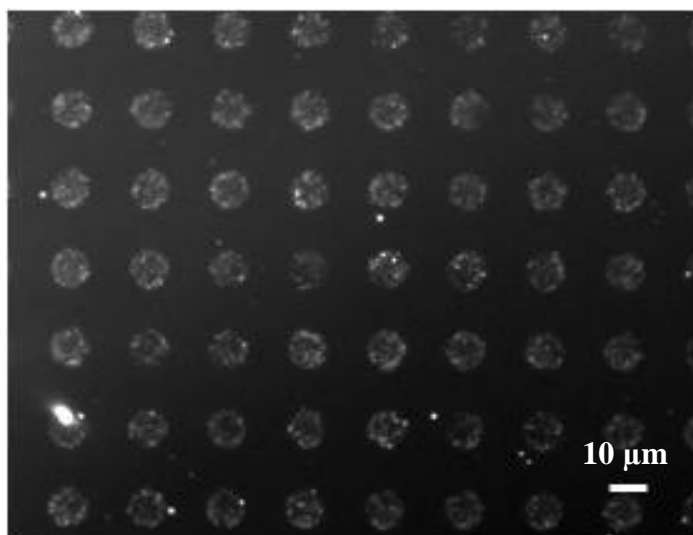


**Figure 3.58:** DF image of the micropattern formed through  $\mu$ CP of Bi-GEPI-5 followed by silver nanoparticle assembly and then, PBS incubation followed by red SA-QD(605) assembly.

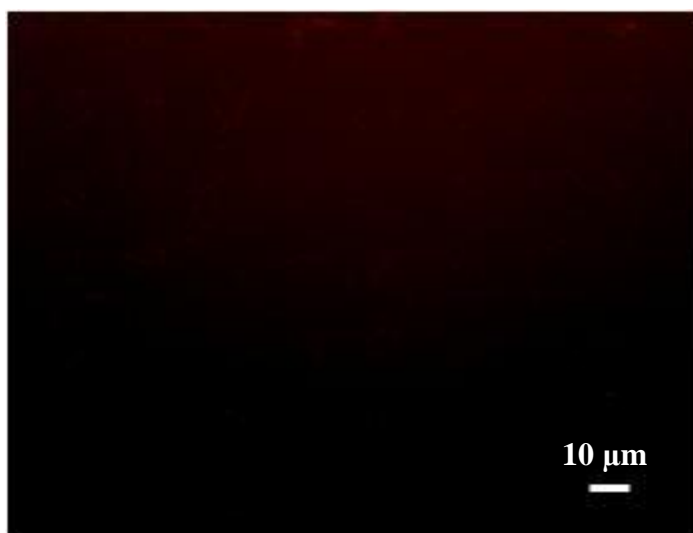


**Figure 3.59:** FM image of the glass substrate prepared through  $\mu$ CP of Bi-GEPI-5 followed by silver nanoparticle assembly and then, PBS incubation followed by SA-QD(605) assembly.

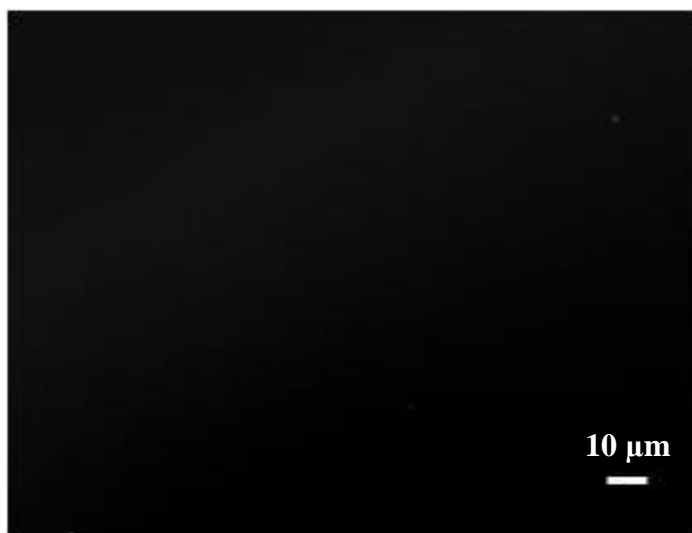


**Figure 3.60:** DF image of the substrate prepared through  $\mu$ CP of PBS followed by silver nanoparticle assembly and then, sequential QBP1-bio and SA-QD(605) assembly.

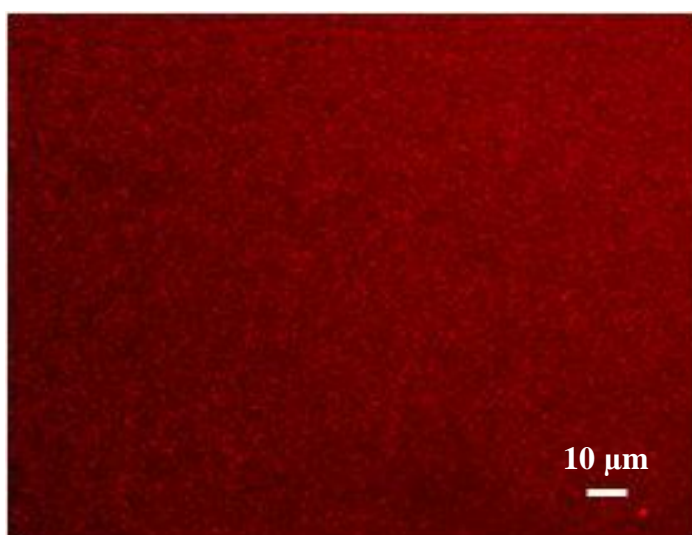


**Figure 3.61:** FM image of the substrate prepared through  $\mu$ CP of PBS followed by silver nanoparticle assembly and then, sequential QBP1-bio and SA-QD(605) assembly.

In the case of choosing Bi-GEPI-5 and QBP1-bio as linkers, complementary micropatterns of both silver nanoparticle and QD on same substrate were achieved. The arrays comprising of silver nanoparticles assembled through microprinted Bi-GEPI-5 on glass cover slip were imaged in dark-field mode (Figure 3.62) and the red QDs surrounding those arrays, attaching to the surface through self-assembled QBP1-bio, were detected in fluorescence mode with QD605 filter (Figure 3.63).



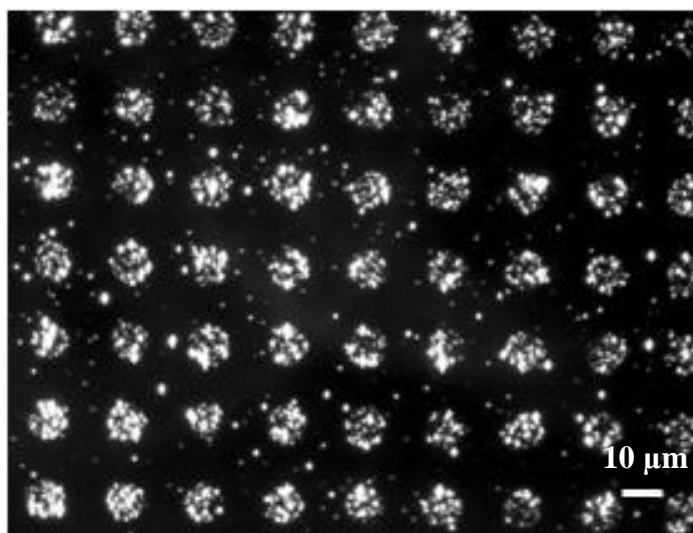


**Figure 3.62:** DF image of the micropattern formed through  $\mu$ CP of Bi-GEPI-5 followed by silver nanoparticle assembly then, sequential QBP1-bio and SA-QD(605) assembly.

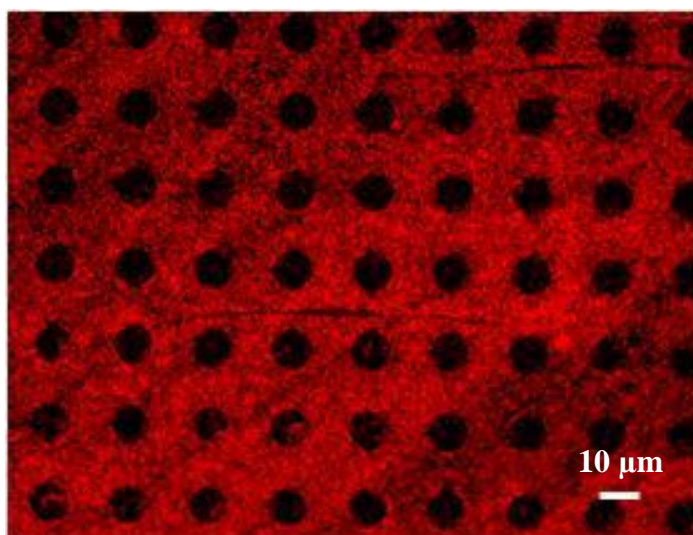


**Figure 3.63:** FM image of the micropattern formed through  $\mu$ CP of Bi-GEPI-5 followed by silver nanoparticle assembly then, sequential QBP1-bio and SA-QD(605) assembly.

### 3.3.4 Microcontact printing of Alkaline phosphatase on gold

In protein and peptide microarray technology, there are several ways, *e.g.*, photolithography [341], soft lithography [153], dip-pen lithography [185], to fabricate micro/nanoscaled platforms. With combination of these methods, advances in GEPI-driven assembly can allow one to prepare biofunctional platforms under ambient conditions. GEPI-mediated assembly of AP onto micropatterned gold substrate was already shown in Figure 3.14 and 3.15. As mentioned earlier in Section

3.1, dense and oriented packing of protein was achieved by using both gold binding sequence and confined gold surface.

Apart from GEPI-mediated assembly, GEPI-protein fusion products can also serve as ink for  $\mu$ CP, forming a probe for subsequent antibody coupling on inorganic surface. In Figure 3.64, assembly of AP antibody through a coupling with micro-contact printed AP/5R-GBP1-AP on gold surface is depicted. The PDMS stamp pre-treated with either AP without GBP insert (Figure 3.64a) or 5GBP1-AP (Figure 3.64b) was brought to contact with gold surface. After washing and drying the substrates, FITC-labeled Anti-AP incubation was carried out on protein-patterned surfaces. The substrates were then characterized by optical microscope in fluorescence mode following final rinsing and drying steps. The control experiment shows that the assembly of Anti-AP was inefficient (Figure 3.65) whereas GBP linkage maintains the immobilization of the protein, 5GBP1-AP (probe), leading a successful Anti-AP (target) assembly (Figure 3.66).

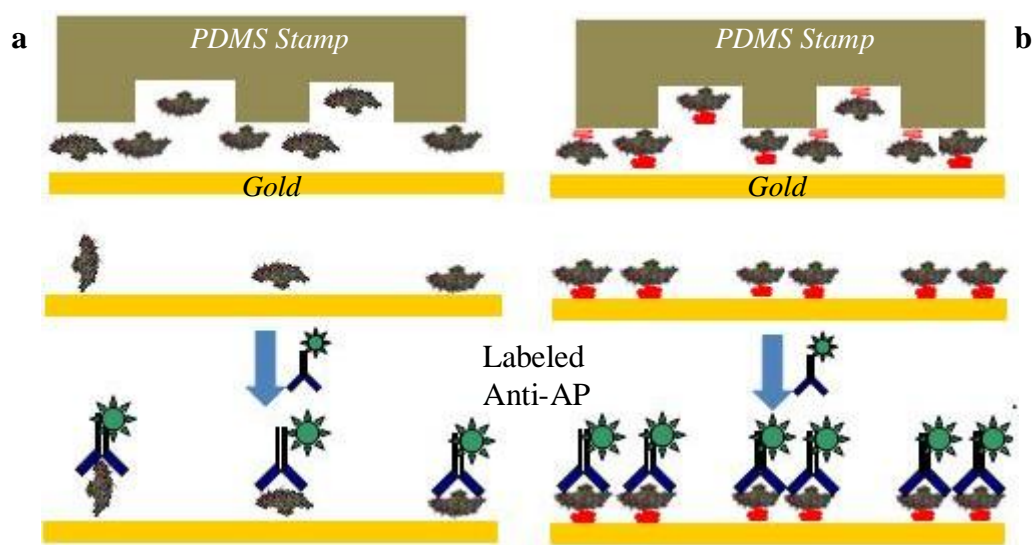


**Figure 3.64:** Schematics for  $\mu$ CP of (a) AP and (b) 5GBP1-AP on gold followed by labeled Anti-AP coupling.



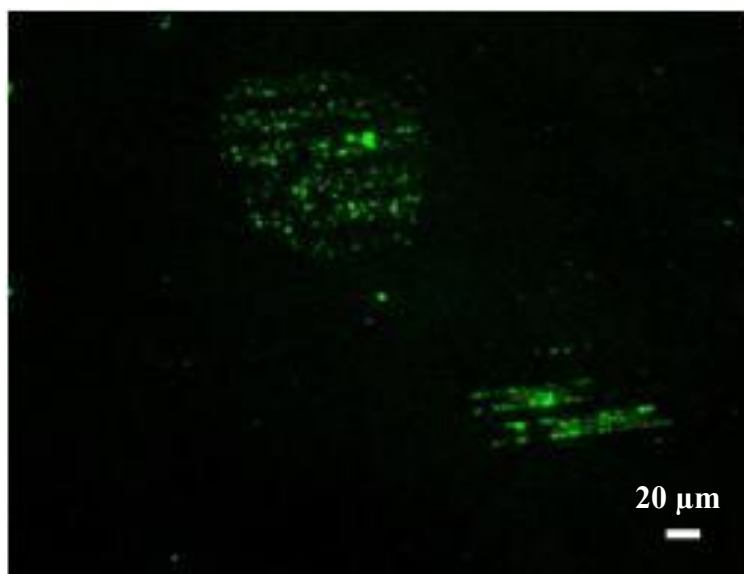


**Figure 3.65:** FM image of the micropattern formed through  $\mu$ CP of AP followed by labeled Anti-AP incubation.

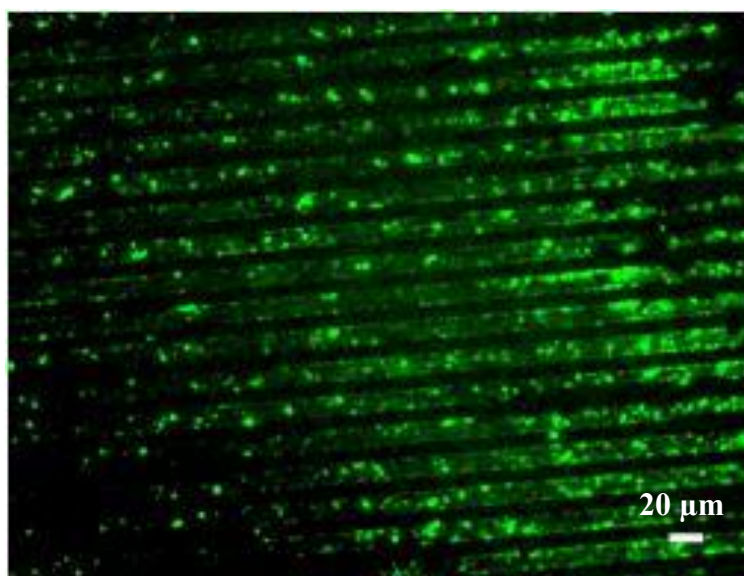


**Figure 3.66:** FM image of the micropattern formed through  $\mu$ CP of 5GBP1-AP followed by labeled Anti-AP incubation.

### 3.3.5 Dip-pen lithography of inorganic-binding peptides

Microprinting and self-assembly of GEPIs on inorganic substrates have provided novel procedures for nanoparticle and biomolecule assembly in a patterned fashion. In this section, direct writing of GEPI was studied by Dip-pen lithography (DPN), yielding submicron patterns.

Dip pen lithography involves couple important steps. The first step is substrate preparation: the substrate is cleaned and rinsed to remove all impurities and produce a flawless surface (see Materials and Methods Section). The AFM tip is then coated with the “ink” to be deposited onto the substrate. Finally, the tip inked with the peptide is brought into contact with the inorganic surface to produce desired patterns. If the peptide is chemically linked (pre-functionalized) with a probe, *e.g.* biotin, then the appropriate target molecule such as SA-QD can be assembled on the patterns formed by deposited ink (Figure 3.67).

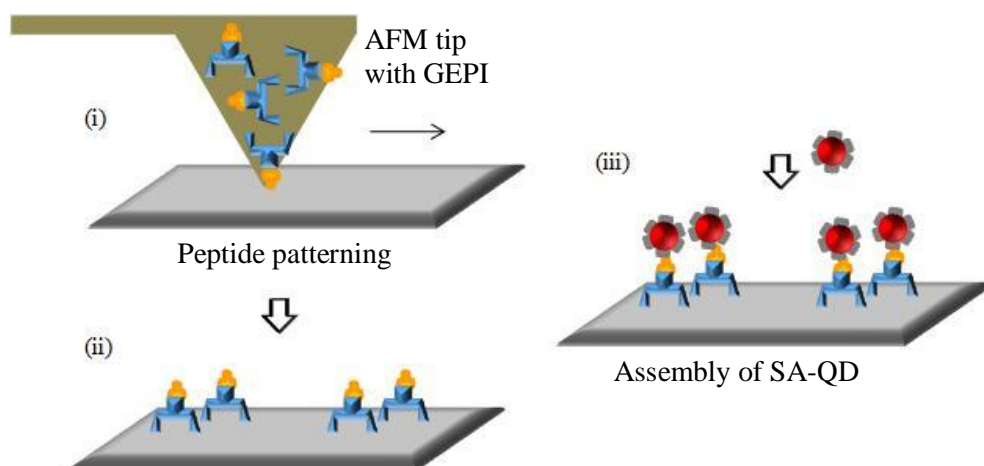


**Figure 3.67:** Schematics for DPN of GEPI-bio on inorganic substrate followed by SA-QD assembly.

Using the procedure shown in Figure 3.67, we could prepare SA-QD microarrays on silica surface where the linker was DPN-deposited QBP1-bio. After ink deposition, the substrate was rinsed thoroughly and then, SA-QD assembly was carried out by incubating the substrate with the solution of SA-QD. The substrate was rinsed again with DI water and dried prior to characterization with fluorescence microscope. Even though the substrate was rinsed, the peptides delivered by the tip still remained on the surface, probing for the next SA-QD assembly. It should be noted that peptide transfer from the tip to the surface did not decrease the binding activity of biotin to the streptavidin (Figure 3.68). The arrays are surrounded by SA-QD conjugates through their non-specific interactions with the surface. As the control, an uncoated and buffer treated tip did not produce a pattern, indicating that the labeling step had occurred through streptavidin-biotin interaction and not through non-specific binding to the scratches created by the tip contacts [336].

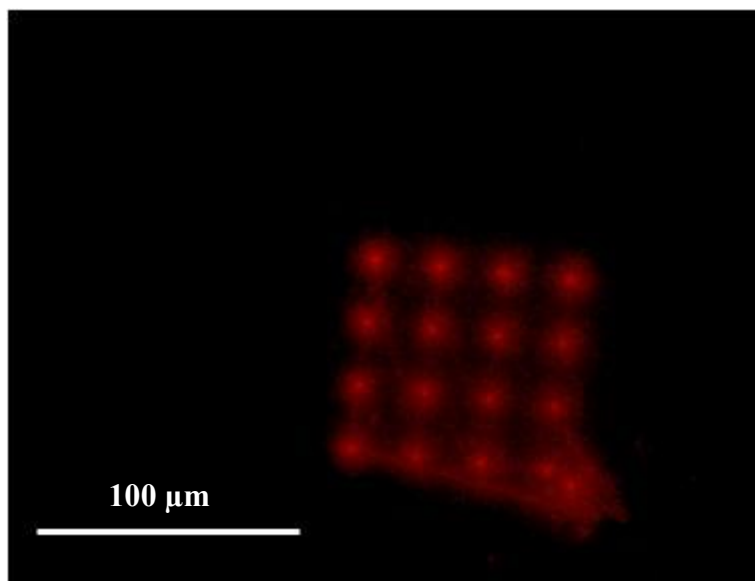


**Figure 3.68:** FM image of the microarray formed through DPN of QBP1-bio followed by SA-QD assembly.

Parallel to this experiment, QBP1 without biotin was also utilized as ink for DPN to fabricate submicron features on the silica substrate. The same steps followed for the previous experiment were carried out, except SA-QD incubation. The substrate was rinsed thoroughly and dried prior to AFM characterization. The lateral force microscopy image of DPN-deposited QBP1 on silica surface is presented in Figure 3.69 [336]. DPN of QBP1 produced lines with down to ~80 nm in width. Moreover, ~110-nm-wide lines are reproducibly written. The effect of the buffer was also studied. It was found that there was almost no difference between water and PC buffer in terms of writing the peptide on silica surface [336].



**Figure 3.69:** LFM image of DPN-patterned QBP1 on silica substrate [336].

### 3.4 LSPR based detection of Biomolecules using GEPI and GEPI-Protein Constructs

#### 3.4.1 Preparation of LSPR active silver nanostructures using NSL

As mentioned earlier (see Section 1.4), noble metal nanostructures are very useful tools for the detection of biomolecules due to their strong optical properties and NSL is one the techniques for fabrication of inorganic nanostructures. This section involves the fabrication of metal nanostructures by NSL towards biosensing.

The protocol for NSL is shown in Figure 1.17 (see also Materials and Methods). As first step, self-assembly of polystyrene beads was carried out, forming a nanomask for the metal deposition. In Figure 3.70, nanomask comprising of beads with 1.5 $\mu$ m in diameter is represented. Following silver deposition, the beads were lifted up by sonication, yielding silver nanostructures shown in Figure 3.71.

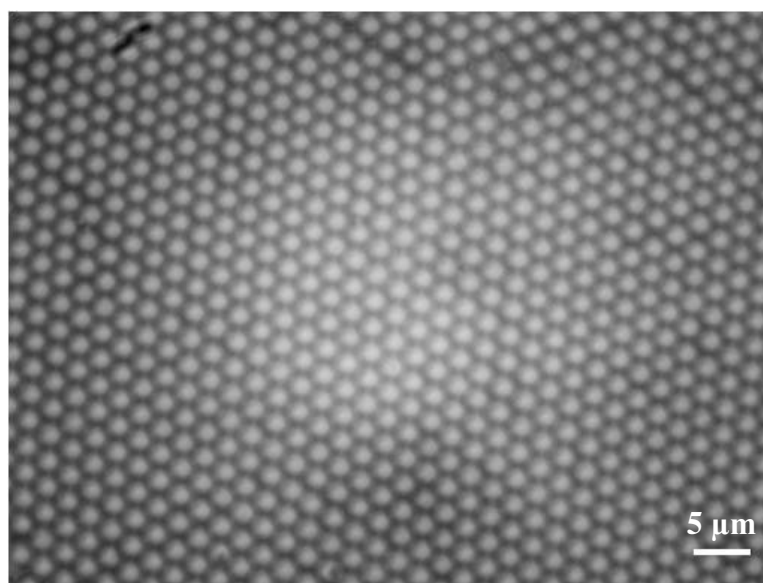


**Figure 3.70:** DF image of polystyrene monolayer prior to silver deposition.

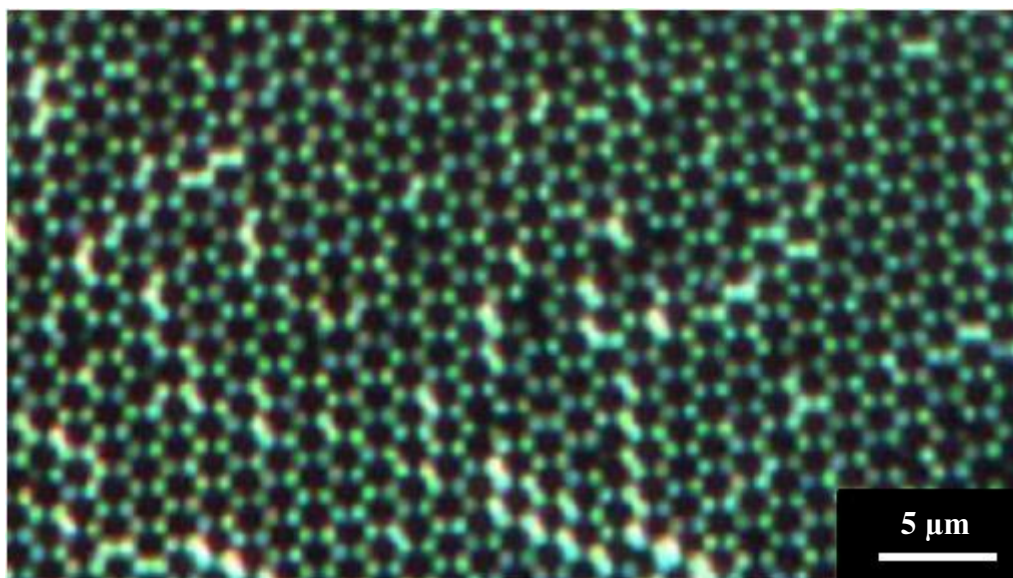


**Figure 3.71:** DF image of NSL-fabricated silver nanostructures following metal deposition and removal of polystyrene beads.

Silver and gold nanotriangles produced using beads with  $0.45\mu\text{m}$ -diameter were characterized by AFM to confirm the dimensions of the array as well as successful bead removal. It was found that we produced metal nanostructures with  $\sim 145\text{-nm}$  in-plane width and  $\sim 50\text{-nm}$  height (Figure 3.72, 3.73, Appendix A4 and 5).

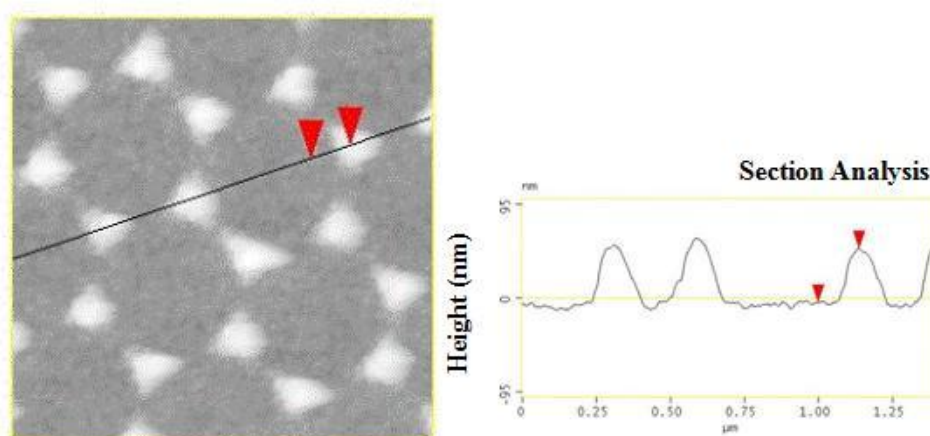


**Figure 3.72:** AFM image of NSL-fabricated silver nanostructures with line profile analysis.

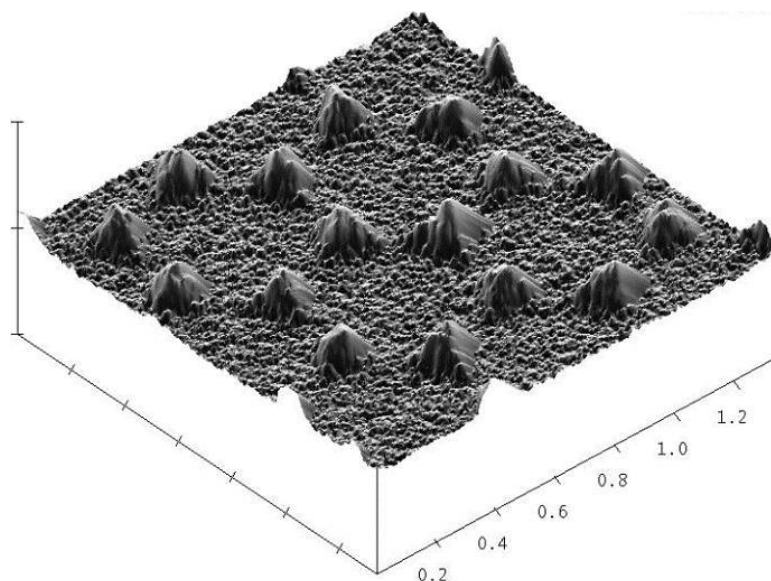


**Figure 3.73:** Pseudo-3-dimensional presentation of the AFM image of NSL-fabricated silver nanostructures shown in Figure 3.72.

### 3.4.2 Probe and target assembly on silver nanostructures

LSPR based biosensors mainly involve two components; an inorganic platform where localized surface plasmons are generated and appropriate probe immobilized onto the platform to detect target molecule. Mostly, noble metal nanoparticles either in solution or attached on a planar surface are used as inorganic platform. Sensing occurs upon any change in surrounding media of those particles and detected by UV-vis spectrometer.

The NSL-fabricated nanoarrays (demonstrated in previous section) have been shown to be good candidate as platform for biosensing [256]. Here, LSPR based biosensor composed of NSL-fabricated silver nanotriangles on glass surface and the biotin as platform and probe, respectively was utilized to detect streptavidin-Alkaline phosphatase conjugate (SA-AP). (see Figure 2.3 for experimental setup). To be able to immobilize the probe onto silver surface, the biotin molecule (probe) was chemically linked to silver binding peptide which was isolated through cell surface display and characterized by SPR ( $k_a = 43093 \text{ M}^{-1} \text{ s}^{-1}$ ,  $k_d = 0.0003 \text{ s}^{-1}$ , Appendix A6).

Figure 3.74 shows the scattering spectra obtained from each step in the detection of SA-AP, involving probe assembly, target assembly and probe regeneration. Basically, from a constant area in the array, the scattering spectra were recorded in water before and after each modification following washing step (see Section 2.7.2). Assembly of biotinylated silver binding peptide (AgBP1-bio) led 6-nm-red shift at



LSPR  $\lambda_{\max}$  (step 1 and 2 in Figure 3.74). After probe assembly, 100 nM of target molecule, SA-AP, was pumped into flowcell resulting in a further 8-nm-red shift, indicating streptavidin binding activity of biotin assembled on silver through GEPI (step 3 in Figure 3.74). Moreover, the nanosensor could also be regenerated by pumping excess amount of biotin into the system (step 4 in Figure 3.74). 7-nm blue shift indicating the removal of target molecule was observed. 1-nm gap between step 3 and 4 in Figure 3.74 was dedicated to non-specific binding of target molecule onto Ag nanoparticles.

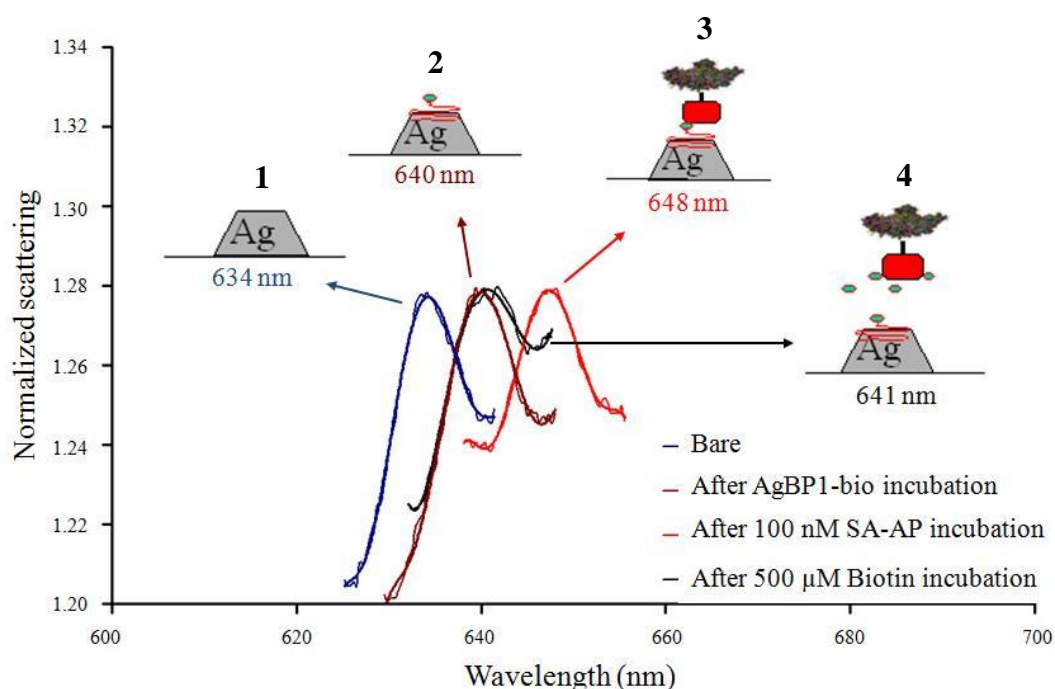


**Figure 3.74:** LSPR spectra of NSL-fabricated Ag nanoarray (nanosphere D= 450 nm, the height of Ag nanotriangle;  $d_m$ = 50nm) for each step in SA-AP detection. Experimental data are represented with their calculated curve fittings.

### 3.4.3 Probe and target assembly on gold nanoparticles immobilized on glass

Apart from NSL, noble metal nanoparticles in colloidal solution can be immobilized onto a transparent surface such as glass, forming a suitable stage for LSPR based detection [281, 348]. Since Bi-GEPIs were successfully utilized for gold nanoparticle immobilization on glass in Section 3.2.1, the resultant substrates could be proper platforms for biosensing. To explore their potential, another LSPR biosensor was designed, where glass substrate with gold nanoparticles immobilized through Bi-GEPI-1 (see Section 3.2.1) and 5GBP1-AP [334] were used as platform and probe, respectively. Here, instead of using the alkanethiol based linkers for the attachment

of protein and nanoparticle to the inorganic surface, the approach was again to use appropriate GEPI sequences to maintain linkage between the interfaces, forming the biosensor.

Firstly, using LSPR spectroscopy, the assembly performance of the fusion protein was investigated and compared with the control molecule, AP wild type (Figure 3.75). The red shift at LSPR  $\lambda_{\max}$  corresponding 5GBP1-AP assembly on gold nanoparticles was more than three times higher than the red shift recorded for AP assembly. Since the size of the molecules are closer to each other, higher red shift of 5GBP1-AP was attributed to higher number of molecules assembled on the gold surface comparing to AP.

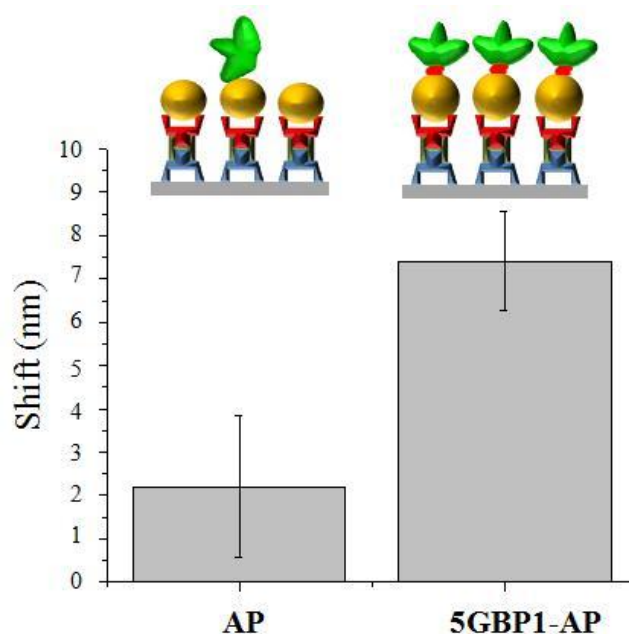


**Figure 3.75:** Comparison of probe assembly by LSPR spectroscopy. The higher red shifts at LSPR  $\lambda_{\max}$  indicate stronger binding of 5GBP1-AP on gold surface than that of AP lacking gold binding peptide.

Next, binding of Anti-AP (target molecule) to probe immobilized on the chip was studied. Here, the signals coming from LSPR  $\lambda_{\max}$  of the gold nanoparticles attached onto the glass surface were recorded before and after the probe assembly, and then after target assembly (see Materials and Methods Section). Figure 3.76 and 3.77 show the LSPR spectra of the each step in Anti-AP detection where 5GBP1-AP and AP were used as probes, respectively. Due to the local refractive index change, the probe and subsequent target assembly resulted in red shifts at the LSPR  $\lambda_{\max}$ .



Since the number of assembled 5GBP1-AP molecules on gold surface is higher than AP, detection of 25  $\mu\text{g/ml}$  Anti-AP solution was achieved by higher shift (Figure 3.76 vs 3.77).

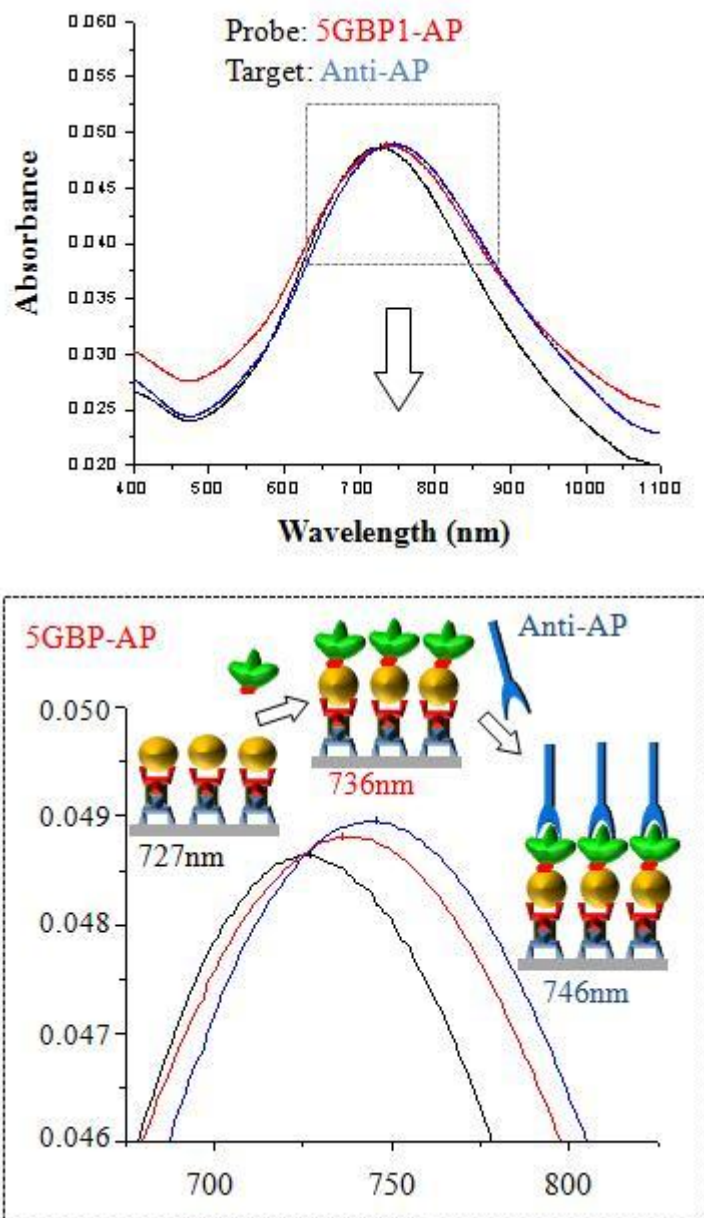


**Figure 3.76:** Immuno-detection of Anti-AP (25  $\mu\text{g/ml}$ ) using LSPR based biosensor composed of gold nanoparticles immobilized through Bi-GEPI-1 and a genetically engineered fusion probe, 5GBP1-AP. LSPR Spectra with  $\lambda_{\text{max}}$  values are highlighted in black for bare, red for probe assembly, and blue for Anti-AP assembly.

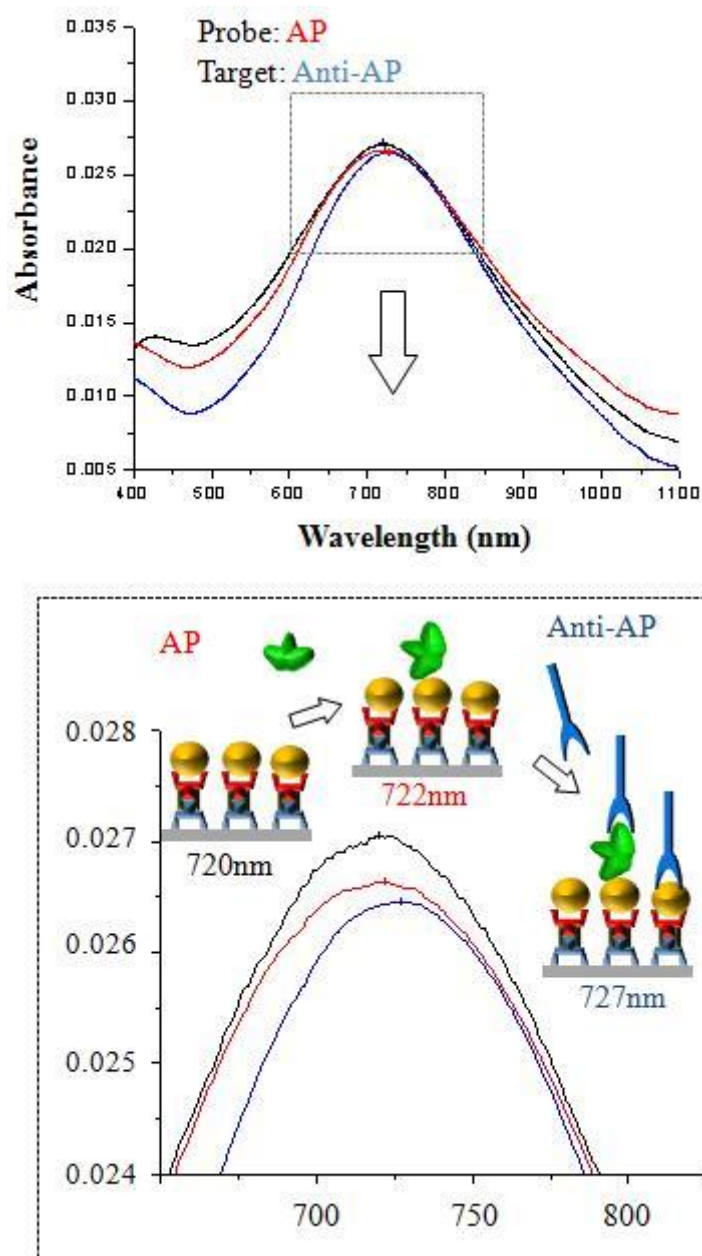


**Figure 3.77:** Immuno-detection of Anti-AP (25  $\mu\text{g/ml}$ ) using LSPR based biosensor composed of gold nanoparticles immobilized through Bi-GEPI-1 and the control protein, AP. LSPR Spectra with  $\lambda_{\text{max}}$  values are highlighted in black for bare, red for probe assembly, and blue for Anti-AP assembly.

The limit of target detection for a biosensor is an important issue. To determine the limit of detection, the Anti-AP concentration dependence on the local refractive index change were investigated in range of 5-100  $\mu\text{g/ml}$ . The red shifts at LSPR  $\lambda_{\text{max}}$  were plotted against Anti-AP concentration (Figure 3.78). The data obtained from two different probes were compared in the same graph. Between 5-50  $\mu\text{g/ml}$ , linear trend was observed and the sensitivity coming from value of the red shift was always

higher when 5GBP1-AP was the probe. For example, in the case of 25  $\mu\text{g/ml}$  Anti-AP detection, the red shift at LSPR  $\lambda_{\text{max}}$  is three times higher for the sensing *via* 5GBP1-AP comparing to AP based sensing, indicating the higher sensitivity. At larger Anti-AP concentrations than 50  $\mu\text{g/ml}$ , the shift became saturated.  $\sim 30$  nM (corresponding to 5  $\mu\text{g/ml}$ ) of target molecule was successfully detected by the LSPR of optical response coming from the gold nanoparticles modified by 5GBP1-AP. Comparing to the streptavidin-biotin reaction, the dynamic range and detection limit for the coupling between 5GBP1-AP and Anti-AP are larger [281]. This reality could be attributed to higher dissociation constant of streptavidin-biotin pair, i.e.  $10^{-15}$  M, than antigen-antibody pair, i.e.  $10^{-9}$  M [348]. The coupling reaction with higher affinity lowers the detection limit, whereas the surface is totally covered at lower concentrations with a large binding constant. Consequently, higher affinity of a binding can enable a lower dynamic range [348].

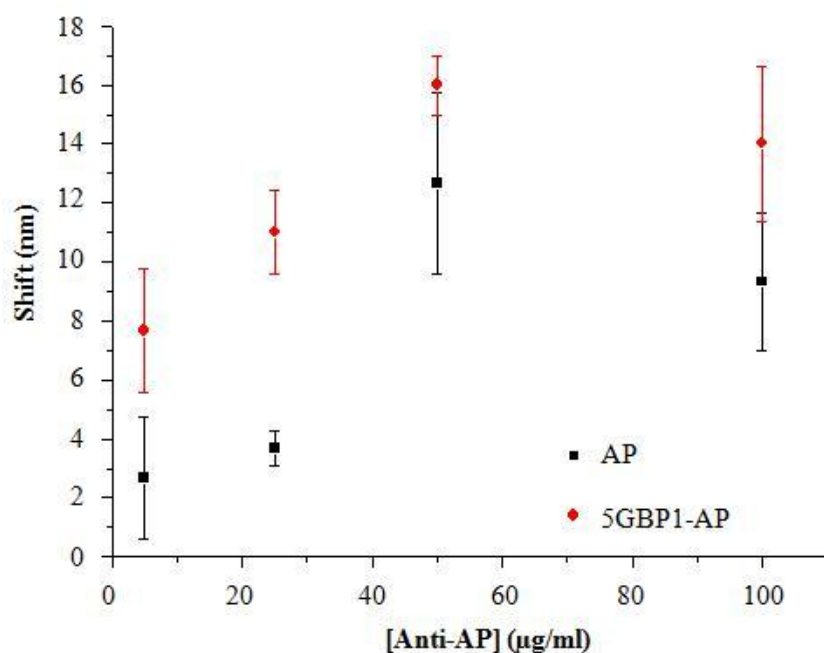


**Figure 3.78:** The red shift upon functionalization of probe-assembled gold nanoparticles on glass slide by Anti-AP with different concentrations. Red dots and black dots indicate the probes, 5GBP1-AP and AP, respectively. The detection range was 5-100  $\mu\text{g/ml}$  (corresponding to  $\sim 30\text{nM}$ -600nM).

Additionally, to investigate the LSPR responses coming from the specific binding between 5GBP1-AP and Anti-AP, two control experiments were carried out (Figure 3.79): 1) Target molecule, Anti-AP was incubated with gold nanoparticles

immobilized on the glass substrate (no probe condition), 2) An analogous molecule, Anti-MBP was incubated with 5GBP1-AP immobilized on gold nanoparticles bound to glass surface (scheme in Figure 3.79). Firstly, LSPR spectra of gold nanoparticles attached on the substrate were recorded before and after incubation with Anti-AP. Nonspecific binding of 30 nM Anti-AP on gold nanoparticles resulted in 5 times lower LSPR shift comparing to that incubated with the probe assembled on gold nanoparticle film (a and b in Figure 3.79, respectively). Secondly, Anti-MBP was incubated with 5GBP1-AP preassembled on gold nanoparticle-coated glass. LSPR spectra were also collected at each step. At the same concentration of antibodies, it turned out that attachment of Anti-AP yielded 5 times higher LSPR shift than that for Anti-MBP (b and c in Figure 3.79, respectively). The red shifts in Figure 3.79 a and c could be attributed to either protein's non-specific affinity to gold surface [350, 351] (a and c in Figure 3.79) or non-specific protein-protein adsorption [352] (c in Figure 3.79).

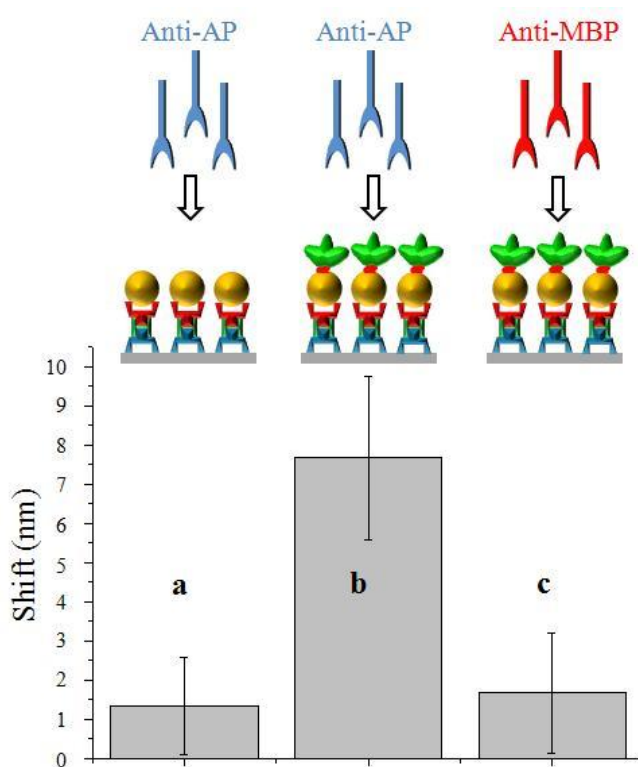


**Figure 3.79:** Red shifts at LSPR  $\lambda_{\max}$  obtained from (a) the non-specific binding of Anti-AP on glass functionalized with gold nanoparticle film, (b) the specific binding of the same target to 5GBP1-AP immobilized on gold nanoparticles attached to the glass cover slip, and (c) the non-specific binding of Anti-MBP on the same substrate represented in b. The target concentration was 30 nM in all cases. Scheme illustrates the scenarios for each case.

Overall results in Section 3.4 show that one can prepare optically active platforms for detection of biomolecules where probe molecule and even inorganic nanostructures can be immobilized and organized using GEPIs with appropriate binding activity. All assembly procedures can be done at ambient conditions such as room temperature, aqueous environment, excluding complex chemical reactions.

### **3.5 Preparation of Gold Nanoparticle-Silica Nanoparticle conjugates and Gold Nanoshells (Silica core)**

#### **3.5.1 Decoration of silica nanoparticles with gold nanoparticles**

In addition to the immobilization of gold nanoparticles on planar silica surface (Section 3.2.1), in this section, GEPI-driven attachment of gold nanoparticles to the larger silica nanoparticle was demonstrated.

Firstly, silica nanoparticles (Figure 3.80 and Appendix A7) and gold nanoparticles were synthesized using Stober method [232] and citrate reduction method [228], respectively (see Materials and Methods).

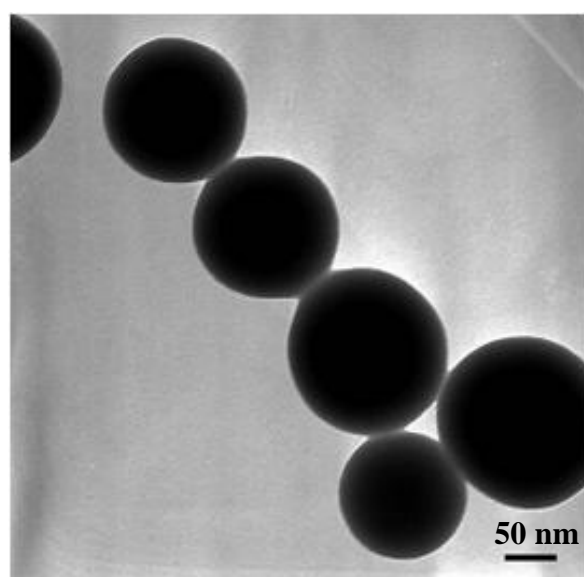


**Figure 3.80:** TEM image of synthesized silica nanoparticles.

Preparation of gold nanosatellites on silica nanoparticles was achieved using the procedure, depicted in Figure 3.81, involving functionalization of silica nanoparticles with Bi-GEPI-1 followed by gold nanoparticle attachment.

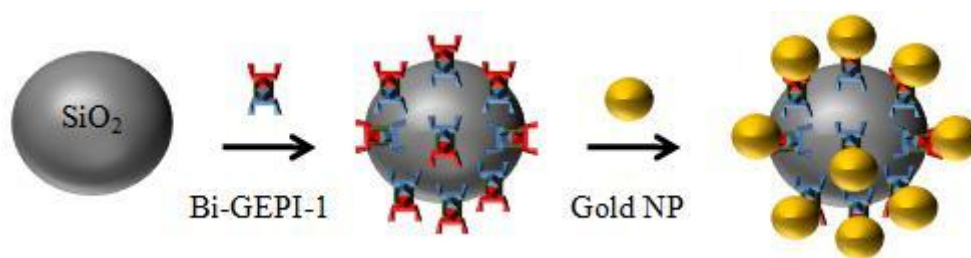


**Figure 3.81:** Gold nanoparticle attachments to silica nanoparticle pre-functionalized by Bi-GEPI-1.

First step was carried out by incubating the silica nanoparticles with Bi-GEPI-1. Since the peptide sequence contains Try and Trp, unbound peptide concentration could be determined through UV measurement at 280 nm following precipitation of silica nanoparticles by centrifugation (see Materials and Methods Section). Subsequently, total number of the bound peptides was calculated by subtracting the initial number of peptides from the number of unbound peptides. Finally, the total number of bound peptides was normalized by total number of silica nanoparticles to find number of bound peptides per silica nanoparticle, i.e. ~40000 molecules per a silica nanoparticle. Resultant silica nanoparticles functionalized with Bi-GEPI-1 were then incubated with the amount of gold nanoparticles in excess of that estimated for full monolayer coverage of the silica core (see Materials and Methods Section), yielding gold nanoparticle assembly onto silica surface. SEM characterization proves the conjugation of silica nanoparticles with gold nanoparticles (Figure 3.82 and Figure 3.83). Moreover, it should be noted that the conjugation doesn't occur when the peptide isn't used as linker (Figure 3.84). The results indicate that the assembly of gold nanoparticles on silica surface is GEPI dependent instead of non-specific interactions between the particles.

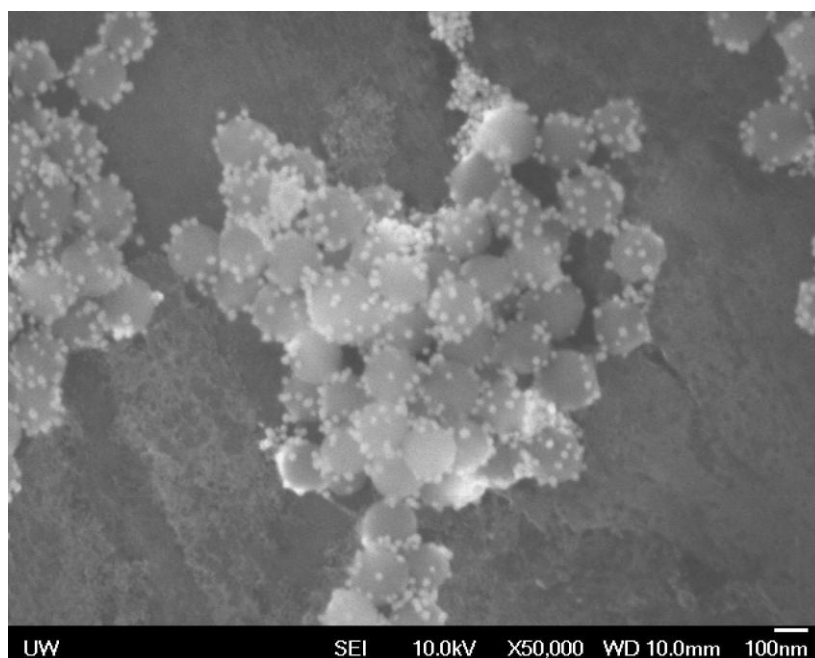


**Figure 3.82:** SEM image of gold nanoparticle attachments to silica nanoparticle pre-functionalized by Bi-GEPI-1 (at lower magnification).

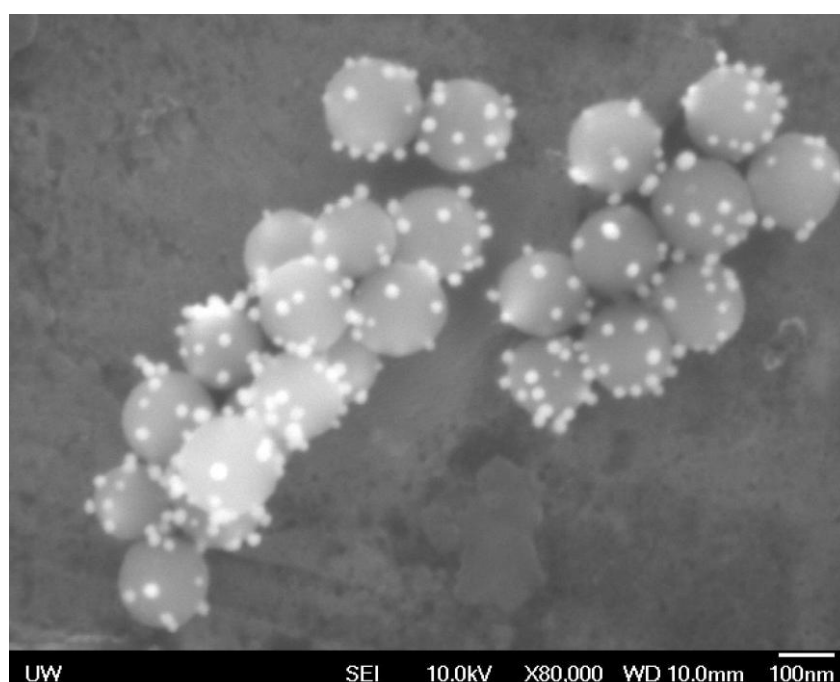


**Figure 3.83:** SEM image of gold nanoparticle attachments to silica nanoparticle pre-functionalized by Bi-GEPI-1 (at higher magnification).

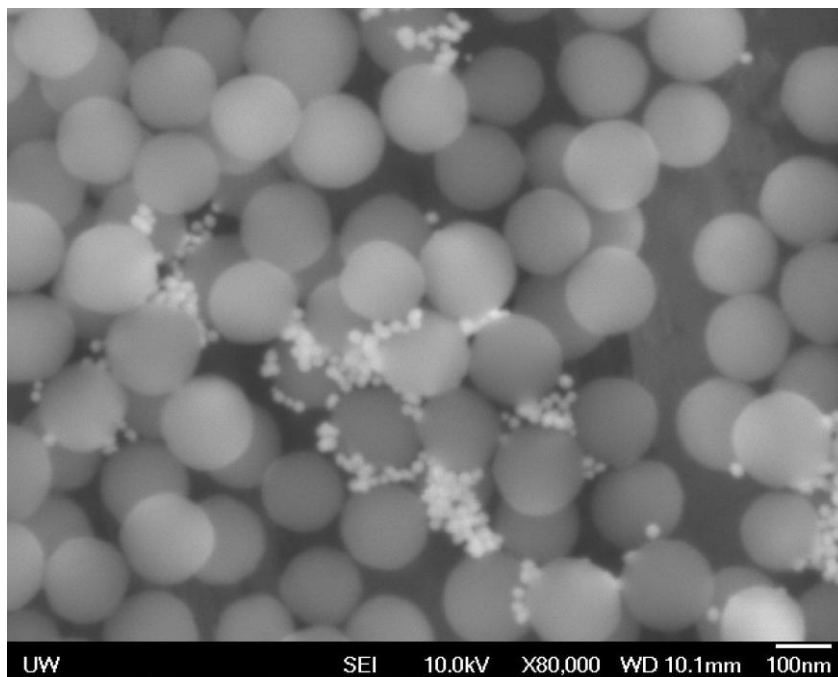


**Figure 3.84:** SEM image of gold nanoparticle attachments to silica nanoparticles in absence of Bi-GEPI-1.

Next, the conjugates and free gold nanoparticles were scanned by UV-vis spectrometer. Core-shell assemblies displayed bimodal extinction maxima, generated presumably by individual and collective plasmon responses from assembled gold nanoparticles on the silica surface, which was red-shifted from LSPR  $\lambda_{\text{max}}$  of free gold nanoparticles (Figure 3.85). Since citrate weakly binds to the gold nanoparticle surface, citrate coated gold nanoparticles are vulnerable in solution, especially very sensitive to salt concentration that may cause agglomeration. Thus they should be coated with strong capping agents or attached to solid support for practical applications in biotechnology. Previously, gold nanoparticle attachment on planar silica substrate was already demonstrated (see Section 3.21). Here, the attachment onto silica surface was also succeeded at nano-scale, providing a strong platform for solution based sensing [61] as well as optical contrast agents [353].



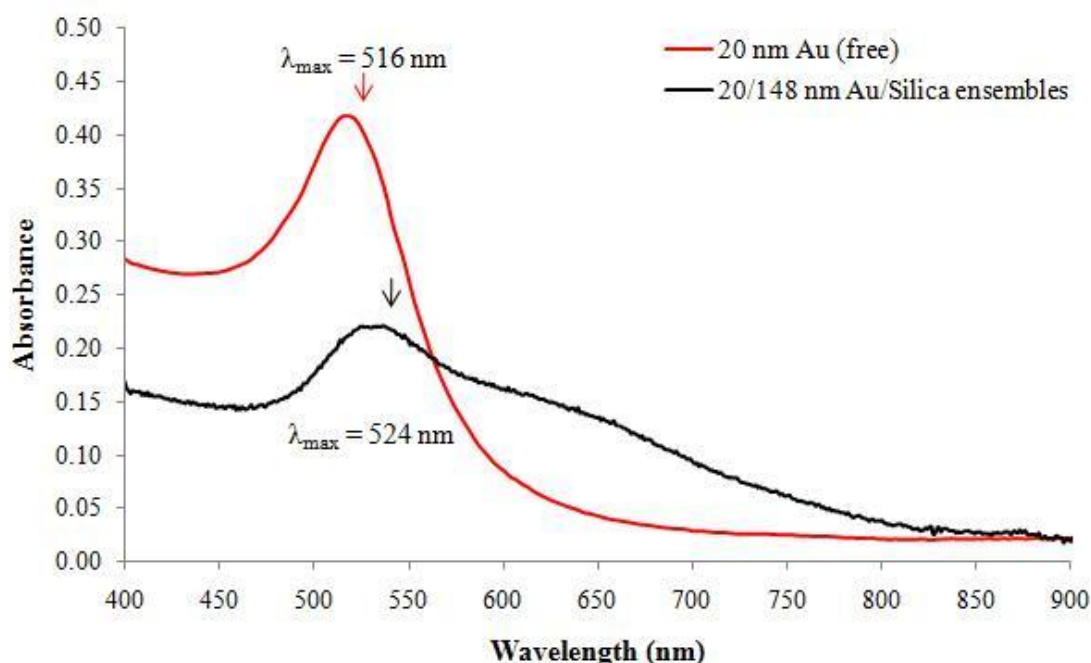


**Figure 3.85:** Extinction spectra of free gold nanoparticles and 20/148 nm Au/SiO<sub>2</sub> ensembles. Arrows indicate the position of the extinction maxima of each spectrum.

### 3.5.2 Gold Formation around Silica nanoparticles

Metal nanoshells consists of two materials; dielectric core, *e.g.* silica and metal thin layer surrounding the core, *e.g.* gold. Conventional approaches for preparation of metal nanoshells generally involve three steps: 1) functionalization of silica nanoparticles with silane-based bifunctional chemicals such as APTES (Step 1 requires heating to form the bonds between silane and silica surface. Also, the reaction should be carried out in fume hood due to toxicity of the linker molecule.), 2) assembly of gold nanoparticles onto silica surface, 3) gold formation around Au/SiO<sub>2</sub> conjugates in presence of gold ion and reducing agent such as, formaldehyde [332]. Simply, the procedure is based on to locate nucleation sites on silica surface followed by gold reduction to form the metal shell around the core. Since gold and silica surfaces do not wet each other, gold formation cannot occur on silica surface unless gold nanoparticles utilized here as nucleation sites are attached to the silica surface through bifunctional linker. Moreover, another crucial point is that thickness and roughness of the metal film are highly dependent on the size of the gold nanoparticle used as nucleation site.

It turned out that gold binding sequences could also have ability in reducing gold ions (+3) to elemental gold (0) [311]. Based on this fact, a new approach for

preparation of gold nanoshells (Au-shell@Silica-core) has been studied. Basically, it has two steps including functionalization of silica nanoparticles with GEPI followed by incubation of peptide-silica conjugates in  $\text{HAuCl}_4$  under reducing conditions (Figure 3.86). Among the bifunctional peptides consisting of silica and gold binding regions, Bi-GEPI-1, -2 and -6 were the candidates. Figure 3.87 shows the number of bifunctional peptides assembled onto one silica nanoparticle following first step (see Materials and Methods Section). All three peptides seemed to have similar silica binding performance. However, Bi-GEPI-6 showed two times better activity in terms of gold formation (see Materials and Methods Section).

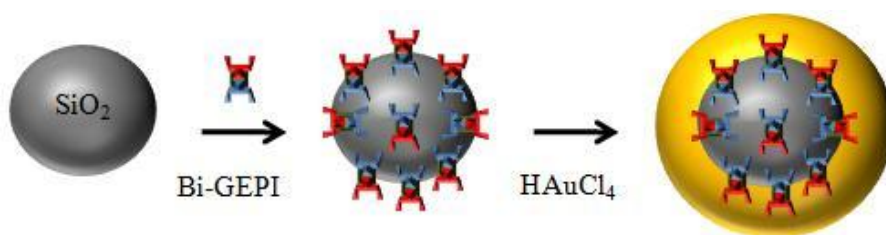


**Figure 3.86:** Scheme for GEPI-based gold nanoshell (Au-shell@Silica-core) preparation.

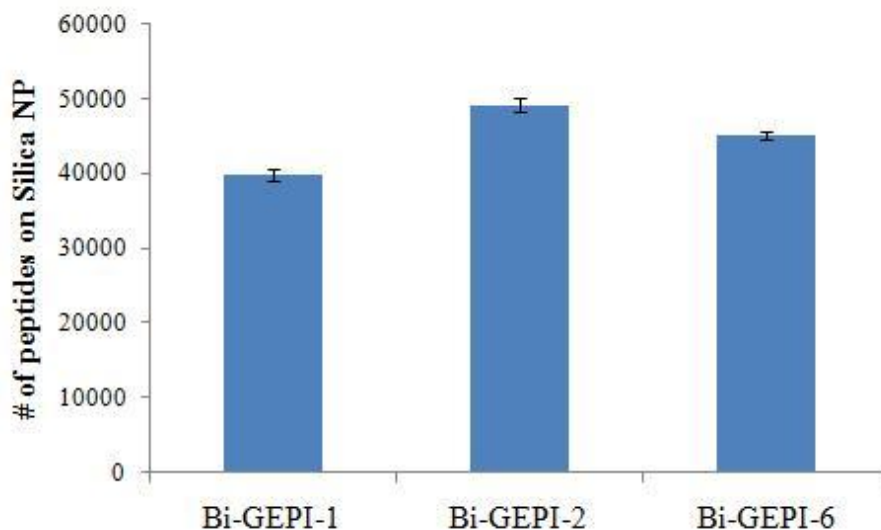


**Figure 3.87:** Comparison for number of bound Bi-GEPIs per silica nanoparticle.

General gold formation procedures involve  $\text{HAuCl}_4$  salt addition at a certain level of concentration causing a lower pH of final solution ( $\sim 2.5$ - $3.0$ ) [221]. This harsh condition can result in peptide detachment from the silica surface. Hence  $\text{K}_2\text{CO}_3$  salt was used to obtain final  $\text{HAuCl}_4$  solution with pH of  $\sim 7.5$  for the second step. So, silica nanoparticle-peptide conjugates were introduced into freshly prepared  $\text{K}_2\text{CO}_3$ -

neutralized  $\text{HAuCl}_4$  solution, resulting in no detectable gold formation around silica nanoparticles till formaldehyde addition. Since formaldehyde is very strong gold-reducing agent in neutral and basic pH conditions, gold formation around silica nanoparticles was occurred upon formaldehyde addition with a color change from colorless to blue. Unfortunately, none of the peptide candidates mentioned above could lead to gold formation by itself (in absence of formaldehyde). It should be noted that the gold formation test mentioned earlier was carried out in acidic  $\text{HAuCl}_4$  solution with free peptides (no attachment to the surface-see Materials and Methods). Most probably, higher pH condition or/and the change in peptide conformation upon binding to silica surface decrease/cancel the gold formation activity of the peptides. Moreover, in presence of formaldehyde, Bi-GEPI-6 was the one that could provide formation of gold nanoshell where the peptide acted as nucleation site on silica surface. To support this hypothesis, two control experiments were also carried out; 1) only silica nanoparticles (without peptide) were exposed to the  $\text{K}_2\text{CO}_3$ -neutralized  $\text{HAuCl}_4$  solution followed by formaldehyde addition, 2) formaldehyde alone was added to the  $\text{K}_2\text{CO}_3$ -neutralized  $\text{HAuCl}_4$  solution. Then, both the sample and the controls were scanned under UV-vis spectrometer. Control solutions revealed extinction spectra that could match with those given by gold nanoparticles in the Vis region. However, silica-peptide conjugates incubated with the  $\text{K}_2\text{CO}_3$ -neutralized  $\text{HAuCl}_4$  solution with formaldehyde displayed an extinction spectrum red shifted to the NIR region (Figure 3.88).

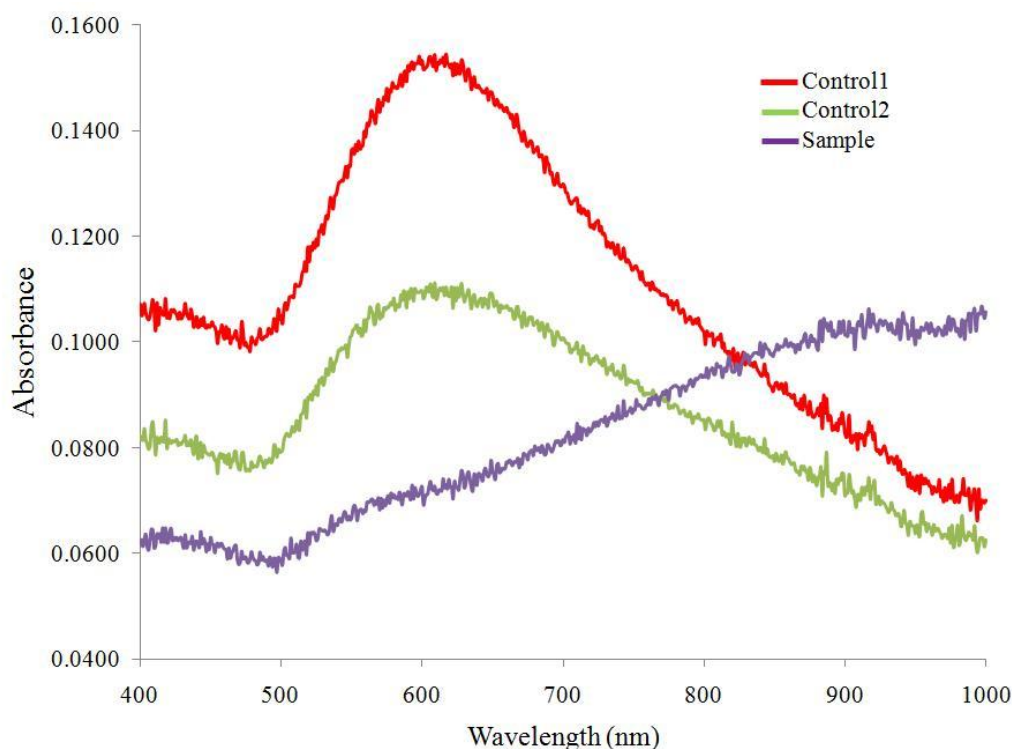


**Figure 3.88:** Extinction spectra of control 1, control 2, and the nanostructures (sample) prepared using the protocol depicted in Figure 3.86 with formaldehyde.

SEM characterization in combination of EDX spectroscopy also proves the presence of individual gold nanoparticles formed by gold reduction with formaldehyde in control 1 and control 2 (Figure 3.89 and Figure 3.90, respectively). In control 1, it is also obvious that there is no gold formation around silica nanoparticles. However, in the case of silica spheres pre-functionalized with Bi-GEPI-6, larger nanostructures ( $315 \pm 39$  nm), possibly Au-shell@Silica-core, were imaged (Figure 3.91 and Figure 3.92) comparing to bare silica ( $148 \pm 10$  nm) and those gold nanoparticles formed in control experiments.

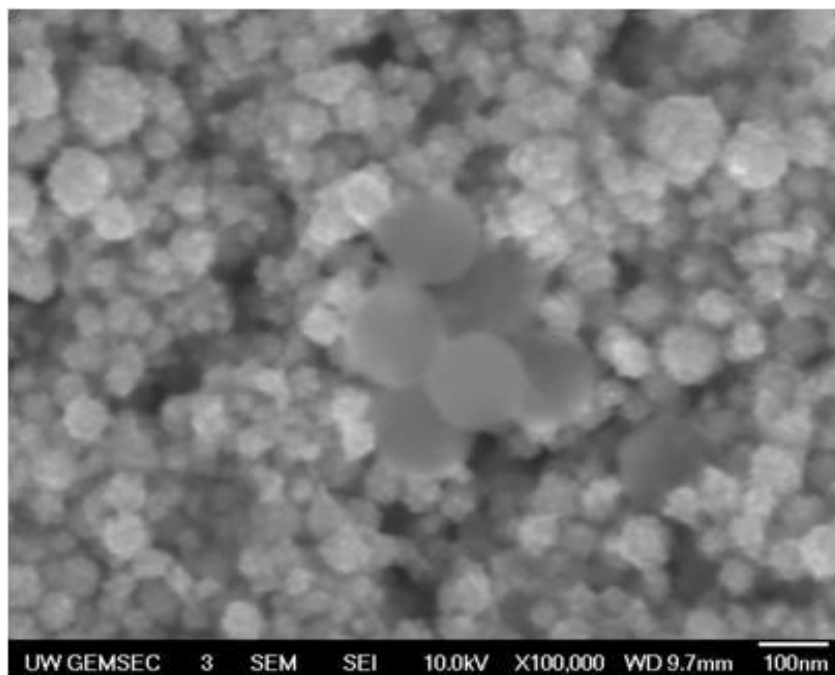


**Figure 3.89:** SEM image of control 1 where only silica nanoparticles were exposed to gold ion solution under reducing condition.

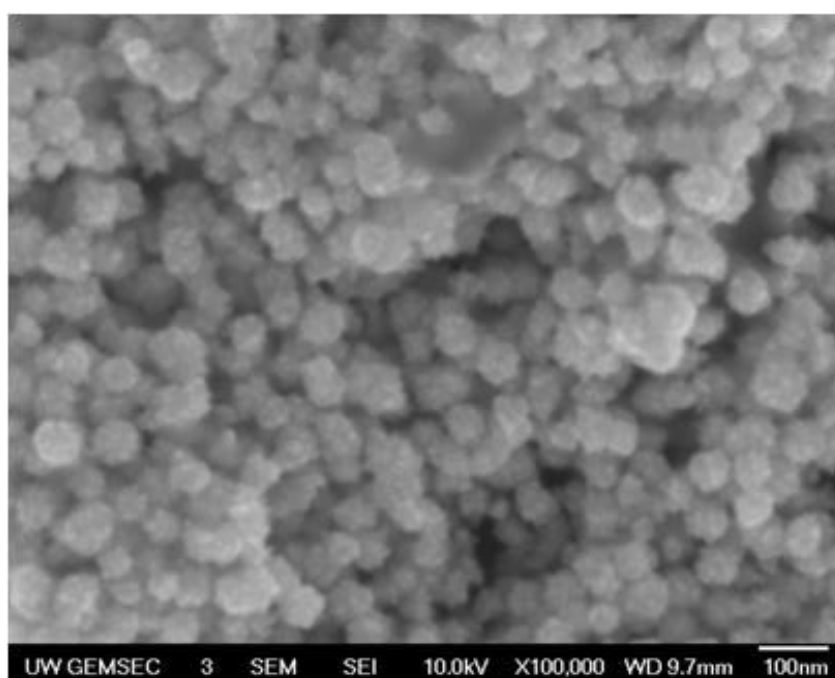


**Figure 3.90:** SEM image of control 2 where only formaldehyde was exposed to gold ion solution.

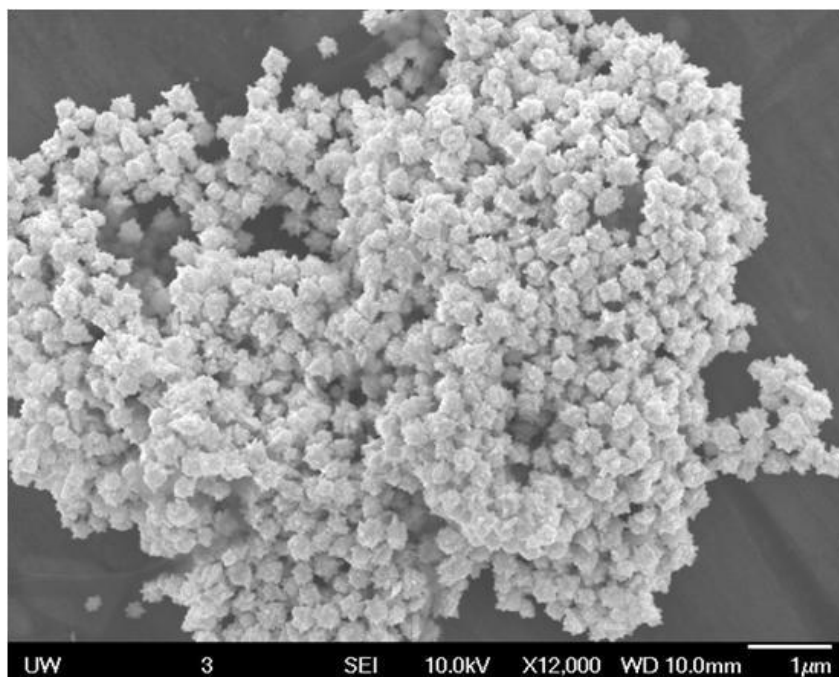


**Figure 3.91:** SEM image of nanostructures synthesized using the protocol shown in Figure 3.86 in combination with formaldehyde (at lower magnification).

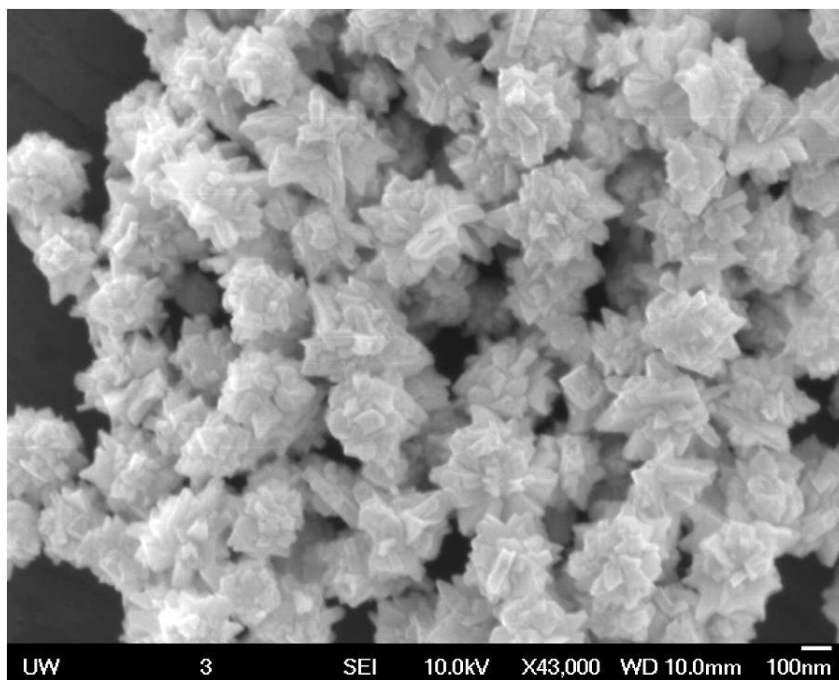


**Figure 3.92:** SEM image of nanostructures synthesized using the protocol shown in Figure 3.86 in combination with formaldehyde (at higher magnification).

EDX spectroscopy was utilized to gain insight into the composition of the nanostructures. Firstly, the probe of EDX detector was separately spotted on bare silica nanoparticle and gold nanoparticle that was formed in control 1. Characteristic silicon signal obtained from the silica nanoparticle (around 1.75 keV) and three signals from the gold nanoparticle (two weak peaks around 1.68 and 2.40 keV; one strong peak around 2.20 keV) were recorded (Figure 3.93 and Figure 3.94, respectively). The intensity of the spectrum presented in Figure 3.94-b is very low around 1.75 keV since the target doesn't have silicon-based compound *i.e.* silica core. Additionally another control spectrum was also recorded from the aluminum background (Appendix A-8) to make sure that there was no interference between the signals coming from the background and gained from the corresponding nanoparticles. Lastly, the EDX spectrum from one of the nanostructures presented in Figure 3.91 and Figure 3.92 was taken displaying both silicon and gold signals. Comparing to Figure 3.94-b, the signal intensities around both 1.68 and 1.75 keV are increased indicating gold-silicon composition rather than single gold content.

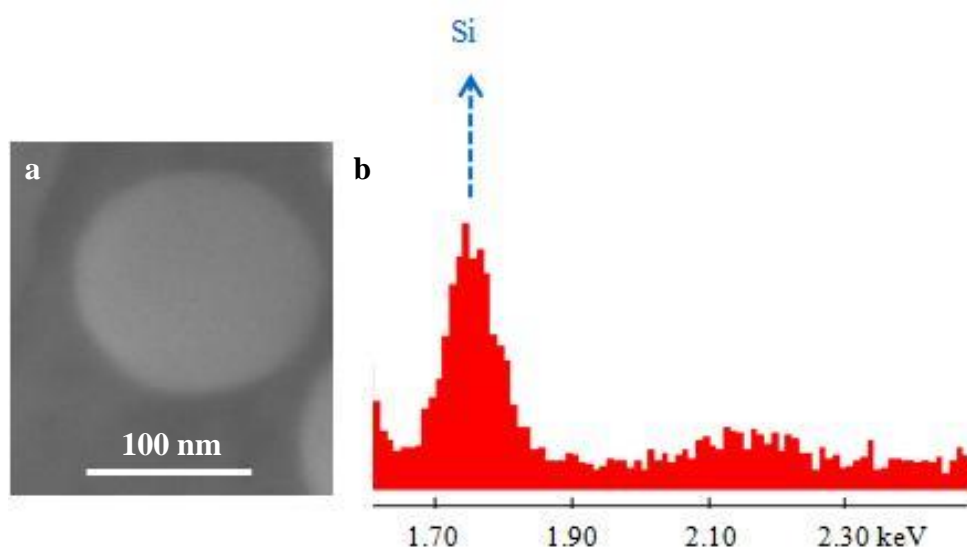


**Figure 3.93:** Characterization of silica nanoparticle by (a) SEM, (b) with EDX spectroscopy. Blue arrow indicates the position of corresponding silicon signal.

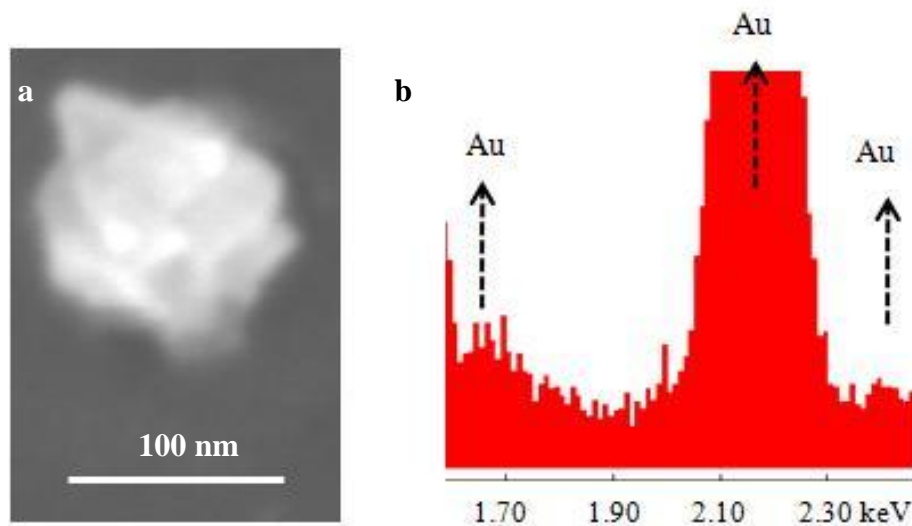


**Figure 3.94:** Characterization of gold nanoparticles obtained from control experiment-1 by (a) SEM, (b) with EDX spectroscopy. Black arrows indicate the positions of corresponding gold signal.

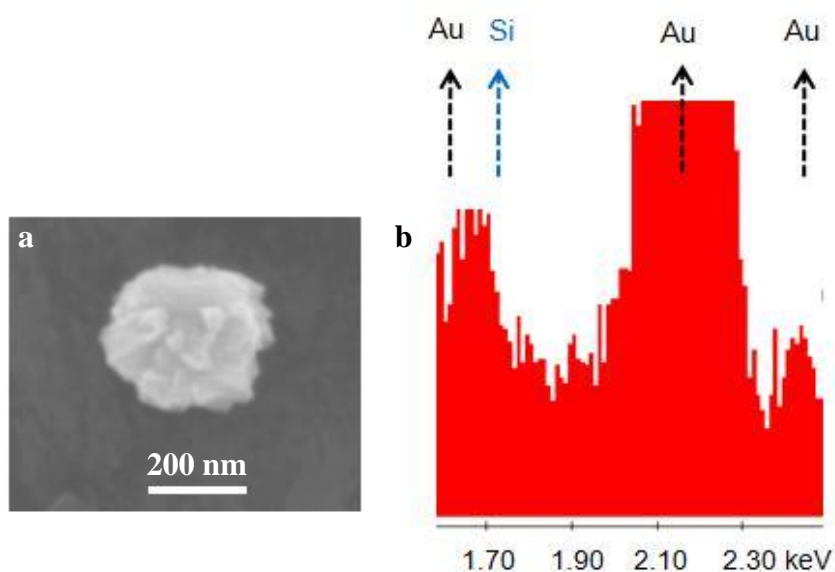


**Figure 3.95:** Characterization of gold nanoshells by (a) SEM, (b) with EDX spectroscopy. Black and blue arrows indicate the positions of corresponding gold and silicon signals, respectively.

Overall results show that gold formation around silica nanoparticle surface is possible with use of bifunctional peptide as nucleation site. Resultant nanostructures have nano spikes resulting in very rough surface. In the literature, it was found that aspartic acid, lysine, arginine, tyrosine, and tryptophan could initiate and control the syntheses of gold nanostructures at room temperature [354-356]. Also, the lysine, arginine, aspartate, glutamate, and histidine residues may sequester metal ions or



metal ion complexes [357]. Subsequently, these amino acid residue-metal ion complexes may subsequently be reduced to metal nanoparticles by addition of external reducing agents [357]. Here, the aa sequence of Bi-GEPI-6 contains tryptophan, arginine, and lysine residues (see Table 2.1). Therefore, gold ions may only bind to the peptides pre-assembled on silica surface leading to gold deposition in presence of formaldehyde or additionally, peptide may also play role in the gold formation step affecting the morphology of the shell. If the morphology is dependent on the peptide, then one can control the surface roughness and even thickness of the metal shell. These issues are still unclear and require further study. Moreover, the gold formation step is very fast and difficult to control since formaldehyde is very strong reducing agent. Other reagents such as hydroxylamine may yield more controlled reaction. As a fact, an inorganic-binding peptide based synthesis procedure was demonstrated for preparation of hybrid nanostructures with an optical plasmon response red shifted into NIR region that is a window for various biomedical applications such as cancer therapy and SERS based detection [230].

### 3.6 Conclusions

Advances in nanotechnology certainly reshape the human life with an increased standard. As novel fabrication techniques at nano-scale are developed with better understanding of the interactions between the nano-entities, production of new devices with advanced features will be available, dominating the life. For sure, nanobiotechnology, branch of nanotechnology, has been also exhibiting great performance in this context. At this point, molecular biomimetics is an important area to help scientists to gain insight on the interactions between biomolecules and nano-components composed of different inorganic materials, which already exist in nature with a certain molecular specificity. With better knowledge on biomolecule-material interaction, one can easily develop new hybrid materials/devices comprised of controlled structures that in turn, will enable better achievement at crucial issues in biotechnology and medicine, *e.g.* rapid disease detection with higher sensitivity. These developments will also increase quality of the outcome from core research in biology involving such as cell-cell or protein-protein interaction studies.

In this thesis, preparation of hybrid functional platforms constituted of GEPI, GEPI-protein constructs, nanoparticles, and inorganic substrates has been demonstrated in

the context of enzyme immobilization and biosensing applications. Taking advantage of molecular biomimetics enabled us to develop new molecular linking systems as well as inorganic synthesis method where, in both cases, GEPI successfully took place proving itself to be an alternative for conventional synthetic reagents such as thiol-, silane- based molecules. Overall experimental protocols involve ambient conditions such as aqueous media with a pH~7.5, room temperature and eliminate chemical reactions requiring complicated procedures with toxic agents.

Firstly, the utilization of inorganic-binding peptides as molecular linkers for the immobilization of enzymes on solid materials was demonstrated. To prove the concept, cell surface display-selected gold binding peptide (GBP1) to self-immobilize AP on a gold surface was used. The enzyme genetically fused to multiple repeats (n= 5, 6, 7, 9) of GBP1 were expressed in *E. coli* cells. The bi-functional activity of the construct, that is, both the gold binding and phosphatase activities, was conserved as demonstrated by spectroscopic and biochemical assays. The hybrid enzyme construct that displayed the highest bi-functional activity was selected for self-immobilization experiments. Both spectroscopic and imaging assays showed that gold-specific linkage provided by GBP1 resulted in higher enzymatic activity compared to the wild-type AP. GBP1 mediated AP immobilization, therefore, provided easier access of the enzyme's active site to the surrounding aqueous media [334].

Moreover, it was also shown that  $\mu$ CP fabricated micro-patterned substrates can be used to increase the number density of the self-immobilized enzymes by providing targeted assembly through a guidance during the assembly process. The consequence of the targeted immobilization of the genetically linked GBP1 is a simultaneous effect of directed self-assembly and higher AP activity per area compared to the wild-type. Self-assembly of the inorganic-binding peptide-linked enzyme on the surface is completed fairly rapidly, that is, within hours. This approach is universal and could be extendable to any solid surface such as platinum, graphite, and silica with the use of appropriate inorganic-binding peptides [334]. Here, although only gold was used as inorganic platform, the method may be applicable in multi-material patterned functional platforms [286] that are addressed through specific inorganic-binding peptide tags, efficient and utilizable for a wide range of applications in bionanotechnology.

Besides protein assembly, nanoparticle immobilization on inorganic substrates was also achieved using Bi-GEPI displaying two inorganic-binding activities under ambient conditions. For gold and silica nanoparticle immobilization, gold-binding sequence was chemically linked to either N-terminus or C-terminus of silica-binding sequence *via* either flexible –GlyGlyGly- linker or rigid –ProProPro- linker, yielding four different bifunctional peptides. In the case of gold nanoparticle immobilization on glass substrate, the results show that location of individual binding regions is important and QBP1 sequence should be at the N terminus of the bifunctional GEPI (Bi-GEPI-2 and Bi-GEPI-2) to achieve higher number of gold nanoparticle attachment. Moreover, the linker choice may also affect the bifunctionality. The rigid linker, triplet of prolin (in Bi-GEPI-2), showed slightly better performance comparing to –GlyGlyGly- linker (in Bi-GEPI-1). However, all four Bi-GEPIs showed similar immobilization activity for silica nanoparticle attachment on gold surface. Assembly of silver nanoparticles was also achieved however bifunctional peptide was only synthesized with flexible linker. Overall, results are promising and can be improved by designing new linkers and inorganic-binding sequences using computational methods.

Multifunctional micro/nanopatterned substrates involving GEPI-driven assembly of inorganic or biological nano-entities were prepared using different lithographic techniques such as  $\mu$ CP and DPN. Inorganic solid-binding peptides were utilized as ink for  $\mu$ CP and DPN printing as well as linker for self-assembly [335, 336]. The results show that molecular constructs based on GEPIs, e.g., QBP1 can be designed with bifunctionality, including both a solid-substrate-binding ability and incorporating a target molecule carrying out a robust function. Firstly, QBP1-based molecular constructs with either fluorescein or biotin displaying nanophotonic or biomolecular recognition functions were used. Furthermore, a procedure involving microcontact printing and self-assembly was carried out using these QBP1-based molecular constructs. Using a combined procedure, one can coassemble fluorescein molecule and SA-QD through QBP1-mediated and targeted self-assembly, respectively, leading to multifunctional micropatterned substrate fabrication. Similarly, this procedure was applied with Bi-GEPI-1 or Bi-GEPI-5 and again, QBP1-bio to coassemble gold or silver nanoparticles and SA-QD in patterned fashion. Here, control experiments proved that success of the “ink” is related with the

peptide sequence since QBP2 called “weak binder” fails to be printed. Additionally, QBP1 showed binding activity towards silica but not to gold, indicating that the binding mechanism is also surface specific [335]. Same strong binder was successfully demonstrated as “ink” for DPN to produce high resolution nanoscale patterns. This fact, therefore, will be considered for the micro/nano-array applications that require high-spatial-resolution surface bifunctionalization followed by targeted assembly, as well as biosynthesis of inorganic materials *via* peptides micro/nano-patterned on the surface [336].

Noble metal nanoparticle based platforms have been utilized in biosensing applications due to their powerful optical properties [6, 224, 256]. NSL is a straight forward and robust technique to produce array of inorganic nanostructures with controlled size and interspacing [255]. NSL-fabricated silver nanostructures were used as LSPR based biosensor in combination with a probe, *i.e.* biotin that was immobilized *via* AgBP1-mediated assembly to detect target molecule, SA-AP. Also, detailed study on fabrication of LSPR based biosensor was carried out using Bi-GEPI-1 to attach gold nanoparticles on glass substrate followed by probe (5GBP1-AP) assembly for immunospecific detection of the target antibody (Anti-AP). Due to the local refractive index increase at interface of gold nanoparticles, binding of probe and target molecules were monitored by LSPR spectroscopy. The results confirmed that gold binding peptide acted as an erector to immobilize Alkaline phosphatase, allowing three times better sensitivity in antibody coupling reaction at lower concentrations comparing to control molecule, AP. Using our model, the detection limit could be down to ~30 nM of target molecule and is compatible with the literature where conventional thiol- and silane-based chemical methods were employed for the attachment of nanoparticles and proteins [348]. In combination of inorganic-binding peptides in bifunctional molecular constructs, *i.e.* 5GBP1-AP, Bi-GEPI-1 and optically active metal noble nanoparticles, these hybrid materials are promising platforms to detect various important biomolecules in bionanotechnology. In addition, targeted assembly of Anti-AP was also demonstrated onto 5GBP1-AP-printed gold, leading to a microarray of target molecule on the substrate.

One of the major advantages for gold and silver nanoparticles is that their optical properties can be tuned for various applications such as contrast imaging [353], SERS based sensing [358]. In addition, solution based applications require higher

stability for the nanoparticles upon exposure to the biological media [359]. A method to prepare nanoscale platform with higher stability and optical function can involve assembly of noble metal nanoparticles onto larger silica nanoparticles. The attachment of gold nanoparticles to the silica surface necessitates a linker at the interface. Here, we used Bi-GEPI-1 to bridge two different inorganic nanoparticles. The SEM results clearly show that the gold attachment was occurred onto silica nanoparticles pre-functionalized by Bi-GEPI-1, leading to red-shift at the plasmon response of the nanoparticles. Future studies will be on the attempts to increase the number of gold nanoparticles attached on silica particle surface since higher attachment densities should strengthen the electromagnetic coupling between nanoparticles on the silica core resulting higher red-shift in their collective plasmon responses [360].

Furthermore, GEPI-assembled silica nanoparticles were used to prepare optically active hybrid nanostructures by reducing gold onto silica surface, forming a metal shell around silica core. Apart from the binding affinities, here bifunctional peptide acted as nucleation site in gold formation step, excluding gold nanoparticle attachment which is a must for those prepared by conventional methods. The final nanostructures with highly rough outer-shell surface showed different optical properties than control nanoparticles. The plasmon peak was shifted to NIR region where various biomedical applications can be carried out. Since the extinction maxima of the metal nanoshells is highly dependent on the size and the shell thickness, control of the shell thickness and the roughness of metal layer will be the topic of the future studies where effect of peptide sequence on gold formation and morphology will be explored.

In conclusion, GEPIs are smart molecules isolated using molecular biology protocols such as phage and cell surface display and subsequently characterized by different qualitative and semi-qualitative techniques, e.g. AFM, QCM, SPR, and FM [7, 279, 298, 323]. Bioinformatics can be also applied to these peptide sequences to improve their binding activity or material specificity [304]. The overall results reported here point out the utilization of GEPI and GEPI fused proteins as building blocks and molecular tools in fabrication of micro/nanoscale hybrid platforms displaying multifunctionality. As a summary;

- GEPIs were shown to be promising linker for the attachment of nanoparticles and biomolecules.
- GBP mediated AP immobilization provided higher enzymatic activity comparing to AP wild type.
- GEPIs were successfully used as ink for patterning techniques, *i.e.*  $\mu$ CP and DPN. Using DPN, sub 100-nm-wide peptide lines were produced.
- Assembly and writing procedures are simple and takes place at ambient conditions (aqueous, room temperature..)
- GEPI mediated AP and nanoparticle immobilization were used to fabricate platforms to detect biomolecules.
- With these sensors, detection at nM range of target concentrations was achieved, requiring very small sample volumes (~150  $\mu$ l).
- Bi-GEPI was used to hybrid nanomaterials that have potential optical properties for biotargeting, sensing and thermal ablation for cancer.

Certainly, GEPI will play critical role in variety of areas such as proteomics, pharmagenomics, protein biosensors, tissue engineering, and nanoparticle-based nanotechnologies (e.g., nanoparticle-based cancer probing) due to great potential of inorganic binding peptides in biotechnology and medicine. Particularly, the following highlights as the future prospects are proposed based on the results presented in this study:

- Enhanced molecular detection *via* LSPR-based bionanosensor,
- Multiple target detection with GEPI-protein constructs,
- Controllable nanoshell formation (shell thickness & surface roughness) and its functionalization for biomedical applications *via* plasmonics,
- Designing and synthesis of GEPI-based heterofunctional molecular constructs as molecular rulers,
- Demonstration of gold & silver nanoparticles for addressable plasmonic structures towards enhanced sensing & detection.



## REFERENCES

- [1] **Feynman, R.**, 1959. There's plenty of room at the bottom. In *The American Physical Society Meeting*, CalTech, California, USA.
- [2] **Papazoglou, E. S. and Parthasarathy, A.**, 2007. *Bionanotechnology*, p 1-14, ed. Enderle, J. D., Morgan & Claypool, New Jersey, USA.
- [3] **Hamley, I. W.**, 2003. Nanotechnology with soft materials, *Angew. Chem. Int. Ed.*, **42**, 1692-1712.
- [4] **Piner, R. D., Zhu, J., Xu, F., Hong, S. H. and Mirkin, C. A.**, 1999. "Dip-pen" Nanolithography, *Science*, **283**, 661-663.
- [5] **Mirkin, C. A., Letsinger, R. L., Mucic, R. C. and Storhoff, J. J.**, 1996. A DNA-based method for rationally assembling nanoparticles into macroscopic materials, *Nature*, **382**, 607-609.
- [6] **Haes, A. J. and Van Duyne, R. P.**, 2002. A nanoscale optical biosensor: Sensitivity and selectivity of an approach based on the localized surface plasmon resonance spectroscopy of triangular silver nanoparticles, *J. Am. Chem. Soc.*, **124**, 10596-10604.
- [7] **Sarikaya, M., Tamerler, C., Jen, A. K. Y., Schulten, K. and Baneyx, F.**, 2003. Molecular biomimetics: Nanotechnology through biology, *Nat. Mater.*, **2**, 577-585.
- [8] **Goodsell, D. S.**, 2004. *Bionanotechnology: Lessons from nature*, p 1-8, ed. Willey-Less, New Jersey, USA.
- [9] **Sarikaya, M., Tamerler, C., Schwartz, D. T. and Baneyx, F. O.**, 2004. Materials assembly and formation using engineered polypeptides, *Annual Review of Materials Research*, **34**, 373-408.
- [10] **Tamerler, C. and Sarikaya, M.**, 2009. Genetically designed peptide-based molecular materials, *Acs Nano*, **3**, 1606-1615.
- [11] **Sarikaya, M.**, 1999. Biomimetics: Materials fabrication through biology, *Proc. Natl. Acad. Sci. U. S. A.*, **96**, 14183-14185.
- [12] **Ball, P.**, 2001. Life's lessons in design, *Nature*, **409**, 413-416.
- [13] **Seeman, N. C. and Belcher, A. M.**, 2002. Emulating biology: Building nanostructures from the bottom up, *Proc. Natl. Acad. Sci. U. S. A.*, **99**, 6451-6455.
- [14] **Vogel, P. D.**, 2005. Nature's design of nanomotors, *Eur. J. Pharm. Biopharm.*, **60**, 267-277.
- [15] **Okten, Z., Churchman, L. S., Rock, R. S. and Spudich, J. A.**, 2004. Myosin vi walks hand-over-hand along actin, *Nat. Struct. Mol. Biol.*, **11**, 884-887.



- [16] **Ferrari, M.**, 2005. Cancer nanotechnology: Opportunities and challenges, *Nature Reviews Cancer*, **5**, 161-171.
- [17] **Rusmini, F., Zhong, Z. Y. and Feijen, J.**, 2007. Protein immobilization strategies for protein biochips, *Biomacromolecules*, **8**, 1775-1789.
- [18] **Castner, D. G. and Ratner, B. D.**, 2002. Biomedical surface science: Foundations to frontiers, *Surf. Sci.*, **500**, 28-60.
- [19] **Blawas, A. S. and Reichert, W. M.**, 1998. Protein patterning, *Biomaterials*, **19**, 595-609.
- [20] **Malmsten, M.**, 2000. Protein adsorption at the solid-liquid interface, in *Protein architecture-interfacing molecular assemblies and immobilization biotechnology* p. 1-23, Eds. Lvov, Y. and Mohwald, H., Marcel Dekker, Inc., New York, USA.
- [21] **Liu, J. Q., Zhang, Q., Remsen, E. E. and Wooley, K. L.**, 2001. Nanostructured materials designed for cell binding and transduction, *Biomacromolecules*, **2**, 362-368.
- [22] **Zhu, H. and Snyder, M.**, 2003. Protein chip technology, *Curr. Opin. Chem. Biol.*, **7**, 55-63.
- [23] **Hanson, K. L., Filipponi, L. and Nicolau, D. V.**, 2004. Biomolecules and cells on surfaces – fundamental concepts, in *Microarray technology and its applications*, p. 23-44, Eds. Muller, U. R. and Nicolau, D. V., Springer, Berlin, Germany.
- [24] **Buijs, J., vandenBerg, P. A. W., Lichtenbelt, J. W. T., Norde, W. and Lyklema, J.**, 1996. Adsorption dynamics of igg and its f(ab')(2) and fc fragments studied by reflectometry, *J. Colloid Interface Sci.*, **178**, 594-605.
- [25] **Norde, W., Macritchie, F., Nowicka, G. and Lyklema, J.**, 1986. Protein adsorption at solid liquid interfaces - reversibility and conformation aspects, *J. Colloid Interface Sci.*, **112**, 447-456.
- [26] **Elwing, H., Welin, S., Askendahl, A. and Lundstrom, I.**, 1988. Adsorption of fibrinogen as a measure of the distribution of methyl-groups on silicon surfaces, *J. Colloid Interface Sci.*, **123**, 306-308.
- [27] **Malmsten, M. and Veide, A.**, 1996. Effects of amino acid composition on protein adsorption, *J. Colloid Interface Sci.*, **178**, 160-167.
- [28] **Malmsten, M., Burns, N. and Veide, A.**, 1998. Electrostatic and hydrophobic effects of oligopeptide insertions on protein adsorption, *J. Colloid Interface Sci.*, **204**, 104-111.
- [29] **Morrisse.Bw and Stromber.Rr**, 1974. Conformation of adsorbed blood proteins by infrared bound fraction measurements, *J. Colloid Interface Sci.*, **46**, 152-164.
- [30] **Malmsten, M., Emoto, K. and Van Alstine, J. M.**, 1998. Effect of chain density on inhibition of protein adsorption by poly(ethylene glycol) based coatings, *J. Colloid Interface Sci.*, **202**, 507-517.

- [31] **Prime, K. L. and Whitesides, G. M.,** 1991. Self-assembled organic monolayers - model systems for studying adsorption of proteins at surfaces, *Science*, **252**, 1164-1167.
- [32] **Sofia, S. J., Premnath, V. and Merrill, E. W.,** 1998. Poly(ethylene oxide) grafted to silicon surfaces: Grafting density and protein adsorption, *Macromolecules*, **31**, 5059-5070.
- [33] **Zhang, M. Q., Desai, T. and Ferrari, M.,** 1998. Proteins and cells on peg immobilized silicon surfaces, *Biomaterials*, **19**, 953-960.
- [34] **Burns, N. L., Vanalstine, J. M. and Harris, J. M.,** 1995. Poly(ethylene glycol) grafted to quartz - analysis in terms of a site-dissociation model of electroosmotic fluid-flow, *Langmuir*, **11**, 2768-2776.
- [35] **Asanov, A. N., DeLucas, L. J., Oldham, P. B. and Wilson, W. W.,** 1997. Interfacial aggregation of bovine serum albumin related to crystallization conditions studied by total internal reflection fluorescence, *J. Colloid Interface Sci.*, **196**, 62-73.
- [36] **Schaaf, P., Dejardin, P., Johner, A. and Schmitt, A.,** 1987. Thermal-denaturation of an adsorbed fibrinogen layer studied by reflectometry, *Langmuir*, **3**, 1128-1131.
- [37] **Elofsson, U. M., Paulsson, M. A., Sellers, P. and Arnebrant, T.,** 1996. Adsorption during heat treatment related to the thermal unfolding aggregation of beta-lactoglobulins a and b, *J. Colloid Interface Sci.*, **183**, 408-415.
- [38] **Arnebrant, T., Barton, K. and Nylander, T.,** 1987. Adsorption of alpha-lactalbumin and beta-lactoglobulin on metal-surfaces versus temperature, *J. Colloid Interface Sci.*, **119**, 383-390.
- [39] **Okubo, M., Azume, I. and Yamamoto, Y.,** 1990. Preferential adsorption of bovine serum-albumin dimer onto polymer microspheres having a heterogeneous surface consisting of hydrophobic and hydrophilic parts, *Colloid. Polym. Sci.*, **268**, 598-603.
- [40] **Lensen, H. G. W., Bargeman, D., Bergveld, P., Smolders, C. A. and Feijen, J.,** 1984. High-performance liquid-chromatography as a technique to measure the competitive adsorption of plasma-proteins onto lattices, *J. Colloid Interface Sci.*, **99**, 1-8.
- [41] **Elofsson, U. M., Paulsson, M. A. and Arnebrant, T.,** 1997. Adsorption of beta-lactoglobulin a and b in relation to self-association: Effect of concentration and ph, *Langmuir*, **13**, 1695-1700.
- [42] **Adamczyk, Z., Siwek, B., Zembala, M. and Belouschek, P.,** 1994. Kinetics of localized adsorption of colloid particles, *Adv. Colloid Interface Sci.*, **48**, 151-280.
- [43] **Billsten, P., Wahlgren, M., Arnebrant, T., McGuire, J. and Elwing, H.,** 1995. Structural-changes of t4 lysozyme upon adsorption to silica nanoparticles measured by circular-dichroism, *J. Colloid Interface Sci.*, **175**, 77-82.

- [44] **Kondo, A. and Mihara, J.**, 1996. Comparison of adsorption and conformation of hemoglobin and myoglobin on various inorganic ultrafine particles, *J. Colloid Interface Sci.*, **177**, 214-221.
- [45] **Kwon, Y., Coleman, M. A. and Camarero, J. A.**, 2006. Selective immobilization of proteins onto solid supports through split-intein-mediated protein trans-splicing, *Angew. Chem. Int. Ed.*, **45**, 1726-1729.
- [46] **Kumada, Y., Tokunaga, Y., Imanaka, H., Imamura, K., Sakiyama, T., Katoh, S. and Nakanishi, K.**, 2006. Screening and characterization of affinity peptide tags specific to polystyrene supports for the orientated immobilization of proteins, *Biotechnol. Prog.*, **22**, 401-405.
- [47] **Blodgett, K. B. and Langmuir, I.**, 1937. Built-up films of barium stearate and their optical properties, *Physical Review*, **51**, 0964-0982.
- [48] **Langmuir, I. and Schaefer, V. J.**, 1938. Activities of urease and pepsin monolayers, *J. Am. Chem. Soc.*, **60**, 1351-1360.
- [49] **Xu, Q. C. and Lam, K. S.**, 2003. Protein and chemical microarrays - powerful tools for proteomics, *J. Biomed. Biotechnol.*, 257-266.
- [50] **Dubrovsky, T. B.**, 2000. Immobilization of protein monolayers on planar solid supports, in *Protein architecture-interfacing molecular assemblies and immobilization biotechnology* p. 25-54, Eds. Lvov, Y. and Mohwald, H., Marcel Dekker, Inc., New York, USA.
- [51] **Jung, Y. W., Kang, H. J., Lee, J. M., Jung, S. O., Yun, W. S., Chung, S. J. and Chung, B. H.**, 2008. Controlled antibody immobilization onto immunoanalytical platforms by synthetic peptide, *Anal. Biochem.*, **374**, 99-105.
- [52] **Bornscheuer, U. T.**, 2003. Immobilizing enzymes: How to create more suitable biocatalysts, *Angew. Chem. Int. Ed.*, **42**, 3336-3337.
- [53] **Watzke, A., Kohn, M., Gutierrez-Rodriguez, M., Wacker, R., Schroder, H., Breinbauer, R., Kuhlmann, J., Alexandrov, K., Niemeyer, C. M., Goody, R. S. and Waldmann, H.**, 2006. Site-selective protein immobilization by staudinger ligation, *Angew. Chem. Int. Ed.*, **45**, 1408-1412.
- [54] **Mrksich, M. and Whitesides, G. M.**, 1996. Using self-assembled monolayers to understand the interactions of man-made surfaces with proteins and cells, *Annu. Rev. Biophys. Biomol. Struct.*, **25**, 55-78.
- [55] **Hoffmann, P. W., Stelzle, M. and Rabolt, J. F.**, 1997. Vapor phase self-assembly of fluorinated monolayers on silicon and germanium oxide, *Langmuir*, **13**, 1877-1880.

- [56] **Westcott, S. L., Oldenburg, S. J., Lee, T. R. and Halas, N. J.,** 1998. Formation and adsorption of clusters of gold nanoparticles onto functionalized silica nanoparticle surfaces, *Langmuir*, **14**, 5396-5401.
- [57] **Willner, I., Rubin, S. and Cohen, Y.,** 1993. Photoregulated binding of spiropyran-modified concanavalin-a to monosaccharide-functionalized self-assembled monolayers on gold electrodes, *J. Am. Chem. Soc.*, **115**, 4937-4938.
- [58] **Mrksich, M., Grunwell, J. R. and Whitesides, G. M.,** 1995. Biospecific adsorption of carbonic-anhydrase to self-assembled monolayers of alkanethiolates that present benzenesulfonamide groups on gold, *J. Am. Chem. Soc.*, **117**, 12009-12010.
- [59] **Knichel, M., Heiduschka, P., Beck, W., Jung, G. and Gopel, W.,** 1995. Utilization of a self-assembled peptide monolayer for an impedimetric immunosensor, *Sens. Actuators, B*, **28**, 85-94.
- [60] **Willey, T. M., Vance, A. L., van Buuren, T., Bostedt, C., Terminello, L. J. and Fadley, C. S.,** 2005. Rapid degradation of alkanethiol-based self-assembled monolayers on gold in ambient laboratory conditions, *Surf. Sci.*, **576**, 188-196.
- [61] **Park, T. J., Lee, S. Y., Lee, S. J., Park, J. P., Yang, K. S., Lee, K. B., Ko, S., Park, J. B., Kim, T., Kim, S. K., Shin, Y. B., Chung, B. H., Ku, S. J., Kim, D. H. and Choi, I. S.,** 2006. Protein nanopatterns and biosensors using gold binding polypeptide as a fusion partner, *Anal. Chem.*, **78**, 7197-7205.
- [62] **Yan, M. D., Cai, S. X., Wybourne, M. N. and Keana, J. F. W.,** 1993. Photochemical functionalization of polymer surfaces and the production of biomolecule-carrying micrometer-scale structures by deep-uv lithography using 4-substituted perfluorophenyl azides, *J. Am. Chem. Soc.*, **115**, 814-816.
- [63] **Yan, M. D., Cai, S. X., Wybourne, M. N. and Keana, J. F. W.,** 1994. N-hydroxysuccinimide ester functionalized perfluorophenyl azides as novel photoactive heterobifunctional cross-linking reagents - the covalent immobilization of biomolecules to polymer surfaces, *Bioconj. Chem.*, **5**, 151-157.
- [64] **Jiang, K. Y., Schadler, L. S., Siegel, R. W., Zhang, X. J., Zhang, H. F. and Terrones, M.,** 2004. Protein immobilization on carbon nanotubes via a two-step process of diimide-activated amidation, *J. Mater. Chem.*, **14**, 37-39.
- [65] **Choi, H. J., Kim, N. H., Chung, B. H. and Seong, G. H.,** 2005. Micropatterning of biomolecules on glass surfaces modified with various functional groups using photoactivatable biotin, *Anal. Biochem.*, **347**, 60-66.

- [66] **Betancor, L., Lopez-Gallego, F., Hidalgo, A., Alonso-Morales, N., Mateo, G., Fernandez-Lafuente, R. and Guisan, J. M.,** 2006. Different mechanisms of protein immobilization on glutaraldehyde activated supports: Effect of support activation and immobilization conditions, *Enzyme Microb. Technol.*, **39**, 877-882.
- [67] **Avseenko, N. V., Morozova, T. Y., Ataullakhanov, F. I. and Morozov, V. N.,** 2001. Immobilization of proteins in immunochemical microarrays fabricated by electrospray deposition, *Anal. Chem.*, **73**, 6047-6052.
- [68] **Xie, W. Z., Wang, D., Du, H. W. and Cheng, J.,** 2002. The analysis of antigen-antibody interactions on protein microarrays, *Progress in Biochemistry and Biophysics*, **29**, 311-315.
- [69] **Zhang, Y. Q., Tao, M. L., Shen, W. D., Zhou, Y. Z., Ding, Y., Ma, Y. and Zhou, W. L.,** 2004. Immobilization of l-asparaginase on the microparticles of the natural silk sericin protein and its characters, *Biomaterials*, **25**, 3751-3759.
- [70] **Rozkiewicz, D. I., Kraan, Y., Werten, M. W. T., de Wolf, F. A., Subramaniam, V., Ravoo, B. J. and Reinhoudt, D. N.,** 2006. Covalent microcontact printing of proteins for cell patterning, *Chemistry-a European Journal*, **12**, 6290-6297.
- [71] **Wacker, R., Schroder, H. and Niemeyer, C. M.,** 2004. Performance of antibody microarrays fabricated by either DNA-directed immobilization, direct spotting, or streptavidin-biotin attachment: A comparative study, *Anal. Biochem.*, **330**, 281-287.
- [72] **Edmiston, P. L., Lee, J. E., Cheng, S. S. and Saavedra, S. S.,** 1997. Molecular orientation distributions in protein films .1. Cytochrome c adsorbed to substrates of variable surface chemistry, *J. Am. Chem. Soc.*, **119**, 560-570.
- [73] **Wood, L. L., Cheng, S. S., Edmiston, P. L. and Saavedra, S. S.,** 1997. Molecular orientation distributions in protein films .2. Site-directed immobilization of yeast cytochrome c on thiol-capped, self-assembled monolayers, *J. Am. Chem. Soc.*, **119**, 571-576.
- [74] **Bhatia, S. K., Shriverlake, L. C., Prior, K. J., Georger, J. H., Calvert, J. M., Bredehorst, R. and Ligler, F. S.,** 1989. Use of thiol-terminal silanes and heterobifunctional crosslinkers for immobilization of antibodies on silica surfaces, *Anal. Biochem.*, **178**, 408-413.
- [75] **Hong, H. G., Jiang, M., Sligar, S. G. and Bohn, P. W.,** 1994. Cysteine-specific surface tethering of genetically-engineered cytochromes for fabrication of metalloprotein nanostructures, *Langmuir*, **10**, 153-158.
- [76] **Jongsma, M. A. and Litjens, R.,** 2006. Self-assembling protein arrays on DNA chips by auto-labeling fusion proteins with a single DNA address, *Proteomics*, **6**, 2650-2655.

- [77] **Corey, D. R., Munozmedellin, D. and Huang, A.,** 1995. Strand invasion by oligonucleotide nuclease conjugates, *Bioconj. Chem.*, **6**, 93-100.
- [78] **Kunath, K., Merdan, T., Hegener, O., Haberlein, H. and Kissel, T.,** 2003. Integrin targeting using rgd-pei conjugates for in vitro gene transfer, *J. Gene Med.*, **5**, 588-599.
- [79] **Masri, M. S. and Friedman, M.,** 1988. Protein reactions with methyl and ethyl vinyl sulfones, *J. Protein Chem.*, **7**, 49-54.
- [80] **Fernandezlafuente, R., Rosell, C. M., Rodriguez, V., Santana, C., Soler, G., Bastida, A. and Guisan, J. M.,** 1993. Preparation of activated supports containing low pk amino-groups - a new tool for protein immobilization via the carboxyl coupling method, *Enzyme Microb. Technol.*, **15**, 546-550.
- [81] **Ducker, R. E., Montague, M. T. and Leggett, G. J.,** 2008. A comparative investigation of methods for protein immobilization on self-assembled monolayers using glutaraldehyde, carbodiimide, and anhydride reagents, *Biointerphases*, **3**, 59-65.
- [82] **Tischer, W. and Wedekind, F.,** 1999. Immobilized enzymes: Methods and applications, in *Biocatalysis - from discovery to application*, p. 95-126, Eds.
- [83] **Soellner, M. B., Dickson, K. A., Nilsson, B. L. and Raines, R. T.,** 2003. Site-specific protein immobilization by staudinger ligation, *J. Am. Chem. Soc.*, **125**, 11790-11791.
- [84] **Duckworth, B. P., Xu, J. H., Taton, T. A., Guo, A. and Distefano, M. D.,** 2006. Site-specific, covalent attachment of proteins to a solid surface, *Bioconj. Chem.*, **17**, 967-974.
- [85] **Rao, S. V., Anderson, K. W. and Bachas, L. G.,** 1998. Oriented immobilization of proteins, *Mikrochim. Acta*, **128**, 127-143.
- [86] **Kolb, H. C., Finn, M. G. and Sharpless, K. B.,** 2001. Click chemistry: Diverse chemical function from a few good reactions, *Angew. Chem. Int. Ed.*, **40**, 2004-+.
- [87] **Sun, X. L., Stabler, C. L., Cazalis, C. S. and Chaikof, E. L.,** 2006. Carbohydrate and protein immobilization onto solid surfaces by sequential diels-alder and azide-alkyne cycloadditions, *Bioconj. Chem.*, **17**, 52-57.
- [88] **Lewis, W. G., Green, L. G., Grynszpan, F., Radic, Z., Carlier, P. R., Taylor, P., Finn, M. G. and Sharpless, K. B.,** 2002. Click chemistry in situ: Acetylcholinesterase as a reaction vessel for the selective assembly of a femtomolar inhibitor from an array of building blocks, *Angew. Chem. Int. Ed.*, **41**, 1053-+.
- [89] **Lummerstorfer, T. and Hoffmann, H.,** 2004. Click chemistry on surfaces: 1,3-dipolar cycloaddition reactions of azide-terminated monolayers on silica, *J. Phys. Chem. B*, **108**, 3963-3966.
- [90] **Tam, J. P., Xu, J. X. and Eom, K. D.,** 2001. Methods and strategies of peptide ligation, *Biopolymers*, **60**, 194-205.

- [91] **Yeo, D. S. Y., Srinivasan, R., Chen, G. Y. J. and Yao, S. Q.,** 2004. Expanded utility of the native chemical ligation reaction, *Chemistry-a European Journal*, **10**, 4664-4672.
- [92] **Kohn, M. and Breinbauer, R.,** 2004. The staudinger ligation - a gift to chemical biology', *Angew. Chem. Int. Ed.*, **43**, 3106-3116.
- [93] **Schmid, E. L., Keller, T. A., Dienes, Z. and Vogel, H.,** 1997. Reversible oriented surface immobilization of functional proteins on oxide surfaces, *Anal. Chem.*, **69**, 1979-1985.
- [94] **Turkova, J.,** 1999. Oriented immobilization of biologically active proteins as a tool for revealing protein interactions and function, *J. Chromatogr. B*, **722**, 11-31.
- [95] **Srisawat, C. and Engelke, D. R.,** 2001. Streptavidin aptamers: Affinity tags for the study of rnas and ribonucleoproteins, *Rna-a Publication of the Rna Society*, **7**, 632-641.
- [96] **Zhen, G. L., Falconnet, D., Kuennemann, E., Voros, J., Spencer, N. D., Textor, M. and Zurcher, S.,** 2006. Nitrilotriacetic acid functionalized graft copolymers: A polymeric interface for selective and reversible binding of histidine-tagged proteins, *Adv. Funct. Mater.*, **16**, 243-251.
- [97] **Ladd, J., Boozer, C., Yu, Q. M., Chen, S. F., Homola, J. and Jiang, S.,** 2004. DNA-directed protein immobilization on mixed self-assembled monolayers via a streptavidin bridge, *Langmuir*, **20**, 8090-8095.
- [98] **Smith, C. L., Milea, J. S. and Nguyen, G. H.,** 2005. Immobilization of nucleic acids using biotin-strept(avidin) systems, in *Immobilisation of DNA on chips ii*, p. 63-90, Eds.
- [99] **Chilkoti, A. and Stayton, P. S.,** 1995. Molecular-origins of the slow streptavidin-biotin dissociation kinetics, *J. Am. Chem. Soc.*, **117**, 10622-10628.
- [100] **Luo, S. F. and Walt, D. R.,** 1989. Avidin biotin coupling as a general-method for preparing enzyme-based fiber-optic sensors, *Analytical Chemistry*, **61**, 1069-1072.
- [101] **Orth, R. N., Clark, T. G. and Craighead, H. G.,** 2003. Avidin-biotin micropatterning methods for biosensor applications, *Biomed. Microdevices*, **5**, 29-34.
- [102] **Spinke, J., Liley, M., Schmitt, F. J., Guder, H. J., Angermaier, L. and Knoll, W.,** 1993. Molecular recognition at self-assembled monolayers - optimization of surface functionalization, *J. Chem. Phys.*, **99**, 7012-7019.
- [103] **Gentz, R., Chen, C. H. and Rosen, C. A.,** 1989. Bioassay for trans-activation using purified human immunodeficiency virus tat-encoded protein - trans-activation requires messenger-rna synthesis, *Proc. Natl. Acad. Sci. U. S. A.*, **86**, 821-824.

- [104] **Hochuli, E., Dobeli, H. and Schacher, A.,** 1987. New metal chelate adsorbent selective for proteins and peptides containing neighboring histidine-residues, *J. Chromatogr.*, **411**, 177-184.
- [105] **Hochuli, E., Bannwarth, W., Dobeli, H., Gentz, R. and Stuber, D.,** 1988. Genetic approach to facilitate purification of recombinant proteins with a novel metal chelate adsorbent, *Bio-Technology*, **6**, 1321-1325.
- [106] **Piesecki, S., Teng, W. Y. and Hochuli, E.,** 1993. Immobilization of beta-galactosidase for application in organic-chemistry using a chelating peptide, *Biotechnol. Bioeng.*, **42**, 178-184.
- [107] **Arnold, F. H.,** 1991. Metal-affinity separations - a new dimension in protein processing, *Bio-Technology*, **9**, 151-156.
- [108] **Ljungquist, C., Breitholtz, A., Brinknilsson, H., Moks, T., Uhlen, M. and Nilsson, B.,** 1989. Immobilization and affinity purification of recombinant proteins using histidine peptide fusions, *Eur. J. Biochem.*, **186**, 563-569.
- [109] **Carlsson, J., Mosbach, K. and Bulow, L.,** 1996. Affinity precipitation and site-specific immobilization of proteins carrying polyhistidine tails, *Biotechnol. Bioeng.*, **51**, 221-228.
- [110] **Gershon, P. D. and Khilko, S.,** 1995. Stable chelating linkage for reversible immobilization of oligohistidine tagged proteins in the biacore surface-plasmon resonance detector, *J. Immunol. Methods*, **183**, 65-76.
- [111] **Sigal, G. B., Bamdad, C., Barberis, A., Strominger, J. and Whitesides, G. M.,** 1996. A self-assembled monolayer for the binding and study of histidine tagged proteins by surface plasmon resonance, *Anal. Chem.*, **68**, 490-497.
- [112] **Kroger, D., Liley, M., Schiweck, W., Skerra, A. and Vogel, H.,** 1999. Immobilization of histidine-tagged proteins on gold surfaces using chelator thioalkanes, *Biosens. Bioelectron.*, **14**, 155-161.
- [113] **Peelle, B. R., Krauland, E. M., Wittrup, K. D. and Belcher, A. M.,** 2005. Design criteria for engineering inorganic material-specific peptides, *Langmuir*, **21**, 6929-6933.
- [114] **Presnova, G., Grigorenko, V., Egorov, A., Ruzgas, T., Lindgren, A., Gorton, L. and Borchers, T.,** 2000. Direct heterogeneous electron transfer of recombinant horseradish peroxidases on gold, *Faraday Discuss.*, 281-289.
- [115] **Slocik, J. M. and Wright, D. W.,** 2003. Biomimetic mineralization of noble metal nanoclusters, *Biomacromolecules*, **4**, 1135-1141.
- [116] **Martel, R. R., Rounseville, M. P. and Botros, I. W.,** 2004. Array formats, in *Microarray technology and its applications*, p. 3-22, Eds. Muller, U. R. and Nicolau, D. V., Springer, Berlin, Germany.
- [117] **Niemeyer, C. M.,** 2002. The developments of semisynthetic DNA-protein conjugates, *Trends Biotechnol.*, **20**, 395-401.



- [118] **Niemeyer, C. M.**, 2000. Self-assembled nanostructures based on DNA: Towards the development of nanobiotechnology, *Curr. Opin. Chem. Biol.*, **4**, 609-618.
- [119] **Seeman, N. C.**, 1999. DNA engineering and its application to nanotechnology, *Trends Biotechnol.*, **17**, 437-443.
- [120] **Hendrickson, E. R., Truby, T. M. H., Joerger, R. D., Majarian, W. R. and Ebersole, R. C.**, 1995. A sensitivity multianalyte immunoassay using covalent DNA-labeled antibodies and polymerase chain-reaction, *Nucleic Acids Res.*, **23**, 522-529.
- [121] **Schweitzer, B., Wiltshire, S., Lambert, J., O'Malley, S., Kukanskis, K., Zhu, Z. R., Kingsmore, S. F., Lizardi, P. M. and Ward, D. C.**, 2000. Immunoassays with rolling circle DNA amplification: A versatile platform for ultrasensitive antigen detection, *Proc. Natl. Acad. Sci. U. S. A.*, **97**, 10113-10119.
- [122] **Ghosh, S. S., Kao, P. M., McCue, A. W. and Chappelle, H. L.**, 1990. Use of maleimide-thiol coupling chemistry for efficient syntheses of oligonucleotide-enzyme conjugate hybridization probes, *Bioconj. Chem.*, **1**, 71-76.
- [123] **E. Kynclova, A. Hartig and Schalkhammer, T.**, 1995. Oligonucleotide labelled lipase as a new sensitive hybridization probe and its use in bio-assays and biosensors, *J. Mol. Recognit.*, **8**, 139-145.
- [124] **Scouten, W. H. and Konecny, P.**, 1992. Reversible immobilization of antibodies on magnetic beads, *Anal. Biochem.*, **205**, 313-318.
- [125] **Niemeyer, C. M., Sano, T., Smith, C. L. and Cantor, C. R.**, 1994. Oligonucleotide-directed self-assembly of proteins - semisynthetic DNA streptavidin hybrid molecules as connectors for the generation of macroscopic arrays and the construction of supramolecular bioconjugates, *Nucleic Acids Res.*, **22**, 5530-5539.
- [126] **Niemeyer, C. M., Boldt, L., Ceyhan, B. and Blohm, D.**, 1999. DNA-directed immobilization: Efficient, reversible, and site-selective surface binding of proteins by means of covalent DNA-streptavidin conjugates, *Anal. Biochem.*, **268**, 54-63.
- [127] **Niemeyer, C. M.**, 2001. Bioorganic applications of semisynthetic DNA-protein conjugates, *Chemistry-a European Journal*, **7**, 3189-3195.
- [128] **Patolsky, F., Ranjit, K. T., Lichtenstein, A. and Willner, I.**, 2000. Dendritic amplification of DNA analysis by oligonucleotide-functionalized au-nanoparticles, *Chem. Commun.*, 1025-1026.
- [129] **He, L., Musick, M. D., Nicewarner, S. R., Salinas, F. G., Benkovic, S. J., Natan, M. J. and Keating, C. D.**, 2000. Colloidal au-enhanced surface plasmon resonance for ultrasensitive detection of DNA hybridization, *J. Am. Chem. Soc.*, **122**, 9071-9077.
- [130] **Niemeyer, C. M. and Ceyhan, B.**, 2001. DNA-directed functionalization of colloidal gold with proteins, *Angew. Chem. Int. Ed.*, **40**, 3685-+.

- [131] **Demers, L. M., Park, S. J., Taton, T. A., Li, Z. and Mirkin, C. A.,** 2001. Orthogonal assembly of nanoparticle building blocks on dip-pen nanolithographically generated templates of DNA, *Angew. Chem. Int. Ed.*, **40**, 3071-3073.
- [132] **Lesaicherre, M. L., Lue, R. Y. P., Chen, G. Y. J., Zhu, Q. and Yao, S. Q.,** 2002. Intein-mediated biotinylation of proteins and its application in a protein microarray, *J. Am. Chem. Soc.*, **124**, 8768-8769.
- [133] **Furuse, M., Fujita, K., Hiiragi, T., Fujimoto, K. and Tsukita, S.,** 1998. Claudin-1 and -2: Novel integral membrane proteins localizing at tight junctions with no sequence similarity to occludin, *J. Cell Biol.*, **141**, 1539-1550.
- [134] **Terpe, K.,** 2003. Overview of tag protein fusions: From molecular and biochemical fundamentals to commercial systems, *Appl. Microbiol. Biotechnol.*, **60**, 523-533.
- [135] **Pryor, K. D. and Leiting, B.,** 1997. High-level expression of soluble protein in escherichia coli using a his(6)-tag and maltose-binding-protein double-affinity fusion system, *Protein Expression Purif.*, **10**, 309-319.
- [136] **Waugh, D. S.,** 2005. Making the most of affinity tags, *Trends Biotechnol.*, **23**, 316-320.
- [137] **Jenny, R. J., Mann, K. G. and Lundblad, R. L.,** 2003. A critical review of the methods for cleavage of fusion proteins with thrombin and factor xa, *Protein Expression Purif.*, **31**, 1-11.
- [138] **Lichty, J. J., Malecki, J. L., Agnew, H. D., Michelson-Horowitz, D. J. and Tan, S.,** 2005. Comparison of affinity tags for protein purification, *Protein Expression Purif.*, **41**, 98-105.
- [139] **Lu, B., Smyth, M. R. and Okennedy, R.,** 1996. Oriented immobilization of antibodies and its applications in immunoassays and immunosensors, *Analyst*, **121**, R29-R32.
- [140] **Tomizaki, K. Y., Usui, K. and Mihara, H.,** 2005. Protein-detecting microarrays: Current accomplishments and requirements, *ChemBioChem*, **6**, 783-799.
- [141] **Uttamchandani, M., Wang, J. and Yao, S. Q.,** 2006. Protein and small molecule microarrays: Powerful tools for high-throughput proteomics, *Molecular Biosystems*, **2**, 58-68.
- [142] **Wodicka, L., Dong, H. L., Mittmann, M., Ho, M. H. and Lockhart, D. J.,** 1997. Genome-wide expression monitoring in saccharomyces cerevisiae, *Nat. Biotechnol.*, **15**, 1359-1367.
- [143] **Lockhart, D. J., Dong, H. L., Byrne, M. C., Follettie, M. T., Gallo, M. V., Chee, M. S., Mittmann, M., Wang, C. W., Kobayashi, M., Horton, H. and Brown, E. L.,** 1996. Expression monitoring by hybridization to high-density oligonucleotide arrays, *Nat. Biotechnol.*, **14**, 1675-1680.

- [144] **Li, C. and Wong, W. H.**, 2001. Model-based analysis of oligonucleotide arrays: Expression index computation and outlier detection, *Proc. Natl. Acad. Sci. U. S. A.*, **98**, 31-36.
- [145] **Schweitzer, B. and Kingsmore, S. F.**, 2002. Measuring proteins on microarrays, *Curr. Opin. Biotechnol.*, **13**, 14-19.
- [146] **Love, K. R. and Seeberger, P. H.**, 2002. Carbohydrate arrays as tools for glycomics, *Angew. Chem. Int. Ed.*, **41**, 3583-3586.
- [147] **Lam, K. S. and Renil, M.**, 2002. From combinatorial chemistry to chemical microarray, *Curr. Opin. Chem. Biol.*, **6**, 353-358.
- [148] **Wu, R. Z., Bailey, S. N. and Sabatini, D. M.**, 2002. Cell-biological applications of transfected-cell microarrays, *Trends Cell Biol.*, **12**, 485-488.
- [149] **Fejzo, M. S. and Slamon, D. J.**, 2001. Frozen tumor tissue microarray technology for analysis of tumor rna, DNA, and proteins, *Am. J. Pathol.*, **159**, 1645-1650.
- [150] **de Wildt, R. M. T., Mundy, C. R., Gorick, B. D. and Tomlinson, I. M.**, 2000. Antibody arrays for high-throughput screening of antibody-antigen interactions, *Nat. Biotechnol.*, **18**, 989-994.
- [151] **Anderson, L. and Seilhamer, J.**, 1997. A comparison of selected mrna and protein abundances in human liver, *Electrophoresis*, **18**, 533-537.
- [152] **Gygi, S. P., Rochon, Y., Franza, B. R. and Aebersold, R.**, 1999. Correlation between protein and mrna abundance in yeast, *Mol. Cell. Biol.*, **19**, 1720-1730.
- [153] **Xia, Y. N. and Whitesides, G. M.**, 1998. Soft lithography, *Annual Review of Materials Science*, **28**, 153-184.
- [154] **Scholl, M., Sprossler, C., Denyer, M., Krause, M., Nakajima, K., Maelicke, A., Knoll, W. and Offenhausser, A.**, 2000. Ordered networks of rat hippocampal neurons attached to silicon oxide surfaces, *J. Neurosci. Methods*, **104**, 65-75.
- [155] **Ding, L., Zhou, W. W., Chu, H. B., Jin, Z., Zhang, Y. and Li, Y.**, 2006. Direct preparation and patterning of iron oxide nanoparticles via microcontact printing on silicon wafers for the growth of single-walled carbon nanotubes, *Chemistry of Materials*, **18**, 4109-4114.
- [156] **Kim, Y. K., Park, S. J., Koo, J. P., Oh, D. J., Kim, G. T., Hong, S. and Ha, J. S.**, 2006. Controlled direct patterning of v2o5 nanowires onto sio2 substrates by a microcontact printing technique, *Nanotechnology*, **17**, 1375-1379.
- [157] **McDonald, J. C., Duffy, D. C., Anderson, J. R., Chiu, D. T., Wu, H. K., Schueller, O. J. A. and Whitesides, G. M.**, 2000. Fabrication of microfluidic systems in poly(dimethylsiloxane), *Electrophoresis*, **21**, 27-40.

- [158] **Carlsson, J., Winqvist, F., Danielsson, B. and Lundstrom, I.,** 2005. Biosensor discrimination of meat juice from various animals using a lectin panel and ellipsometry, *Anal. Chim. Acta*, **547**, 229-236.
- [159] **Pla-Roca, M., Fernandez, J. G., Mills, C. A., Martinez, E. and Samitier, J.,** 2007. Micro/nanopatterning of proteins via contact printing using high aspect ratio pmma stamps and nanoimprint apparatus, *Langmuir*, **23**, 8614-8618.
- [160] **Bernard, A., Renault, J. P., Michel, B., Bosshard, H. R. and Delamarche, E.,** 2000. Microcontact printing of proteins, *Adv. Mater.*, **12**, 1067-1070.
- [161] **Tan, J. L., Tien, J. and Chen, C. S.,** 2002. Microcontact printing of proteins on mixed self-assembled monolayers, *Langmuir*, **18**, 519-523.
- [162] **Kane, R. S., Takayama, S., Ostuni, E., Ingber, D. E. and Whitesides, G. M.,** 1999. Patterning proteins and cells using soft lithography, *Biomaterials*, **20**, 2363-2376.
- [163] **Yang, Z. P. and Chilkoti, A.,** 2000. Microstamping of a biological ligand onto an activated polymer surface, *Adv. Mater.*, **12**, 413-+.
- [164] **Inglis, W., Sanders, G. H. W., Williams, P. M., Davies, M. C., Roberts, C. J. and Tendler, S. J. B.,** 2001. A simple method for biocompatible polymer based spatially controlled adsorption of blood plasma proteins to a surface, *Langmuir*, **17**, 7402-7405.
- [165] **Xia, Y. N. and Whitesides, G. M.,** 1998. Soft lithography, *Angew. Chem. Int. Ed.*, **37**, 551-575.
- [166] **Kumar, A. and Whitesides, G. M.,** 1993. Features of gold having micrometer to centimeter dimensions can be formed through a combination of stamping with an elastomeric stamp and an alkanethiol ink followed by chemical etching, *Appl. Phys. Lett.*, **63**, 2002-2004.
- [167] **Bieri, C., Ernst, O. P., Heyse, S., Hofmann, K. P. and Vogel, H.,** 1999. Micropatterned immobilization of a g protein-coupled receptor and direct detection of g protein activation, *Nat. Biotechnol.*, **17**, 1105-1108.
- [168] **Lopez, G. P., Biebuyck, H. A., Harter, R., Kumar, A. and Whitesides, G. M.,** 1993. Fabrication and imaging of 2-dimensional patterns of proteins adsorbed on self-assembled monolayers by scanning electron-microscopy, *J. Am. Chem. Soc.*, **115**, 10774-10781.
- [169] **Bernard, A., Delamarche, E., Schmid, H., Michel, B., Bosshard, H. R. and Biebuyck, H.,** 1998. Printing patterns of proteins, *Langmuir*, **14**, 2225-2229.
- [170] **Hyun, J., Zhu, Y. J., Liebmman-Vinson, A., Beebe, T. P. and Chilkoti, A.,** 2001. Microstamping on an activated polymer surface: Patterning biotin and streptavidin onto common polymeric biomaterials, *Langmuir*, **17**, 6358-6367.

- [171] **Hovis, J. S. and Boxer, S. G.**, 2000. Patterning barriers to lateral diffusion in supported lipid bilayer membranes by blotting and stamping, *Langmuir*, **16**, 894-897.
- [172] **James, C. D., Davis, R. C., Kam, L., Craighead, H. G., Isaacson, M., Turner, J. N. and Shain, W.**, 1998. Patterned protein layers on solid substrates by thin stamp microcontact printing, *Langmuir*, **14**, 741-744.
- [173] **Branch, D. W., Corey, J. M., Weyhenmeyer, J. A., Brewer, G. J. and Wheeler, B. C.**, 1998. Microstamp patterns of biomolecules for high-resolution neuronal networks, *Med Biol Eng Comput*, **36**, 135-141.
- [174] **St John, P. M., Davis, R., Cady, N., Czajka, J., Batt, C. A. and Craighead, H. G.**, 1998. Diffraction-based cell detection using a microcontact printed antibody grating, *Anal. Chem.*, **70**, 1108-1111.
- [175] **Homola, J., Lu, H. B. and Yee, S. S.**, 1999. Dual-channel surface plasmon resonance sensor with spectral discrimination of sensing channels using dielectric overlayer, *Electron. Lett*, **35**, 1105-1106.
- [176] **Garrison, M. D., McDevitt, T. C., Luginbuhl, R., Giachelli, C. M., Stayton, P. and Ratner, B. D.**, 2000. Quantitative interrogation of micropatterned biomolecules by surface force microscopy, *Ultramicroscopy*, **82**, 193-202.
- [177] **Freeman, J. W., Wright, L. D. and Laurencin, C. T.**, 2008 Nanofabrication techniques, in *Biomedical nanostructures*, p. 3-24, Eds. Gonsalves, K. E., Halberstadt, C. R., Laurencin, C. T. and Nair, L. S., John Wiley & Sons, Inc. , New Jersey, USA.
- [178] **Lee, K. B., Lim, J. H. and Mirkin, C. A.**, 2003. Protein nanostructures formed via direct-write dip-pen nanolithography, *J. Am. Chem. Soc.*, **125**, 5588-5589.
- [179] **Ding, L., Li, Y., Chu, H. B., Li, X. M. and Liu, J.**, 2005. Creation of cadmium sulfide nanostructures using afm dip-pen nanolithography, *J. Phys. Chem. B*, **109**, 22337-22340.
- [180] **Jaschke, M. and Butt, H. J.**, 1995. Deposition of organic material by the tip of a scanning force microscope, *Langmuir*, **11**, 1061-1064.
- [181] **Berggren, K. K., Bard, A., Wilbur, J. L., Gillaspay, J. D., Helg, A. G., McClelland, J. J., Rolston, S. L., Phillips, W. D., Prentiss, M. and Whitesides, G. M.**, 1995. Microlithography by using neutral metastable atoms and self-assembled monolayers, *Science*, **269**, 1255-1257.
- [182] **Bottomley, L. A.**, 1998. Scanning probe microscopy, *Anal. Chem.*, **70**, 425r-475r.
- [183] **Nyffenegger, R. M. and Penner, R. M.**, 1997. Nanometer-scale surface modification using the scanning probe microscope: Progress since 1991, *Chem. Rev.*, **97**, 1195-1230.

- [184] **Demers, L. M., Ginger, D. S., Park, S. J., Li, Z., Chung, S. W. and Mirkin, C. A.,** 2002. Direct patterning of modified oligonucleotides on metals and insulators by dip-pen nanolithography, *Science*, **296**, 1836-1838.
- [185] **Lee, K. B., Park, S. J., Mirkin, C. A., Smith, J. C. and Mrksich, M.,** 2002. Protein nanoarrays generated by dip-pen nanolithography, *Science*, **295**, 1702-1705.
- [186] **Kenseth, J. R., Harnisch, J. A., Jones, V. W. and Porter, M. D.,** 2001. Investigation of approaches for the fabrication of protein patterns by scanning probe lithography, *Langmuir*, **17**, 4105-4112.
- [187] **Lee, K. B., Kim, E. Y., Mirkin, C. A. and Wolinsky, S. M.,** 2004. The use of nanoarrays for highly sensitive and selective detection of human immunodeficiency virus type 1 in plasma, *Nano Lett.*, **4**, 1869-1872.
- [188] **Lee, M., Kang, D. K., Yang, H. K., Park, K. H., Choe, S. Y., Kang, C., Chang, S. I., Han, M. H. and Kang, I. C.,** 2006. Protein nanoarray on prolinker (tm) surface constructed by atomic force microscopy dip-pen nanolithography for analysis of protein interaction, *Proteomics*, **6**, 1094-1103.
- [189] **Lim, J. H., Ginger, D. S., Lee, K. B., Heo, J., Nam, J. M. and Mirkin, C. A.,** 2003. Direct-write dip-pen nanolithography of proteins on modified silicon oxide surfaces, *Angew. Chem. Int. Ed.*, **42**, 2309-2312.
- [190] **Jiang, H. Z. and Stupp, S. I.,** 2005. Dip-pen patterning and surface assembly of peptide amphiphiles, *Langmuir*, **21**, 5242-5246.
- [191] **Cho, Y. and Ivanisevic, A.,** 2004. Siox surfaces with lithographic features composed of a tat peptide, *J. Phys. Chem. B*, **108**, 15223-15228.
- [192] **Cho, Y. and Ivanisevic, A.,** 2005. Tat peptide immobilization on gold surfaces: A comparison study with a thiolated peptide and alkylthiols using afm, xps, and ft-irras, *J. Phys. Chem. B*, **109**, 6225-6232.
- [193] **Chung, S. W., Ginger, D. S., Morales, M. W., Zhang, Z. F., Chandrasekhar, V., Ratner, M. A. and Mirkin, C. A.,** 2005. Top-down meets bottom-up: Dip-pen nanolithography and DNA-directed assembly of nanoscale electrical circuits, *Small*, **1**, 64-69.
- [194] **Smith, J. C., Lee, K. B., Wang, Q., Finn, M. G., Johnson, J. E., Mrksich, M. and Mirkin, C. A.,** 2003. Nanopatterning the chemospecific immobilization of cowpea mosaic virus capsid, *Nano Lett.*, **3**, 883-886.
- [195] **Vega, R. A., Maspoch, D., Salaita, K. and Mirkin, C. A.,** 2005. Nanoarrays of single virus particles, *Angew. Chem. Int. Ed.*, **44**, 6013-6015.

- [196] **Cheung, C. L., Camarero, J. A., Woods, B. W., Lin, T. W., Johnson, J. E. and De Yoreo, J. J.,** 2003. Fabrication of assembled virus nanostructures on templates of chemoselective linkers formed by scanning probe nanolithography, *J. Am. Chem. Soc.*, **125**, 6848-6849.
- [197] **Rozhok, S., Shen, C. K. F., Littler, P. L. H., Fan, Z. F., Liu, C., Mirkin, C. A. and Holz, R. C.,** 2005. Methods for fabricating microarrays of motile bacteria, *Small*, **1**, 445-451.
- [198] **Salaita, K., Wang, Y. H. and Mirkin, C. A.,** 2007. Applications of dip-pen nanolithography, *Nature Nanotechnology*, **2**, 145-155.
- [199] **Gates, B. D., Xu, Q. B., Stewart, M., Ryan, D., Willson, C. G. and Whitesides, G. M.,** 2005. New approaches to nanofabrication: Molding, printing, and other techniques, *Chem. Rev.*, **105**, 1171-1196.
- [200] **Healy, K. E., Thomas, C. H., Rezanian, A., Kim, J. E., McKeown, P. J., Lom, B. and Hockberger, P. E.,** 1996. Kinetics of bone cell organization and mineralization on materials with patterned surface chemistry, *Biomaterials*, **17**, 195-208.
- [201] **Lom, B., Healy, K. E. and Hockberger, P. E.,** 1993. A versatile technique for patterning biomolecules onto glass coverslips, *J. Neurosci. Methods*, **50**, 385-397.
- [202] **Britland, S., Perezarnaud, E., Clark, P., McGinn, B., Connolly, P. and Moores, G.,** 1992. Micropatterning proteins and synthetic peptides on solid supports - a novel application for microelectronics fabrication technology, *Biotechnol. Prog.*, **8**, 155-160.
- [203] **Sigrist, H., Collioud, A., Clemence, J. F., Gao, H., Luginbuhl, R., Sanger, M. and Sundarababu, G.,** 1995. Surface immobilization of biomolecules by light, *Optical Engineering*, **34**, 2339-2348.
- [204] **Das, M. and Fox, C. F.,** 1979. Chemical cross-linking in biology, *Annu. Rev. Biophys. Bioeng.*, **8**, 165-193.
- [205] **Hahn, M. S., Taite, L. J., Moon, J. J., Rowland, M. C., Ruffino, K. A. and West, J. L.,** 2006. Photolithographic patterning of polyethylene glycol hydrogels, *Biomaterials*, **27**, 2519-2524.
- [206] **Sugawara, T. and Matsuda, T.,** 1995. Photochemical surface derivatization of a peptide-containing arg-gly-asp (rgd), *J. Biomed. Mater. Res.*, **29**, 1047-1052.
- [207] **Pease, A. C., Solas, D., Sullivan, E. J., Cronin, M. T., Holmes, C. P. and Fodor, S. P. A.,** 1994. Light-generated oligonucleotide arrays for rapid DNA-sequence analysis, *Proc. Natl. Acad. Sci. U. S. A.*, **91**, 5022-5026.
- [208] **Gao, H., Sanger, M., Luginbuhl, R. and Sigrist, H.,** 1995. Immunosensing with photoimmobilized immunoreagents on planar optical-wave guides, *Biosens. Bioelectron.*, **10**, 317-328.

- [209] **Nukavarapu, S. P., Kumbar, S. G., Nair, L. S. and Laurencin, C. T.,** 2008 Nanostructures for tissue engineering/regenerative medicine, in *Biomedical nanostructures*, p. 377-408, Eds. Gonsalves, K. E., Halberstadt, C. R., Laurencin, C. T. and Nair, L. S., John Wiley & Sons, Inc. , New Jersey, USA.
- [210] **Jang, Y. H., Oh, S. Y. and Park, J. K.,** 2006. In situ electrochemical enzyme immunoassay on a microchip with surface-functionalized poly(dimethylsiloxane) channel, *Enzyme Microb. Technol.*, **39**, 1122-1127.
- [211] **Cao, T. B., Wei, F., Jiao, X. M., Chen, J. Y., Liao, W., Zhao, X. and Cao, W. X.,** 2003. Micropatterns of protein and conducting polymer molecules fabricated by layer-by-layer self-assembly and photolithography techniques, *Langmuir*, **19**, 8127-8129.
- [212] **Mooney, J. F., Hunt, A. J., McIntosh, J. R., Liberko, C. A., Walba, D. M. and Rogers, C. T.,** 1996. Patterning of functional antibodies and other proteins by photolithography of silane monolayers, *Proc. Natl. Acad. Sci. U. S. A.*, **93**, 12287-12291.
- [213] **Hui, E. E. and Bhatia, S. N.,** 2007. Microscale control of cell contact and spacing via three-component surface patterning, *Langmuir*, **23**, 4103-4107.
- [214] **Popescu, D. C., van Leeuwen, E. N. M., Rossi, N. A. A., Holder, S. J., Jansen, J. A. and Sommerdijk, N. A. J. M.,** 2006. Shaping amorphous calcium carbonate films into 2d model substrates for bone cell culture, *Angew. Chem. Int. Ed.*, **45**, 1762-1767.
- [215] **Fodor, S. P. A., Read, J. L., Pirrung, M. C., Stryer, L., Lu, A. T. and Solas, D.,** 1991. Light-directed, spatially addressable parallel chemical synthesis, *Science*, **251**, 767-773.
- [216] **He, W., Gonsalves, K. E., Pickett, J. H. and Halberstadt, C.,** 2003. Synthesis, characterization, and preliminary biological study of poly(3-(tert-butoxycarbonyl)-n-vinyl-2-pyrrolidone), *Biomacromolecules*, **4**, 75-79.
- [217] **Douvas, A., Argitis, P., Diakoumakos, C. D., Misiakos, K., Dimotikali, D. and Kakabakos, S. E.,** 2001. Photolithographic patterning of proteins with photoresists processable under biocompatible conditions, *Journal of Vacuum Science & Technology B*, **19**, 2820-2824.
- [218] **Niemeyer, C. M.,** 2001. Nanoparticles, proteins, and nucleic acids: Biotechnology meets materials science, *Angew. Chem. Int. Ed.*, **40**, 4128-4158.
- [219] **Whitesides, G. M., Mathias, J. P. and Seto, C. T.,** 1991. Molecular self-assembly and nanochemistry - a chemical strategy for the synthesis of nanostructures, *Science*, **254**, 1312-1319.
- [220] **Alivisatos, A. P.,** 1996. Semiconductor clusters, nanocrystals, and quantum dots, *Science*, **271**, 933-937.



- [221] **Daniel, M. C. and Astruc, D.**, 2004. Gold nanoparticles: Assembly, supramolecular chemistry, quantum-size-related properties, and applications toward biology, catalysis, and nanotechnology, *Chemical Reviews*, **104**, 293-346.
- [222] **Wiley, B. J., Im, S. H., Li, Z. Y., McLellan, J., Siekkinen, A. and Xia, Y. A.**, 2006. Maneuvering the surface plasmon resonance of silver nanostructures through shape-controlled synthesis, *J. Phys. Chem. B*, **110**, 15666-15675.
- [223] **Pankhurst, Q. A., Connolly, J., Jones, S. K. and Dobson, J.**, 2003. Applications of magnetic nanoparticles in biomedicine, *Journal of Physics D-Applied Physics*, **36**, R167-R181.
- [224] **Xia, Y. N. and Halas, N. J.**, 2005. Shape-controlled synthesis and surface plasmonic properties of metallic nanostructures, *MRS Bull.*, **30**, 338-344.
- [225] **Sun, Y. G. and Xia, Y. N.**, 2002. Shape-controlled synthesis of gold and silver nanoparticles, *Science*, **298**, 2176-2179.
- [226] **Liz-Marzan, L. M.**, 2006. Tailoring surface plasmons through the morphology and assembly of metal nanoparticles, *Langmuir*, **22**, 32-41.
- [227] **Jin, R. C., Cao, Y. W., Mirkin, C. A., Kelly, K. L., Schatz, G. C. and Zheng, J. G.**, 2001. Photoinduced conversion of silver nanospheres to nanoprisms, *Science*, **294**, 1901-1903.
- [228] **Turkevich, J., Stevenson, P. C. and Hillier, J.**, 1951. A study of the nucleation and growth processes in the synthesis of colloidal gold, *Discuss. Faraday Soc.*, 55-&.
- [229] **Brown, K. R. and Natan, M. J.**, 1998. Hydroxylamine seeding of colloidal au nanoparticles in solution and on surfaces, *Langmuir*, **14**, 726-728.
- [230] **Hirsch, L. R., Gobin, A. M., Lowery, A. R., Tam, F., Drezek, R. A., Halas, N. J. and West, J. L.**, 2006. Metal nanoshells, *Annals of Biomedical Engineering*, **34**, 15-22.
- [231] **Zhou, H. S., Honma, I., Komiyama, H. and Haus, J. W.**, 1994. Controlled synthesis and quantum-size effect in gold-coated nanoparticles, *Physical Review B*, **50**, 12052-12056.
- [232] **Stober, W., Fink, A. and Bohn, E.**, 1968. Controlled growth of monodisperse silica spheres in micron size range, *J. Colloid Interface Sci.*, **26**, 62-&.
- [233] **Medintz, I. L., Uyeda, H. T., Goldman, E. R. and Mattoussi, H.**, 2005. Quantum dot bioconjugates for imaging, labelling and sensing, *Nat. Mater.*, **4**, 435-446.
- [234] **Murray, C. B., Norris, D. J. and Bawendi, M. G.**, 1993. Synthesis and characterization of nearly monodisperse cde (e = s, se, te) semiconductor nanocrystallites, *J. Am. Chem. Soc.*, **115**, 8706-8715.

- [235] **Dabbousi, B. O., Bawendi, M. G., Onitsuka, O. and Rubner, M. F.,** 1995. Electroluminescence from cdse quantum-dot polymer composites, *Appl. Phys. Lett.*, **66**, 1316-1318.
- [236] **Mattoussi, H., Cumming, A. W., Murray, C. B., Bawendi, M. G. and Ober, R.,** 1996. Characterization of cdse nanocrystallite dispersions by small angle x-ray scattering, *J. Chem. Phys.*, **105**, 9890-9896.
- [237] **Mattoussi, H., Cumming, A. W., Murray, C. B., Bawendi, M. G. and Ober, R.,** 1998. Properties of cdse nanocrystal dispersions in the dilute regime: Structure and interparticle interactions, *Physical Review B*, **58**, 7850-7863.
- [238] **Hines, M. A. and Guyot-Sionnest, P.,** 1998. Bright uv-blue luminescent colloidal znse nanocrystals, *J. Phys. Chem. B*, **102**, 3655-3657.
- [239] **Guzelian, A. A., Banin, U., Kadavanich, A. V., Peng, X. and Alivisatos, A. P.,** 1996. Colloidal chemical synthesis and characterization of inas nanocrystal quantum dots, *Appl. Phys. Lett.*, **69**, 1432-1434.
- [240] **Guzelian, A. A., Katari, J. E. B., Kadavanich, A. V., Banin, U., Hamad, K., Juban, E., Alivisatos, A. P., Wolters, R. H., Arnold, C. C. and Heath, J. R.,** 1996. Synthesis of size-selected, surface-passivated inp nanocrystals, *J. Phys. Chem.*, **100**, 7212-7219.
- [241] **Guerreiro, P. T., Ten, S., Borrelli, N. F., Butty, J., Jabbour, G. E. and Peyghambarian, N.,** 1997. Pbs quantum-dot doped grasses as saturable absorbers for mode locking of a cr:Forsterite laser, *Appl. Phys. Lett.*, **71**, 1595-1597.
- [242] **Stewart, M. D., Patterson, K., Somervell, M. H. and Willson, C. G.,** 2000. Organic imaging materials: A view of the future, *J. Phys. Org. Chem.*, **13**, 767-774.
- [243] **Willson, C. G. and Trinquet, B. C.,** 2003. The evolution of materials for the photolithographic process, *J. Photopolym. Sci. Technol.*, **16**, 621-627.
- [244] **Goethals, A. M., De Bisschop, P., Hermans, J., Jonckheere, R., Van Roey, F., Van den Heuvel, D., Eliat, A. and Ronse, K.,** 2003. Introducing 157nm full field lithography, *J. Photopolym. Sci. Technol.*, **16**, 549-556.
- [245] **Golovkina, V. N., Nealey, P. F., Cerrina, F., Taylor, J. W., Solak, H. H., David, C. and Gobrecht, J.,** 2004. Exploring the ultimate resolution of positive-tone chemically amplified resists: 26 nm dense lines using extreme ultraviolet interference lithography, *Journal of Vacuum Science & Technology B*, **22**, 99-103.
- [246] **Brainard, R. L., Cobb, J. and Cutler, C. A.,** 2003. Current status of euv photoresists, *J. Photopolym. Sci. Technol.*, **16**, 401-410.
- [247] **Larruquert, J. I. and Keski-Kuha, R. A. M.,** 2002. Sub-quarter-wave multilayer coatings with high reflectance in the extreme ultraviolet, *Appl. Opt.*, **41**, 5398-5404.

- [248] **Li, Y. Q., Ota, K. and Murakami, K.,** 2003. Thermal and structural deformation and its impact on optical performance of projection optics for extreme ultraviolet lithography, *Journal of Vacuum Science & Technology B*, **21**, 127-129.
- [249] **Xia, Y. N., Rogers, J. A., Paul, K. E. and Whitesides, G. M.,** 1999. Unconventional methods for fabricating and patterning nanostructures, *Chem. Rev.*, **99**, 1823-1848.
- [250] **Url-1,** [www.Aph.Uni-karlsruhe.De/wegener/data/image/research/eb1.Jpg](http://www.Aph.Uni-karlsruhe.De/wegener/data/image/research/eb1.Jpg), accessed at 27.08.2009
- [251] **Batson, P. E.,** 1993. Simultaneous stem imaging and electron-energy-loss spectroscopy with atomic-column sensitivity, *Nature*, **366**, 727-728.
- [252] **Muller, D. A., Tzou, Y., Raj, R. and Silcox, J.,** 1993. Mapping sp(2) and sp(3) states of carbon at subnanometer spatial-resolution, *Nature*, **366**, 725-727.
- [253] **Smith, H. I. and Craighead, H. G.,** 1990. Nanofabrication, *Physics Today*, **43**, 24-30.
- [254] **Gibson, J. M.,** 1997. Reading and writing with electron beams, *Physics Today*, **50**, 56-61.
- [255] **Haes, A. J., Haynes, C. L., McFarland, A. D., Schatz, G. C., Van Duyne, R. R. and Zou, S. L.,** 2005. Plasmonic materials for surface-enhanced sensing and spectroscopy, *MRS Bull.*, **30**, 368-375.
- [256] **Anker, J. N., Hall, W. P., Lyandres, O., Shah, N. C., Zhao, J. and Van Duyne, R. P.,** 2008. Biosensing with plasmonic nanosensors, *Nat. Mater.*, **7**, 442-453.
- [257] **Yonzon, C. R., Stuart, D. A., Zhang, X. Y., McFarland, A. D., Haynes, C. L. and Van Duyne, R. P.,** 2005. Towards advanced chemical and biological nanosensors - an overview, *Talanta*, **67**, 438-448.
- [258] **Haes, A. J., Chang, L., Klein, W. L. and Van Duyne, R. P.,** 2005. Detection of a biomarker for alzheimer's disease from synthetic and clinical samples using a nanoscale optical biosensor, *J. Am. Chem. Soc.*, **127**, 2264-2271.
- [259] **Litorja, M., Haynes, C. L., Haes, A. J., Jensen, T. R. and Van Duyne, R. P.,** 2001. Surface-enhanced raman scattering detected temperature programmed desorption: Optical properties, nanostructure, and stability of silver film over sio2 nanosphere surfaces, *J. Phys. Chem. B*, **105**, 6907-6915.
- [260] **Dick, L. A., McFarland, A. D., Haynes, C. L. and Van Duyne, R. P.,** 2002. Metal film over nanosphere (mfon) electrodes for surface-enhanced raman spectroscopy (sers): Improvements in surface nanostructure stability and suppression of irreversible loss, *J. Phys. Chem. B*, **106**, 853-860.

- [261] **Stuart, D. A., Yonzon, C. R., Zhang, X. Y., Lyandres, O., Shah, N. C., Glucksberg, M. R., Walsh, J. T. and Van Duyne, R. P., 2005.** Glucose sensing using near-infrared surface-enhanced raman spectroscopy: Gold surfaces, 10-day stability, and improved accuracy, *Anal. Chem.*, **77**, 4013-4019.
- [262] **Zhang, X. Y., Young, M. A., Lyandres, O. and Van Duyne, R. P., 2005.** Rapid detection of an anthrax biomarker by surface-enhanced raman spectroscopy, *J. Am. Chem. Soc.*, **127**, 4484-4489.
- [263] **Nakamura, H. and Karube, I., 2003.** Current research activity in biosensors, *Anal. Bioanal. Chem.*, **377**, 446-468.
- [264] **Scheller, F. W., Wollenberger, U., Warsinke, A. and Lisdat, F., 2001.** Research and development in biosensors, *Curr. Opin. Biotechnol.*, **12**, 35-40.
- [265] **Altschuh, D., Oncul, S. and Demchenko, A. P., 2006.** Fluorescence sensing of intermolecular interactions and development of direct molecular biosensors, *J. Mol. Recognit.*, **19**, 459-477.
- [266] **McFarland, S. A. and Finney, N. S., 2001.** Fluorescent chemosensors based on conformational restriction of a biaryl fluorophore, *J. Am. Chem. Soc.*, **123**, 1260-1261.
- [267] **Aoki, S., Zulkefeli, M., Shiro, M., Kohsako, M., Takeda, K. and Kimura, E., 2005.** A luminescence sensor of inositol 1,4,5-triphosphate and its model compound by ruthenium-templated assembly of a bis(zn<sup>2+</sup>-cyclen) complex having a 2,2'-bipyridyl linker (cyclen=1,4,7,10-tetraazacyclododecane), *J. Am. Chem. Soc.*, **127**, 9129-9139.
- [268] **Chudakov, D. M., Lukyanov, S. and Lukyanov, K. A., 2005.** Fluorescent proteins as a toolkit for in vivo imaging, *Trends Biotechnol.*, **23**, 605-613.
- [269] **Knemeyer, J. P., Marme, N. and Sauer, M., 2000.** Probes for detection of specific DNA sequences at the single-molecule level, *Anal. Chem.*, **72**, 3717-3724.
- [270] **Demchenko, A. P., 2005.** The problem of self-calibration of fluorescence signal in microscale sensor systems, *Lab on a Chip*, **5**, 1210-1223.
- [271] **Willems, K. A. and Van Duyne, R. P., 2007.** Localized surface plasmon resonance spectroscopy and sensing, *Annu. Rev. Phys. Chem.*, **58**, 267-297.
- [272] **Miller, M. M. and Lazarides, A. A., 2005.** Sensitivity of metal nanoparticle surface plasmon resonance to the dielectric environment, *J. Phys. Chem. B*, **109**, 21556-21565.
- [273] **Malmqvist, M., 1993.** Biospecific interaction analysis using biosensor technology, *Nature*, **361**, 186-187.
- [274] **Berger, C. E. H., Beumer, T. A. M., Kooyman, R. P. H. and Greve, J., 1998.** Surface plasmon resonance multisensing, *Anal. Chem.*, **70**, 703-706.

- [275] **Hamamoto, K., Micheletto, R., Oyama, M., Umar, A. A., Kawai, S. and Kawakami, Y.,** 2006. An original planar multireflection system for sensing using the local surface plasmon resonance of gold nanospheres, *Journal of Optics a-Pure and Applied Optics*, **8**, 268-271.
- [276] **Prasad, P. N.,** 2003. *Intoduction to biophotonics*, p ed. John Wiley & Sons, Inc., New Jersey, USA.
- [277] **Knobloch, H., Brunner, H., Leitner, A., Aussenegg, F. and Knoll, W.,** 1993. Probing the evanescent field of propagating plasmon surface-polaritons by fluorescence and raman spectroscopies, *J. Chem. Phys.*, **98**, 10093-10095.
- [278] **Homola, J., Yee, S. S. and Gauglitz, G.,** 1999. Surface plasmon resonance sensors: Review, *Sens. Actuators, B*, **54**, 3-15.
- [279] **Seker, U. O. S., Wilson, B., Dincer, S., Kim, I. W., Oren, E. E., Evans, J. S., Tamerler, C. and Sarikaya, M.,** 2007. Adsorption behavior of linear and cyclic genetically engineered platinum binding peptides, *Langmuir*, **23**, 7895-7900.
- [280] **Abdulhalim, I.,** 2009. Enhancing the sensitivity of surface-plasmon resonance sensors, *SPIE-Newsroom*, 1-3.
- [281] **Nath, N. and Chilkoti, A.,** 2004. Label-free biosensing by surface plasmon resonance of nanoparticles on glass: Optimization of nanoparticle size, *Analytical Chemistry*, **76**, 5370-5378.
- [282] **Haes, A. J. and Van Duyne, R. P.,** 2004. A unified view of propagating and localized surface plasmon resonance biosensors, *Anal. Bioanal. Chem.*, **379**, 920-930.
- [283] **Jung, L. S., Campbell, C. T., Chinowsky, T. M., Mar, M. N. and Yee, S. S.,** 1998. Quantitative interpretation of the response of surface plasmon resonance sensors to adsorbed films, *Langmuir*, **14**, 5636-5648.
- [284] **Tamerler, C. and Sarikaya, M.,** 2009. Molecular biomimetics: Nanotechnology and bionanotechnology using genetically engineered peptides, *Philosophical Transactions of the Royal Society a-Mathematical Physical and Engineering Sciences*, **367**, 1705-1726.
- [285] **Zin, M. T., Ma, H., Sarikaya, M. and Jen, A. K. Y.,** 2005. Assembly of gold nanoparticles using genetically engineered polypeptides, *Small*, **1**, 698-702.
- [286] **Tamerler, C., Duman, M., Oren, E. E., Gungormus, M., Xiong, X. R., Kacar, T., Parviz, B. A. and Sarikaya, M.,** 2006. Materials specificity and directed assembly of a gold-binding peptide, *Small*, **2**, 1372-1378.

- [287] **Dai, H. X., Choe, W. S., Thai, C. K., Sarikaya, M., Traxler, B. A., Baneyx, F. and Schwartz, D. T.,** 2005. Nonequilibrium synthesis and assembly of hybrid inorganic-protein nanostructures using an engineered DNA binding protein, *J. Am. Chem. Soc.*, **127**, 15637-15643.
- [288] **Gungormus, M., Fong, H., Kim, I. W., Evans, J. S., Tamerler, C. and Sarikaya, M.,** 2008. Regulation of in vitro calcium phosphate mineralization by combinatorially selected hydroxyapatite-binding peptides, *Biomacromolecules*, **9**, 966-973.
- [289] **Falini, G., Albeck, S., Weiner, S. and Addadi, L.,** 1996. Control of aragonite or calcite polymorphism by mollusk shell macromolecules, *Science*, **271**, 67-69.
- [290] **Hunter, G. K. and Goldberg, H. A.,** 1993. Nucleation of hydroxyapatite by bone sialoprotein, *Proc. Natl. Acad. Sci. U. S. A.*, **90**, 8562-8565.
- [291] **Paine, M. L. and Snead, M. L.,** 1997. Protein interactions during assembly of the enamel organic extracellular matrix, *J. Bone Miner. Res.*, **12**, 221-227.
- [292] **Fan, Y., Sun, Z. and Moradian-Oldak, J.,** 2009. Controlled remineralization of enamel in the presence of amelogenin and fluoride, *Biomaterials*, **30**, 478-483.
- [293] **Kroger, N., Deutzmann, R., Bergsdorf, C. and Sumper, M.,** 2000. Species-specific polyamines from diatoms control silica morphology, *Proc. Natl. Acad. Sci. U. S. A.*, **97**, 14133-14138.
- [294] **Shimizu, K., Cha, J., Stucky, G. D. and Morse, D. E.,** 1998. Silicatein alpha: Cathepsin L-like protein in sponge biosilica, *Proc. Natl. Acad. Sci. U. S. A.*, **95**, 6234-6238.
- [295] **Kroger, N., Deutzmann, R. and Sumper, M.,** 1999. Polycationic peptides from diatom biosilica that direct silica nanosphere formation, *Science*, **286**, 1129-1132.
- [296] **Goobes, R., Goobes, G., Shaw, W. J., Drobny, G. P., Campbell, C. T. and Stayton, P. S.,** 2007. Thermodynamic roles of basic amino acids in statherin recognition of hydroxyapatite, *Biochemistry (Mosc)*. **46**, 4725-4733.
- [297] **Brown, S.,** 1992. Engineered iron oxide-adhesion mutants of the escherichia-coli phage-lambda receptor, *Proc. Natl. Acad. Sci. U. S. A.*, **89**, 8651-8655.
- [298] **Hnilova, M., Oren, E. E., Seker, U. O. S., Wilson, B. R., Collino, S., Evans, J. S., Tamerler, C. and Sarikaya, M.,** 2008. Effect of molecular conformations on the adsorption behavior of gold-binding peptides, *Langmuir*, **24**, 12440-12445.
- [299] **Brown, S.,** 1997. Metal-recognition by repeating polypeptides, *Nat. Biotechnol.*, **15**, 269-272.
- [300] **Naik, R. R., Stringer, S. J., Agarwal, G., Jones, S. E. and Stone, M. O.,** 2002. Biomimetic synthesis and patterning of silver nanoparticles, *Nat. Mater.*, **1**, 169-172.

- [301] **Whaley, S. R., English, D. S., Hu, E. L., Barbara, P. F. and Belcher, A. M.,** 2000. Selection of peptides with semiconductor binding specificity for directed nanocrystal assembly, *Nature*, **405**, 665-668.
- [302] **Lee, S. W., Mao, C. B., Flynn, C. E. and Belcher, A. M.,** 2002. Ordering of quantum dots using genetically engineered viruses, *Science*, **296**, 892-895.
- [303] **Krauland, E. M., Pelle, B. R., Wittrup, K. D. and Belcher, A. M.,** 2007. Peptide tags for enhanced cellular and protein adhesion to single-crystal line sapphire, *Biotechnol. Bioeng.*, **97**, 1009-1020.
- [304] **Oren, E. E., Tamerler, C., Sahin, D., Hnilova, M., Seker, U. O. S., Sarikaya, M. and Samudrala, R.,** 2007. A novel knowledge-based approach to design inorganic-binding peptides, *Bioinformatics*, **23**, 2816-2822.
- [305] **Thai, C. K., Dai, H. X., Sastry, M. S. R., Sarikaya, M., Schwartz, D. T. and Baneyx, F.,** 2004. Identification and characterization of cu<sub>2</sub>O- and ZnO-binding polypeptides by escherichia coli cell surface display: Toward an understanding of metal oxide binding, *Biotechnology and Bioengineering*, **87**, 129-137.
- [306] **Sano, K. I., Sasaki, H. and Shiba, K.,** 2005. Specificity and biomineralization activities of Ti-binding peptide-1 (tbp-1), *Langmuir*, **21**, 3090-3095.
- [307] **Kenan, D. J., Walsh, E. B., Meyers, S. R., O'Toole, G. A., Carruthers, E. G., Lee, W. K., Zauscher, S., Prata, C. A. H. and Grinstaff, M. W.,** 2006. Peptide-peg amphiphiles as cytophobic coatings for mammalian and bacterial cells, *Chem. Biol.*, **13**, 695-700.
- [308] **Adey, N. B., Mataragnon, A. H., Rider, J. E., Carter, J. M. and Kay, B. K.,** 1995. Characterization of phage that bind plastic from phage-displayed random peptide libraries, *Gene*, **156**, 27-31.
- [309] **Smith, G. P. and Petrenko, V. A.,** 1997. Phage display, *Chem. Rev.*, **97**, 391-410.
- [310] **Donatan, S., Yazici, H., Bermek, H., Sarikaya, M., Tamerler, C. and Urgen, M.,** 2009. Physical elution in phage display selection of inorganic-binding peptides, *Materials Science & Engineering C-Biomimetic and Supramolecular Systems*, **29**, 14-19.
- [311] **Brown, S., Sarikaya, M. and Johnson, E.,** 2000. A genetic analysis of crystal growth, *J. Mol. Biol.*, **299**, 725-735.
- [312] **Evans, J. S., Samudrala, R., Walsh, T. R., Oren, E. E. and Tamerler, C.,** 2008. Molecular design of inorganic-binding polypeptides, *MRS Bull.*, **33**, 514-518.
- [313] **Addadi, L. and Weiner, S.,** 1985. Interactions between acidic proteins and crystals - stereochemical requirements in biomineralization, *Proc. Natl. Acad. Sci. U. S. A.*, **82**, 4110-4114.
- [314] **Mann, S.,** 1988. Molecular recognition in biomineralization, *Nature*, **332**, 119-124.

- [315] **Attwood, T. K.**, 2000. Genomics - the babel of bioinformatics, *Science*, **290**, 471-473.
- [316] **Needleman, S. B. and Wunsch, C. D.**, 1970. A general method applicable to search for similarities in amino acid sequence of 2 proteins, *J. Mol. Biol.*, **48**, 443-&.
- [317] **Henikoff, S. and Henikoff, J. G.**, 1992. Amino-acid substitution matrices from protein blocks, *Proc. Natl. Acad. Sci. U. S. A.*, **89**, 10915-10919.
- [318] **Tamerler, C., Oren, E. E., Duman, M., Venkatasubramanian, E. and Sarikaya, M.**, 2006. Adsorption kinetics of an engineered gold binding peptide by surface plasmon resonance spectroscopy and a quartz crystal microbalance, *Langmuir*, **22**, 7712-7718.
- [319] **Suzuki, N., Sarikaya, M. and Ohuchi, F. S.**, 2007. Adsorption of genetically engineered proteins studied by time-of-flight secondary ion mass spectrometry (tof-sims). Part b: Hierarchical cluster analysis (hca), *Surf. Interface Anal.*, **39**, 427-433.
- [320] **Haris, P. I. and Chapman, D.**, 1995. The conformational-analysis of peptides using fourier-transform ir spectroscopy, *Biopolymers*, **37**, 251-263.
- [321] **Kulp, J. L., Sarikaya, M. and Evans, J. S.**, 2004. Molecular characterization of a prokaryotic polypeptide sequence that catalyzes au crystal formation, *J. Mater. Chem.*, **14**, 2325-2332.
- [322] **So, C. R., Tamerler, C. and Sarikaya, M.**, 2009. Adsorption, diffusion, and self-assembly of an engineered gold-binding peptide on au(111) investigated by atomic force microscopy, *Angew. Chem. Int. Ed.*, **48**, 5174-5177.
- [323] **So, C. R., Kulp, J. L., Oren, E. E., Zareie, H., Tamerler, C., Evans, J. S. and Sarikaya, M.**, 2009. Molecular recognition and supramolecular self-assembly of a genetically engineered gold binding peptide on au{111}, *Acs Nano*, **3**, 1525-1531.
- [324] **Drexler, K. E.**, 1994. Molecular nanomachines - physical principles and implementation strategies, *Annu. Rev. Biophys. Biomol. Struct.*, **23**, 377-405.
- [325] **Ryu, D. D. Y. and Nam, D. H.**, 2000. Recent progress in biomolecular engineering, *Biotechnol. Prog.*, **16**, 2-16.
- [326] **Ishikawa, K., Yamada, K., Kumagai, S., Sano, K. I., Shiba, K., Yamashita, I. and Kobayashi, M.**, 2008. Adsorption properties of a gold-binding peptide assessed by its attachment to a recombinant apoferritin molecule, *Applied Physics Express*, **1**, -.
- [327] **Woodbury, R. G., Wendin, C., Clendenning, J., Melendez, J., Elkind, J., Bartholomew, D., Brown, S. and Furlong, C. E.**, 1998. Construction of biosensors using a gold-binding polypeptide and a miniature integrated surface plasmon resonance sensor, *Biosens. Bioelectron.*, **13**, 1117-1126.



- [328] **Brott, L. L., Naik, R. R., Pikas, D. J., Kirkpatrick, S. M., Tomlin, D. W., Whitlock, P. W., Clarson, S. J. and Stone, M. O.,** 2001. Ultrafast holographic nanopatterning of biocatalytically formed silica, *Nature*, **413**, 291-293.
- [329] **Sarikaya, M., Fong, H., Frech, D. W. and Humbert, R.,** 1999. Biomimetic assembly of nanostructured materials, *Bioceramics*, **293**, 83-97.
- [330] **Url-2,** [www.Expasy.Ch/](http://www.Expasy.Ch/), accessed at 12.08.2009
- [331] **Chen, Y., Munechika, K. and Ginger, D. S.,** 2007. Dependence of fluorescence intensity on the spectral overlap between fluorophores and plasmon resonant single silver nanoparticles, *Nano Lett.*, **7**, 690-696.
- [332] **Pham, T., Jackson, J. B., Halas, N. J. and Lee, T. R.,** 2002. Preparation and characterization of gold nanoshells coated with self-assembled monolayers, *Langmuir*, **18**, 4915-4920.
- [333] **Bradford, M. M.,** 1976. Rapid and sensitive method for quantitation of microgram quantities of protein utilizing principle of protein-dye binding, *Anal. Biochem.*, **72**, 248-254.
- [334] **Kacar, T., Zin, M. T., So, C., Wilson, B., Ma, H., Gul-Karaguler, N., Jen, A. K. Y., Sarikaya, M. and Tamerler, C.,** 2009. Directed self-immobilization of alkaline phosphatase on micro-patterned substrates via genetically fused metal-binding peptide, *Biotechnol. Bioeng.*, **103**, 696-705.
- [335] **Kacar, T., Ray, J., Gungormus, M., Oren, E. E., Tamerler, C. and Sarikaya, M.,** 2009. Quartz binding peptides as molecular linkers towards fabricating multifunctional micropatterned substrates, *Advanced Materials*, **21**, 295-299.
- [336] **Wei, J. H., Kacar, T., Tamerler, C., Sarikaya, M. and Ginger, D. S.,** 2009. Nanopatterning peptides as bifunctional inks for templated assembly, *Small*, **5**, 689-693.
- [337] **Anderson, R. A., Bosron, W. F., Kennedy, F. S. and Vallee, B. L.,** 1975. Role of magnesium in escherichia-coli alkaline-phosphatase, *Proc. Natl. Acad. Sci. U. S. A.*, **72**, 2989-2993.
- [338] **Url-3,** [www.Rcsb.Org/pdb/home/home.Do](http://www.Rcsb.Org/pdb/home/home.Do), accessed at 31.08.2009
- [339] **Karpovich, D. S. and Blanchard, G. J.,** 1994. Direct measurement of the adsorption-kinetics of alkanethiolate self-assembled monolayers on a microcrystalline gold surface, *Langmuir*, **10**, 3315-3322.
- [340] **Schessler, H. M., Karpovich, D. S. and Blanchard, G. J.,** 1996. Quantitating the balance between enthalpic and entropic forces in alkanethiol/gold monolayer self assembly, *J. Am. Chem. Soc.*, **118**, 9645-9651.
- [341] **Revzin, A., Russell, R. J., Yadavalli, V. K., Koh, W. G., Deister, C., Hile, D. D., Mellott, M. B. and Pishko, M. V.,** 2001. Fabrication of poly(ethylene glycol) hydrogel microstructures using photolithography, *Langmuir*, **17**, 5440-5447.

- [342] **Prime, K. L. and Whitesides, G. M.,** 1993. Adsorption of proteins onto surfaces containing end-attached oligo(ethylene oxide) - a model system using self-assembled monolayers, *J. Am. Chem. Soc.*, **115**, 10714-10721.
- [343] **Zhou, H. X. and Dill, K. A.,** 2001. Stabilization of proteins in confined spaces, *Biochemistry (Mosc)*. **40**, 11289-11293.
- [344] **Kasemo, B.,** 2002. Biological surface science, *Surf. Sci.*, **500**, 656-677.
- [345] **Shao, W. H., Zhang, X. E., Liu, H. and Zhang, Z. P.,** 2000. Anchor-chain molecular system for orientation control in enzyme immobilization, *Bioconj. Chem.*, **11**, 822-826.
- [346] **Zhang, J. K. and Cass, A. E. G.,** 2001. A study of his-tagged alkaline phosphatase immobilization on a nanoporous nickel-titanium dioxide film, *Analytical Biochemistry*, **292**, 307-310.
- [347] **Manoil, C. and Traxler, B.,** 2000. Insertion of in-frame sequence tags into proteins using transposons, *Methods-a Companion to Methods in Enzymology*, **20**, 55-61.
- [348] **Fujiwara, K., Watarai, H., Itoh, H., Nakahama, E. and Ogawa, N.,** 2006. Measurement of antibody binding to protein immobilized on gold nanoparticles by localized surface plasmon spectroscopy, *Analytical and Bioanalytical Chemistry*, **386**, 639-644.
- [349] **Feng, J., Gao, C. Y., Wang, B. and Shen, J. C.,** 2004. Co-patterning chitosan and bovine serum albumin on an aldehyde-enriched glass substrate by microcontact printing, *Thin Solid Films*, **460**, 286-290.
- [350] **Ostuni, E., Yan, L. and Whitesides, G. M.,** 1999. The interaction of proteins and cells with self-assembled monolayers of alkanethiolates on gold and silver, *Colloids and Surfaces B-Biointerfaces*, **15**, 3-30.
- [351] **Piehl, J., Brecht, A., Geckeler, K. E. and Gauglitz, G.,** 1996. Surface modification for direct immunoprobes, *Biosensors & Bioelectronics*, **11**, 579-590.
- [352] **Brogan, K. L., Shin, J. H. and Schoenfisch, M. H.,** 2004. Influence of surfactants and antibody immobilization strategy on reducing nonspecific protein interactions for molecular recognition force microscopy, *Langmuir*, **20**, 9729-9735.
- [353] **Boppart, S. A., Bouma, B. E., Pitris, C., Southern, J. F., Brezinski, M. E. and Fujimoto, J. G.,** 1998. In vivo cellular optical coherence tomography imaging, *Nat. Med.*, **4**, 861-865.
- [354] **Shao, Y., Jin, Y. D. and Dong, S. J.,** 2004. Synthesis of gold nanoplates by aspartate reduction of gold chloride, *Chem. Commun.*, 1104-1105.

- [355] **Selvakannan, P., Mandal, S., Phadtare, S., Gole, A., Pasricha, R., Adyanthaya, S. D. and Sastry, M.,** 2004. Water-dispersible tryptophan-protected gold nanoparticles prepared by the spontaneous reduction of aqueous chloroaurate ions by the amino acid, *J. Colloid Interface Sci.*, **269**, 97-102.
- [356] **Bhargava, S. K., Booth, J. M., Agrawal, S., Coloe, P. and Kar, G.,** 2005. Gold nanoparticle formation during bromoaurate reduction by amino acids, *Langmuir*, **21**, 5949-5956.
- [357] **Dickerson, M. B., Sandhage, K. H. and Naik, R. R.,** 2008. Protein- and peptide-directed syntheses of inorganic materials, *Chem. Rev.*, **108**, 4935-4978.
- [358] **Kneipp, K., Kneipp, H., Itzkan, I., Dasari, R. R. and Feld, M. S.,** 1999. Ultrasensitive chemical analysis by raman spectroscopy, *Chem. Rev.*, **99**, 2957-+.
- [359] **Levy, R., Thanh, N. T. K., Doty, R. C., Hussain, I., Nichols, R. J., Schiffrin, D. J., Brust, M. and Fernig, D. G.,** 2004. Rational and combinatorial design of peptide capping ligands for gold nanoparticles, *J. Am. Chem. Soc.*, **126**, 10076-10084.
- [360] **Sadtler, B. and Wei, A.,** 2002. Spherical ensembles of gold nanoparticles on silica: Electrostatic and size effects, *Chem. Commun.*, 1604-1605.

## **APPENDICES**

**APPENDIX A.1:** SPR adsorption isotherms of QBP1 and QBP2 on silica-coated SPR chip.

**APPENDIX A.2:** QBP1-F pattern on glass by using “Affiliation” PDMS-stamp.

**APPENDIX A.3:**  $\mu$ CP of PBS buffer on quartz followed by SA-QD(605) incubation.

**APPENDIX A.4:** NSL-fabricated Au nanostructures.

**APPENDIX A.5:** 3D representation of NSL-fabricated Au nanostructures.

**APPENDIX A.6:** SPR profile of AgBP1 on silver-coated SPR chip.

**APPENDIX A.7:** Silica nanoparticles synthesized by Stober method.

**APPENDIX A.8:** EDX spectrum from Al-background.

**APPENDIX A.1:** SPR adsorption isotherms of QBP1 and QBP2 on silica-coated SPR chip.

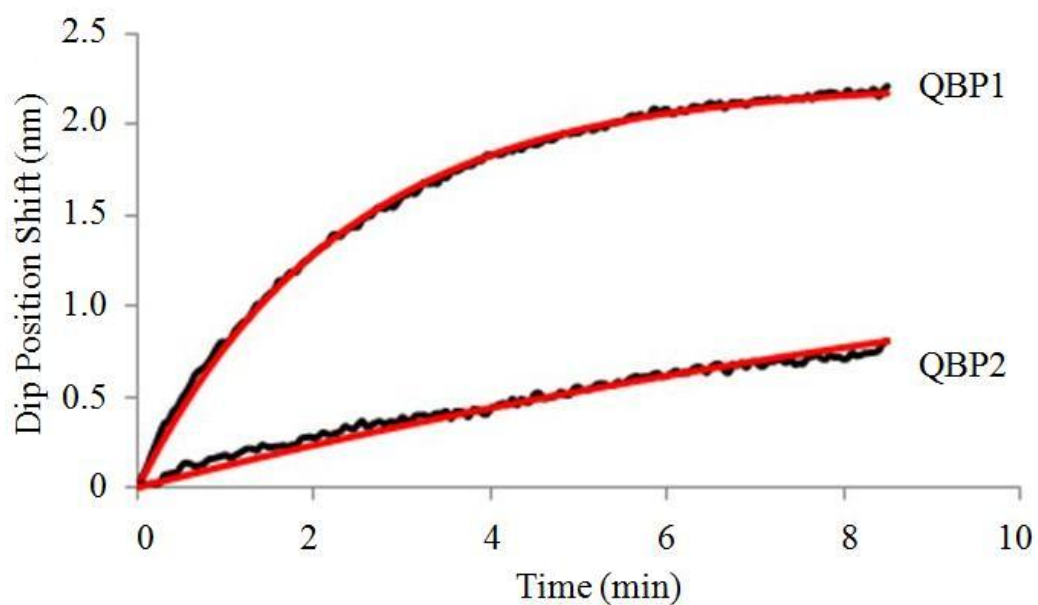


**Figure A.1 :** Adsorption isotherms for QBP1 and QBP2 based on SPR spectroscopy. Black lines represent the experimental data and red lines are for the fits calculated using the Langmuir isotherm (by U.O. Seker).

**APPENDIX A.2:** QBP1-F pattern on glass by using “Affiliation” PDMS-stamp.



**Figure A.2:** FM images of the glass substrate after micropatterning of QBP1-F.

**APPENDIX A.3:**  $\mu$ CP of PBS buffer on quartz followed by SA-QD(605) incubation.

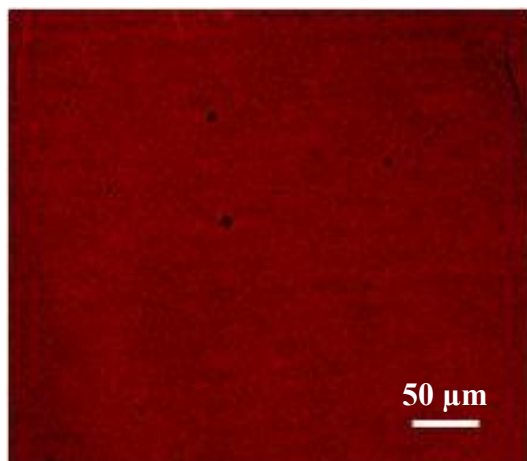


**Figure A.3:** FM image of PBS buffer-stamped quartz substrate following SA-QD(605) incubation.

**APPENDIX A.4:** NSL-fabricated Au nanostructures.

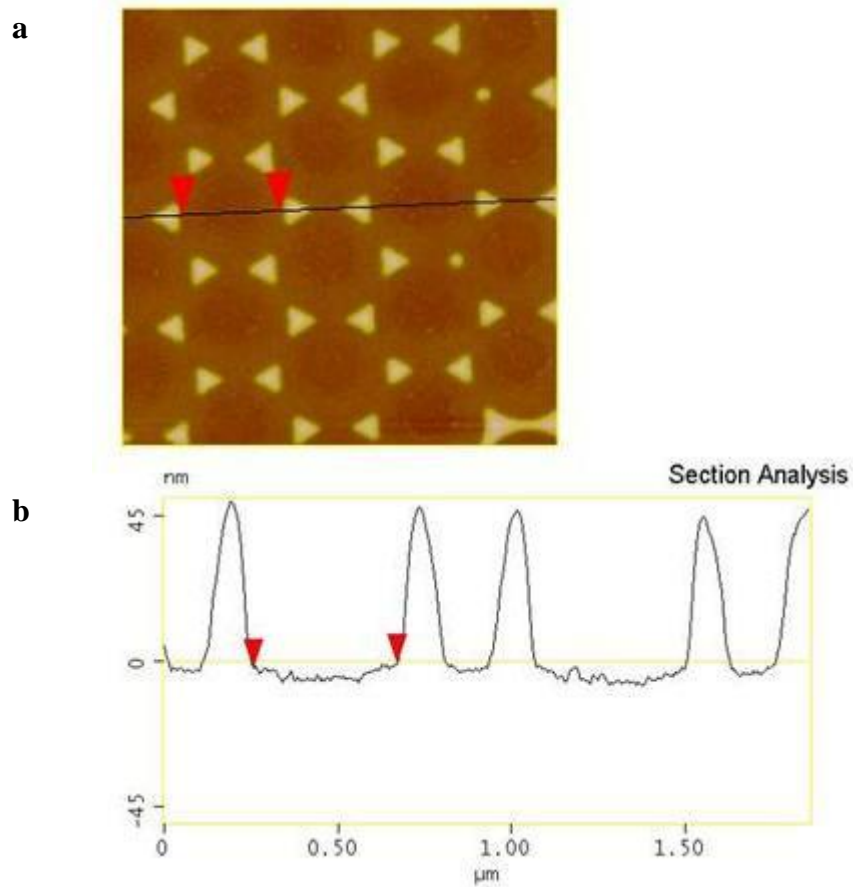


**Figure A.4:** (a) AFM image of NSL-fabricated Au NP array, (b) Section analysis (by C. So).



**APPENDIX A.5:** 3D representation of NSL-fabricated Au nanostructures.

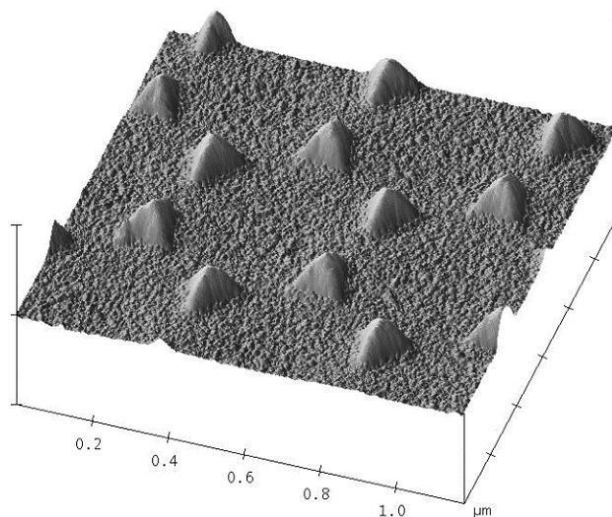


**Figure A.5:** 3D AFM image of NSL-fabricated Au NP array represented in Figure A.4 (by C. So).

**APPENDIX A.6:** SPR profile of AgBP1 on silver-coated SPR chip.

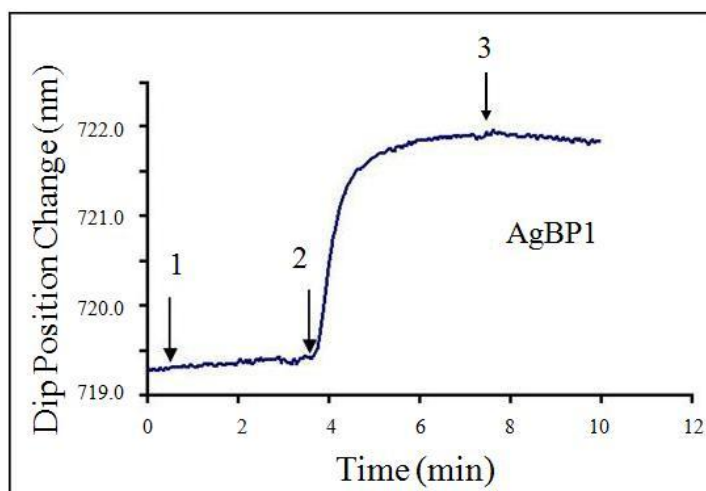


**Figure A.6:** SPR sensogram upon binding of AgBP1 on silver coated-SPR chip; 1. Buffer injection, 2. Peptide solution injection, 3. Washing with buffer. (by B. Wilson).

**APPENDIX A.7:** Silica nanoparticles synthesized by Stober method.

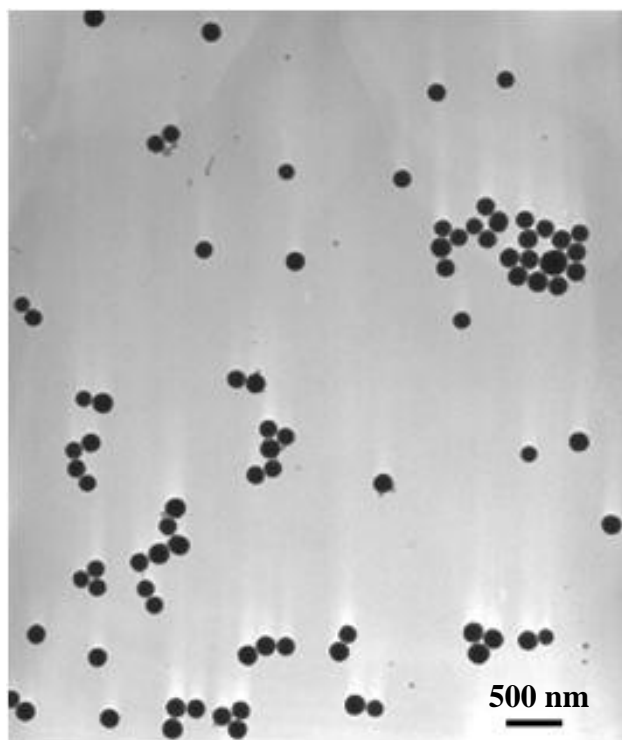


**Figure A.7:** TEM image of synthesized silica NPs.

**APPENDIX A.8:** EDX spectrum from Al-background.

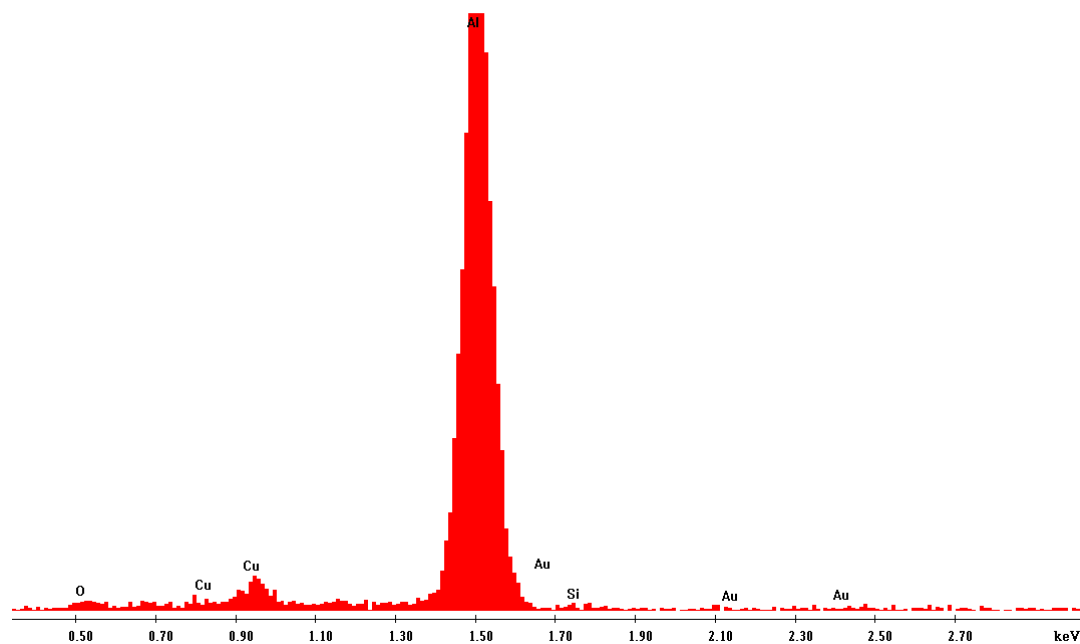


**Figure A.8:** EDX spectrum was taken from blank spot on Aluminum mount (as background), showing negligible Si and Au signals.



## CURRICULUM VITA



**Candidate's full name:** Turgay Kaçar

**Place and date of birth:** Istanbul, Turkey 09/05/1979

**Permanent Address:** Üsküdar- İstanbul

### Universities and

**Colleges attended:** I.T.U. Molecular Biology-Genetics and Biotechnology (Ph.D.)  
I.T.U. Polymer Science and Technology (M.Sc.)  
Marmara University, Chemistry Dept. (B.Sc.)  
Haydarpaşa College

### Publications:

- Tamerler, C., Khatayevich, D., Gungormus, M., **Kacar, T.**, Oren, EE., Hnilova, M., Sarikaya, M., 2010: Molecular Biomimetics: GEPI-Based Biological Routes to Technology. *Peptide Science*, 94 (1) 78-94.
- **Kacar, T.**, Zin, MT., So, C., Wilson, B., Ma, H., Gul-Karaguler, N., Jen, AK-Y., Sarikaya, M. and Tamerler, C., 2009: Directed Self-Immobilization of Alkaline Phosphatase on Micro-patterned Substrates via Genetically-Fused Metal-Binding Peptide. *Biotechnology and Bioengineering* 103, 696-705.
- Wei, JH., **Kacar, T.**, Tamerler, C., Sarikaya, M. and Ginger DS., 2009: Nanopatterning peptides as Bi-functional Inks for Templated assembly. *Small*, 5 689-693.
- **Kacar, T.**, Ray, J., Gungormus, M., Oren, EE., Tamerler, C., Sarikaya, M., 2009: Quartz Binding Peptides as Molecular Linkers Towards Fabricating Multifunctional Micropatterned Substrates. *Advanced Materials*, 21 295-299.
- Tamerler, C., **Kacar, T.**, Sahin, D., Fong, H., Sarikaya, M., 2007: Genetically Engineered Polypeptides for Inorganics: A Utility in Biological Materials Science and Engineering. *Materials Science & Engineering C-Biomimetic and Supramolecular Systems* 27 (3) 558-564.

- Tamerler, C., Duman, M., Oren, EE., Gungormus, M., Xiong, XR., **Kacar, T.**, Parviz, BA., Sarikaya, M., 2006: Materials specificity and directed assembly of a gold-binding peptide. *Small* 2 (11) 1372-1378.
- Serhatli, IE., **Kacar, T.**, 2006: Synthesis of Liquid Crystalline-Amorphous Block Copolymers by Combination of CFRP and ATRP Mechanisms. *Journal of Applied Polymer Science* 99 (6) 3187–94.
- Serhatli, IE., **Kacar, T.**, Onen, A., 2003: Synthesis of Liquid Crystalline-Amorphous Block Copolymers by the Combination of Atom Transfer and Photoinduced Radical Polymerization Mechanisms. *Journal of Polymer Science Part A: Polymer Chemistry* 41 (13) 1892-1903.
- **Kacar, T.**, 2002: New Synthetic Approach for the Liquid Crystalline-Amorphous Block Copolymers. *M.Sc. thesis*.